Living microalgae-textile and cyanobacteria-loofah biocomposites for intensified carbon capture, utilisation and storage

A Thesis Submitted By

Pichaya In-na

For the Degree of Doctor of Philosophy

School of Engineering
Newcastle University

December 2020

Abstract

Microalgae and cyanobacteria have been intensively studied as biological routes for carbon capture. Conventionally, they are cultivated in suspension within open ponds or enclosed photobioreactors (PBR); however, these systems suffer from many drawbacks including large land and water consumption, slow mass transfer rates, and high risk of contamination. This thesis presents a biocomposite culture system to overcome these disadvantages by immobilising cells onto solid supports (textiles and loofah sponge) using non-toxic hydrogel and latex-based binders.

The performance of *Chlorella vulgaris* (a eukaryote microalga) textile-based hydrogel top coated biocomposites were tested in semi-batch CO_2 absorption tests, resulting in enhanced CO_2 capture. The highest CO_2 absorption rate was 1.82 ± 0.10 g CO_2 $g^{-1}_{biomass}$ d^{-1} from coated cotton biocomposites, followed by 1.55 ± 0.27 g CO_2 $g^{-1}_{biomass}$ d^{-1} from uncoated cotton biocomposites. There was some degradation of the cotton, which could limit operational lifetime of the biocomposites.

Loofah-based *Synechococcus elongatus* (prokaryote cyanobacterium) latex-based biocomposites had CO_2 absorption rates of 0.68 ± 0.18 and 0.93 ± 0.30 g CO_2 $g^{-1}_{biomass}$ d^{-1} for *S. elongatus* strain PCC 7942 (PCC) and CCAP 1479/1A (CCAP) respectively; however, cell outgrowth occurred midway through the trials.

The formulations of synthetic latex binders were adjusted using different styrene/butyl acrylate blends and a coalescence agent (i.e. Texanol™), increasing CO_2 uptake rates by 14-20 and 3-8 fold for CCAP and PCC relative to their suspension controls. The CCAP biocomposites lasted in excess of 12 weeks whereas the PCC biocomposites experienced cell leaching after four weeks.

A simplified techno-economic analysis was conducted, revealing that water and energy consumption were significantly reduced compared to raceway ponds, flat plate PBRs and biofilm-based PBRs.

Acknowledgement

First and foremost, I would like to express my heartfelt gratitude to my supervisors, Dr Jonathan G. M. Lee and Dr Gary S. Caldwell who continuously support my PhD journey and we have gone through challenges and obstacles together as a team. Their excellent supervision, patience, motivation, encouragement, wealth of knowledge, and guidance will not be forgotten. This thesis would not have become one piece without their tremendous help. They pushed me beyond my normal capacity and made me realise my true potential. It is a great honour and a pleasure to work with both of you. I would not have professionally become who I am today.

My sincere appreciation goes to Adam Wallace, who assisted in the development of the biocomposites screening protocol in Chapter 4. During my visit to North Carolina State University, United States, our experiences in the laboratory and his hospitality are memorable.

To all the academic and non-academic staff of the School of Engineering and the School of Natural and Environmental Sciences at Newcastle University (especially Justine McGruther, Rob Dixon, Kevin Brown, Ashley Craig, Michael Foster, Peter McParlin, David Whitaker, and Charlotte Anderson), I would like to express my warm appreciation for their technical support.

I wish to also extend my gratitude to the following people who supported me one way or another during my research work; Dr Abbas Umar, Rachel Hart, Assia Stefanova, Matthew Pickersgill and Matthew Walker. Your support was valuable and it made my PhD journey full of enthusiasm and enjoyment.

Same recognition goes to all the Bachelor's and Master's students; Edouard Thouvenin, Jack He, Robin Kaur, Hamza Zaib, Ryan Marchington, Fergal Byrne, and Chloe Allen, who I worked with throughout my study. They inspired me to keep going and I wish them bright and successful future.

An exceptional appreciation goes to Elliot Sharp, who worked alongside me on research work in Chapter 5 and was there whenever I came across challenges as well as Prof. Justin Perry and Dr Matthew Unthank from Northumbria University for insightful advises and guidance.

To Newcastle University, I gratefully acknowledge the Doctoral scholarship award that made my PhD study possible and for being my second home not only for my PhD study, but also my Bachelor's and Master's degrees.

I would like to also thank all of my friends including the ones in my office who believed in me during my self-doubt moments and persuaded me to take a break during stressful times. This appreciation also goes to a very special person, Chris Dixon.

At last, to my entire family, my father (Dr Nophadol In-na), mother (Dr Yuwaree In-na), grandmothers in heaven, and brother (Jirakit In-na) who stayed by my side despite long hours in the lab, at the keyboard, or at university, I am grateful to have them in my life.

<div align="right">

Pichaya In-na
Newcastle University
December 2020

</div>

Publications and conferences

Publications:

- **Pichaya In-na,** Abbas A. Umar, Gary S. Caldwell, Adam D. Wallace, Michael C. Flickinger, and Jonathan G.M. Lee. "Loofah-based microalgae and cyanobacteria biocomposites for intensifying carbon dioxide capture". Journal of CO_2 Utilization. 2020. DOI: https://doi.org/10.1016/j.jcou.2020.101348 (Chapter 4 of this Thesis).

- **Pichaya In-na,** Gary S. Caldwell, and Jonathan G.M. Lee. "Microalgae-textile biocomposites deliver enhanced carbon dioxide capture". Submitted to Journal of Industrial Textiles. (Chapter 3 of this Thesis).

- **Pichaya In-na,** Elliot Sharp, Gary S. Caldwell, Matthew Unthank, Justin Perry, and Jonathan G.M. Lee. "Engineered living photosynthetic biocomposites for intensified carbon capture". To be submitted to Communications Biology. (Chapter 5 of this Thesis).

- **Pichaya In-na,** Fergal Bryne, Gary S. Caldwell, and Jonathan G.M. Lee. "Preliminary techno-economic analysis of living biocomposites for carbon capture from breweries". To be submitted to Algal Research. (Chapter 6 of this Thesis).

Conferences:

- **Pichaya In-na**, Abbas A. Umar, Adam D. Wallace, Jonathan G.M. Lee, Gary S. Caldwell, and Michael C. Flickinger. "Algae biocomposites for carbon capture and storage". Poster presentation at the 14th International Conference on Greenhouse Gas Control Technologies, Melbourne, Australia. 21st – 25th October 2018.

- **Pichaya In-na**, Jonathan G.M. Lee, Gary S. Caldwell, and Michael C. Flickinger. "Development of biocomposites using loofah scaffold with immobilised cyanobacteria for carbon capture and utilisation". Oral presentation at the 12th European Symposium on Biochemical Engineering Sciences, Lisbon, Portugal. 9th – 12th September 2018.

- **Pichaya In-na**, Jonathan G.M. Lee, Gary S. Caldwell, and Michael C. Flickinger. "Carbon capture and conversion using textile-based algae biocomposites". Poster presentation at the 8th International Conference on Algal Biomass, Biofuels & Bioproducts, Seattle, WA, USA. 11th – 13th June 2018.

Table of contents

List of figures

Chapter 3

Chapter 4

Chapter 5

Chapter 6

List of tables

Chapter 5

Chapter 6

Chapter 7

Abbreviations and notation

Abbreviations

2D	2-dimensional
3D	3-dimensional
3PGA	3-phosphoglycerate
AA	Acrylic acid
AFOLU	Agriculture, forestry and other land use
ATP	Adenosine triphosphate
ANOVA	One-way analysis of variance
BA	Butyl acrylate
BECCS	Bioenergy with carbon capture and storage
BOD	biochemical oxygen demand
CCM	CO_2 concentrating mechanism
CCS	Carbon capture and storage
CCU	Carbon capture and utilisation
COD	chemical oxygen demand
Ci	Inorganic carbon
DAC	Direct air capture
EPS	Extracellular polymeric substances
Fv/Fm	Maximum photosystem II quantum yield
G3P	3-carbon molecules G3P
GHG	Greenhouse gases
MC	Membrane contractor
MEA	Monoethanolamine
MGS	Membrane gas separation
MFFT	Minimum film formation temperature
NET	Negative emissions technology
NADPH	Nicotinamide adenine dinucleotide phosphate
PBR	Photobioreactor
PAR	Photosynthetic active radiation

PS	Apparent rate of photosynthesis
PSI	Photosystem I
PSII	Photosystem II
PZ	Piperazine
IDW	Immobilised dried weight
IPCC	Intergovernmental Panel on Climate Change
RuBisCo	Ribulose-1,5-bisphosphate carboxylase/oxygenase
RuBP	Ribulose-1, 5- biphosphate
SEM	Scanning electron microscopy
St	Styrene
SA	Surface area
TEA	Technoeconomic analysis
WCP	Wet cell paste

Notation

d	day
dH_2O	Deionised water
g	gram
Gt	Gigatonnes
L	Litre
mL	Millilitre
m	metre
t	tonnes
Tg	glass transition temperature
h	hour
w/w	weight to weight
V	Volume
v/v	volume to volume
yr	year

Chapter 1

Introduction

1.1 Project background

Mitigating global warming is a serious matter if humanity is to prevent major permanent environmental damage. The recent Intergovernmental Panel on Climate Change (IPCC) report (Rogelj et al., 2018) states that GHG emissions must be urgently reduced to prevent the global average temperature exceeding 1.5 °C above pre-industrial levels. To achieve this, net carbon dioxide (CO_2) emissions need to be reduced to zero, i.e. "carbon neutrality" — the quantity of CO_2 released to atmosphere must be removed at the same rate. The IPCC published four scenarios which demonstrate that CO_2 removal will play a vital role in limiting global average temperature rise to 1.5 °C. In the most favourable and practical scenario, bioenergy with carbon capture and storage (BECCS)—considered the most promising carbon capture and storage (CCS) technology—is classed as a negative emission technology. However, the land required to employ BECCS would consume around 25-80% of current crop growing land. There is emerging interest in utilising microalgae and cyanobacteria within BECCS.

Microalgae and cyanobacteria have been intensively studied as biological routes for carbon capture for the last 40 years. Conventional algae cultivation relies on suspension (free cell culture) within open ponds or enclosed photobioreactors (PBR); however, these have drawbacks which limit their practicality for industrial scale CO_2 removal, including; large land and water consumption, slow CO_2 mass transfer rates, and a high risk of biological contamination (Singh and Dhar, 2019, Noble et al., 2012, Kumar et al., 2011, Ho et al., 2011). Biofilm-based PBRs overcome some of the drawbacks, but contamination risk is still present and biomass detachment can limit productivity (Mantzorou and Ververidis, 2019). In this thesis, a novel bioinspired concept of living algae biocomposites is developed to intensify carbon capture. Biocomposites (3D) or biocoatings (2D) are technologies that utilise cell immobilisation to entrap or adhere a concentrated population of microorganisms onto solid substrates without compromising biological performance. Biocomposites should be able to overcome the disadvantages of suspension and biofilm systems by: 1) immobilising the cells onto solid supports with non-toxic binders or coatings; 2) protecting microalgae and cyanobacteria from contamination; and, 3) significantly reducing water and land requirements.

1.2   Aims and objectives

The aim of this research is to develop inexpensive living biocomposites that have higher rates of CO_2 absorption compared to suspension cultures, with a long operational lifespan (more than 1000 h as an initial target). The specific objectives are, to:

1. Identify suitable non-toxic solid supports, immobilisation techniques, and adhesive binding materials for producing long lasting biocomposites.

2. Develop a screening protocol to identify non-toxic binders and adhesion ability to a chosen solid support for biocomposite production with selected microalgae and cyanobacteria.

3. Test CO_2 uptake performances of the biocomposites against their suspension controls in a semi-batch system as well as monitor biocomposites robustness (for up to 1000 h) without water or nutrient refreshment.

4. Assess carbohydrate accumulation of the biocomposites from the CO_2 absorption tests against suspension controls.

5. Conduct a preliminary technoeconomic analysis on the best performing biocomposites against alternative cultivation systems.

1.3   Hypotheses

In nature, microalgae and cyanobacteria can live on or within solid surfaces and are even found living symbiotically in lichen underneath a protective layer of fungus filaments. Inspired by this, the following hypotheses were developed:

1) *The survival of microalgae and cyanobacteria is prolonged when immobilised with non-toxic coatings onto suitable solid substrates;*

2) *Immobilisation will increase CO_2 absorption rates relative to suspension cultures; and*

3) *Living biocomposites are more economically and sustainably feasible than conventional algae cultivation systems for CCS applications.*

1.4   Outline of thesis

This thesis was written with each chapter in the style of journal paper. All chapters were written by the primary author, Pichaya In-na, and edited by Dr Jonathan Lee and Dr Gary Caldwell. In particular, Dr Jonathan Lee helped with the CO_2 absorption kinetics model in Chapter 4. All experimental work and data collection were conducted by the primary author unless otherwise stated. Each chapter describes the following:

Chapter two – In this Chapter, the relevant literature is reviewed to provide insights into the current development of various CCS technologies (post-, pre- and oxy-fuel- combustion) and algae technologies (open ponds, PBRs, biofilms and algal immobilisation techniques) in terms of their technical aspects and CO_2 transfer. Advantages and disadvantages of each technology are discussed where possible. Photosynthesis and CO_2 transfer pathways of microalgae and cyanobacteria are also explained. Among the immobilisation techniques, latex immobilisation is the primary focus as a potential breakthrough technology. Diverse solid supports that may be used for developing biocomposites (particularly loofah sponge) are also discussed.

Chapter three – In this Chapter, microalgae-textile biocomposites are developed using hydrogels as a topcoat to immobilise *Chlorella vulgaris* onto natural and synthetic textiles. The textile biocomposites were operated with substantially reduced water use, offering a "low-water low-maintenance" system that overcomes many issues inherit with conventional open pond or suspension based PBR systems, tackling both CO_2 emissions and water shortage issues.

Chapter four – This Chapter aims to demonstrate that living cyanobacteria biocomposites made from inexpensive loofah scaffolds with latex immobilisation can intensify CO_2 absorption rates relative to suspension cultures. Effective, simple, and rapid binder screening protocols are developed using two strains of *Synechococcus elongatus* cyanobacteria (CCAP 1479/1A and PCC 7942). The analysis of the kinetic CO_2 absorption model of the biocomposites are also conducted.

Chapter five – This study identifies a desirable chemical composition for acrylic latex binders (based on varying the styrene/butyl acrylate monomer blends and levels of a commercial coalescence agent) and investigates the photosynthetic responses of cyanobacteria exposed to acrylic latex formulations. The best performing binders are tested in semi-batch CO_2 absorption tests without water and nutrient refreshment. In addition, the total carbohydrate content of the tested biocomposites is determined to inform potential paths to carbon utilisation.

Chapter six – A simplified techno-economic analysis and estimation of CO_2 avoidance costs are conducted on the best performing biocomposites against other algae cultivation systems, with emphasis on the brewing industry. The work also identifies some pitfalls of the biocomposite technology and makes constructive suggestions where possible. Unlike other algae technologies, it should be noted that the biocomposites are designed with the aim of maximising CO_2 uptake rates instead of maximising algae biomass production. The estimated

CO_2 avoidance costs of the biocomposites provide the economic values of biocomposites against other CCS technologies.

Chapter seven – The final chapter summarises all the findings in this thesis and provides a future vision of the biocomposites within and beyond CCS applications. The future vision outlines key design criteria, potential challenges, a proposed design, and possible improvements that should be considered for scaling for pilot-scale CCS application. A design of a pilot-scale biocomposite system is proposed based on three different case studies. In closing, other potential biocomposites applications are discussed, emphasising their versatility and potential benefits to society.

Chapter 2

Literature review

Abstract

Carbon capture and storage (CCS) will play a vital role in mitigating global warming by limiting the rise in global average temperatures to 1.5 ℃. CCS technologies are well developed; however, drawbacks including expensive infrastructure and environmental impacts from using toxic chemicals are concerns. Among the CCS options, bioenergy with carbon capture and storage (BECCS) is deemed the most promising, but the land requirement to achieve the mitigation scenario (estimated at 25-80% of current crop growing land) is impractical and threatens food security. Integrating algae technologies within a BECCS context could potentially reduce land consumption. In this Chapter, CCS technologies (post-, pre- and oxy-fuel- combustion) and algae technologies (open ponds, photobioreactors (PBRs), biofilms, and algal immobilisation techniques) are discussed in terms of their technical aspects and CO_2 transfer. Open ponds and PBRs have significant water demand coupled with slow CO_2 mass transfer rates. Biofilms can overcome these drawbacks, but they suffer from high biological contamination risk and have short operational lifespans unfavourable for long-term carbon capture. Applying biocoatings or biocomposites that immobilise algae appear to enhance CO_2 mass transfer and limit biocontamination, but have yet to overcome issues of short service life. This chapter will focus on latex immobilisation as a potential breakthrough technology. Its use in combination with diverse solid support matrices (particularly loofah sponge) are also discussed.

2.1 Introduction

Since the industrial age, human activities that emit greenhouse gases (GHG) have contributed substantially to global climate change (Leeham and Allen, 2013). Currently, the atmospheric level of carbon dioxide (CO_2) exceeds 400 ppm and is predicted to reach 730 to 1,200 ppm by 2100 (Meehl and Stocker, 2007). If substantive mitigation measures are not enacted (and soon) (Adams and Caldeira, 2008), major environmental impacts (including ocean acidification, ocean heatwaves, ocean scale deoxygenation and destructive sea level rise) will accelerate, catastrophically affecting biodiversity, food webs and the planetary biosphere (Collins and Knutti, 2014).

The recent Intergovernmental Panel on Climate Change (IPCC) report (Rogelj et al., 2018) states that GHG emissions must be urgently reduced to prevent the global average temperature exceeding 1.5 °C above pre-industrial levels. To achieve this, net CO_2 emissions need to be reduced to zero, i.e. "carbon neutrality" — the quantity of CO_2 released to atmosphere must be removed at the same rate. Despite high carbon pricing enforcement and policies relating to CO_2 mitigation being in place, cumulative residual CO_2 emissions from various sectors (e.g. transportation, buildings, agriculture) are predicted to remain significant at 850–1150 $GtCO_2$ between 2016 – 2100 (Luderer et al., 2018), due to increases in global population, food and energy demand. Thus, removal of CO_2 from the atmosphere is necessary (Luderer et al., 2018).

The IPCC published four scenarios (Figure 2.1) for limiting global average temperature rise to 1.5 °C. Major differences between scenarios were based on assumptions for food and energy demand, and the rigid enforcement of climate policies (Rogelj et al., 2018), within which CO_2 removal plays a vital role. CO_2 removal falls into two categories; carbon capture and storage (CCS) and carbon capture and utilisation (CCU). CCS is deemed to have the higher contribution potential for net negative emissions whereas CCU provides economic benefits by reusing the CO_2 in many industrial processes (Baena-Moreno et al., 2018). Gabrielli et al. (2020) compared CCS, CCU and an additional biological route (farming biomass for chemicals production). All routes were feasible but with different benefits and drawbacks. For CCS, the application mainly depended on the availability of suitable geological storage sites. CCU had 10 to 25 times higher energy consumption than the other two routes, whilst the biological routes suffer from massive land requirements of around 40 and 400 times higher than the CCU and CCS routes respectively.

Agriculture, forestry and other land use (AFOLU) were used in the models as a means to reduce CO_2 emission with good land and livestock management (Smith et al., 2014). Three out of four scenarios included bioenergy with carbon capture and storage (BECCS) because it is considered a negative emission technology, in which the CO_2 is absorbed by plants, stored as biomass, with the CO_2 released during biomass conversion to biofuels captured and stored in geological sites (Minx et al., 2018). The scenarios considered the median CO_2 removal by BECCS (Figure 2.1) to be 12 $GtCO_2\,yr^{-1}$; equivalent to one quarter of current emissions (Rogelj et al., 2018). Apart from the P4 scenario, others considered no or limited overshoot of CO_2 emissions (such as from continued global population growth and the emissions problems

therein). Hence, the P4 scenario was deemed the best practical option to maintain temperature rises below 1.5 °C.
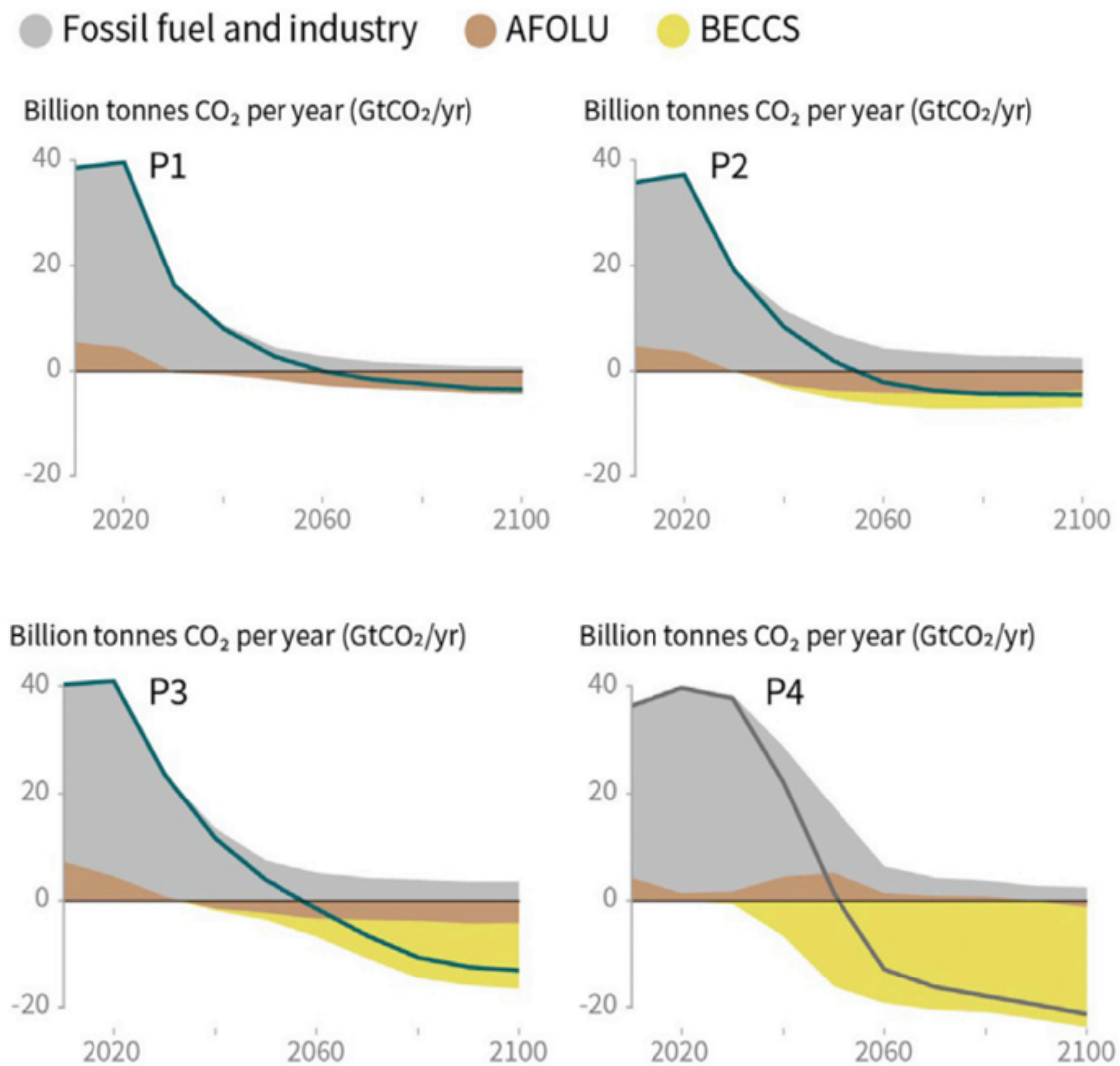
Figure 2.1 A breakdown of contributions to global net CO_2 emissions in four mitigation scenarios to limit mean global temperature rise to 1.5 ℃. P1: AFOLU is the only CO_2 removal option and relies on innovations with lower energy demand, P2: Society shifts towards sustainability with healthy lifestyles, low-carbon technologies, and limited BECCS. P3: Society and technology follows the same historical patterns with small reductions in energy demand and greater BECCS contribution than P2 scenario. P4: Intensive use of energy and resources with high energy demand and livestock production, with major emissions removal through BECCS (Rogelj et al., 2018).

2.2 Carbon capture technologies

2.2.1 Overview of carbon capture -storage (CCS) and -utilisation (CCU)

Carbon capture systems can be integrated in three main steps: 1) separating and capturing CO_2, 2) compressing and transporting the CO_2 gas, and 3) storing the CO_2 in sequestration sites or utilising the captured CO_2 for chemical products or energy supply. There are various capture processes, which can be divided into three main categories; post-combustion, pre-combustion and oxy-fuel combustion (Table 2.1).

Table 2.1 Categories of carbon capture technologies with their advantages and disadvantages (Leung et al., 2014, Hetti et al., 2020).

Capture category	Description	Advantages	Disadvantages
Post-combustion	Removes CO_2 after combustion of fuel from flue gases	- Can be easily retrofitted into existing industrial infrastructure - Most developed technology minimising risk	- High implementation cost and energy consumption - Low CO_2 concentration in flue gases can affect capture efficiency - Location specific
Pre-combustion	Removes CO_2 from fuel by reacting with oxygen or steam to obtain H_2 and CO_2	Can obtain high concentration of CO_2 in the output stream	- Difficult to implement in existing power plants - Complex processes and lack of operational experience
Oxy-fuel	Combust fuel with pure oxygen instead of air	Can achieve very high purity of CO_2	- Requires expensive air separation unit - Has high efficiency drop and energy penalty

Post-combustion technology is typically only implemented with flue gases and is able to capture high CO_2 concentrations for various applications e.g. enhanced oil recovery (Raza et al., 2019). Current post-combustion systems include chemical absorption, adsorption, cryogenic distillation, and membrane separation. Pre-combustion systems recover CO_2 by reacting with oxygen or steam to obtain highly concentrated CO_2 and H_2. The CO_2 is separated

and stored while the H_2 is normally used in other industries. For oxy-fuel combustion, CO_2 and H_2O are the products of fuel combustion with pure oxygen supplied via cryogenic or membrane routes instead of air, in which water is separated by condensation (Pires et al., 2011). Other than those categories, direct air capture (DAC) is considered a negative emissions technologies (NET) focusing on sequestration of atmospheric CO_2. DAC technologies have recently been developed to commercial scales, e.g. Climeworks and Carbon Engineering (Table 2.2). However, all current DAC systems rely on toxic amine-based chemicals and are required tremendous amount of energy (Pritchard et al., 2015).

Despite various technology developments, CCS remains an expensive operation (Salvi and Jindal, 2019). BECCS, another NET, has value added benefits of job creation and being a potentially sustainable alternative to the fossil energy sector (Minx et al., 2018); however, BECCS can pose environmental threats to biodiversity, soil quality, and may compete with agricultural land use (Fajardy et al., 2019).

The final destination of the captured CO_2 can be divided into two main routes, carbon capture and storage (CCS) and carbon capture and utilisation (CCU). CCS is deemed to have the higher contribution for net negative emissions whereas CCU provides economic benefits by reusing the CO_2 in industrial processes (Baena-Moreno et al., 2018). Gabrielli et al. (2020) compared CCS, CCU and an additional biological route (farming biomass for chemicals production). All routes are technically feasible but with different benefits and drawbacks. The application of CCS mainly depends on the availability of suitable geological storage sites. CCU had 10 to 25 times higher energy consumption than the other two routes, whilst the biological route suffers from massive land requirement of around 40 and 400 times higher than the CCU and CCS routes respectively.

2.2.2 Chemical absorption-stripping process

Chemical absorption is the most advanced technology for CO_2 removal from flue gases. It has been widely used for more than 60 years for CO_2 and H_2S removals from natural gas, and recent decades for post-combustion capture (Dutcher et al., 2015), involving absorption and stripping systems using solvents. A typical chemical absorption-stripping process designed for a power plant (Figure 2.2) begins with a stream of flue gas which is passed through a column packed with an aqueous amine-based solution to absorb CO_2. Once the amine solution is saturated, it is transferred into a stripper to be reversed into a reusable solution by heating to 100–120 °C,

normally using waste steam from the power plant (Wang et al., 2011). The released CO_2 is compressed and transported for either sequestration or utilisation.
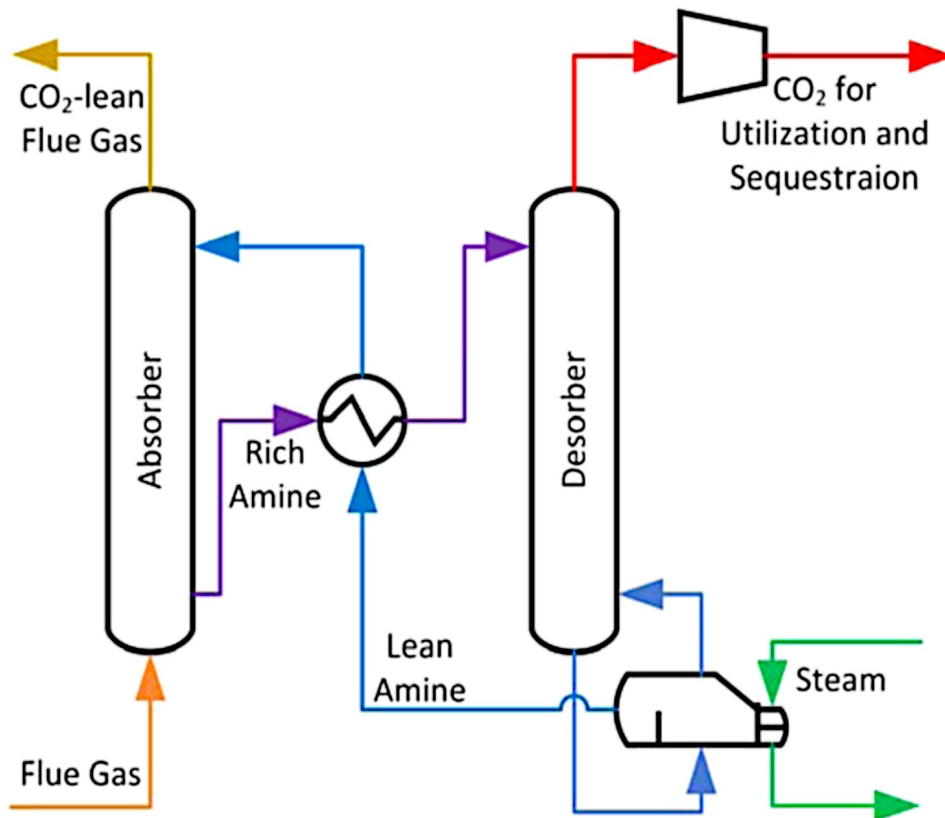
Figure 2.2 A process diagram of a chemical absorption-stripping unit. The CO_2 absorber is typically an amine-based solution, a desorber separates the captured CO_2 from the rich amine-based solution and passes the lean amine-based solution to a cooler before returning it to the absorber (Dutcher et al., 2015).

Monoethanolamine (MEA) is the commonly used as benchmark solvent because of its high CO_2 absorption rate, delivering up to 90% CO_2 removal (Dutcher et al., 2015). However, MEA is environmentally toxic and its thermal and oxidative degradation leads to corrosion in the operating equipment, causing the process to be inefficient and hazardous (Saeed et al., 2018). Many alternatives have been explored such as piperazine (PZ) with 90 to 99.1% CO_2 removal (Gao et al., 2019), and various amine-blend solvents (Saeed et al., 2018, Chen and Lin, 2018). Various process optimisations and intensifications including types of packing (Pascu et al., 2015), rotating packed bed absorbers (Lee et al., 2017, Jassim et al., 2007) and solvent modelling (Mazari et al., 2020) can improve process efficiency. There is a recent interest in using solid rather than aqueous amines to lower the energy requirement (Dutcher et al., 2015).

2.2.3 Adsorption

Adsorption is a cheaper alternative to absorption-based CO_2 capture because of the reduced CO_2 separation cost, lower regeneration energy and minimised pressure losses (Jiang et al., 2019). Examples of post-combustion adsorption-based technologies include pressure swing-, vacuum swing-, temperature swing- and electric temperature swing adsorption. Solid adsorbent can be classified into two types: 1) chemical (chemisorption) – amine-based adsorbents, and 2) physical (physisorption) – carbons, zeolites and metal-organic materials (Sayari et al., 2011). The former separates CO_2 by selective reaction with surface bound amine groups, while the latter exploits non-bonding interactions (Chaffee et al., 2007). Although, adsorption is considered a better option than absorption, there are many disadvantages including low selectivity of CO_2 when adsorbing flue gases with low CO_2 concentration, a lack of development in oxidative stability of porous adsorbent materials, and lowered CO_2 capture efficiency due to water in flue gases (Siegelman et al., 2019).

2.2.4 Chemical looping

Chemical looping involves reduction through multiple sub-reactions and regeneration of a solid carrier (also called looping material) performed in spatially separated reactors (Galvita et al., 2013). These reactors can be divided into air and fuel reactors. Firstly, metal oxide (M_xO_y) is normally used as the looping material to react with fossil fuels to capture a concentrated CO_2 stream produced at the outlet of the process. Later, once the carrier is depleted, it is regenerated by re-oxidation with air, steam or CO_2 (Nandy et al., 2016). The main advantage of chemical looping is that air and fuel are not mixed, resulting in the products of fuel conversion never being diluted with N_2 (Mendiara et al., 2018), which eliminates the need for a further separation unit. However, there are many challenges for implementing the technology due to complex process engineering designs with complicated interactions between solids and gases, handling material stability and optimising reactor configurations (Veser and Müller, 2016).

2.2.5 Cryogenics

The cryogenic approach for CO_2 removal is based on different gas condensation and de-sublimation properties to separate CO_2 from flue gases, extracting CO_2 of a purity over 99.99% (Brunetti et al., 2010). The recovered CO_2 can be used for chemical products including fertilisers or food. With cryogenic CO_2 capture the use of chemical solvents and physical sorbents is eliminated (Keshavarz et al., 2019). Examples include cryogenic distillation (Holmes and Ryan, 1982), cryogenic packed bed (Tuinier et al., 2011b), Stirling cooler strategy (Song et al., 2012), and the CryoCell system (Hart and Gnanendran, 2009). Nevertheless,

electricity consumption is a concern when using refrigerating supply (chills to –140 °C) (Tuinier et al., 2011a), although it is possible to reduce the energy requirement by supplying a low-cost cold energy source such as liquefied natural gas, see Song et al. (2019a). Impurities from flue gases (e.g. sulfur oxides, nitrogen oxides, and mercury) can decrease the overall process efficiency if heat exchanger designs are not properly implemented (Tan et al., 2017).

2.2.6 Membrane-based system

Membranes operate like a filter, with performance dependent on their permeability and selectivity to certain molecules (Ji and Zhao, 2017). Membrane-based technologies can be applied to post- and pre-combustion CO_2 capture pathways. Two main options are membrane gas separation (MGS) and membrane contractor (MC) (Figure 2.3). The former is based on the mechanism of selective surface diffusion or ion-conducting membranes to diffuse across a dense membrane matrix into the permeate side for desorption (Wang et al., 2013), while the latter uses a highly hydrophobic microporous membrane for promoting mass transfer, with the CO_2 selectivity dominated by the solvent (Purwasasmita et al., 2015). MGS systems are commonly used for CO_2/CH_4 separation from natural gas (Siagian et al., 2019). Both systems have drawbacks that affect their durability and long-term performance. The polymeric membrane used for MGS has to deal with plasticisation (Sanders et al., 2013), there is a trade-off between permeability and selectivity (Robeson, 2008), and physical aging (Sanders et al., 2013). MC membranes face different challenges including wetting phenomena, fouling and membrane-solvent compatibility (Luis et al., 2012).
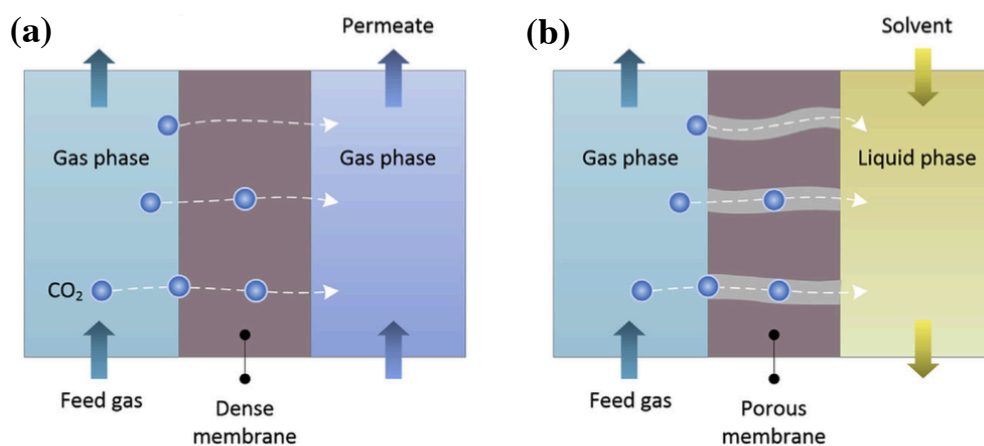
Figure 2.3 Schematics of (a) membrane gas separation (MGS) and (b) membrane contractor (MC). MGS uses a dense membrane that utilises selective surface diffusion with the gas phase on the other side, while MC uses porous membranes with liquid solvent on the other side that has high CO_2 selectivity (Siagian et al., 2019).

2.2.7 Direct Air Capture (DAC)

Direct air capture (DAC) can be categorised into two approaches: 1) absorption – CO_2 dissolves into a sorbent, and 2) adsorption – CO_2 adheres to the sorbent's surface (Sanz-Perez et al., 2016). Once captured, the sorbents are treated and CO_2 molecules are released for sequestration or utilisation. For DAC using absorption (Figure 2.4), the most common liquid absorbents are potassium or sodium hydroxide (strong base) that allow CO_2 molecules to chemically react to form a carbonate solution. The carbonate solution is then combined with a calcium hydroxide ($Ca(OH)_2$) solution in a precipitator to obtain solid calcium carbonate ($CaCO_3$) as a precipitate. While the base solution is being regenerated, $CaCO_3$ is transferred, dried and reacted with oxygen in a calcination process at temperatures above 700 °C (Lackner et al., 1999), forming pure CO_2 and calcium oxide (CaO), with the CO_2 being captured and the CaO converted back into $Ca(OH)_2$ via hydration.
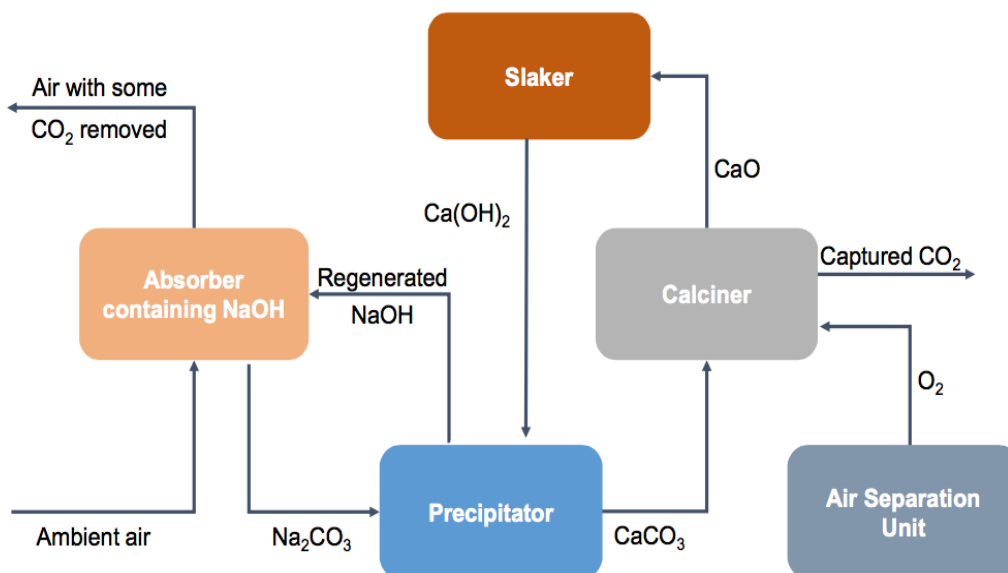
Figure 2.4 A flow diagram of DAC processes starting with an absorber unit to pull the ambient air into the unit. Once NaOH has reacted with CO_2, N_2CO_3 is formed and delivered to a precipitator unit to generate $CaCO_3$. The $CaCO_3$ is transferred to a calciner to react with O_2, and CO_2 is captured. The by product CaO is typically recycled back into a slaker unit for hydration and re-used in the precipitator (Gambhir and Tavoni, 2019).

For adsorption-based methods, solid sorbents (normally amine-based supports) are used to adsorb atmospheric CO_2. Examples of adsorption-based DAC processes are steam stripping (Li et al., 2010), temperature-vacuum swing (Wurzbacher et al., 2012), and moisture swing (Lackner, 2009). At present, Carbon Engineering (Canada), Climeworks (Switzerland), Global

Thermostat (USA), Infinitree LLC (USA), Skytree or Giaura (The Netherlands), and Oy Hydrocell Ltd. (Finland) are companies involved in developing DAC systems (Table 2.2).

Table 2.2 List of companies with commercial DAC technologies (E. Bajamundi et al., 2019).

Company	Location	Sorbent	CO_2 capture rate	Website
Carbon Engineering	Squamish, BC, Canada	Aqueous potassium hydroxide (KOH)	500,000 metric tons per year	https://carboneng ineering.com/
Climeworks	Zürich, Switzerland	Nanofibrillated cellulose grafted with aminosilane	50 tons per year per machine (6 CO_2 filters)	https://www.clim eworks.com/
Global Thermostat	New York, NY, USA	Carbon cubes coated with amine	20 – 500 tons per year per m^2	https://globalther mostat.com/
Infinitree LLC	New York, NY, USA	Ion exchange sorbent	N/A	http://www.infini treellc.com/
Skytree or Giaura	Amsterdam, The Netherlands	Sorbent used in spacecraft	N/A	https://www.skyt ree.eu/
Oy Hydrocell Ltd	Järvenpää, Finland	Amine based sorbent	3800 g CO_2 d^{-1}	https://hydrocell.f i/en/

One advantage of DAC is the process can address distributed emissions sources unlike conventional amine-based scrubber systems which are location-specific (Gambhir and Tavoni, 2019). However, thermodynamically, the minimum average energy requirement for DAC is three times higher than conventional CO_2 capture from flue gases (Pritchard et al., 2015). This is due to the driving force of sorption rate in DAC being 300 times lower than for flue gas absorbers, resulting in increased minimum work (House et al., 2011). The ecological impact of chemicals is another concern as the chemicals used in the DAC process are highly corrosive and the sodium or potassium hydroxide sorbent would need to be produced as a by-product from chlorine synthesis (Gambhir and Tavoni, 2019), thereby increasing toxic chlorine gas production (Realmonte et al., 2019).

2.2.8 Bioenergy with Carbon Capture and Storage (BECCS)

BECCS is considered to be a promising negative emissions technology (NET) because the total amount of atmospheric CO_2 absorbed via biological means and CO_2 captured during biomass to energy conversion is more than the amount of CO_2 released from energy use during the conversion (Figure 2.5). BECCS can be a good transition for existing coal-fired power plants, preventing job losses and providing economic support without government subsides (Cabral et al., 2019), as well as promoting job creation (Minx et al., 2018). BECCS is also likely to be more socially acceptable because of its green and sustainable public perception compared to fossil fuel CCS (Kemper, 2015). Fuss et al. (2018) compared the effectiveness of other biological NETs that utilise photosynthesis against BECCS, including afforestation/reforestation, soil carbon sequestration, biochar, and ocean fertilization, determining that BECCS was the best option with a carbon removal potential of 0.5–5 $GtCO_2$ yr^{-1} with CO_2 removal costs of 100–200 US\$ $t^{-1}CO_2$. However, the cost CO_2 capture for BECCS depends on the route taken for bioenergy, either as bioelectricity or biofuel (Rogelj et al., 2015).
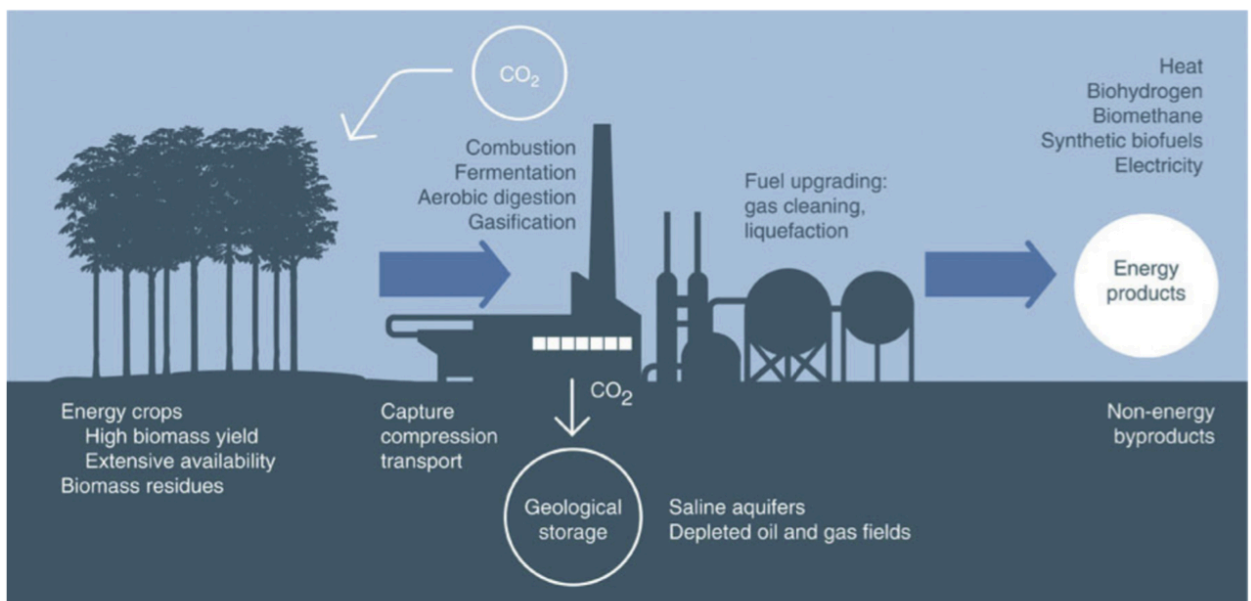
Figure 2.5 BECCS process diagram from plantation, to fixation of atmospheric CO_2 with high biomass yield, to conversion of energy products. After harvest, biomass is transported for conversion through combustion, fermentation, gasification, or anerobic digestion. During conversion, the released CO_2 is captured and stored. The energy products can be heat, biofuels, or electricity (Kemper, 2015).

BECCS is limited by environmental challenges such as massive land use, intensive water consumption, and loss of biodiversity and soil health (Fajardy et al., 2019). In addition, the net

CO_2 removal have been questioned because of difficulty in predicting CO_2 emissions from growing, processing and transporting the biomass to the power station (Fajardy et al., 2019). To reach the 1.5 °C target, BECCS would consume 0.4 to 1.2 billion hectares of land, i.e. 25 to 80% of the current global cropland (Harper et al., 2018), threatening global food security. With this pressure on land use, a concept of combining microalgae cultivation and BECCS has emerged. Microalgae can provide an alternative to traditional biomass. Microalgae, including cyanobacteria (blue-green algae), are more efficient at biologically sequestrating CO_2 than conventional terrestrial plants (Sayre, 2010). Their advantages over other biomass sources include: 1) high photosynthetic efficiency and growth rates that allow frequent harvests, 2) low quality water such as wastewater can be utilised, 3) land competition with agriculture can be eliminated, and 4) many species have high tolerances to SOx and NOx enabling CO_2 capture from flue gases (Choi et al., 2019). They also possess a versatile ability to convert CO_2 into various valuable products (Suarez Garcia et al., 2018).

2.3 Photosynthesis, microalgae and cyanobacteria

2.3.1 Photosynthesis

Photosynthesis is a biochemical CO_2 fixation process (equation 2.1), which is driven by energy from light (photons), and is responsible on an annual basis for converting approximately 200 billion tonnes of CO_2 into complex organic compounds and generating around 140 billion tonnes of oxygen (as the reaction by-product) (Johnson, 2016). There are two main chemical reactions in photosynthesis: 1) Light dependent reactions - happens in the presence of light, and 2) Light independent (dark) reactions - happens in both the absence and presence of light.

$$\text{Overall photosynthesis reaction: } CO_2 + 2H_2O \rightarrow (CH_2O) + H_2O + O_2 \quad (2.1)$$
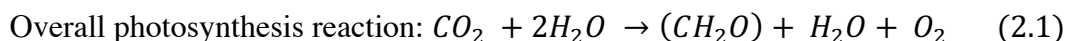
The light dependent reactions take place in the thylakoid membrane (Figure 2.6) to produce nicotinamide adenine dinucleotide phosphate (NADPH) and adenosine triphosphate (ATP) molecules from light-driven electron and proton transfers. The electron transfer starts with water splitting by light. The light is harvested by pigments arranged into two photosystems i.e. Photosystem I (PSI) and II (PSII), which absorb light at optimal wavelengths of 700 and 680 nm respectively. This water splitting reaction releases and accumulates protons creating concentration gradient that drives ATP synthesis.
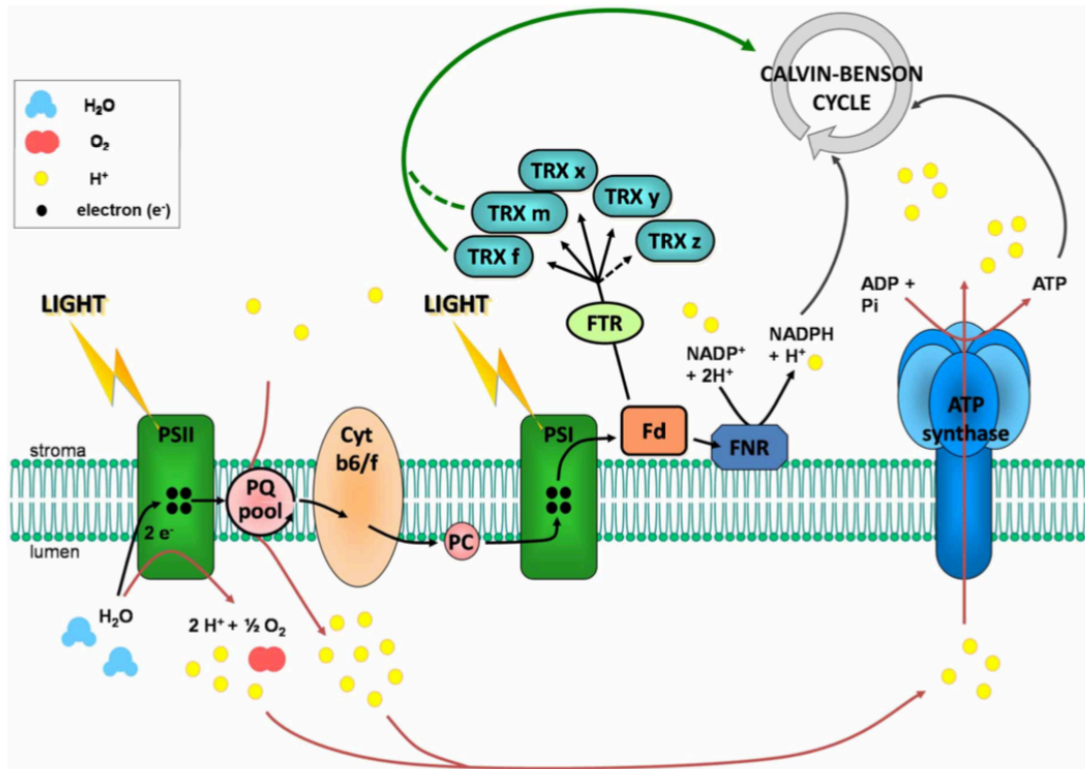
Figure 2.6 Photosynthetic electron transfer chain in the thylakoid membrane (Michelet et al., 2013).

The molecules of ATP and NADPH are used as energy sources for the light independent reactions to fix CO_2 into carbohydrates via the Calvin-Benson-Bassham cycle (Figure 2.7), which occurs in the stroma of the chloroplast (Zhang, 2015). The cycle can be divided into three phases:

1) **Carbon fixation**: The enzyme ribulose-1,5-bisphosphate carboxylase/oxygenase (RuBisCo) catalyses gaseous CO_2 to react with RuBP inside the chloroplast producing six molecules of 3-phosphoglycerate (3PGA) or known as three carbon organic acids (Durall and Lindblad, 2015).

$$3RuBP + 3CO_2 \rightarrow 6\ 3 - phosphoglycerate$$
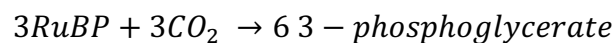
2) **Reduction reaction**: 3PGA reacts with ATP and NADPH to form single 3-carbon molecules (G3P), with one of its six parts removed for storage or use by the plant.

$$6\ 3 - phosphoglycerate + 6\ ATP + 6NADPH \rightarrow 5\ G3P + 1\ G3P$$

3) **Ribulose-1, 5- biphosphate (RuBP) regenerations**: the leftovers of G3P recycle back into the cycle to regenerate more RuBP to drive the carbon fixation stage (Silverstein et al., 2007).

$$5\ G3P + 3ATP \rightarrow 3RuBP$$

Figure 2.7 A schematic of Calvin-Benson-Bassham cycle with eleven enzymes involved including RuBisCo enzyme (Michelet et al., 2013).

It was found that four out of eleven enzymes involved in the cycle appeared to have a low activity in the dark and were activated in the light through thioredoxin-dependent reduction of regulatory disulfide bonds (Michelet et al., 2013). It is also possible to manipulate the cycle to efficiently convert CO_2 into a C2 metabolite acetyl-CoA sugar without net carbon loss, in which the pathway was tested with *Synechococcus elongatus* PCC 7942 (Yu et al., 2018).

2.3.2 CO_2 mass transfer in an algae suspension system

To understand photosynthesis in aquatic and marine environments it is necessary to understand mass transfer or dissolution of CO_2 in water. When water is exposed to atmosphere, CO_2 dissolves by molecule diffusion from gas to liquid phases, in which partial pressure differences is the main driving force (Morse and Mackenzie, 1990). A part of the aqueous CO_2 reacts with H_2O to form a bicarbonate (HCO_3^-) with a hydrogen ion (H^+) or carbonic acid (H_2CO_3). The HCO_3^- and H^+ react forming a carbonate ion (CO_3^{2-}) with $2H^+$. This sequence (equation 2.2) is a reversible hydration process. At equilibrium, the stoichiometric equilibrium constant of CO_3^{2-} is generally the lowest ($\sim\times 10^{-9}$) followed by HCO_3^- ($\sim\times 10^{-6}$) and H_2CO_3 ($\sim\times 10^{-2}$) at 25 °C and

18

1 bar pressure (~1 atm), meaning that CO_3^{2-} is less likely to form in nature compared to other dissolved inorganic carbon (Ci) molecules (Morse and Mackenzie, 1990). HCO_3^- formation is the rate-determining step (Stirling and Papai, 2010).

$$CO_2(gas) \leftrightarrow CO_2(aq.) + H_2O \leftrightarrow H_2CO_3 \leftrightarrow HCO_3^- + H^+ \leftrightarrow CO_3^{2-} + 2H^+ \quad (2.2)$$
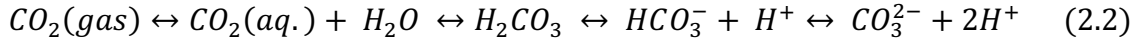
Distribution of dissolved Ci depends on pH, the concentration of aqueous H^+, salinity, and temperature (Morse and Mackenzie, 1990). For instance, under neutral or acidic conditions, H_2CO_3 is directly produced from the dissolved CO_2 and H_2O, but HCO_3^- and CO_3^{2-} are more likely to form if pH exceeds 8 (Stirling and Papai, 2010). The molecular diffusion coefficient of CO_3^{2-} was the lowest ($0.81 \times 10^{-9}\,m^2\,s^{-1}$) compared to the dissolved CO_2 and HCO_3^- ($2.02 \times 10^{-9}\,m^2\,s^{-1}$ and $1.17 \times 10^{-9}\,m^2\,s^{-1}$ respectively) at 25 °C with 1 atm pressure (Zeebe, 2011).

With these low diffusion rates many microalgae and cyanobacteria have developed a CO_2 concentrating mechanism (CCM) involving five modes of Ci transporters to accumulate dissolved Ci. Three modes are HCO_3^- transporters (BCT1, SbtA and BicA) and the other two are CO_2 uptake systems (NDH-1_4 and NDH-1_3) (Kupriyanova et al., 2013). The activation of the CCM depends on the CO_2 concentration (Figure 2.8). For instance, if the cyanobacterium *Synechococcus elongatus* PCC 7942 is exposed to high CO_2 concentration (2% v/v or more), the CCM would be in constitutive mode as there is no Ci transfer limitation (Price et al., 2008). During the constitutive CCM, only one CO_2 uptake system (NDH-1_4) is active with possibly a low level of one HCO_3^- transporter (SbtA). For the fully induced CCM, all five modes activate to gather CO_2 and HCO_3^- into the cells. Accumulation of HCO_3^- within the cell can be as high as 1000-fold with respect to the total external Ci level (Price et al., 1998). Since HCO_3^- is an ionic molecule, HCO_3^- is 1000 times less permeable to lipid membranes than the uncharged CO_2 molecule, which is a preferrable form of Ci for accumulation (Mangan and Brenner, 2014). The permeability of the cell membrane to HCO_3^- and CO_2 were reported as 3×10^{-9} and 0.3 cm s^{-1} respectively. Despite the high permeability of CO_2, the CO_2 uptake systems assist in preventing the CO_2 molecules escape by recapturing and recycling leaked CO_2 (Price and Badger, 1989). For cyanobacteria, once the HCO_3^- molecules transfer into carboxysomes (a subcellular microcompartment), carbonic anhydrase is used as a catalyst to convert HCO_3^- into CO_2 for photosynthesis.
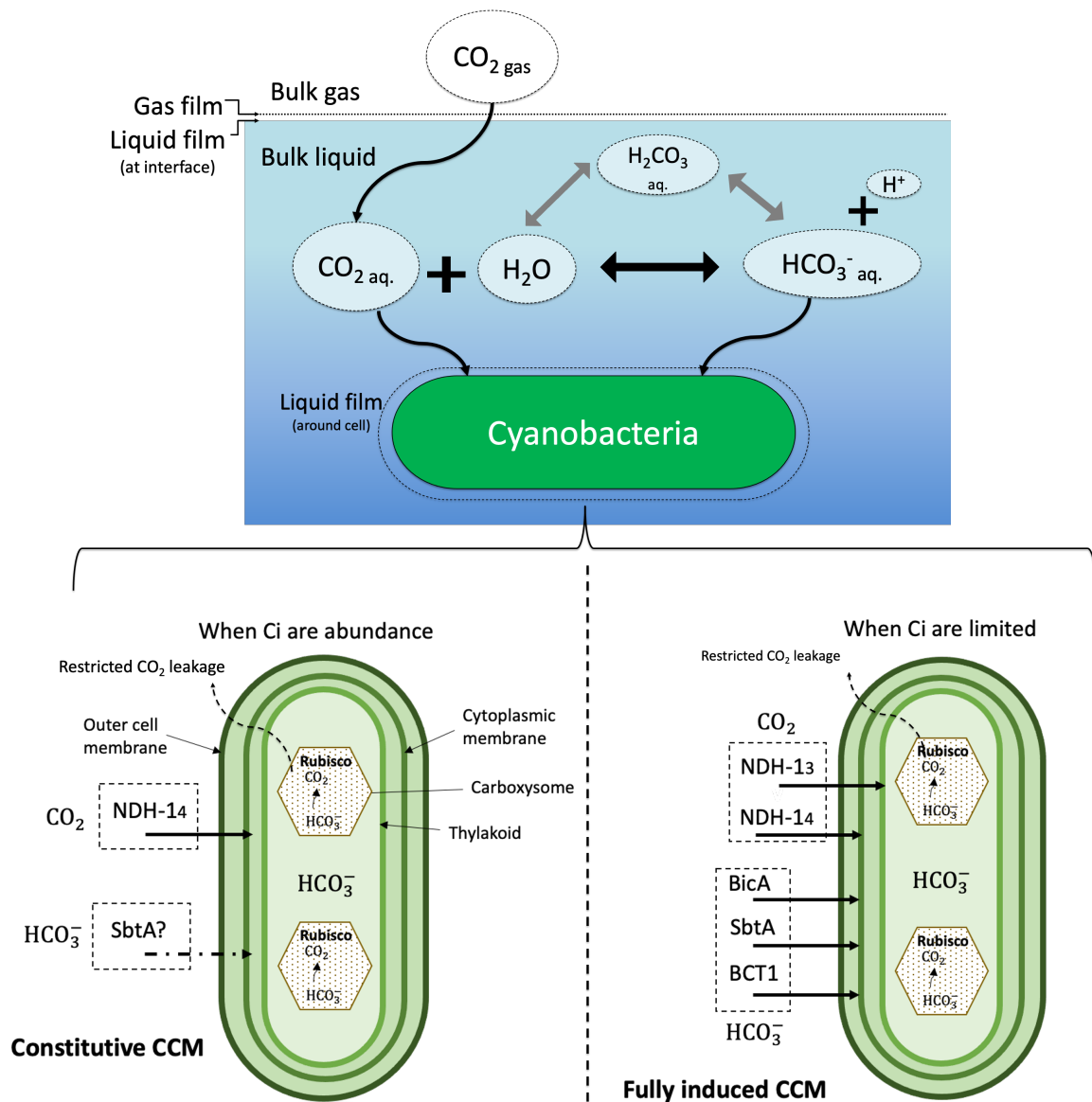
Figure 2.8 A schematic of CO_2 transfer into water, pathways of dissolved Ci formations, and Ci diffusion to cyanobacteria with two CCM scenarios. Constitutive CCM occurs when Ci are in abundance, while fully induced CCM activates during Ci limitation. Adapted from (Price et al., 2008).

2.3.3 Microalgae and cyanobacteria for carbon capture

2.3.3.1 *Microalgae*

Most microalgae and cyanobacteria are ten times more efficient at converting solar energy into biomass than terrestrial plants (Moreira and Pires, 2016). For conventional terrestrial plants, less than 0.5% of the solar energy is converted into plant biomass, whereas microalgae can convert more than 10% (Tsai et al., 2015). Microalgae can duplicate 100 times faster than terrestrial plants resulting in higher biomass productivity (Cheah et al., 2015). For every 1 kg of microalgae biomass production, around 1.83 kg of CO_2 can be fixed (Jiang et al., 2013).

According to Ho et al. (2011), *Botryococcus braunii*, *Chlorella vulgaris*, *Chlorella kessleri*, *Chlorocuccum littorale*, *Scenedesmus sp.*, *Chlamydomonas reinhardtii* and *Spirulina* sp. are commonly used microalgae and cyanobacteria for CO_2 sequestration and BECCS, Figure 2.9, (Choi et al., 2019). Many have particular characteristics including: 1) the ability to assimilate large quantities of CO_2, 2) good tolerance of impurities (SOx and NOx) present in flue gases, 3) having a reasonable high temperature tolerance, and 4) can use various water sources such as saline drainage water, brine, seawater, or industrial wastewater.
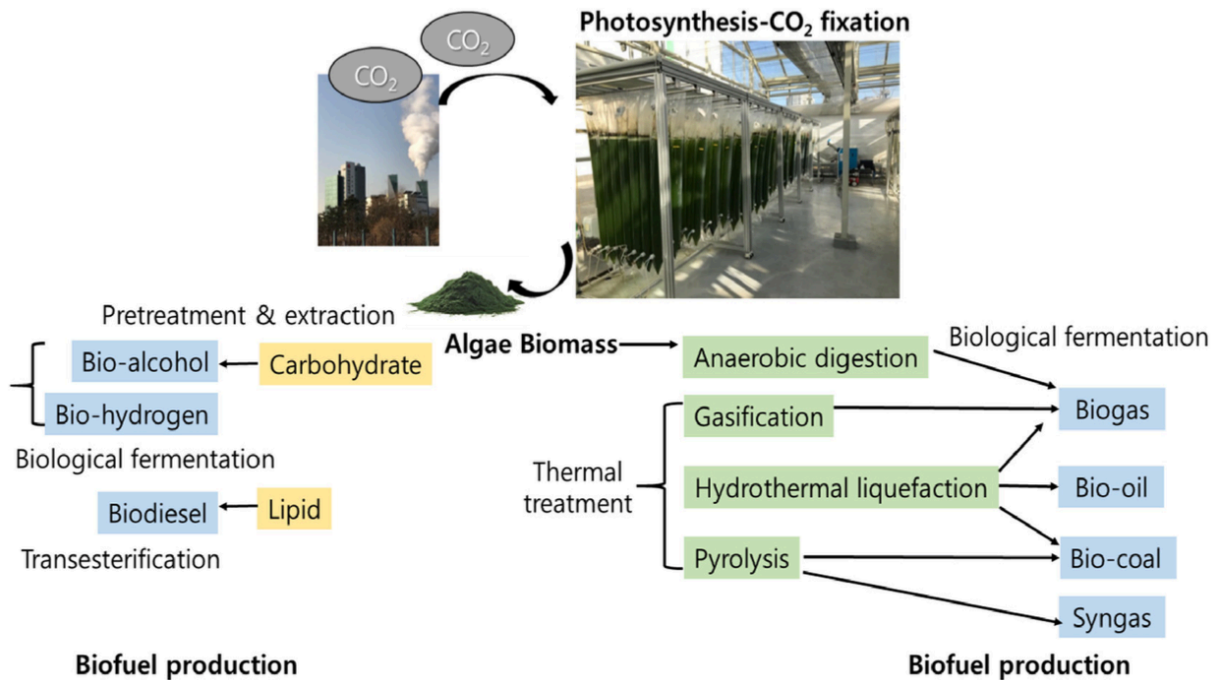
Figure 2.9 Concept of integrating algae with BECCS processes. Algae cultivation can be implemented next to a power plant to absorb CO_2 via photosynthesis. Pre-treatment and extraction of carbohydrate or lipid from the dried biomass can be used to generate biofuels. Another route is to use anerobic digestion or thermal treatment to directly convert the whole algae biomass (Choi et al., 2019).

Salih (2011) reported that efficiency of CO_2 consumption is related to microalgae CO_2 concentration tolerance, and many genera such as *Scenedemus* and *Chlorella* have maximum CO_2 concentration tolerances of up to 60% and 40% respectively. The concentration of CO_2 in flue gas typically range from 15%-20% v/v (Song et al., 2004), which means that many microalgae species can survive and capture carbon from the flue gas. Numerous studies have investigated *Chlorella* species for CO_2 fixation under many CO_2 sources (Table 2.3). Ho et al. (2011) reported that some *Chlorella* species can removed CO_2 at rates of 800–1000 mg per L of suspension culture per day as well as removing SOx, NOx and volatile organic compounds

from flue gases, whereas most microalgae species have CO_2 consumption rates between 200–600 mg per litre of suspension culture per day. Clément-Larosière et al. (2014) investigated the effect of light intensities on *Chlorella vulgaris* with two CO_2 concentrations (2 and 13% v/v) and reported the maximum CO_2 removal rate was 0.98 g CO_2 L^{-1} day^{-1} at 13% v/v CO_2 and light intensity of 180 μmol m^{-2} s^{-1}. Douskova et al. (2009) used *C. vulgaris* for biomass production applying two CO_2 sources, flue gas from a municipal waste incinerator with 10-13% v/v CO_2 and a mixture of pure 11% v/v CO_2 and air. The CO_2 fixation rate was higher when the flue gas was used (4.4 g CO_2 L^{-1} d^{-1}) than the control gas (3.0 g CO_2 L^{-1} d^{-1}).

Table 2.3 *Chlorella* species with biomass yield and their CO_2 fixation rate or removal percentage. Adapted from (Cheah et al., 2015). (PBR = photobioreactor).

Chlorella species	Initial CO_2 (%) (v/v)	CO_2 fixation rate (g L^{-1} d^{-1})	% Removal achieved (v/v)	Biomass yield (g L^{-1})	Cultivation system	References
C. vulgaris	0.03 (Air)	0.06	92.2	~0.315	Sequential bioreactor	(Lam et al., 2012)
C. vulgaris	0.09 (Air)	3.55	96.9	0.9	Membrane-sparged helical tubular bioreactor	(Fan et al., 2008)
C. vulgaris	2	0.43	57.03	2.03	Vertical tubular bioreactor	(Yeh and Chang, 2011)
C. vulgaris	5	0.25	86.7	1.94	Fermenter	(Sydney et al., 2010)
C. vulgaris	5	1.5	35	~0.73	Sequential bioreactor	(Lam et al., 2012)
Chlorella sp.	0.038	0.06	60	0.4	Lab scale PBR	(Ramkrishnan et al., 2014)

Chlorella sp.	0.106	3.55	80	0.7	Lab scale PBR	(Ramkrishnan et al., 2014)
Chlorella sp.	1	6.24	59	0.19	Lab scale flask method	(Ramanan et al., 2010)
Chlorella sp.	5	0.86	27	0.196	Bubble column	(Chiu et al., 2008)
Chlorella sp.	5	0.7	1.5	2.02	Vertical tubular bioreactor	(Ryu et al., 2009)
Chlorella sp.	5	0.2	51	0.28	Lab scale flask method	(Ramanan et al., 2010)
Chlorella sp.	10	0.25	46	2.25	Lab scale flask method	(Ramanan et al., 2010)
Chlorella sp.	10	0.13	63	5.15	Air lift PBR	(Chiu et al., 2009a)
Chlorella sp.	15	0.75	85.6	0.95	Sequential bioreactor	(Cheng et al., 2013)
Chlorella sp.	10	0.89	46	2.25	Open race-way pond	(Ramanan et al., 2010)

Note: All studies used different culture conditions including light source/intensity, temperature, culture volume, starting inoculation concentration, and cultivation time. A fair comparison is not possible unless standard cultivation conditions are performed.

2.3.3.2 Cyanobacteria

Cyanobacteria (a.k.a. blue-green algae) are an ancient phylum of photosynthetic (prokaryote) bacteria. They undergo oxygenic photosynthesis i.e. release oxygen, and are responsible for capturing almost one quarter of the world's CO_2 emissions (Rosgaard et al., 2012). It is believed that they were responsible for the "Great Oxygenation Event" (Ligrone, 2019) circa 2000 – 3500 million years ago that delivered the oxygen rich atmosphere that defines the present Earth's atmosphere. Their sizes can range from 1 to over 30 μm for unicellular and filamentous species respectively (Percival et al., 2004). They are photosynthetic organisms that can easily

survive in the harsh environment with minimal light, CO_2 and water sources. Interestingly, Rosgaard et al. (2012) mentions that cyanobacteria have a number of advantages over algae and plants such as less complex intracellular structures and cell walls, which facilitates CO_2 diffusion across the cells, and some species can also utilise N_2 gas as the sole source of nitrogen, whereas algae and plants cannot unless symbiotic N_2-fixing bacteria are present. Cyanobacteria also contain numerous species that can be categorised into mesophilic or thermophilic species growing at temperature from 13-45 °C and 42-75 °C respectively (Ono and Cuello, 2007). Thermophilic species are more suitable for capturing CO_2 from power-plant flue gas because of their higher temperature tolerance which reduces cooling costs for the flue gas stream.

In nature, cyanobacteria can be found in places with a presence of water including stream sediments, lakes, reservoirs, marine waters, and even in waste discharges and treatment effluents. Typically, cyanobacterial blooms in surface waters happen during summer months, in which densities can easily exceed 500 cells per mL (Percival et al., 2004). In the UK 75% of the blooms consist of toxins leading to a public misconception about their toxicity to humans, whereas only around 25 species can have adverse health effects (Percival et al., 2004). Cyanobacteria can also be vital bio-agents/bio-fertilizer to substitute the application of chemical fertilizers and pesticides to achieve sustainable agriculture (Singh et al., 2016). They can enrich soil quality by producing bioactive compounds for crop growth particularly those that can fix atmospheric N_2 and the fixed nitrogen may be released as ammonia, polypeptides, free amino acids, etc. through secretion or microbial degradation after their death (Subramanian and Sundaram, 1986). It was estimated that around 20-30 kg N ha^{-1} can be provided by cyanobacteria (Issa et al., 2014).

Table 2.4 CO_2 fixation rates of *Synechococcus* species. (PBR = photobioreactor).

Species and strain	CO_2 fixation rates	Cultivation systems	Reference
S. elongatus PCC 7942	450 mg L^{-1} d^{-1} (nitrogen starvation), 350 mg L^{-1} d^{-1} (nitrogen repletion)	Lab scale flat plate PBR	(Choi et al., 2016)
Synechococcus 2973	12.2 mmol $gDCW^{-1}$ h^{-1}	Lab scale PBR	(Abernathy et al., 2017)
Synechococcus 2973	6.7 mmol $gDCW^{-1}$ h^{-1}	Lab scale shaking flask	(Abernathy et al., 2017)
Synechococcus 7942	5.1 mmol $gDCW^{-1}$ h^{-1}	Lab scale PBR	(Abernathy et al., 2017)
S. elongatus	1.26 g L^{-1} d^{-1}	Lab scale conical flask PBR	(Hashemi et al., 2020)
Synechococcus PCC 7942	0.6 g L^{-1} d^{-1}	Lab scale oblong flat flasks	(Kajiwara et al., 1997)
Synechococcus sp. PCC6301	0.43 g L^{-1} d^{-1}	Lab scale stirred tank PBR	(Suh et al., 1998)
Synechococcus sp. PCC6301	0.75 g L^{-1} d^{-1}	Lab scale fluorescence lamp PBR	(Suh et al., 1998)
Synechococcus sp. PCC6301	0.66 g L^{-1} d^{-1}	Lab scale optical fibre PBR	(Suh et al., 1998)
Synechococcus sp. PCC6301	0.92 g L^{-1} d^{-1}	Lab scale fluorescence lamp/ optical fibre PBR	(Suh et al., 1998)

Note: All studies used different culture conditions including light source/intensity, temperature, culture volume, starting inoculation concentration, and cultivation time. A fair comparison is not possible unless standard cultivation conditions are performed.

Synechococcus elongatus is one of the most commonly used cyanobacteria in the research community and may be considered as a model cyanobacterium. It has been extensively studied for genetic engineering for CO_2 fixation enhancement and acclimation to nutrient

stresses for various biochemical products (Schwarz and Forchhammer, 2005, Liang et al., 2018). Most studies have reported performance of this species by its biomass productivity. A number of studies reporting CO_2 fixation rates are shown in Table 2.4. A few studies utilised nitrogen starvation to force the cyanobacteria into producing carbohydrates (Möllers et al., 2014, Aikawa et al., 2014). During nitrogen limitation, the expression of genes relating to CO_2 uptake were up-regulated in *S. elongatus* PCC 7942, resulting in higher CO_2 uptake compared to nitrogen replete conditions (Choi et al., 2016). Recently, *S. elongatus* was tested with a constant simulated flue gases (10% v/v CO_2 concentration) from a power plant and reported a maximum CO_2 fixation rate of 1.26 g L^{-1} d^{-1} with a continuous light supply (Hashemi et al., 2020). Furthermore, two *Synechococcus* strains (PCC 8806 and PCC 8807), were able to calcify CO_2 to an extent to form a $CaCO_3$ precipitate (Lee et al., 2004), which could potentially be a long term carbon store within concrete constructions i.e. biomineralisation. *S. elongatus* PCC 7942 was also reported to produce carbonate precipitates under specific culture conditions (Kamennaya et al., 2012).

2.4 Biochemical products of microalgae and cyanobacteria

There are four primary biochemical components in microalgae; proteins, carbohydrates, nucleic acids and lipids, which vary depending on algae species and can be manipulated under different cultivation conditions. The energy values of lipids, proteins, and carbohydrates are 37.6, 16.7 and 15.7 kJ g^{-1} respectively (Sajjadi et al., 2018). Many biochemicals produced by microalgae and cyanobacteria can be utilised in industrial applications e.g. biofuels, pharmaceutical products, pigments, nutrient food supplements, bio-plastics, etc. (Khanra et al., 2018). Microalgae containing >30% oil by dry weight biomass could surpass the oil yield per area of palm oil by over 10 fold (Deng et al., 2009). Most lipids are stored as triglycerides (TAGs), which are mainly saturated fatty acids and some unsaturated fatty acids. Many studies have tried to increase lipid production by nutrient starvation (particularly nitrogen) and by metabolic engineering. When nitrogen is deficient the carbon from the carbon fixation process is converted into lipids or carbohydrates as the main storage compounds instead of synthesizing protein (Klok et al., 2014). Numerous studies have reported carbohydrate accumulation in microalgae and cyanobacteria under nitrogen starvation ranging from 40 to 74% in dry weight biomass, with most microalgae accumulating carbohydrates as starch and cyanobacteria as glycogen (Depraetere et al., 2015, Dragone et al., 2011, Branyikova et al., 2011, Sassano et al., 2010, Möllers et al., 2014, Philippis et al., 1992). The most abundant storage carbohydrates are glucose, rhamnose, xylose, and mannose.

Microalgae and cyanobacteria can have total protein content varying from 6 to 70% in dry biomass (Becker, 2007). Only a few species, including *Chlorella* sp., *Scenedesmus* sp. and *Arthrospira* sp. (c.f. *Spirulina* sp.) are commercialised for large-scale production (Becker, 2007). *Chlorella* sp. are popular sources of microalgae protein, with content ranging from 51-58% w/w dry weight, including essential amino acids (Bleakley and Hayes, 2017). *Arthrospira*, a genus of filamentous cyanobacteria, has the highest recorded protein content of any whole food; 65% more than dried skimmed milk (36%), soy flour (37%), chicken (24%), fish (24%), beef (22%) and peanuts (26%) (Barka and Blecker, 2016). Numerous natural photosynthetic pigments have been extracted from microalgae and cyanobacteria (e.g. phycobilins, chlorophylls, and carotenoids including β-carotene) and have functional properties with value to humanity, including antioxidant, anti-inflammatory and anticancer properties, and have been shown to benefit eye-health and lower the risk of heart disease. These pigments are recognised as high value products (Novoveská et al., 2019), with a market worth of up to £1 billion (Khanra et al., 2018). Recently, many microalgae species (Arashiro et al., 2020) were investigated to remediate industrial wastewater and produce extractable high value phycobiliproteins, which highlight both the environmental and economic benefits of microalgae. However, many studies have reported pigment degradation during macronutrient depletion (Schwarz and Forchhammer, 2005, Sauer et al., 2001).

2.5   Current algae technologies

There are three main algae cultivation technologies: open (ponds and raceways), closed (PBRs) and biofilm systems. Factors such as cost, CO_2 capture source, desired products and nutrient source all contribute to the selection of the most appropriate cultivation system (Cheah et al., 2015).

2.5.1   Open ponds

Commercial algae ponds for CO_2 absorption have been in development since the 1950s. Open algae pond systems can be separated into two types; natural and artificial. Raceway ponds are the most widely used for commercial cultivation (see Figure 2.10a). Typically, depth ranges between 15-25 cm and a paddle wheel is used for agitation to provide circulation and aid mixing of the nutrient medium. Pond temperature is generally not controlled and the light environment is dependent on the local climate and latitude (Murthy, 2011, Shilton, 2006). In theory, biomass productivity could be more than 40 g m^{-2} d^{-1}, but it is generally reported to be much lower—within the range of 16-19 g m^{-2} d^{-1} due to mass transfer limitation from slow diffusion of dissolved CO_2 into the water medium from the atmosphere (de Godos et al., 2014). In addition,

algae slow their CO_2 uptake rate at night and on cloudy days (Parmar et al., 2011). This would require gas storage facilities to contain CO_2 from flue gases adding extra expense.

A 40,000 L capacity multi-layer bioreactor open pond system sited in open space (Figure 2.9b) was tested for wastewater treatment (Zhou et al., 2014). The structure of the multi-layer bioreactor comprised several tiers of tanks stacked on top of each other with the nutrient medium flowing under gravity and pumped back to the top (Figure 2.10b). It was reported that the biomass productivity ranged from 19 to 23 g m^{-2} d^{-1} (Min et al., 2014) which was higher than conventional open pond systems (Zhou et al., 2014). This arrangement was designed to reduce land consumption, but required artificial light supplementation which would increase costs. Despite being more land use efficient, issues with contamination and water loss remained. Efforts have been made with plastic covers to reduce contamination risk and water evaporation (Razzak et al., 2013). Li et al. (2013) found that a transparent cover over a raceway can potentially increase CO_2 fixation efficiency to 95%. However, additional costs, difficulty in maintenance, and contamination issues will remain (Jiménez et al., 2003).
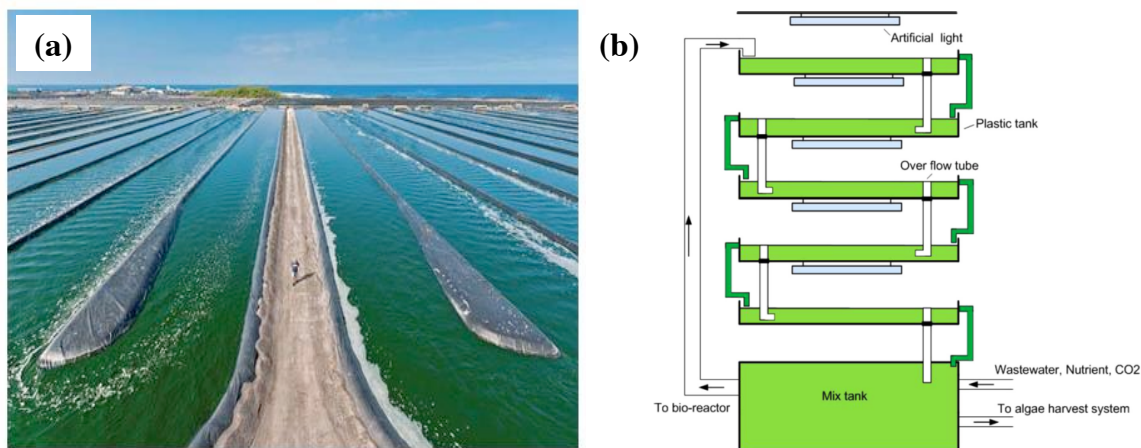
Figure 2.10 (a) raceway algae pond (RoboPlant, 2013) and (b) multi-layer bioreactor (Zhou et al., 2014).

2.5.2 Closed photobioreactors (PBRs)

Enclosed PBRs have been developed to overcome many of the disadvantages of open systems (Klinthong, 2015, Kumar, 2011), and to enhance photosynthesis, mass transfer of CO_2 and O_2, and minimise light shading (Ho et al., 2012). PBR designs include; tubular, airlift, flat panel and bags (Figure 2.11). Some studies report that the potential for CO_2 capture of some PBRs were comparable to amine-based solvent absorption (Keffer and Kleinheinz, 2002, Tola and Pettinau, 2014).
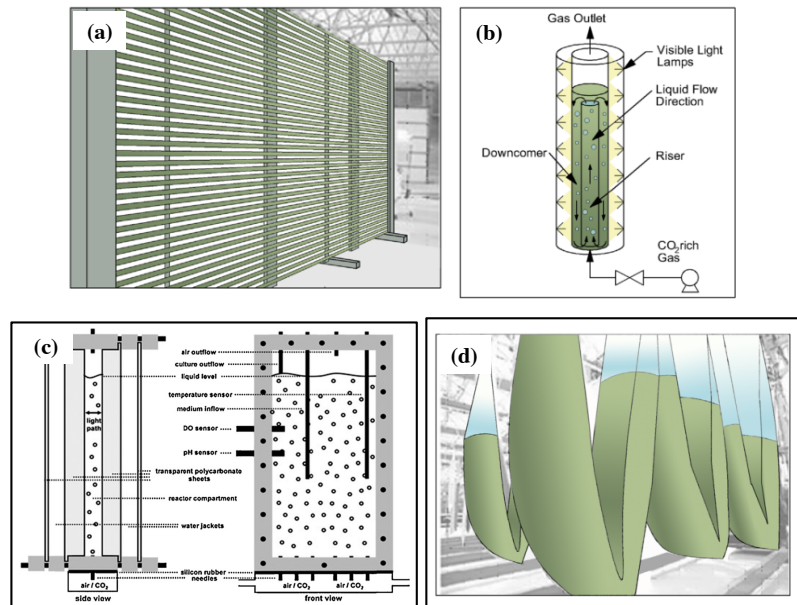
Figure 2.11 PBR designs: a) horizontal tubular, b) bubble column airlift, c) flat panel, and d) large scale plastic bag PBRs. Adapted from (Singh and Sharma, 2012, Razzak et al., 2013).

2.5.2.1 *Tubular photobioreactors*

Tubular PBRs are made of transparent glass or plastic tubes (5-20 cm in diameter). The system is normally connected to a large reservoir and overhead tubes for effective circulation. An airlift device can also be used to enable good exchange of CO_2 and O_2 between the liquid medium and the aeration gas (Xu et al., 2009). Flow rates are typically between 30 and 50 cm s^{-1} to provide sufficient mixing, avoid cell deposition, and ensure adequate distribution of light to individual cells (Razzak et al., 2013). A major issue with tubular PBRs is that a strong CO_2 concentration gradient can develop in long tubes which can starve some cells and affect carbon fixation by creating a pH gradient (Xu et al., 2009).

2.5.2.2 *Airlift bubble column photobioreactors*

An airlift PBR divides fluid volume into two interconnected zones with a baffle or draft tube. The liquid circular motion and micro- macro-bubbles improves gas mass transfer and increases light exposure (Lam et al., 2012). Increasing the aeration rate can effectively distribute CO_2 and prevent O_2 accumulation, but can also affect biological performance of some microalgae due to high shear stress (Xu et al., 2009). An alternative mixing mechanism, such as pneumatical agitation, can achieve a mass transfer coefficient of 0.006 s^{-1} and the lower liquid circulation velocity can lower shear stress (Xu et al., 2009). Gas mass transfer can also be improved with a rubber membrane diffuser or dual spargers (Xu et al., 2009, Eriksen et al., 1998). However, this aeration mode has complex flow patterns which make it difficult to scale up (Razzak et al., 2013). Recently, a split column airlift PBR was developed which helped to overcome the scale

up issue, with biomass productivity reported to be 15-30% higher than conventional bubble column systems (Fernandes et al., 2014). Nevertheless, further scale up and optimisation of flow patterns are still challenging.

2.5.2.3 *Flat plate photobioreactors*

Flat plate PBRs have particularly large surface area to volume ratios, providing sufficient light transmission to support a high biomass yield. The reactors are typically designed to ensure short light paths, and baffles can be installed for aeration (Ho et al., 2011). Gas is introduced via a perforated tube at the bottom of the reactor. Suitable aeration rates are 0.023–1.000 vvm for 5-10% v/v CO_2/air mixture (Zhao and Su, 2014). Flat plate PBRs offer efficient light distribution when implemented vertically (Hu et al., 1996, Pluz et al., 1995). Flat panel PBRs can be scalable to 1000–2000 L, but drawbacks exist such as difficulty in temperature control, growth restriction near the wall region and hydrodynamic stress (Razzak et al., 2013).

2.5.2.4 *Polyethylene bag photobioreactors*

Bag PBRs have low installation costs. Bags can and be hung outside, and air flow is normally introduced from the bottom of the bag and vented at the top to increase mixing and avoid cell settlement (Razzak et al., 2017). Disadvantages of bags include inadequate mixing in some zones and the bag itself is a fragile container with a short operational lifespan (Huang et al., 2017). Zhu et al. (2017) tried to integrate bags with a rocking platform to increase mixing *Euhalothece sp*. ZM001 cultivation, but the mass transfer coefficient was highly variable, ranging from 0.57 to 33.49 h^{-1}, and it could be difficult to obtain consistent process control as well as increase the total installation cost. Bag systems retain the advantages of closed systems, whilst being cheap, and do not have a high-energy consumption (Cheah et al., 2015).

2.5.2.5 *Membrane photobioreactors*

Membrane PBRs are modified versions of air lift or tubular PBRs, with the integration of a membrane to overcome mass transfer limitation. The membrane generates fine bubbles that facilitate CO_2 dissolving in the medium Lam et al. (2012). A good membrane PBR should have good CO_2 distribution, limit oxygen accumulation, be mechanically robust, and have high resistance to corrosion and fouling. However, fine bubbles can resulted in cloudy conditions inside the reactor hindering light penetration. Lam et al. (2012) suggested separating light and gas supply systems into distinct components, but this would increase capital cost and be difficult to scale.

2.6 Microalgae biofilm formation

Microalgal biofilms can consist of a single microalga species or a mixture of algae with other organisms such as bacteria, fungi or cyanobacteria – these are commonly known as biofouling biofilms (Wang et al., 2017). The monospecific biofilms are more appropriate for targeted product synthesis whereas the biofouling biofilms are more suitable for wastewater bioremediation due to the combination of autotrophic and heterotrophic metabolisms (Mantzorou and Ververidis, 2019). Figure 2.12 shows a formation biofilm with microalgae and other microorganisms.

Biofilm formation can be initiated by cells producing extracellular polymeric substances (EPS) to assist attachment onto surfaces and form a stable matrix (Figure 2.12). The main components of EPS include polysaccharides, proteins (both enzymes and structural), nucleic acids (DNA) and lipids, with each having different functionalities (Xiao and Zheng, 2016).
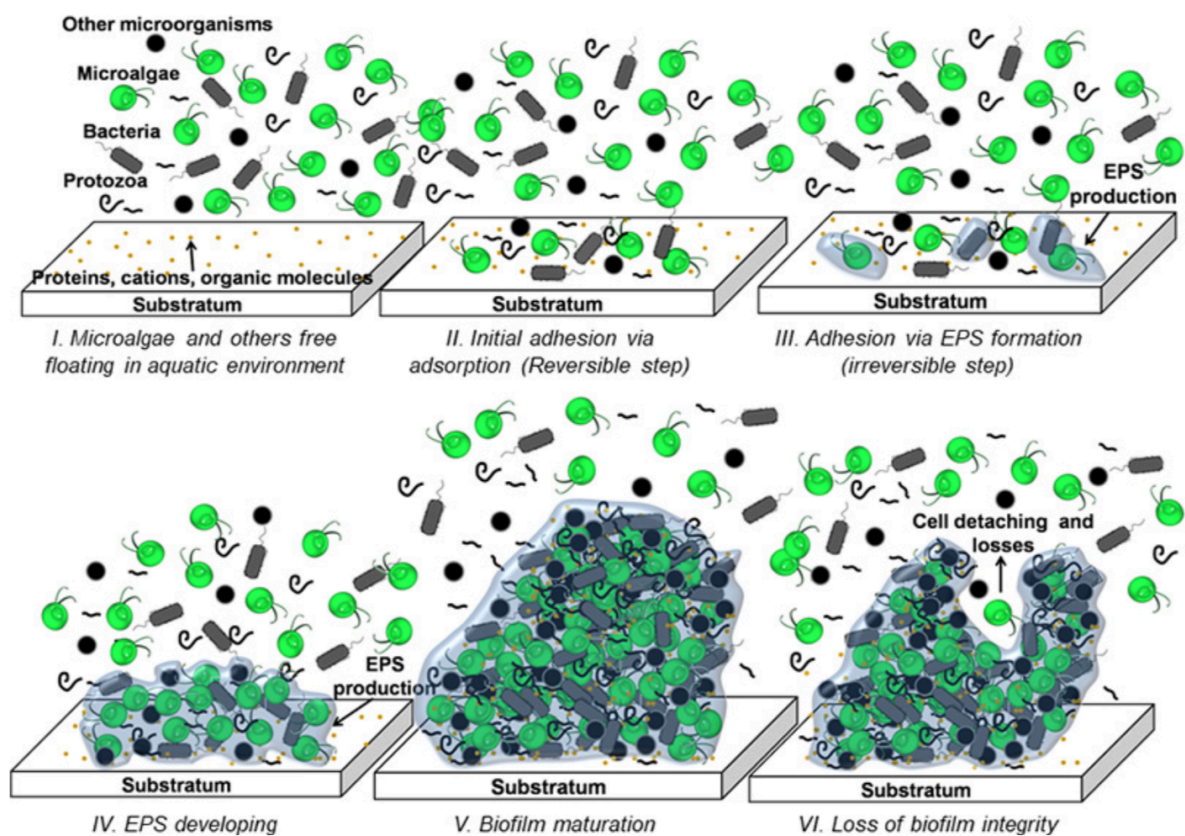
Figure 2.12 Formation of a biofilm consisted of microalgae and other microorganisms on a substrate. The first two stages are reversible before extracellular polymeric substances (EPS) formation. The biofilm losses its integrity in the final stage and eventually cell detachment occurs (Mantzorou and Ververidis, 2019).

2.7 Microalgae biofilm-based photobioreactors

Biofilm-based (or attached cultivation) PBRs have been developed to combat the drawbacks of both open and closed PBRs by ultimately moving away from suspension cultures, with improved light distribution and gas mass transfer (Mantzorou and Ververidis, 2019). Most biofilm systems have been developed for wastewater treatment. Biofilm-based photobioreactors can be divided into three types (Figure 2.13): 1) permanently immersed biofilms – always submerged in liquid medium, 2) biofilms between two phases – continuously alternate between gaseous and liquid phases, and 3) permeated biofilms – liquid medium is provided through the substrate material/substratum (Berner et al., 2014)
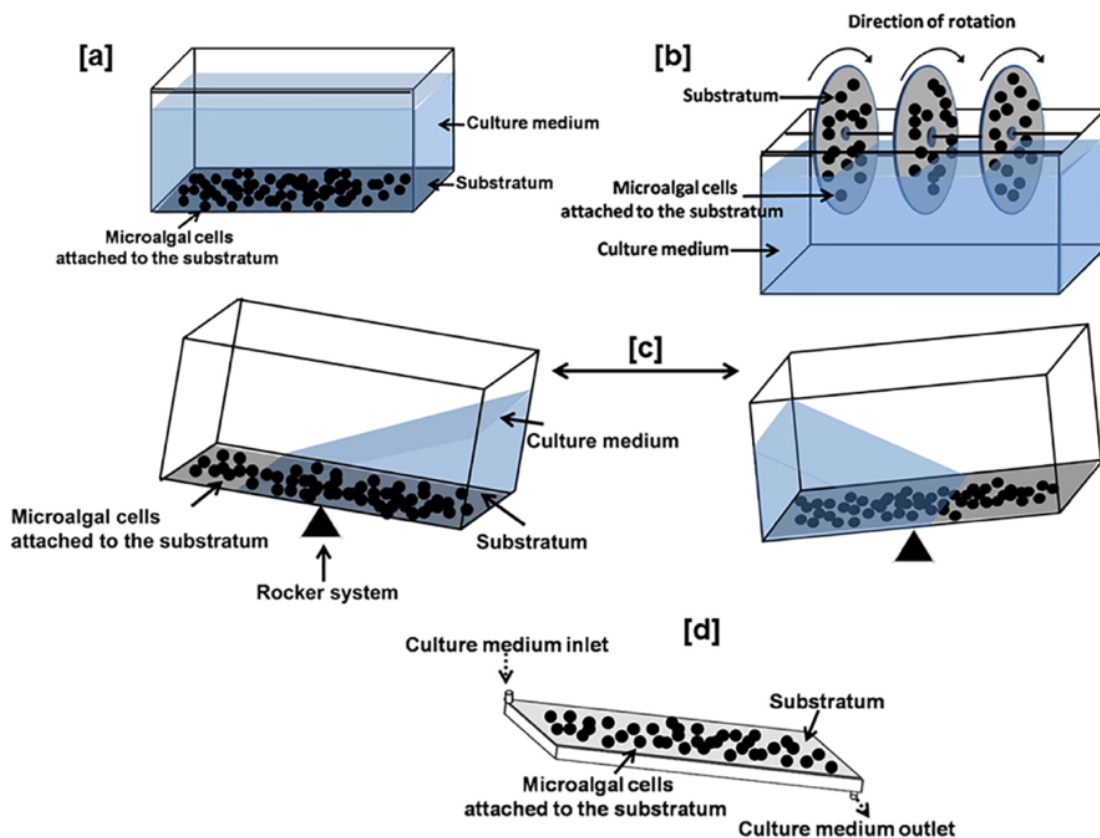
Figure 2.13 Simplified process diagrams to illustrate (a) permanently immersed biofilms; (b) and (c) biofilms between two phases; and (d) permeated biofilms (Mantzorou and Ververidis, 2019).

Advantages and disadvantages of each system type are listed in Table 2.5. Although biofilm PBRs seem to eliminate many disadvantages of open and closed systems, the biofilm are still prone to biological contamination, particularly those with pure cultures. They also suffer from biomass detachment which causes sedimentation issues and may pollute the aquatic environment (Mantzorou and Ververidis, 2019). Surface erosion and fouling of supporting materials are other drawbacks (Mantzorou and Ververidis, 2019). There is emerging interest in

immobilising microalgae and cyanobacteria to overcome drawbacks inherent with biofilm systems.

Table 2.5 Advantages and disadvantages of open, closed and biofilm systems (Singh and Sharma, 2012, Mantzorou and Ververidis, 2019).

Systems	Advantages	Disadvantages
Open	- Easy to build - Low capital cost - Can use natural light source	- High contamination risk - High operation cost - Requires large land areas - Lower biomass productivity than closed systems - Inconsistent light source - High water requirement - Difficult biomass harvesting - Insufficient mixing
Closed	- Better control of pH, temperature, light and CO_2 concentration - Prevent contamination and allow axenic algal cultivation - Less CO_2 and water losses - Higher biomass productivities than open systems are possible - Can produce high purity products	- Complex bioreactor designs - Difficult biomass harvesting including dewatering stage (energy intensive) - Still use substantial amounts of water - High operation cost because of intensive energy requirement - Potential hydrodynamic stress on culture
Biofilms	- Require less water consumption than suspension cultures - Small land use - Easy biomass harvesting as dewatering stage can be excluded - Better light and mass transfers compared to suspension cultures	- Corrosion or erosion on supporting materials - Still prone to contamination - Potential biomass loss from cell detachment

2.8 Algae biocomposite technologies

2.8.1 Biomimicry from lichen

Over millions of years, mutually beneficial symbiotic relationships have developed between photosynthetic cells (photobionts) and fungi to form composite organisms termed lichens. Photobionts are either algae and/or cyanobacteria living underneath a thin layer of fungi (cortex) (Figure 2.14).
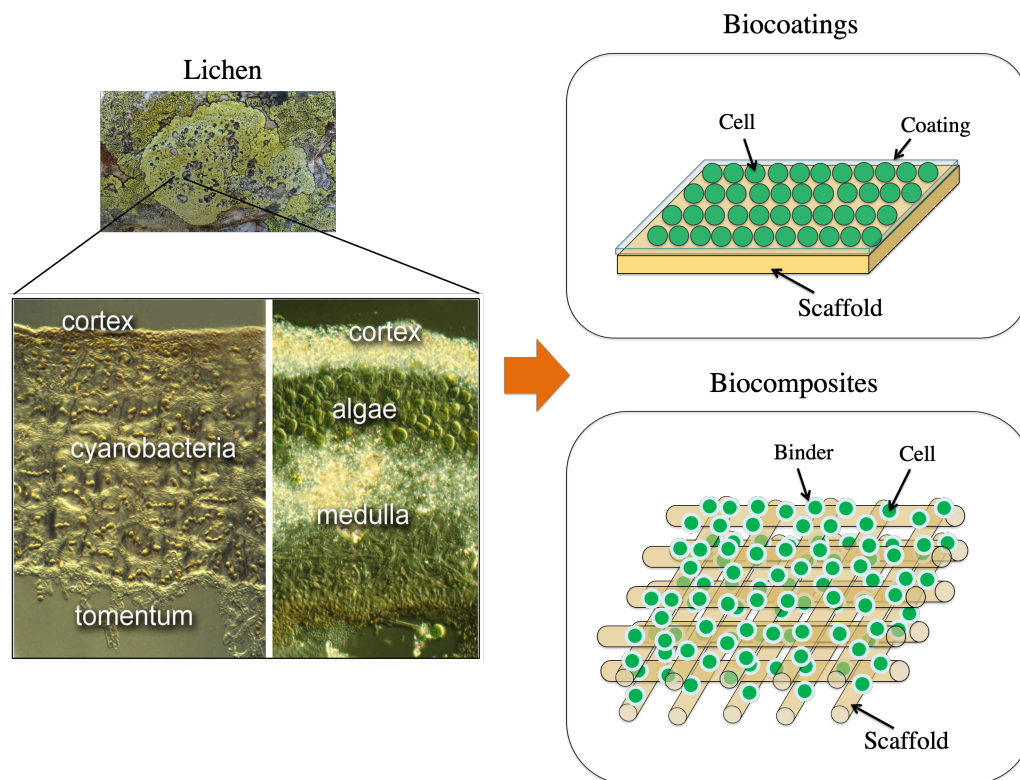
Figure 2.14 Structure of biocoatings (2D) and biocomposites (3D) comprising living cells, coating/binder, and scaffold - inspired by the structure of lichen. Modified from (Bungartz et al., 2002).

The cortex protects the photobionts from the outside environment, while the fungus host benefits from the carbohydrates produced by the embedded photobionts. The fungus does not harm their photobionts but influences their growth and cell turnover rates (Honegger, 2009). Most lichens have the ability to tolerate drought and extreme temperatures, survive under a scarcity of key nutrients and hibernate as a dormancy state (Honegger, 2009). More than 12% of Earth's land mass are lichen covered (Watkinson, 2015). These self-sustained microsystems demonstrate that algae/cyanobacteria can live long lives and operate under minimal quantities of water. There are moves in the research community to mimic the lichen system as a means to intensify current algae-based technologies with a concentrated population of

34

algae/cyanobacteria mixed or embedded with suitable non-toxic adhesive binders and coated onto solid hydrophilic substrates (Figure 2.14). The binders should be able to protect the cells from bacterial contamination and retain the cells on the substrate. Ideally, the substrate needs to be able to transfer nutrients to the cells. This concept is known as biocoating or biocomposite technology.

There have been a number of studies aiming to develop biocoatings and biocomposites with different microorganisms for many applications, including biofuel production, gas and chemical synthesis, environmental remediation, and as biosensors (Berger, 2009, Carballeira et al., 2009, Demain, 2009, Rao et al., 2009). Biocoatings (2-dimensional) and biocomposites (3-dimensional) are processes that utilise cell immobilisation techniques to entrap a concentrated population of microorganisms onto solid supports. They are different from biofilms because the microorganisms are entrapped within the structure and created with an intention of no cell growth. Many have successfully reported that biocoatings and biocomposites can intensify biological performance relative to suspension cultures including CO_2 capture (End and Schöning, 2004, Flickinger et al., 2009, Gosse et al., 2010, Flickinger et al., 2007). To successfully deliver the concept of living algae biocomposites, immobilisation methods, selection of binders, and solid substrates are the key elements that have to be considered.

2.8.2   Immobilisation techniques

Immobilisation of microalgae and cyanobacteria has been studied for bioremediation (Kesaano and Sims, 2014). According to the DOE (1985), immobilisation offers several advantages such as increased culture density, with minimised water and land requirements. There are six different immobilisation types (Mallick, 2002): 1) affinity binding, 2) adsorption, 3) covalent coupling, 4) confinement in a liquid-liquid emulsion, 5) capture behind a semi-permeable membrane, and 6) entrapment within polymers (Figure 2.15). These techniques can be separated into passive and active methods. Passive immobilisation utilises the natural attachment ability of microorganisms to natural or synthetic surfaces (i.e. adsorption), while active immobilisation uses artificial techniques including flocculent agents, chemical attachment, and gel/polymer entrapment (Cohan, 2001, Moreno-Garrido, 2008). Affinity immobilisation is a very mild method and is based on complementary biomolecular interactions which do not involve drastic reactions and no chemical exposure. The method is often used for purification or separation of biomolecule mixtures and a desorption step is required to extract compounds from the immobilised substrate (Magdeldin and Moser, 2012). Adsorption immobilisation is a reversible process involving cells that strongly adhere to the sorbent.

Covalent coupling is a well-known immobilisation technique for enzymes, but not for living cells because cell division can lead to cell leakage from loose bonding (Mallick, 2002). Confinement in liquid-liquid emulsions is an aqueous method in which phase separation occurs from two different water-soluble polymers based on their surface properties and the microorganisms are trapped between the two phases (Mallick, 2002). For semi-permeable membranes, the cells are immobilised onto the membrane and this technique is often used for biosensor fabrication (Mallick, 2002). However, this method causes excessive accumulation of biomass growth on the substrate, which leads to high pressure and damages the membrane (Mallick, 2002). Entrapment and encapsulation in polymers are the most common immobilisation methods, in which the cells are captured in a matrix made from synthetic polymers (e.g. acrylamide, polyurethanes, polyvinyl, polystyrene), proteins (e.g. gelatine, collagen, egg white) or natural polysaccharides (e.g. agars, carrageenan, alginates) (Moreno-Garrido, 2008). These two techniques have been widely used to immobilise many algae species on various polymers for wastewater and biosensor applications.

Affinity binding

Adsorption

Covalent coupling

Confinement in liquid-liquid emulsion

Capture behind semi-permeable membrane

Polymer entrapment
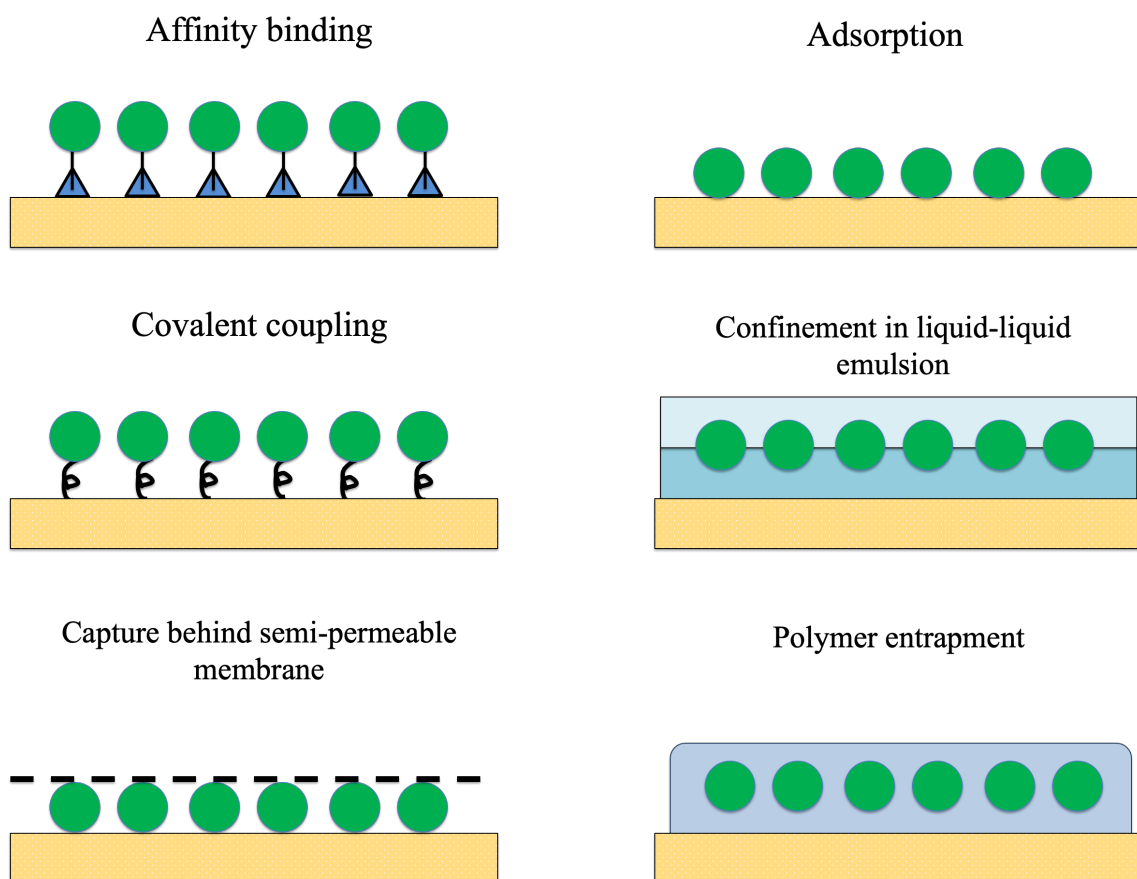
Figure 2.15 Types of immobilisation techniques that are used to immobilise microalgae cells onto a substrate. Adsorption is a passive method, while affinity binding, covalent coupling,

confinement in liquid-liquid emulsion, capture behind semi-permeable membrane, and porous polymer entrapment are active methods.

2.8.3 Effects of immobilisation on microorganisms

A number of studies have found that immobilising microalgae or bacteria can improve cell growth and chlorophyll content. Mallick and Rai (1992) reported that immobilising *Anabaena* and *Chlorella* in alginate over 15 days in growth medium resulted in a higher chlorophyll yield than suspension cultures. Yashveer (2003) also used alginate to investigate photosynthetic activity, lipid and hydrocarbon production of two *Botryococcus* species immobilised in alginate beads. There were significant increases in chlorophyll, carotenoids, dry weight and lipids compared to suspension cultures. Chlorophyll content of immobilised cells was found to be more than that of free cells (Moreno-Garrido, 2008), which may be due to higher light exposure resulting in enhanced pigment synthesis (Hameed A.S.M. and O., 2007). Mallick (2002) reported that immobilised cells have greater oxygen evolution that free cells. It was reported that 90% of chlorophyll content was retained after three months of incubation when cells were immobilised, while free cells showed increased in pheophytinization (molecules that broke down chlorophyll) after one week (Mallick, 2002). Some studies have reported toxicity of some immobilising techniques; for example, Bashan (1986) found a decrease in bacteria populations when immobilised within alginate beads. Also, during immobilisation in polymers, chemical forces and interactions between the matrix and the cell wall can cause significant stresses on both the material and the entrapped microorganisms (de-Bashan and Bashan, 2010).

2.8.4 Latex polymer immobilisation

The first immobilisation of microorganisms (yeast and *E. coli*) using latex polymers was conducted in 1991 (Bunning et al., 1991). The mixture was coated onto an activated carbon particle mesh and calcium carbonate was mixed into the biocoating to generate porosity. Since then, there have been several studies that have attempted to immobilise many microorganisms (mostly bacteria) with various latex polymers onto different solid supports (Flickinger et al., 2017, Flickinger et al., 2007, Cortez et al., 2017).

Immobilisation to a substrate using latex follows a general latex film formation (Winnik, 1997) but with a concentrated population of cells presented within the latex formulation (Figure 2.16). Initially, the aqueous latex formulation is placed onto a desired solid substrate. Over time, the dispersion medium (typically water) evaporates forcing latex particles to be in close contact with each other. Eventually, the latex particles deform and pack around the microorganism if

the drying temperature is more than or equal to the minimum film formation temperature (MFFT). If the drying temperature is below the MFFT the film can take a powdery form with weak mechanical strength (Steward et al., 2000). Lastly, an interdiffusion across particle boundaries occurs to provide mechanical entanglements forming a homogenous film to entrap the cells. This happens when the drying temperature is over a glass transition temperature (Tg) of latex particles, which is closely related to the MFFT. The Tg defines the physical property of the latex polymer coating, which can either be in a rubbery (drying above Tg) or glassy state (drying below Tg) (Ebnesajjad, 2016).
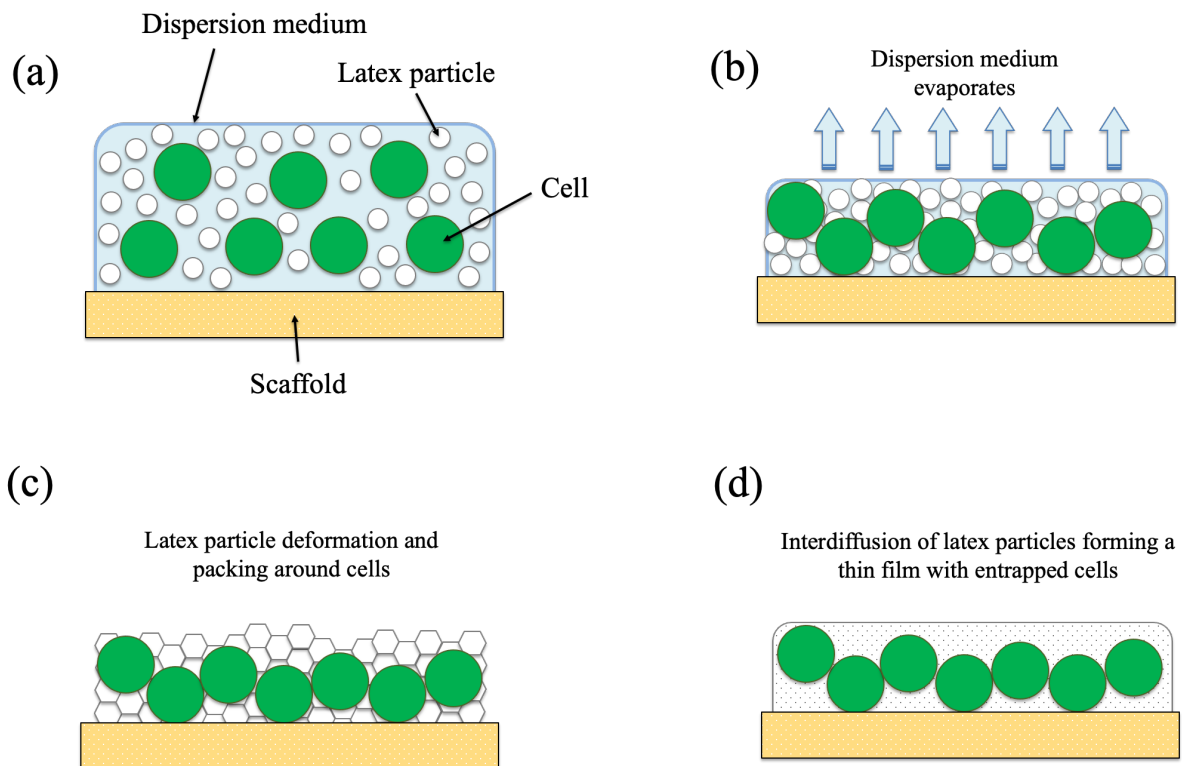
Figure 2.16 Stages of latex cell immobilisation onto a solid scaffold; (a) applying latex formulation with concentrated cell paste onto scaffold; (b) drying of latex formulation, in which evaporation of dispersion medium occurs and latex particles and drawn together; (c) deformation of latex particles around the cells; (d) interdiffusion across particle boundaries to form a homogeneous thin film with cells inside the coatings.

2.8.4.1 Latex immobilisation with photosynthetic microorganisms

Photosynthetic microorganisms have been entrapped using latex polymers. Bernal et al. (2014) immobilised cyanobacteria (*Synechococcus* PCC7002, *Synechocystis* PCC6308, *Synechocystis* PCC6803, and *Anabaena* PCC7120) onto filter paper using acrylate copolymer

latex to produce artificial leaf biocomposites for hydrogen production with a service life of up to 500 h. The specific photosynthetic rate was enhanced by up to 10 times compared to the suspension controls. Martens and Hall (1994) immobilised *Synechococcus* PCC6301 with different latex emulsions on a carbon electrode and reported that the cells maintained nearly 100% of photosynthetic activity upon rehydration. Jenkins (2013) demonstrated that photosynthetic coatings (i.e. artificial leaves) made with *Chlamydomonas reinhardtii* and *Rhodopseudomonas palustris* immobilised with adhesive waterborne latex were able to retain photohydrogen production for more than 90 h. The coatings were manufactured using the convective-sedimentation assembly, which assisted in forming uniform thin coating onto the filter paper substrate.

Wallace (2018) demonstrated a similar concept by constructing flexible biomimetic artificial leaves using *C. reinhardtii* or *C. vulgaris* immobilised with mixtures of high and low glass transition temperature (Tg) latex particles onto paper within a silicon-based organic polymer microfluidic cell. The combination of *C. vulgaris* and latex coatings obtained CO_2 uptake rates of up to 12.1 ± 1.8 mmol m^{-2} h^{-1} under 100 μmol m^{-2} s^{-1}, which compared favorably with the CO_2 uptake rate of natural *Arabidopsis* leaves (around 18 mmol m^{-2} h^{-1} at 100 μmol m^{-2} s^{-1}). Umar (2018) tested microalgae biocomposites created from immobilising *C. vulgaris*, *Dunaliella salina* and *Nannochloropsis oculata* with latex binders onto loofah scaffolds in both semi-batch and continuous CO_2 absorption tests over 8- and 6-week periods. The CO_2 absorption rates were significantly enhanced up to 15 times from their suspension controls. In addition, the lipid content of immobilised *C. vulgaris* and *D. salina* were increased by up to 69.4% and 66.2% dry weight biomass respectively.

Apart from algae, some studies have investigated the photosynthetic bacterium *Rhodopseudomonas palustris* with latex immobilisation. For example, Gosse et al. (2007) fabricated thin biocoatings of highly concentrated *R. palustris* CGA009 and found that the coatings sustained their viability after more than three months of hydrated storage in the dark and over one year when stored at -80 °C. Later, the same research group reported the biocoating generated hydrogen for more than 4000 h (Gosse et al., 2010). They also demonstrated that humidity during long-term storage was the main influence on H_2 production (Piskorska et al., 2013).

2.8.4.2 Advantages of latex polymer entrapments

There are several advantages of latex polymer immobilisation including: thinness, low cost, the potential for engineered multi-layer deposition, a highly concentrated cell density, increased longevity of microbes, and high flexibility (Cortez et al., 2017). Biocoatings and biocomposites made from latex polymer entrapment differ significantly from natural biofilms and cells immobilised in hydrogels (Figure 2.17). Unlike those systems, the thin latex coatings can deposit a highly concentrated population of microorganisms (500-1000 fold compared to suspension cultures) onto a confined space for gas diffusion and retain their viability (Lyngberg et al., 2001, Lyngberg et al., 1999a). Natural biofilms do not have strong protective barriers causing biomass loss and resulting in a short operation lifespan, despite EPS being produced for self-adhesion (Mantzorou and Ververidis, 2019). Compared to hydrogel encapsulation, the gel structure also has poor mechanical strength for long term operation and cannot survive in extreme dry conditions (Flickinger et al., 2017). Many have reported that cells grow out of the gel matrices after a certain period of nutrient exposure. Also, hydrogel coatings thickness can range from 100 microns to millimetres thick (Flickinger et al., 2007), while latex coatings can be 2 to <50 μm (Flickinger et al., 2017). As a result, the cells in the hydrogel would likely have higher CO_2 transfer limitation than the cells entrapped in latexes.
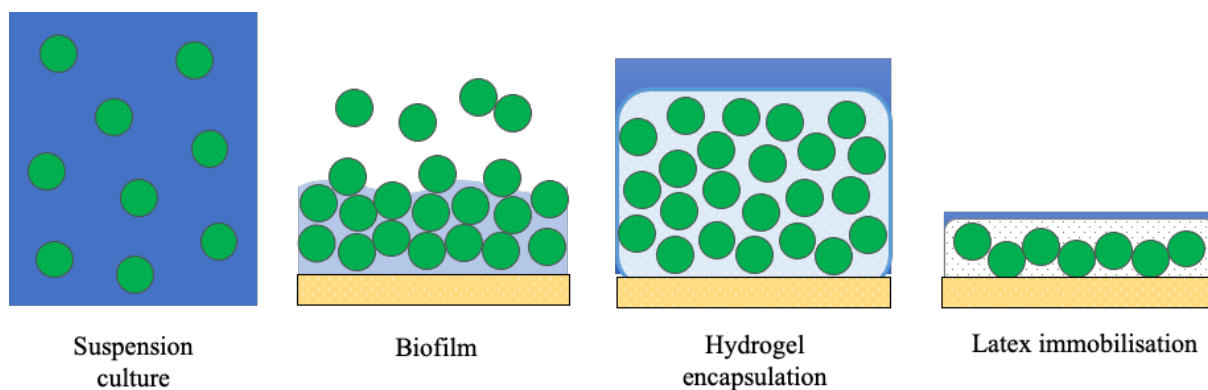
Figure 2.17 Comparison of different systems including suspension culture, biofilm, hydrogel encapsulation and latex immobilisation. Cell density of suspension culture is lower than other systems. Cells in biofilm system can detach due to weak EPS adhesion and no physical barrier. Hydrogels have greater thickness than latex coatings.

Latex coatings can be made with high precision and controlled thickness using techniques such as Mayer rod drawdown and convective assembly methods (Figure 2.18). The former has been used to immobilise *E. coli* with acrylate/vinyl acetate copolymer latex binders, in which near thickness uniformity (approx. 80 μm) was achieved (Swope and Flickinger,

1996). The total cell viability (~95%) was reported for several weeks after rehydration. Mayer rods are typically wrapped with metal wires and the wire size is used to control the coating thickness (Wallace, 2018). The drawdown technique were also successfully used to perform multi-layered coatings with coating thickness of 5-65 μm on top of the substrate diameter of 12.5-35 mm (Lyngberg et al., 1999a). However, the Mayer rod drawdown generally generates coatings that are >10 μm in thickness due to limited wire diameter. The convective assembly method enables the creation of layer-by-layer coatings with rapid, well-ordered, and scalable fabrication (Jenkins et al., 2012). These coating deposition methods enable biocomposites to obtain thinner coatings (~2 to ~75 μm) than the traditional hydrogels and natural biofilms, but they may also have difficulty in scaling up with the same precision.
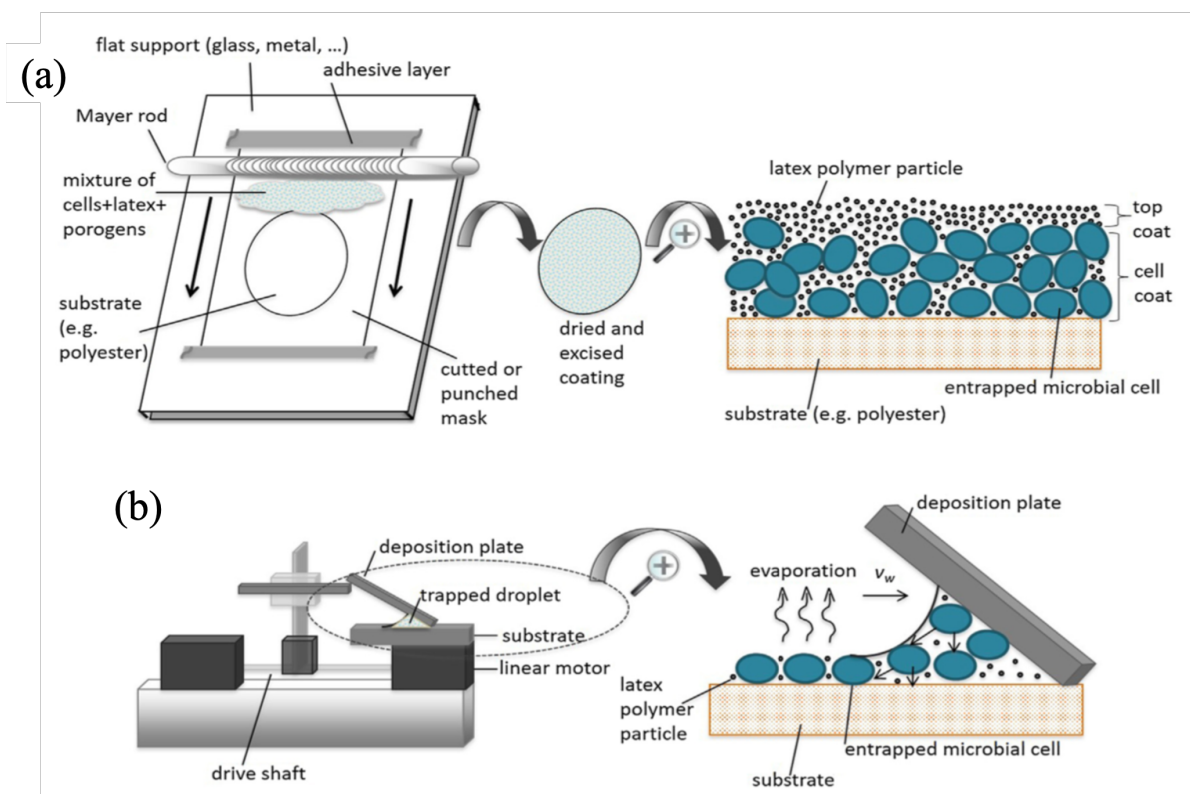
Figure 2.18 Schematic of (a) Mayer rod drawdown, and (b) a convective assembly deposition method for latex cell immobilisation (Cortez et al., 2017).

Another advantage of latex coating is its affordability and the readiness of available non-toxic waterborne latex emulsions (Marrion and Guy, 2004, Flickinger et al., 2009). Latexes have been widely used in industrial settings such as the printing and coating industries to ensure strong adhesiveness, greater flexibility and porosity of the products (Thiagarajan et al., 1999). The infrastructure of coating technology is already in place for scaling up the biocomposites once they are properly optimised. Furthermore, the addition of osmoprotectants (e.g. glycerol)

41

may increase cell stability and protection to cells during drying (Jenkins et al., 2012, Flickinger et al., 2007), allowing them to retain their biological activity for 1000 h after re-hydration (Gosse et al., 2010).

2.8.4.3 Challenges in latex polymer optimisation

Flickinger et al. (2017) outlined many challenges to fabricating and optimising biocoatings from latex immobilisation, such as strong wet adhesion, resistance of living microbes upon drying, porosity generation, and non-destructive measurements of the biological performance of the immobilised cells. A good approach to evaluate strong wet adhesion could be through a screening process of non-toxic latex polymer candidates with the microorganisms of interest on the surface of targeted supports (Umar, 2018). To assist the biocoating drying stage, sugars or osmoprotectant additives are normally used to protect microbes against desiccation (Cortez et al., 2017, Fidaleo et al., 2006). For example, Lyngberg et al. (1999b) used glycerol, sucrose or trehalose during the drying process of *E.coli* mixed with latex emulsions to protect cell viability and enhance the porosity of the biocoatings; although the film formation continued after the additives leached from the coatings. Another intriguing alternative is arrested coalescence using non-film forming particles (bimodal blends) mixed into the coating formulation to increase the porosity of coatings, which have been used with fungi and bacteria (Jenkins et al., 2012, Chen et al., 2020). However, the use of bimodal blends may decrease light transmission to the immobilised photosynthetic cells hindering biological performance unless the particles are sufficiently transparent. In addition, the non-film forming particles have to be non-toxic to the microorganisms, inert (non-reactive to latex), ideally smaller sizes than the immobilised cells, and larger than latex particles (Flickinger et al., 2007).

A major obstacle of immobilising microbes with latex was the limitation to analyse cell viability in biocoatings and biocomposites. Differential viability staining and laser scanning confocal microscopy could be applied to determine the biological performance but with limited depth of penetration into coatings due to photobleaching (Swope and Flickinger, 1996).

2.8.5 Solid supporting materials

Many immobilisation methods have been developed using a wide range of supporting materials including hydrogels and synthetic and natural polymers, with various microorganisms including bacteria, fungus, and algae (Table 2.6). An ideal matrix for cell immobilisation should have the following desirable characteristics (Mallick, 2002, Saeed and Iqbal, 2013):
1) High surface area with tendency for cell adhesion;

2) Provide sufficient photo-transparency to enable photosynthesis;

3) Non-toxic to immobilised cells and support cell viability;

4) Retain good mechanical strength for long operational stability;

5) No adverse effects on biological performance;

6) Should allow exchange of gas and nutrient transfer;

7) Be inexpensive and easily scale up.

In most studies, entrapment and adsorption have been employed to immobilise or test desired microorganisms with the selected immobilising matrices. With the entrapment method, the microorganisms were mixed with the matrix solution, and for hydrogels the rigid gel structure is formed once chemically cross-linked. There is emerging interest in using 3D printing with hydrogels. Lode et al. (2015) printed with alginate-based hydrogel to entrap *Chlamydomonas reinhartii* and reported the chlorophyll content of increased by 16 times after 12 days and an oxygen production rate of 0.25 mg L^{-1} h^{-1} was achieved. For adsorption, the immobilising matrices were inoculated with suspension culture until the cells adhered to their surfaces.

Table 2.6 Examples of studies with various combinations of microorganisms, immobilisation techniques, and immobilised matrices.

Type	Species	Immobilising matrix	Immobilisation technique	References
Green alga	*Selenastrum capricornutum*	Alginate beads	Entrapment	(Faafeng et al., 1994)
Green alga	*Chlamydomonas reinhartii*	Alginate hydrogels	Entrapment	(Lode et al., 2015)
Fungus	*Saccharomyces cerevisiae*	Agar/carrageenan hydrogels	Entrapment	(Kuu and Polack, 1983)
Fungus	*Phaffia rhodozyma*	Alginate mixed with chitosan beads	Entrapment	(Serp et al., 2000)

Green alga	*Scenedesmus obliquus*	Kappa-carrageenan beads	Entrapment	(Chevalier and Noue, 1985)
Green alga	*Chlorella vulgaris*	Carrageenan/alginate beads	Entrapment	(Lau et al., 1997)
Bacteria	*Pseudomonas carrageenovora*	Iota-, lambda-, and kappa-carrageenan hydrogels	Entrapment	(Wong and Tam, 2013)
Cyanobacteria	*Synechococcus* sp.	Chitosan	Entrapment	(Aguilar-May et al., 2007)
Bacteria	*E. coli* ATCC 11505	Chitosan beads	Entrapment	(Nomanbhay and Hussain, 2015)
Green alga	*Chlorella vulgaris*	Chitosan mixed with paper pulp	Entrapment	(Ekins-Coward et al., 2019)
Red alga	*Porphyridium cruentum*	Polyurethane foam	Entrapment (pre-polymerisation)	(Thepenier and Gudin, 1985)
Fungus	*Phanerochaete chrysosporium*	Polyvinylchloride, Stainless steel, Polyurethane foam, and Scotch-Brite	Adsorption	(Guimaraes et al., 2002)

Green alga	*Chlorella vulgaris*	Polystyrene and	Adsorption	(Travieso et
	C. kessleri	polyurethane		al., 1996)
	Scenedesmus quadricauda	foams		
Fungus	*Aspergillus niger* ATCC 10864	Polyester cloth	Adsorption	(Villena and Gutierrez-Correa, 2006)
Green alga	*Scenedesmus* sp. LX1	Polyester microfibres	Adsorption	(Xu et al., 2017)
Green alga	*Chlorella vulgaris* UTEX 265	Cotton sheet	Adsorption	(Gross and Wen, 2014)
Green alga	*Chlorella minutissima* *Chlamydomonas* sp.	Cotton cloth	Adsorption	Prasad et al. (2016a)

Solid supports can be divided into synthetic- and natural-based polymers. They can also be classified as inorganic (zeolite, clay, porous glass, active charcoal, and ceramics) or organic materials, in which the organic polymers are more abundant than the inorganic ones (Cassidy et al., 1996). Most natural polymers are derived from polysaccharides such as agar, chitosan, alginate, and carrageenan. Alginate and carrageenan have been studied extensively as immobilising matrices, but they are fragile and unstable for long term carbon capture operations. Attempts have been made to mix different hydrogels with other solid supports. For instance, Serp et al. (2000) mixed alginate and chitosan to immobilise *Phaffia rhodozyma* and the combination doubled mechanical resistance. Another recent example was from Ekins-Coward et al. (2019), in which chitosan was incorporated into a paper pulp mixture.

Synthetic supports such as polypropylene, polyethylene, polyvinylchloride, polyurethane and polyacrylonitrile are more mechanically robust than natural gel polymers. Polyurethane is a popular material for pilot scale applications for wastewater treatment (Guimaraes et al., 2002). However, Thepenier and Gudin (1985) tried to immobilise *Porphyridium cruentum* during polymerisation of polyurethane foam and found that a large proportion of the microalgae were

destroyed because of pre-polymer composition and physico-chemical reactions. Nevertheless, cell division and recolonisation in the foam structure were observed after removing the lysed cells by rinsing with nutrient medium.

There have been a number of studies using polyester sheets as matrices (Villena and Gutierrez-Correa, 2006, Xu et al., 2017). A natural alternative to polyester sheet is cotton. Gross et al. (2013) used various supporting materials such as armid fiberglass, chamois cloth and cotton duct in a rotating algal biofilm system and discovered that the cotton sheet obtained the best results for algae growth, durability and cost effectiveness. Different cotton based materials i.e. cotton duct, rag, denim and corduroy have also been investigated (Gross et al., 2013). Recently, Prasad et al. (2016a) conducted an experiment for conservation of microalgae using cotton pieces and discovered that the algae preserved their photosynthetic activity for up to 18 months.

Loofah sponge (aka *Luffa* plant) is another promising immobilising matrix, offering a natural high surface area 3D scaffold. Loofah has been used for microorganism (both microalgae and fungi) immobilisation in various applications including bioremediation., with enhanced biosorption performance compared to suspension culture controls (Akhtar et al., 2004b, Iqbal and Edyvean, 2005, Akhtar et al., 2003b, Sriharsha et al., 2017). Loofah has also been studied for blending with plastics to create bioplastics packaging (Masmoudi et al., 2016), and has been tested for numerous biotechnology applications (Acosta-Rubí et al., 2017, Baena-Moreno et al., 2018, Stella and Vijayalakshmi, 2019, Zainab et al., 2019, Saeed and Iqbal, 2013). The highly porous structure should support excellent gas exchange and facilitate reasonable effective light transmission for immobilised phototrophs. Additionally, its hydrophilic property is effective at retaining moisture within the structure (Chen et al., 2018).

Table 2.7 summarises studies using loofah as a solid support. Most focused on heavy metal recovery and all reported enhanced biological performances once the cells were immobilised. They also employed adsorption as an immobilisation technique to adhere the cells, which is a reversible process (Mallick, 2002). Recently, Umar (2018) combined loofah with latex immobilisation of *Chlorella vulgaris* and *Dunaliella salina* to produce algae biocomposites for carbon capture. The CO_2 absorption rates were significantly higher than suspension controls and the immobilised microalgae accumulated lipid up to 66-69% of biomass dry weight.

Table 2.7 Studies with loofah as a solid support for microalgae and cyanobacteria immobilisation.

Type	Immobilised species	Biotechnological application	References
Red microalga	*Porphyridium cruentum*	First report of loofah immobilised algae. There was no significance difference in biomass productivity compared with suspension cultures.	(Iqbal and Zafar, 1993b)
Red microalga	*P. cruentum*	Immobilised cells were able to grow in a limiting growth medium for 50 days.	(Iqbal and Zafar, 1993a)
Green microalga	*Chlorella sorokiniana*	Removed 97% of nickel (Ni^{2+}) from water within 5 mins. Retained 92.9% of initial removal after 5 reuse cycles.	(Akhtar et al., 2003a)
Green microalga	*C. sorokiniana*	Achieved maximum nickel Ni^{2+} removal rates of 60.38 mg $g^{-1}_{biomass}$ and 48.08 mg $g^{-1}_{biomass}$ from water for immobilised and free cell culture.	(Akhtar et al., 2004b)
Green microalga	*C. sorokiniana*	Removed 73.2% of the total metal of a continuous contaminated water flow column with cadmium removal capacity of 192 mg $g^{-1}_{biomass}$.	(Akhtar et al., 2003b)
Green microalga	*C. sorokiniana*	Achieved maximum lead(II) (Pb^{2+}) removal rates of 123.67 and 108.04 mg $g^{-1}_{biomass}$ from water for immobilised and free cell culture.	(Akhtar et al., 2004a)

Green microalga	*C. sorokiniana*	Achieved maximum chromium (Cr^{3+}) removal rates of 69.26 and 58.80 mg $g^{-1}_{biomass}$ from water for immobilised and free cell culture.	(Akhtar et al., 2008)
Cyanobacteria	*Synechococcus* sp.	Increased cadmium (Cd^{2+}) biosorption by 21% compared to suspension cultures. Achieved 96% adsorption of Cd^{2+} within 5 mins.	(Saeed and Iqbal, 2006)
Green microalga	*Scenedesmus obliquus* CNW-N	Removal of cadmium (Cd^{2+}) with adsorption capacity of 38.4 mg within 15.5 h.	(Chen et al., 2014)
Green microalga	*C. vulgaris*	Immobilised with latex binders onto loofah scaffold and achieved CO_2 absorption of 0.17 g CO_2 $g^{-1}_{biomass}$ d^{-1} with continuous gaseous 5% v/v CO_2 exposure for 42 days.	(Umar, 2018)
Green microalga	*Dunaliella salina*	Immobilised with latex binders onto loofah scaffold and achieved CO_2 absorption rate of 0.25 g CO_2 $g^{-1}_{biomass}$ d^{-1} with continuous gaseous 5% v/v CO_2 exposure for 42 days.	(Umar, 2018)

2.9   Conclusion

Conventional CCS technologies are complex, expensive and can cause potential secondary pollution. There is great interest in algae technologies for carbon capture, but conventional cultivation systems have many disadvantages. Biofilm-based PBRs have poor cell adhesion and are undesirable for long term CCS application. Latex biocomposites or biocoatings have many advantages include higher cell density than suspension cultures, provide protection against contamination and prevent cell loss, and enhance CO_2 transfer by eliminating the slow CO_2 diffusion in water. Non-toxic loofah sponge has a good 3D surface area, good mechanical strength, and sufficient porosity for gas exchange and light access. Microalgae immobilised with a combination of latex coating onto loofah has significantly increased CO_2 absorption rates compared to suspension culture controls. To date, no researcher has tried to immobilise cyanobacteria with this unique combination to recreate nature inspired "living biocomposites" for intensified long-term carbon capture.

Chapter 3

Microalgae-textile biocomposites deliver enhanced carbon dioxide capture

Abstract

Microalgae offer a biological route to capture industrial carbon dioxide (CO_2) emissions; however, conventional cultivation systems (open ponds and photobioreactors) have many drawbacks—including high land and water demands—that limit their utility for affordable and sustainable CO_2 abatement. In this study we demonstrate the CO_2 capture performance of prototype living algae biocomposites that use textiles as a solid substrate. *Chlorella vulgaris* were attached to 100% cotton and 100% polyester sheets, of which half were coated with kappa-carrageenan as a gel topcoat to enhance microalgae retention. The biocomposites were tested in 28 days semi-batch CO_2 absorption tests using a 5% v/v CO_2/air gas mixture. The biocomposites absorbed significantly more CO_2 than suspension culture controls, with the highest CO_2 absorption rate being 1.82 ± 0.10 g CO_2 $g^{-1}_{biomass}$ d^{-1} from the coated cotton biocomposites, followed by 1.55 ± 0.27 g CO_2 $g^{-1}_{biomass}$ d^{-1} from the uncoated cotton biocomposites. The coated and uncoated polyester biocomposites had comparatively lower CO_2 absorption rates (0.49 ± 0.04 and 0.42 ± 0.03 g CO_2 $g^{-1}_{biomass}$ d^{-1} respectively), likely due to the hydrophobic and surface charges of the materials affecting microalgae adhesion and retention. A two weeks attachment test on cotton/polyester blends revealed some deterioration of the cotton which could limit the operational longevity of the biocomposites. Despite these issues, the CO_2 abatement values compare favourably with other *Chlorella* CO_2 capture studies with the added benefit of much reduced water usage and, if constructed vertically, a greatly reduced land requirement. End-of-life textiles upcycled as microalgae biocomposites would reduce the amount of waste materials sent for incineration or landfill, and deliver a concurrent socioeconomic good through CO_2 capture.

Keywords: Textiles, fabric, living biocomposites, intensified carbon capture, engineered biofilm

3.1 Introduction

Some microalgae are capable of efficient photosynthetic carbon fixation, potentially removing 1.83 kg of CO_2 for every 1 kg of microalgae biomass produced (Jiang et al., 2013). The practical aspects of this carbon capture potential have been explored for carbon sequestration (Cheah et al., 2015, Moreira and Pires, 2016, Bernal et al., 2017, Song et al., 2019b, Míguez et al., 2020); however, the very nature of suspension based cultivation techniques—growing microalgae in either ponds or photobioreactors (PBR)—presents a major techno-economic bottleneck. Conventional suspension-based cultivation systems typically have large land footprints, require substantial quantities of water, have high maintenance burdens, and are prone to contamination by competing and/or infectious microbes (Singh and Dhar, 2019, Noble et al., 2012, Kumar et al., 2011, Ho et al., 2011). Additionally, limitations on CO_2 mass transfer between the gas-liquid phases in ponds and PBRs further limits process efficiency (Fu et al., 2019, Lu et al., 2020).

Alternative approaches to suspension cultivation, primarily based on cell immobilisation or engineered biofilms (Strieth et al., 2018), are showing promise for certain applications, wastewater bioremediation for example (Zhao et al., 2018, Zhou et al., 2018, Wu et al., 2019, Gou et al., 2020, Chaiwong et al., 2020, Kesaano and Sims, 2014). However, the development of similar systems for CO_2 capture are in their infancy (Bernal et al., 2017, Cortez et al., 2017, Ekins-Coward et al., 2019, Flickinger et al., 2017). These systems, also known as biocomposites, typically immobilise microorganisms onto solid surfaces or within hydrogels. Hydrogels using substances extracted from natural sources such as alginate, carrageenan and chitosan have been shown to support enhanced photosynthetic performance relative to their suspension culture controls (Lau et al., 1997, Lode et al., 2015, Yashveer, 2003) and do not compromise their biological performance (Chevalier and Noue, 1985, Tosa et al., 1979, Lau et al., 1997, Wang and Hettwer, 1982). However, studies that randomly mix the cells within the hydrogel matrix generally suffer biomass loss over time, either driven externally through environmental degradation of the hydrogel structure or internally due to outgrowth of the microalgae. The application of hydrogels as a topcoat as opposed to the sole encapsulating matrix would represent a novel iteration of the hydrogel approach, similar to gel coating applications on food surfaces that prolong shelf life (Rojas-Grau et al., 2009). Of the various types of hydrogel, carrageenan has been extensively used to immobilise microalgae and other microorganisms because of its affordable price, with some studies reporting that the gel enhanced biological performance compared to other hydrogels (e.g. alginate) and suspended

cell cultures (Chevalier and Noue, 1985, Tosa et al., 1979, Lau et al., 1997, Wang and Hettwer, 1982).

A solid substrate to coat with cells and hydrogel is required to produce stable algae biocomposite systems. Several supporting materials (scaffolds), including various textiles, have been explored. Biocomposites made from cellulose-based materials (i.e. cotton) tended to support improved cell attachment with increased biomass yield compared to other substrates (Gross et al., 2013, Christenson and Sims, 2012, Christenson and Sims, 2011). Interestingly, Prasad et al. (Prasad et al., 2016b) found that cotton cloth was capable of preserving microalgae viability for up to 18 months, offering an intriguing opportunity to evaluate the potential of cotton-based biocomposites for sustained carbon capture applications; however, concern remain for cotton's longevity in permanently wetted situations. A more robust textile, such as polyester cloth, may offer more confidence for long term operation. Indeed, polyester has previously been used for biofilm systems, including microalgae (Villena and Gutierrez-Correa, 2006, Møretrø and Langsrud, 2004, Xu et al., 2017). Furthermore, upcycling disposed textiles as scaffolds for biocomposites would reduce the amount of textile waste going into incinerators or landfill by extending the end-of-life period.

In the current study we evaluated the suitability of cotton and polyester materials for textile based microalgae (*Chlorella vulgaris*) biocomposites for carbon capture applications. Kappa-carrageenan was implemented as a topcoat to retain the microalgae on the textile substrate. We also investigated whether there was any effect of textile blends on natural immobilisation (i.e. without a topcoat) and whether biocomposite robustness could be improved.

3.2 Materials and methods

3.2.1 Textiles

Four polyester and cotton blends (100% polyester, 100PE; 80% polyester + 20% cotton, 80PE; 65% polyester + 35% cotton, 65PE; and 100% cotton, 100C) were purchased from Aow RungRuang Co. Ltd (Bangkok, Thailand). The textile sheets were washed with deionised water (dH$_2$O), autoclaved at 125 °C for a 15 mins cycle, oven dried at 105 °C for 3 h and left in a desiccator for 24 h before use.

The weave pattern and fibre density was characterised by scanning electron microscopy (SEM) using a Hitachi TM 3000 SEM (Figs 3.3 & 3.4). The sterile textiles were cut into 5 × 5

mm squares and attached to 12 mm diameter pin stubs using carbon tape and imaged at × 60 magnification. For side imaging, a sample was placed vertically against each side of a transparent acrylic cube (5 × 5 × 5 mm) that was attached to a pin stub with carbon tape and imaged at ×180 magnification. Images were analysed using ImageJ software to calculate yarn thickness (yarn being the spun thread comprising a number of material fibres), the number of fibres per yarn, fibre circumference, void space and surface area (Figure 3.1). The surface area was calculated using equation 3.1.

The multipoint tool was used to count each fibre per yarn.

The polygon tool was used to trace and measure fiber circumference.

The straight-line tool was used to measure yarn diameter.

1) Image was cropped and duplicated with a real scale set.
2) The threshold of the cropped image was adjusted to distinguish between empty spaces and fibres.
3) The red highlighted area was measured and subtracted to obtain the percentage difference in area (considered to be void spaces).

80PE before contrasting

80PE after contrasting

Figure 3.1 ImageJ analysis to determine: (a) number of fibre per yarn, (b) fibre circumference, (c) yarn thickness, (d) step by step definition of void space, and (e) an example of before and after contrasting of 80% polyester and 20% cotton (80PE).

$$SA \ (cm^2) = V_{textile} \ (cm^3) \times Fibres \ per \ yarn \ \times \frac{Fibre \ circumference \ (cm)}{Analysed \ area \ (cm^2)} \quad (3.1)$$

pH can be an important determinant of microalgae survival on inert materials. A standard water extraction method was applied to determine the textile's pH (AATCC, 2007). In triplicates, 250 mL of dH_2O was boiled in a beaker for 10 mins and 10 g of coarsely ground (pestle and mortar) textile was added. The beaker was covered with a watch glass, boiled for another 10 mins, then allowed to cool to 20 °C before filtering through a stainless steel mesh (1 mm aperture) lab standard sieve. The filtrate pH was measured using a glass probe pH meter (Mettler Toledo Seven Compact) against controls of boiled dH_2O without textiles.

3.2.2 Cultivation of microalgae

Chlorella vulgaris CCAP 211/63 was cultivated in BG-11 medium (containing 1.5 g/L $NaNO_3$, 0.036 g/L $CaCl_2 \cdot 2H_2O$, 0.075 g/L $MgSO_4 \cdot 7H_2O$, 0.04 g/L K_2HPO_4 and 0.02 g/L Na_2CO_3; Sigma Aldrich, UK) in 10 L Nalgene polycarbonate carboys with a constant air supply from a KOI AIR 50 Blagdon aquarium pump. Cultures were maintained at 18 ± 2 °C with a 16:8 h light:dark cycle with 2,500 lux ($\approx 30.5 \ \mu$mol m^{-2} s^{-1}; (Thimijan and Heins, 1982)) of illumination provided by 30W daylight-type fluorescent tubes (Sylvania Luxline Plus, n = 6).

3.2.3 Production of textile-based algae biocomposites

For the CO_2 fixation trials only 100C and 100PE were used. Sterile sheets of 100C and 100PE (n = 12) were cut into strips (6 × 1 cm height × width) and weighed before being submerged in an algae suspension (250 mL) in a beaker with a lid, and gently stirred every two days for 14 days. After two weeks, the cells had attached to the textiles. Biomass dry weight of the attached algae was determined in weekly sacrificial sampling (n = 3) by oven drying the materials at 105 °C for 3 h and leaving them in a desiccator for 24 h before re-weighed.

Half of the samples were subjected to a topcoat. The topcoat was made by mixing kappa-carrageenan powder (from >99.9% pure powder; Sigma Aldrich, UK) to obtain 0.0125M in sterile dH_2O at 50 °C for 30 mins until homogeneous. Twenty milliliters of solution was poured onto the textile samples in a Petri dish and stored at 4 °C for 1 h to accelerate the gelation process. The coated samples were removed from the gel solution and submerged in 0.5M KCl (Sigma Aldrich, UK) for 1 h to strength the gel topcoat. A schematic of the production process is presented in Figure 3.2.
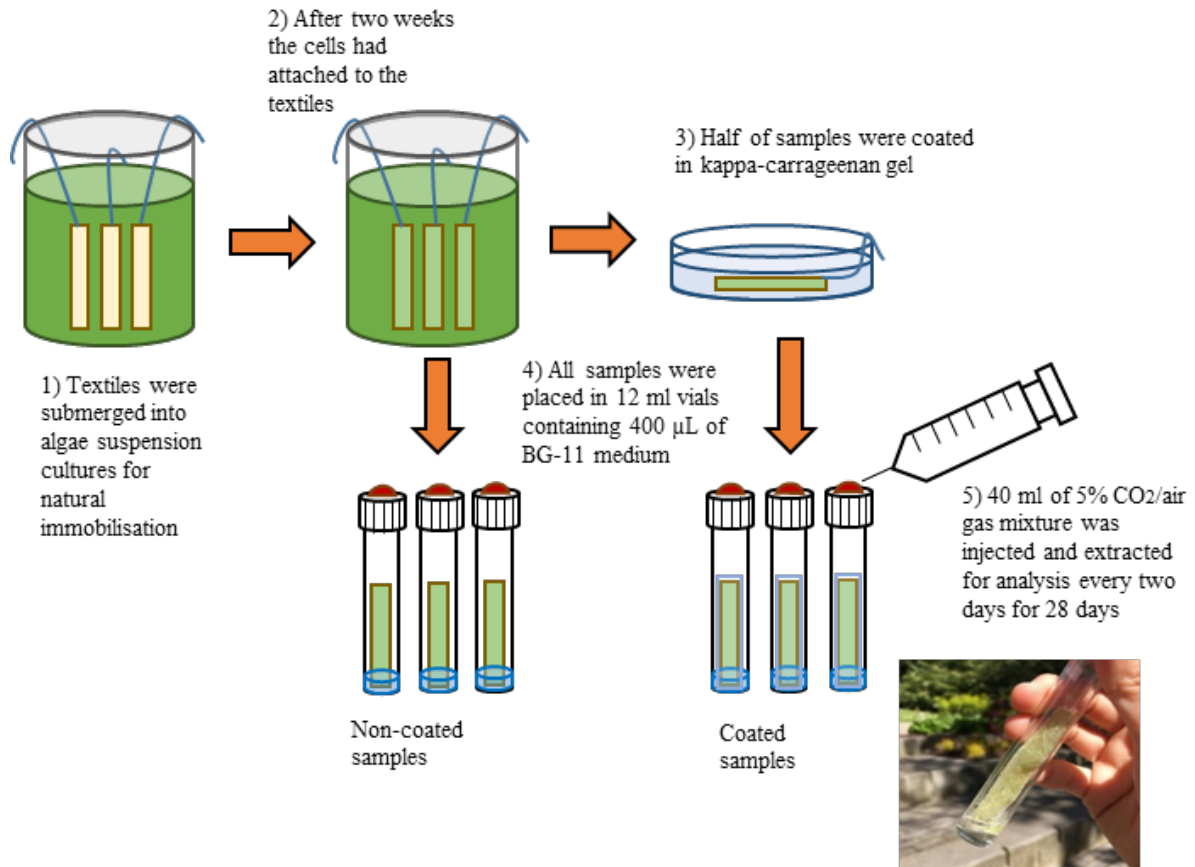
Figure 3.2 A schematic of textile biocomposite production and testing process under batch CO_2 exposure for a period of 28 days.

3.2.4 CO₂ absorption test and chlorophyll monitoring

Each 6 cm biocomposite sample (n = 3 per treatment) was placed in a 12 mL air tight vial and immersed to a depth of 1 cm in 400 μL of BG-11 medium. No further nutrients were added throughout the experiment and no manual wetting of the biocomposites was conducted. Forty milliliters of 5% v/v CO_2/air gas mixture was injected into each vial using a 60 mL airtight syringe. The samples were incubated under the same light and temperature conditions as the main microalgae cultures. The percentage of CO_2 was measured in each vial every second day for 28 days by injecting 40 mL of extracted gas into a GeoTech G100 CO_2 meter. The equivalent volume of 5% v/v CO_2/air gas mix was then refreshed into the vial. CO_2 fixation rate was calculated using equation 3.2, where Mr_{CO2} is the molar ratio of CO_2.

$$CO_2 \text{ fixation rate } \left(g_{CO_2} \; g_{biomass}^{-1} day^{-1}\right)$$
$$= \frac{\% \; CO_2 \; consumed \; \times \; Initial \; mole_{CO2} \; \times Mr_{CO2}}{Dry \; weight \; biomass \; used \; \times 2 \; days} \qquad (3.2)$$

An estimation was made of the total number of immobilised cells using *C. vulgaris* cell size, based on the following assumptions: 1) all cells were of equal size (5 μm measured using a Leica DMi 8 microscope with LasX software), 2) the cells were attached uniformly as a single layer, 3) the cells had not attached between the yarn gaps, and 4) there was no cell division after attachment and coating. With the first assumption, the cell size can be adjusted within the range of 5-10 μm for *C. vulgaris* depending on culture conditions. The chlorophyll *a* content of the immobilised cells was monitored every second day by placing the sample onto a glass microscope slide and measuring fluorescence in a FLUOstar Optima BMG LabTech fluorometer at an excitation of 430 nm.

To estimate the number of cells that had detached from the biocomposites and transported into the growth medium, 10 μL of the liquid medium of each replicate was sampled weekly and cell density determined at ×200 magnification using an Improved Neubauer haemocytometer. Cell density and the percentage of cells released was calculated using equation 3.3 (Moheimani et al., 2013). In the calculation, it was assumed that cell division was negligible within the biocomposites under nitrogen depletion and once released into the media.

$$\% \, cell \, released \; = \frac{cell \, density \; \times 0.4 \, ml}{Estimated \, no. \, of \, cells \, attached \, to \, the \, textile} \qquad (3.3)$$

3.2.5 Natural attachment test on cotton, polyester and cotton-polyester blends

Autoclaved textiles of all four types were cut into 1 cm^2, weighed, and placed into a 24-multiwell plate. Two millilitres of algae culture was added into each well. For abiotic controls, 2 mL of BG-11 without algae was added. The plate was incubated for 14 days at the same light and temperature conditions as the algae cultures. The samples were gently agitated every two days using forward and reverse pipetting, and sacrificially analysed for chlorophyll *a* extraction and dry weight determination. The chlorophyll *a* extraction procedure was modified from Sartory and Grobbelaar, and Henriques et al. (Sartory and Grobbelaar, 1984, Henriques et al., 2007). Samples were ground in a 1.5 mL Eppendorf tube using a micro pestle. One millilitre of 90% v/v ethanol solution was added to each tube, vortexed for 10 to 20 sec (Vortex Genie 2, Scientific Industries, Inc.), then heated at 78 °C for 5 mins and left to stand for 24 h in the dark at 20 °C. The supernatant was analysed for absorbance at 663, 645, 630 and 750 nm. The quantity of chlorophyll *a* per unit surface area of textiles (cm^2) was calculated using equation 3.4 specifically for 90% ethanol solution, in which *A* is absorbance at a particular wavelength.

$$\frac{Chl\ a\ (\mu g)}{Surface\ area\ (cm^2)}$$
$$= \frac{11.64(A_{663} - A_{750}) - 2.16(A_{645} - A_{750}) - 0.1(A_{630} - A_{750})}{Estimated\ surface\ area\ of\ textile\ (cm^2)} \qquad (3.4)$$

After the 14 day test, the samples were oven dried at 105 °C for 1 h and left in a desiccator for 24 h before re-weighing. The percentage of material mass change was calculated using equation 3.5.

$$\%\ Dry\ mass\ change = \frac{final\ mass\ - initial\ mass\ (g)}{initial\ mass\ (g)} \qquad (3.5)$$

3.2.6 Statistical analysis

Minitab 18 was used for statistical analysis. Percentage data were arcsine transformed prior to analysis. Normality was tested using the Anderson-Darling test and equality of variance by the Levene's test. Data that met the test assumptions were analysed by one-way analysis of variance (ANOVA), with Tukey's test as a post-hoc analysis. The remaining data were analysed using the non-parametric Friedman test as they were repeated measures. The Wilcoxon sign ranked test was then used to determine significant differences among treatments, which is a common statistical test for comparing repeated measures in a pair (Bellera et al., 2017).

3.3 Results

3.3.1 Characterisation of the textiles

pH varied significantly with the proportion of cotton in the blend, with higher cotton contents leading to increasing alkalinity (100PE = 6.21 ± 0.036, 80PE = 7.01 ± 0.027, 65PE = 7.15 ± 0.026, 100C = 7.23 ± 0.019; Kruskal-Wallis: H = 19.88, DF = 3, P = 0.006); the dH_2O controls were more acidic than the textiles, varying between pH 5.71 and 6.05.

The textiles had plain weave patterns (Hann and Thomas, 2005) with various degrees of tightness. The higher cotton blends presented rougher surfaces (Figure 3.3). There were significant differences in percentage void space between the textiles (ANOVA: F = 6.96, DF = 3, P = 0.013; Table 3.1), with 80PE having a tighter weave than both 100C and 65PE. There was no relationship between textile composition and void space. There was significant variation in the fibre density per yarn (ANOVA: F = 145.98, DF = 3, P = <0.001; Table 3.1, Figure 3.4), with each textile significantly different from each other. 65PE had the highest fibre density (138

± 8 fibres per yarn) while 100PE had the lowest (30 ± 4 fibres per yarn). The circumference of each fibre also varied (Kruskal-Wallis: H = 9.76, DF = 3, P = 0.022) with 100PE fibres significantly larger (75.39 ± 7.03 μm) and 80PE significantly smaller (38.62 ± 1.27 μm) than the others. Yarn thickness varied between textiles (ANOVA: F = 4.43, DF = 3, P = 0.041) with 65PE having the thickest weave (371.68 ± 59.86 μm) and 80PE the thinnest (235.50 ± 28.99 μm). Surface area varied between fabrics (Kruskal-Wallis: H = 9.67, DF = 3, P = 0.022) with 80PE presenting a significantly smaller area than the other textiles (1.10 ± 0.03 cm^2 cm^{-3}; Mann-Whitney W = 10, DF = 3, P = 0.03) while 100PE presented a significantly larger area than the others (2.82 ± 0.09 cm^2 cm^{-3}; Mann-Whitney W = 10, DF = 3, P = 0.03).
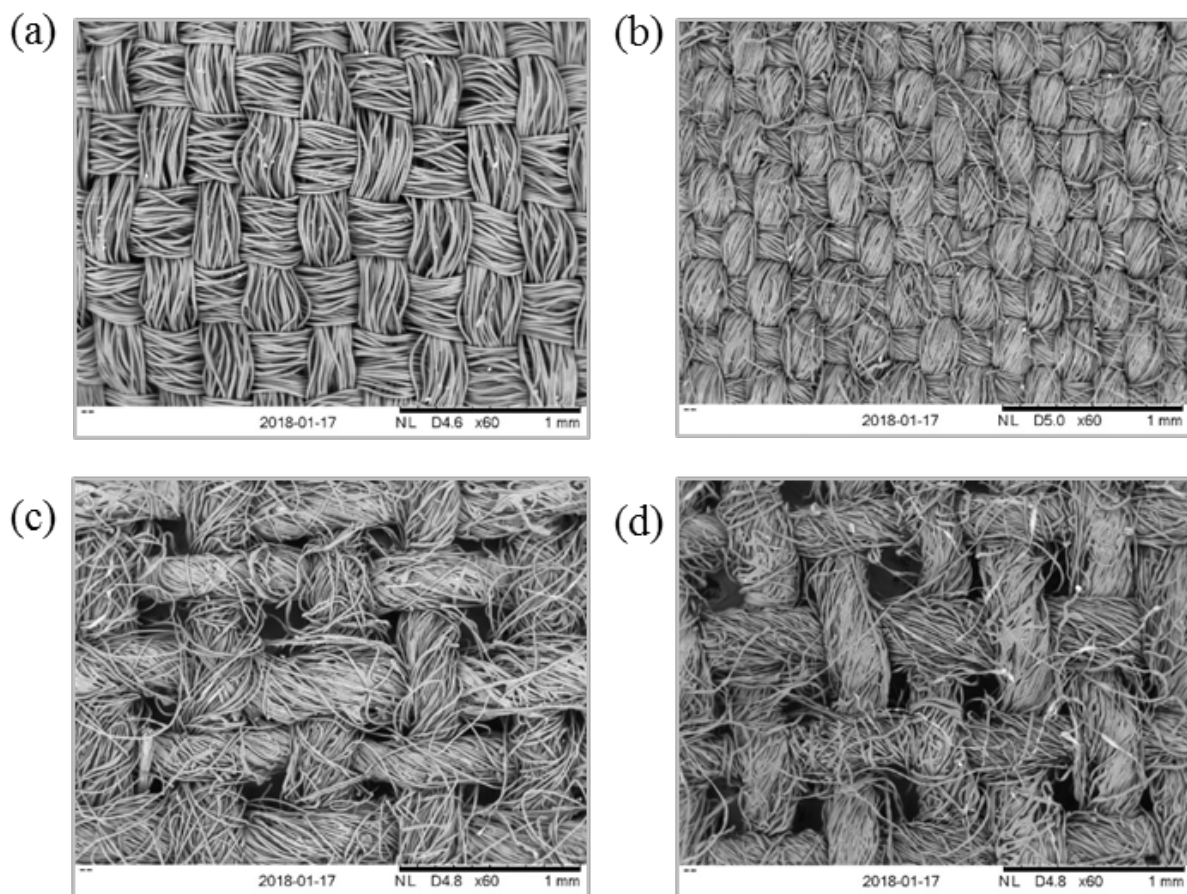
Figure 3.3 SEM images (top view) of: (a) 100% polyester (100PE), (b) 80% polyester and 20% cotton (80PE), (c) 65% polyester and 35% cotton (65PE), and (d) 100% cotton (100C).
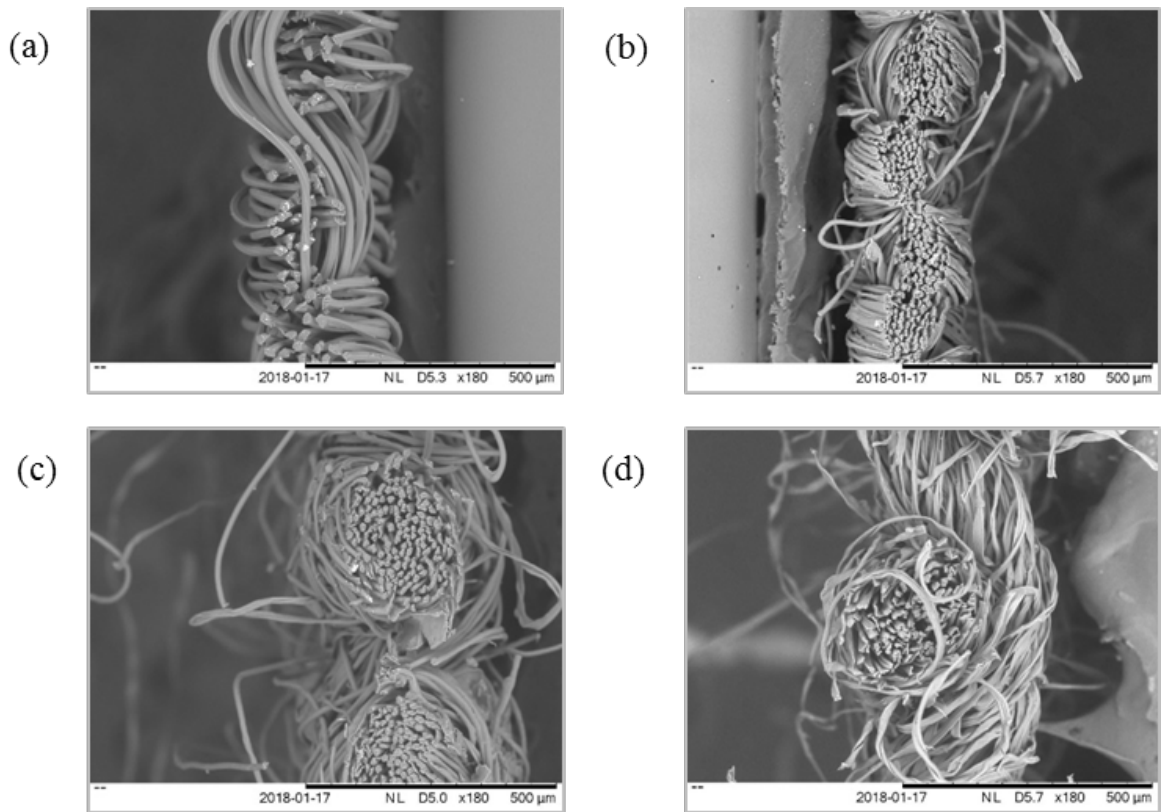
Figure 3.4 SEM images (side view) of: (a) 100% polyester (100PE), (b) 80% polyester and 20% cotton (80PE), (c) 65% polyester and 35% cotton (65PE), and (d) 100% cotton (100C).

Table 3.1 Characteristics of textiles analysed from SEM images using ImageJ software. Measured parameters were: the number of fibres per yarn, fibre circumference, yarn thickness (diameter), estimated surface area available for cell attachment, and the percentage void space. Mean ± StDev.

Type	Fibres per yarn	Fibre circumference (μm)	Yarn thickness (μm)	Surface area (cm^2)	Void space (%)
100C	93 ± 7	54.74 ± 12.09	309.24 ± 16.31	2.05 ± 0.45	25.05 ± 4.43
65PE	138 ± 8	44.71 ± 3.35	371.68 ± 59.86	2.01 ± 0.22	24.77 ± 4.58
80PE	72 ± 7	38.62 ± 1.27	235.50 ± 28.99	1.10 ± 0.03	14.12 ± 2.33
100PE	30 ± 4	75.39 ± 7.03	308.26 ± 60.96	2.82 ± 0.09	16.77 ± 2.11

3.3.2 CO₂ uptakes and chlorophyll *a* content

The cotton biocomposites had the highest net cumulative CO_2 fixation rates (Figure 3.5) irrespective of whether a topcoat was applied (coated = 1.82 ± 0.10, uncoated = 1.55 ± 0.27 g CO_2 g^{-1} biomass d^{-1}, coated polyester = 0.49 ± 0.04, uncoated polyester = 0.42 ± 0.03 g CO_2 g^{-1} biomass d^{-1}; Friedman: data vs. treatment: S = 156.36, DF = 3, P = <0.001 data vs. time: S = 194.97, DF = 13, P = <0.001). All biocomposite treatments outperformed the suspension culture controls (0.16 ± 0.01 g CO_2 g^{-1} biomass day^{-1}).
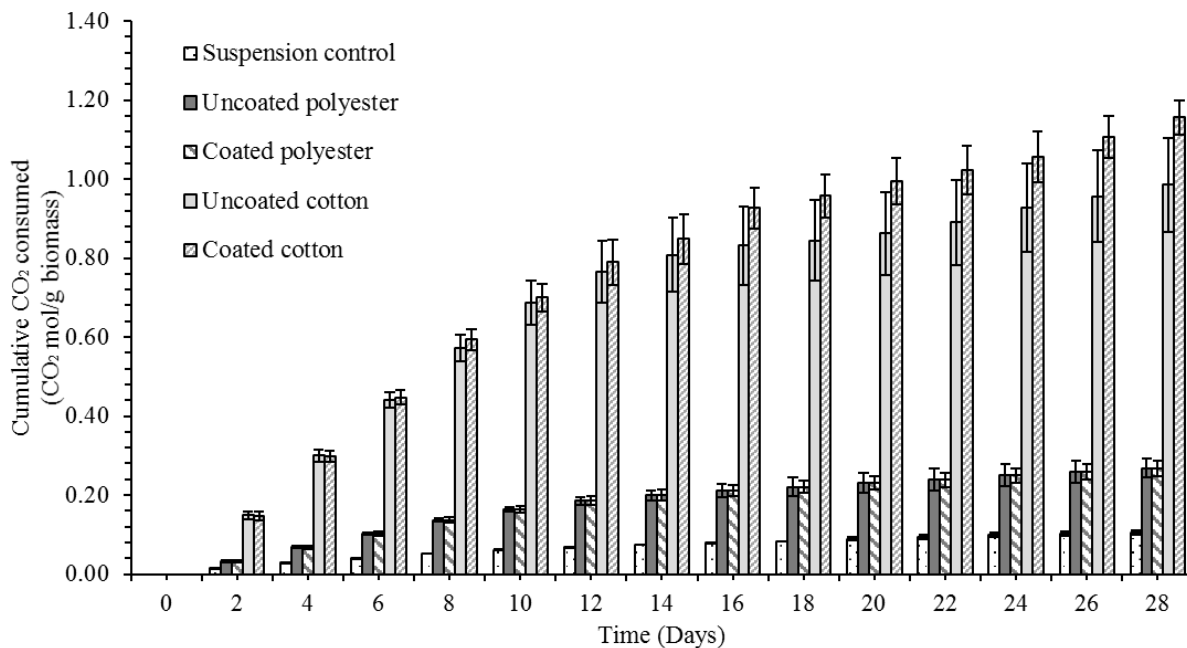
Figure 3.5 Cumulative net CO_2 fixation (mol CO_2/g biomass; mean ± StDev, n = 3) over 28 days for kappa-carrageenan coated and uncoated cotton or polyester based biocomposites and suspension algae culture controls.

The use of the kappa-carrageenan topcoat did improve CO_2 uptake rates (Wilcoxon: cotton; W = 238, DF = 3, P = 0.021; polyester: W = 63, DF = 3, P = <0.001), but the improvement was modest in comparison to the textile type (Wilcoxon: W = 903, DF = 3, P = <0.001).

Chlorophyll fluorescence increased with treatment and time (Friedman: data vs. treatment: S = 99.34, DF = 3, P = <0.001; data vs. time: S = 117.61, DF = 13, P = <0.001). The fluorescence of the uncoated cotton biocomposites increased exponentially from day 10 and peaked on day 18, whereas the fluorescence of the coated cotton biocomposites increased linearly before plateauing from day 24 (Figure 3.6), with the uncoated cotton biocomposites having higher fluorescence than the coated treatment (Wilcoxon: W = 33, DF = 3, P = <0.001).

The polyester biocomposites, which had significantly lower fluorescence than the cotton treatments, plateaued between days 14 and 16. Unlike the cotton treatments, the coated polyesters had higher fluorescence than the uncoated polyesters (Wilcoxon: W = 680, DF = 3, P = 0.004).
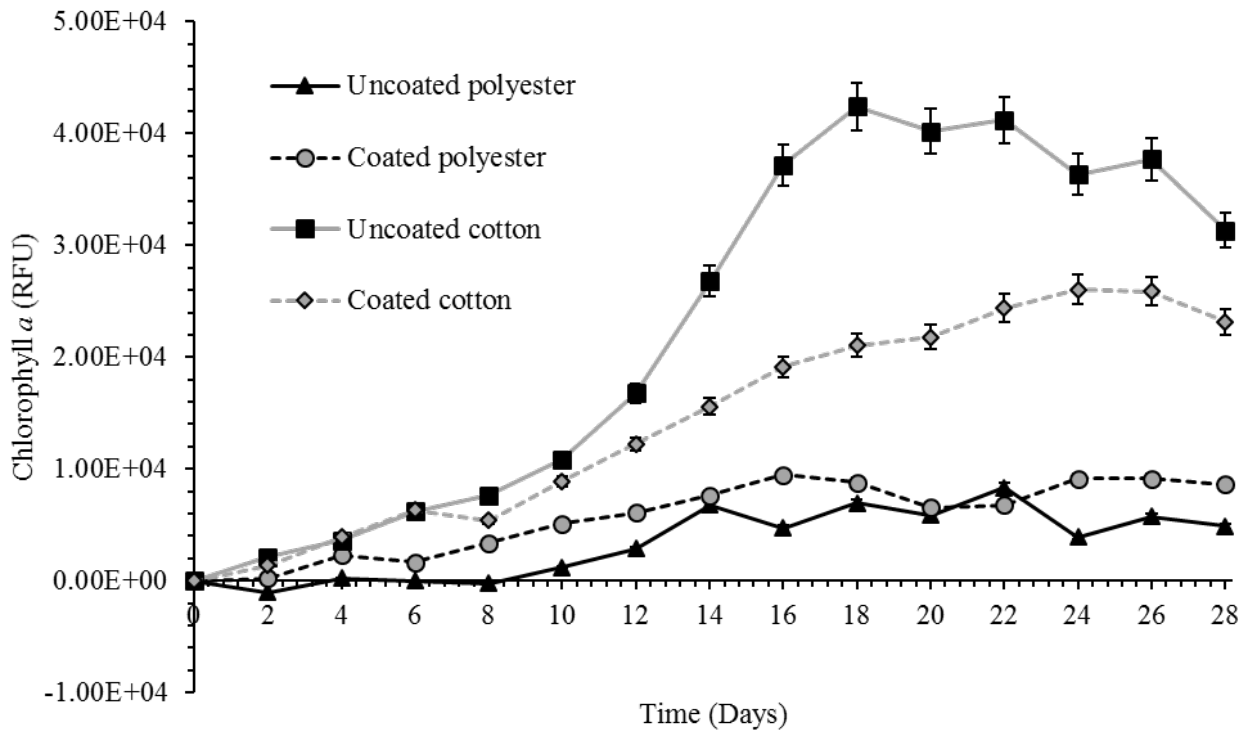
Figure 3.6 Chlorophyll *a* fluorescence intensities (relative fluorescence units; mean ± StDev, n = 3) of kappa-carrageenan coated and uncoated cotton or polyester based biocomposites over 28 days of the CO_2 fixation test.

The trends of net cumulative CO_2 fixation plotted against chlorophyll fluorescence are shown in Figure 3.7. These plots were used to identify which biocomposites were more robust over time by observing relationship between attached biomass and CO_2 removed. It should be noted that the fluorescence measured here cannot be affected by kappa-carrageenan because of different absorbance ranges; i.e. kappa-carrageenan absorbs at 290 nm (Kumoro et al., 2018), while chlorophyll a absorbs at 400 to 700 nm (Kalaji et al., 2017). The uncoated cotton and polyester showed biomass loss and the CO_2 performance seemed to be approaching vertical asymptotes (Figure 3.7c&d). The coated cotton and polyester seemed to indicate linear relationships (Figure 3.7a&b).
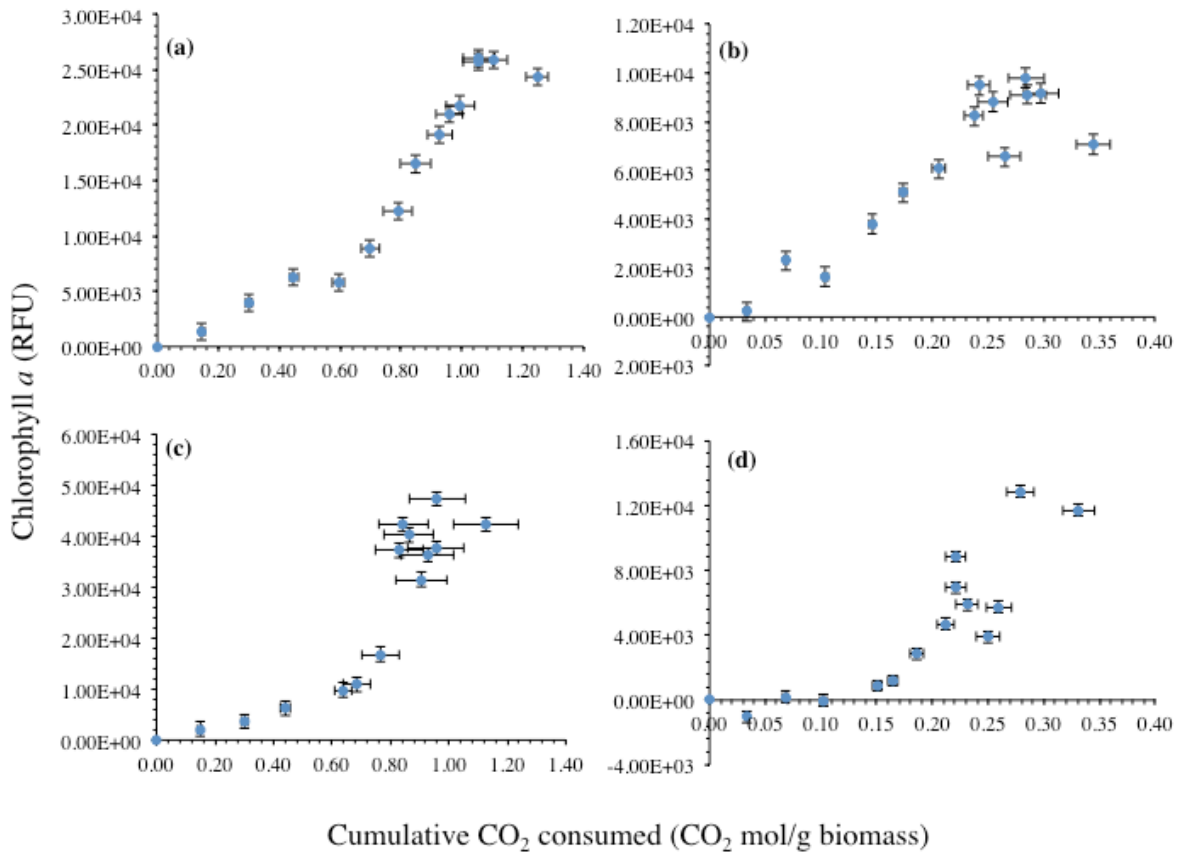
Figure 3.7 Cumulative CO_2 fixation versus chlorophyll a fluorescence intensity over 28 days: a) coated cotton, b) coated polyester, c) uncoated cotton, and d) uncoated polyester based.

3.3.3 Cell detachment

It was noticeable that cells were detaching from the textiles into the BG-11 medium (Figure 3.8 & 3.9), particularly for the uncoated biocomposites (Friedman test: data vs. treatment; S = 40.29, DF = 3, P = <0.001; data vs. time: S = 25.95, DF = 3, P = <0.001). The coated polyester biocomposites had significantly higher cell release than the coated cotton (Wilcoxon: coated, W = 24, P = 0.044) but there was no significant difference between the uncoated biocomposites. The cell release data were used to normalise the CO_2 fixation and chlorophyll fluorescence data to biomass retention (Figure 3.10a&b) (normalised CO_2: Friedman test, data vs. treatment: S = 29.30, DF = 3, P = <0.001, data vs. time: S = 36.0, DF = 3 P = <0.001; normalised chlorophyll a: Friedman test, data vs. treatment: S = 30.70, DF = 3, P = <0.001; data vs. time: S = 29.30, DF = 3, P = <0.001), resulting in higher values in all cases.
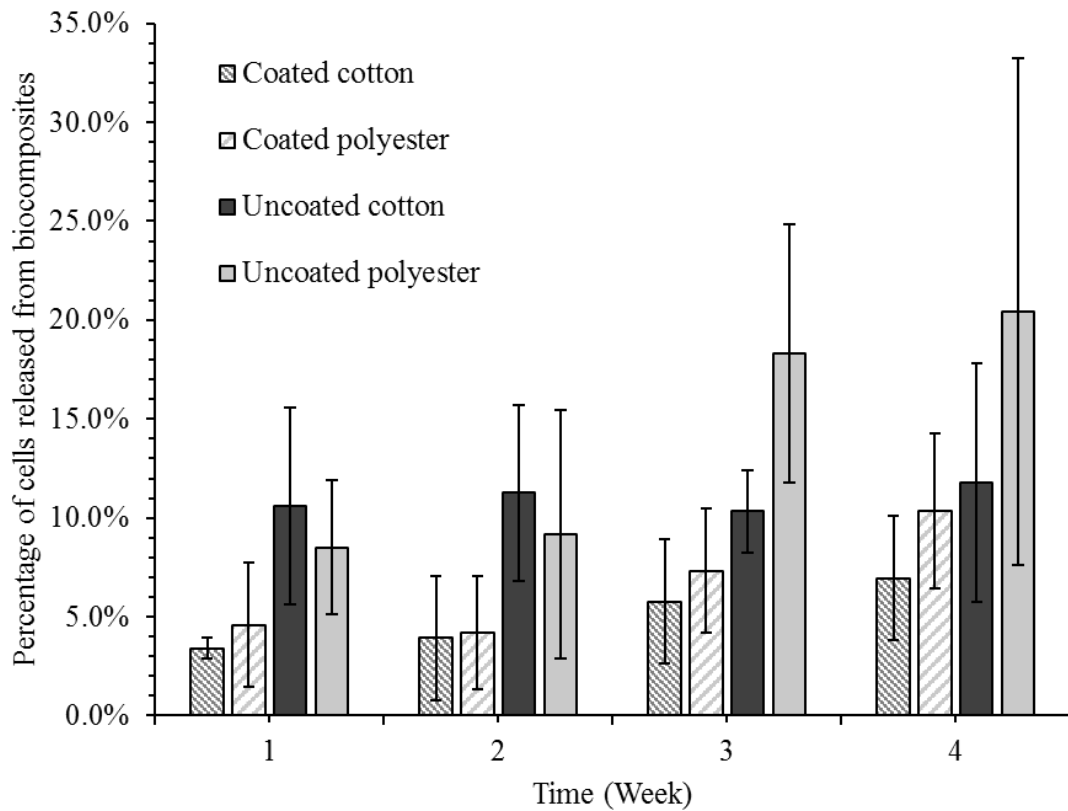
Figure 3.8 The percentage of cells released from the biocomposites (mean ± StDev, n = 3) during the CO_2 fixation test.
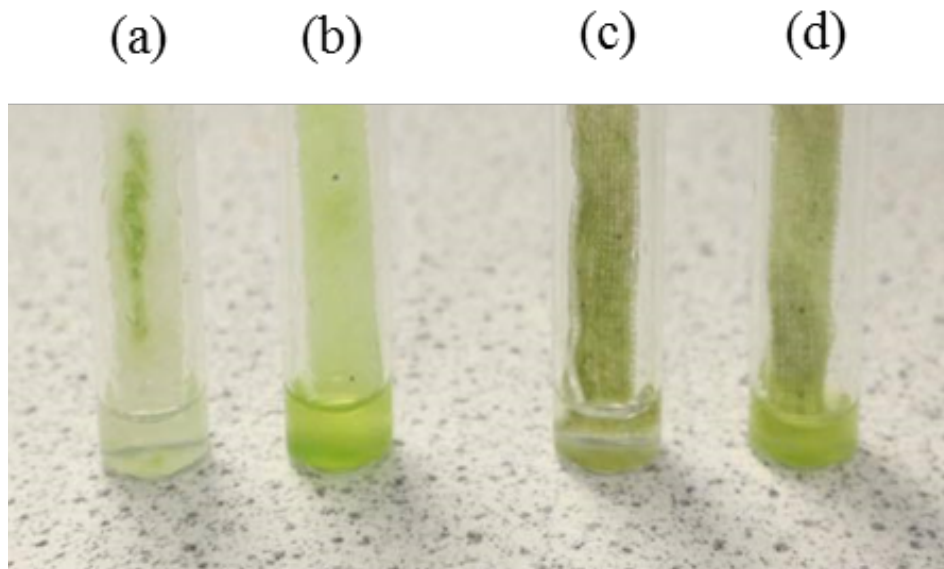
Figure 3.9 Loss of cells from the biocomposite to the BG-11 medium pool for: (a) kappa-carrageenan coated polyester, (b) uncoated polyester, (c) coated cotton, and (d) uncoated cotton biocomposites after one week of the CO_2 fixation test.
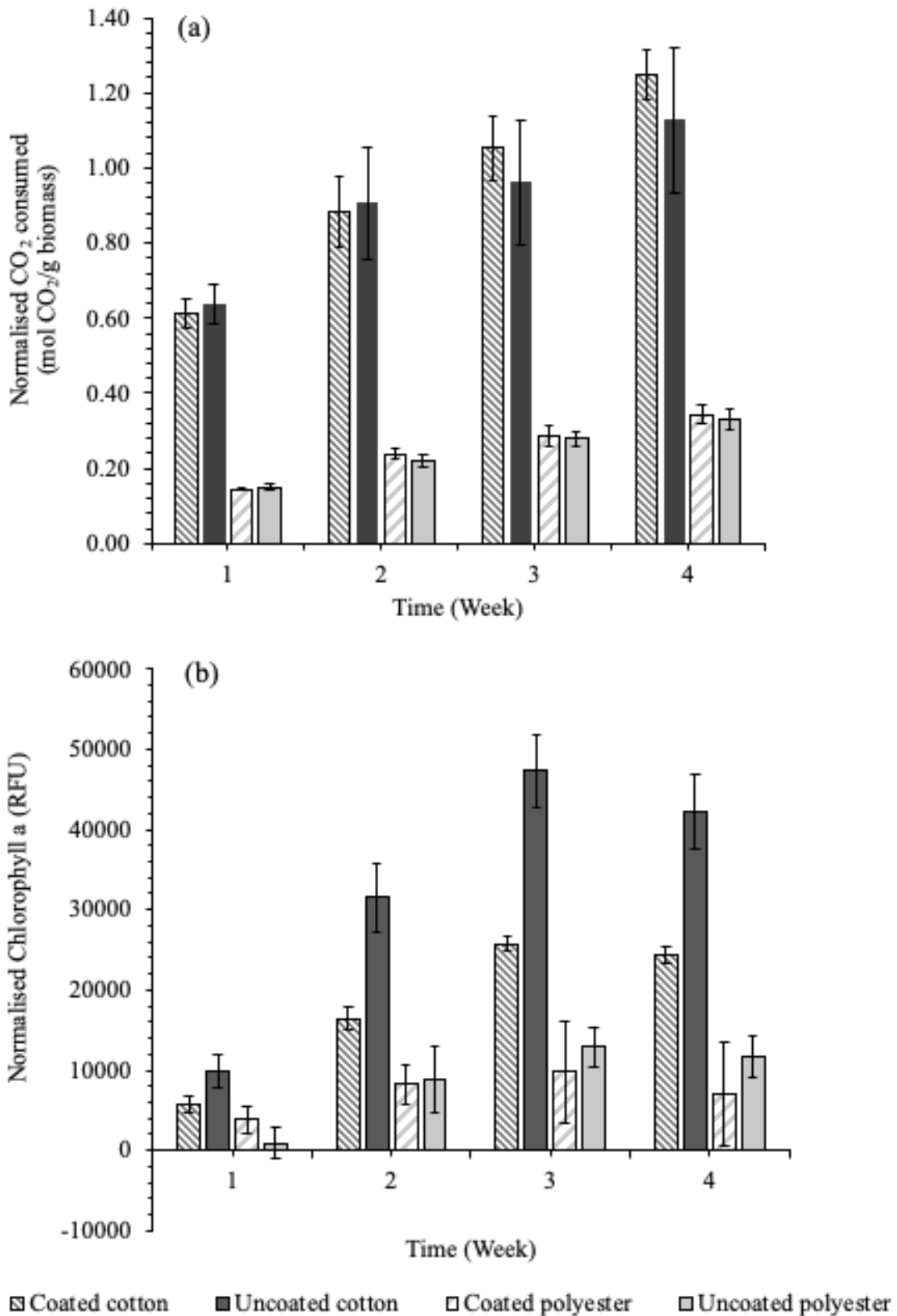
Figure 3.10 Cumulative net CO_2 fixation (a) and change in chlorophyll a fluorescence intensity (b) of biocomposites on a weekly basis normalised to the biomass retained within the biocomposite. Mean ± StDev, n = 3.

3.3.4 Effect of textile blends on natural attachment

After 14 days, *C. vulgaris* had attached to all of the textiles (Figure 3.11a), but the quantity of chlorophyll *a* extracted differed by treatment (ANOVA: F = 5.22, DF = 3, P = 0.027), with the lowest in 100PE (0.794 ± 0.19 μg cm^{-2}), but this was significantly lower than only the 65PE treatment. The abiotic controls indicated that there was mass loss from degradation of the cotton over time (Figure 3.11b) (ANOVA: F = 14.89; DF = 3; P = 0.001). This material loss was used to normalise the percentage biomass change in the samples. There were no significant differences between any of the cotton containing textiles. In contrast, the percentage biomass change was highest for 100PE (2.08 ± 1.11%, median ± range) (ANOVA: F = 25.16, DF = 3, P = <0.001; Figure 3.11c).
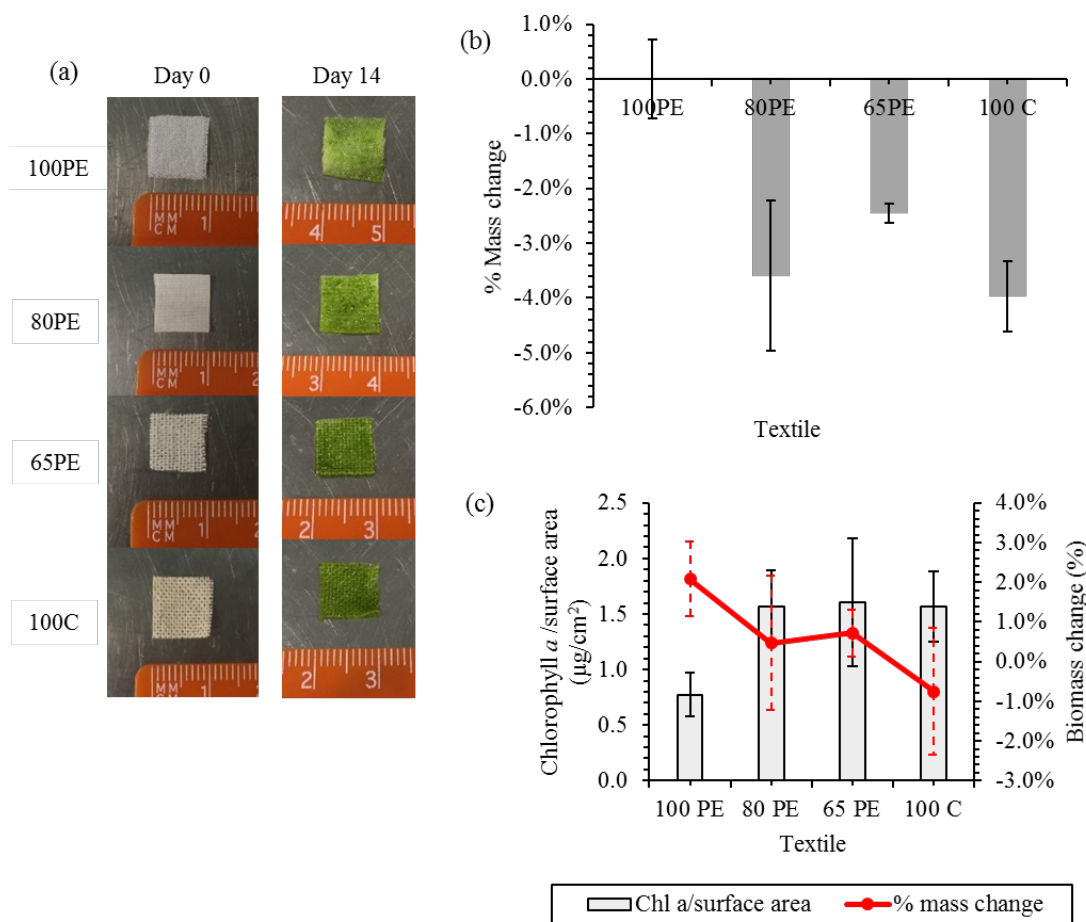
Figure 3.11 Uncoated immobilisation test of different textile blends: 100% polyester (100PE), 80% polyester and 20% cotton (80PE), 65% polyester and 35% cotton (65PE), and 100% cotton (100C). (a) Comparison of textiles on days 0 and 14; (b) percentage mass change of the textiles in abiotic controls exposed to BG-11 medium after 14 days; (c) chlorophyll *a* content and the percentage biomass change of the biocomposites after 14 days. Mean ± StDev, n = 3.

3.4 Discussion

The cotton based biocomposites captured significantly more CO_2 than the polyester versions, while both biocomposite types outperformed the algae suspension controls (Table 3.2). There are no clear explanations based on the physical characteristics of either textile. The cotton had a higher void space percentage than the polyester due to the open weave of the yarns. The polyester presented a larger surface area but this was not translated into greater biomass attachment. The explanation may lie in the greater hydrophilicity of the cotton (Madan et al., 1978), which would allow the cells to access water and dissolved nutrients more effectively. However, this also needs to be considered from the context of the surface charge of the materials. During the cell-attachment stage of the production of the algae biocomposites, the solid surface of the fibres and the ions in the BG-11 media form an electrical double layer. In the BG-11 media there is a layer of bound ions (Stern Layer) and a diffuse layer of less strongly bound ions. Luxbacher and co-workers discuss the electrical double layer in the context of textile surfaces (Luxbacher et al., 2016). The zeta potential measures the net charge within the diffuse layer and can be used to characterise the electrostatic repulsion/attraction between solid surfaces. Over the likely pH range experienced during the experiments (pH 7-8.5), cotton has a surface charge (zeta potential) approximating to -15 to -20 mV, polyester is between -60 to -65 mV (Grancaric A.M. et al., 2005), *Chlorella vulgaris* is -17 to -18 mV (Alkarawi et al., 2018) and kappa-carrageenan is -50 mV (Ellis et al., 2019). The large zeta potential difference between the algae and the polyester fibres would tend to create a repulsive force that does not favour *Chlorella* attachment, leading to the release of algae cells into the BG-11 medium and gravity settling of these cells to the base of the vial (Figure 3.9). The zeta potential of the cotton and *Chlorella* suggests that they will repel each other, although this maybe counteracted the Van der Waals forces of attraction between the complex polysaccharides on the cotton surface and those that surround the cell wall of the *Chlorella* (Notley et al., 2004).

The application of a kappa-carrageenan topcoat marginally enhanced net CO_2 uptake of the cotton biocomposites by retaining the cells on the textiles, despite the uncoated cotton biocomposite having a markedly higher chlorophyll fluorescence. This performance improvement was not mirrored with the polyester. Despite the use of a topcoat, the algae still tended to detach with time, indicating potential degradation of kappa-carrageenan gel. Kappa-carrageenan forms a rigid gel when cross-linked with KCl solution; however, its structure and the capacity for certain chemicals to diffuse through it may still be modified by further exposure to water (Tavassoli-Kafrani et al., 2016). Hence, alternative binding techniques or stronger gel coatings should be explored to increase biocomposite robustness.

Table 3.2 Net CO_2 fixation rates of the textile biocomposites and suspension control.

Treatments	Net CO_2 fixation rate (Mean ± StDev)			
	mmol CO_2 $g^{-1}_{biomass}$ d^{-1}	g CO_2 $g^{-1}_{biomass}$ d^{-1}	mmol CO_2 m^{-2} d^{-1}	g CO_2 m^{-2} d^{-1}
Coated cotton	41.29 ± 2.17	1.82 ± 0.10	106.80 ± 5.60	4.70 ± 0.25
Uncoated cotton	35.17 ± 6.06	1.55 ± 0.27	90.96 ± 15.68	4.00 ± 0.69
Coated polyester	11.09 ± 0.85	0.49 ± 0.04	91.58 ± 7.00	4.03 ± 0.31
Uncoated polyester	9.55 ± 0.72	0.42 ± 0.03	78.92 ± 5.94	3.47 ± 0.26
Suspension	3.73 ± 0.31	0.16 ± 0.01	27.63 ± 2.29	1.22 ± 0.10

Table 3.3 Comparison of net CO_2 fixation rates with other *Chlorella* based studies.

Species and strain	System description	CO$_2$ fixation rate		Reference
		(mmol CO_2 m^{-2} d^{-1})	(g CO_2 g^{-1} $_{biomass}$ d^{-1})	
C. vulgaris ESP-31	1L vertical tubular photobioreactor at 25 °C, light: 60 mol m^{-2} s^{-1}	89.39*	0.21*	(Yeh and Chang, 2011)
Chlorella sp.	10L cylindrical glass reactor at 26 °C; light: 87.75 μmol m^{-2} s^{-1}	227.9*	0.624	(Pourjamshidian et al., 2019)
C. vulgaris CCAP 211/11B	2.4L cylindroconical bubble-column photobioreactor; light: illuminated area 0.1096 cm^2	-	0.24*	(Clément-Larosière et al., 2014)
C. vulgaris	250 mL culture in cylindrical glass column; light: 250 μmol m^{-2} s^{-1}	6.74*	0.30*	(Znad et al., 2019)
Chlorella fusca LEB 111	Cultivated on CO_2 adsorbent nanofibers in 0.45 L PBR at 25 °C; light: 41.6 μmol m^{-2} s^{-1}	-	0.27	(Vaz et al., 2019)
C. vulgaris	15 L tubular reactor at 25 °C with continuous 8% v/v CO_2 (100 L h^{-1}); light: >twice daylight	-	0.91	(Adamczyk et al., 2016)
C. vulgaris	Coated cotton biocomposite at 18 °C; light: 16:8 photoperiod at 30.5 μmol m^{-2} s^{-1} with 5% v/v CO_2 in semi-batch	106.8	1.82	This study
C. vulgaris	Coated polyester biocomposite at 18 °C; light: 16:8 photoperiod at 30.5 μmol m^{-2} s^{-1} with 5% v/v CO_2 in semi-batch	91.58	0.49	This study

*Estimated values from given experimental setups and information from the studies.

Following the initial experiments comparing cotton with polyester, an experiment was conducted using uncoated cotton/polyester blends to ascertain whether textile blends could overcome the limitations of the respective pure fabrics. As for the CO_2 fixation experiments, passive cell attachment was used whereby the textiles were immersed in BG-11 containing *C. vulgaris* for 14 days; however, a separate BG-11 only treatment was run to investigate the structural robustness of the textiles (determined as textile mass change). There was a noticeable mass lost on all the cotton-containing textiles over the 14 days, indicating biodegradation of the cotton, although there was no relationship with the proportion of cotton in the blend. The polyester-only material had no net mass change. These data were then used to normalise the mass change due to biomass growth from the microalgae experiment, showing that despite increased chlorophyll content (biomass loading was determined by chlorophyll *a* extraction rather than in situ fluorescence) relative to the polyester-only treatment, all cotton containing biocomposites either maintained mass or lost mass in the case of cotton-only. These data indicate that during the cell loading phase of biocomposite fabrication, natural fibres (i.e. cotton) can be degraded and may therefore perform sub-optimally. By extrapolation, if we apply this knowledge retrospectively to the CO_2 capture trials it is clear that there are performance gains to be made if the degradation of the cotton can be slowed or eliminated. It would be important to determine whether the degradation rate of the cotton when totally submerged in growth media was the same during high humidity exposure as defined the CO_2 fixation trials. This would be broadly in line with other studies using cotton as an attachment substrate (Gross et al., 2013, Christenson and Sims, 2011, Christenson and Sims, 2012, Rajendran and Hu, 2016). Similarly, it will be necessary to determine whether topcoats can, in addition to promoting cell retention, also protect the cotton from degradation.

It is not straightforward to compare our study with other microalgae-based studies for carbon capture as there are not any agreed standards, with trials having differing conditions such as light exposure, culture arrangement, nutrient provision and the algae species used. Further, there are no agreed standards for data reporting. The majority of studies have grown microalgae in suspension at various scales and using a broad suite of photobioreactor designs and configurations; very few have used biofilm techniques (either natural or engineered) (Clément-Larosière et al., 2014, Yeh and Chang, 2011, Pourjamshidian et al., 2019, Znad et al., 2019, Adamczyk et al., 2016, Vaz et al., 2019). In Table 3.3, we attempt to compare our study with others that have used *Chlorella* species. The textile biocomposites' net CO_2 absorption rates compared favourably, particularly the cotton system when calculated on a per unit biomass basis (g CO_2 $g^{-1}_{biomass}$ d^{-1}). Vaz et al. (Vaz et al., 2019) cultivated *C. fusca* cells onto nanofibers,

attaining 0.27 g CO_2 g^{-1}$_{biomass}$ day^{-1}; our biocomposites outperformed this by almost seven- and twofold for coated cotton (1.82 ± 0.10 g CO_2 g^{-1}$_{biomass}$ d^{-1}) and coated polyester (0.49 ± 0.04 g CO_2 g^{-1}$_{biomass}$ d^{-1}) respectively.

It should also be noted that most photobioreactor studies use significant quantities of water whereas our biocomposites require only small volumes to operate; in effect only requiring a humid atmosphere, enabling our system to both tackle CO_2 emissions and address water shortage issues. However, the overall sustainability of these biocomposites needs to be viewed in the context of the environmental impact of the cotton growing industry, particularly its very high water demand (Duque Schumacher et al., 2020, Esteve-Turrillas and de la Guardia, 2017). Nonetheless, future studies should consider evaluating the potential to utilise recycled cotton e.g. from the fashion industry. CO_2 capture biocomposites may offer an alternative use for end-of-life clothing and other textiles.

3.5 Conclusion

Textile biocomposites developed in the current study had enhanced CO_2 capture compared to their suspension controls. Textile biocomposites operate successfully with substantially reduced water use, offering a "low-water low-maintenance" system that overcomes many issues incumbent in conventional open pond or suspension based photobioreactor systems. However, issues surrounding the degradation of both the gel topcoat and the cotton substrates need to be overcome to extend the operational life of the biocomposites.

Chapter 4

Living loofah-based cyanobacteria biocomposites for intensifying and sustaining carbon dioxide capture

Abstract

Microalgae and cyanobacteria have been evaluated for biological CO_2 capture from flue gases for over 40 years; however, commercial open ponds and photobioreactors suffer many drawbacks including a slow rate of CO_2 capture and high water usage. An intensified 3D cell immobilisation approach with a small water demand is evaluated here by coating latex binders onto defined surface area (947 m^2 m^{-3}) and void space (81.78 ± 4.41 %) loofah sponge scaffolds to form porous 3D biocomposites with two strains of *Synechococcus elongatus* cyanobacteria. Latex binder toxicity and adhesion screening protocols were established to select adhesive binders for eight weeks semi-batch CO_2 fixation trials. Six commercial bio-based binders (Replebin®) were tested and found that AURO 321 and 320 were non-toxic to cyanobacteria. The average net CO_2 fixation rates were 0.68 ± 0.18 and 0.93 ± 0.30 g CO_2 $g^{-1}_{biomass}$ d^{-1} for *S. elongatus* PCC 7942 and *S. elongatus* CCAP 1479/1A respectively. These rates were enhanced by 9-10 folds compared to their suspension controls. This equates to predicted CO_2 capture of scaled systems up to 340.11 ± 110 tCO_2 $t^{-1}_{biomass}$ yr^{-1}.

Keywords: living biocomposites, cyanobacteria, carbon capture and storage; intensified carbon capture, latex immobilisation

4.1 Introduction

Carbon capture and storage (CCS) technologies are being developed as part of a suite of approaches to combat CO_2-driven climate warming (Cuéllar-Franca and Azapagic, 2015, Leung et al., 2014, Haszeldine, 2009). CCS technologies are considered particularly relevant for major point source emitters such as power stations, cement factories and steelworks. Several CCS technologies can capture CO_2 from flue gas, including solvent-based chemical absorption approaches (e.g. monoethanolamine), together with cryogenic, membrane and adsorption methods (Wilberforce et al., 2019). Post capture, the CO_2 can be injected directly into geological reservoirs for long-term sequestration. However, these processes are expensive, require suitable geological features and, paradoxically, are energy intensive with a substantial carbon footprint (Wolsky et al., 1994).

CCS renders the CO_2 permanently inaccessible. A parallel approach centred on carbon capture and utilisation (CCU — also known as carbon capture and conversion) aims to repurpose the captured CO_2 for use in industrial processes, e.g. ammonia and cement manufacture, or to transform it into chemically stable consumer goods, e.g. plastics (Baena-Moreno et al., 2018). CCU approaches are advantageous insomuch as they produce marketable goods at the end of the CO_2 value chain (potentially offsetting some of the associated CO_2 capture costs) (Markewitz et al., 2012); however, this is at the expense of the degree of permanency of CO_2 sequestration. CCU should therefore be regarded as adding additional short term loops (on a geological scale) into the global carbon cycle rather than facilitating permanent CO_2 storage (Cuéllar-Franca and Azapagic, 2015).

It is possible to mimic nature and capture CO_2 using biological approaches by harnessing and engineering the innate CO_2-fixing capabilities of photoautotrophic organisms (plants, algae, phototrophic bacteria) (Singh and Dhar, 2019, Noble et al., 2012). Phototrophs fix CO_2 into sugars using the bidirectional enzyme ribulose-1,5-bisphosphate carboxylase/oxygenase (RuBisCo), with algae and cyanobacteria further benefiting from carbonic anhydrase as a carbon concentrating mechanism (Mondal et al., 2016). CO_2 captured through biological pathways is particularly amenable for CCU exploitation, potentially yielding additional benefits over and above the final carbon product, such as remediating wastewaters (de-Bashan and Bashan, 2010). However, to support their carbon fixing pathways phototrophs require exposure to light (natural or artificial) in addition to water and nutrients; thus adding significant costs to the process (Singh and Dhar, 2019).

Numerous studies have shown that microalgae and cyanobacteria absorb CO_2 from industrial flue gas (up to 20% v/v) (Olaizola, 2003b), with evidence that some species may even prefer flue gas over pure CO_2 streams (Douskova et al., 2009). These organisms (depending on species) can readily convert CO_2 into valuable metabolites e.g. lipids for biodiesel conversion or synthesis of bioplastics, with some species (especially those belonging to the *Synechococcus* and *Synechocystis* genera) capable of storing CO_2 as calcium carbonate ($CaCO_3$); potentially consolidating both CCU and CCS in one organism (Lee et al., 2004). Furthermore, many microalgae and cyanobacteria can tolerate reasonably high temperatures (Hanagata et al., 1992), thus reducing the need for flue gas cooling prior to contact.

Approximately, 70% of trials of microalgae and cyanobacteria for carbon capture have used open pond systems. Open ponds are relatively inexpensive to build, however they require substantial land and water, and are vulnerable to biological contamination (Borowitzka, 1999). Further, open culture systems are exposed to variable weather and climate conditions, which compromise performance. Closed culture systems (photobioreactors, PBR) can overcome many of these drawbacks and support enhanced biomass productivity for greater CO_2 removal and wastewater treatment (Naderi et al., 2015, Kumar et al., 2011, Chiu et al., 2009b). However, PBRs are complex and more expensive to construct and maintain (Cheah et al., 2015). Additionally, PBRs use significant volumes of water, have limitations in terms of uniform illumination, and are more energy intensive for mixing and CO_2 mass transfer than open ponds. This increases the production cost of algal biomass to around 9 to 10 € kg^{-1} biomass for an ideal PBR compared with 1.6 to 1.8 € kg^{-1} for an ideal raceway pond system (Slade and Bauen, 2013).

If microalgae and cyanobacteria are to make meaningful contributions to CCS and CCU, new approaches that significantly intensify the rate of CO_2 absorption are needed. One such approach — the concentration, encapsulation and immobilisation of photosynthetic organisms within a thin matrix coating — draws inspiration from plant leaves and natural biofilms. These matrix-entrapped live organisms, also known as biocomposites, are being evaluated for applications such as intensifying wastewater treatment, microbial air purification, and carbon capture (de-Bashan and Bashan, 2010). The increased cell loading facilitated by immobilisation can significantly enhance volumetric absorption productivity, biosorption capacity and microalgae specific activity (Eroglu et al., 2015). In addition, biocomposites require less space and are easy to handle (Mallick, 2002, Tamponnet et al., 1985). However, the mechanical limitations of the predominant immobilisation technology (hydrogels) fails to support cells for

long-term storage under dry or frozen conditions, resulting in cell damage and leaching (Webb and Dervakos, 1996). Alternative adhesive coating techniques that are robust, inexpensive and easy to implement at scale using industrial coating technology may overcome these problems.

One non-hydrogel approach was developed by Bernal (Bernal et al., 2014), wherein cyanobacteria within a latex binder wet coating on hydrated paper yielded a 10-fold greater specific photosynthetic rate relative to suspension cultures, with CO_2 fixation sustained for up to 500 hours. Additionally, Flickinger (Flickinger et al., 2007) argued that nanoporous latex coatings protect the cells from bacterial contamination.

In addition to paper scaffold systems, numerous synthetic scaffolds have been tested with varying degrees of success, including textiles, polyurethane foam, porous glass and ceramics (de-Bashan and Bashan, 2010, Martins et al., 2013); however, fixation rate and performance suffered from poor cell retention and/or toxicity. Natural scaffold materials may present more options. Loofah sponge H(the dried fruit of the edible *Luffa* plant) offers a natural high surface area scaffold with three-dimensional (3D) geometry. Commercially, the xylem-rich fibrous structure is used as a bathing and exfoliating aide, has been studied for blending with plastics to create bioplastics packaging (Masmoudi et al., 2016), and has been tested for numerous biotechnology applications (Acosta-Rubí et al., 2017, Baena-Moreno et al., 2018, Stella and Vijayalakshmi, 2019, Zainab et al., 2019, Saeed and Iqbal, 2013). Loofah should be suitable for phototroph immobilisation as the highly porous structure should support excellent gas exchange and facilitate effective light transmission to a reasonable depth. Additionally, the fibres are moderately hydrophilic (Chen et al., 2018) which may prove effective at retaining moisture within the structure. Microalgae and fungi have successfully been immobilised onto loofah for metal recovery from wastewater, producing enhanced biosorption capacities relative to suspension culture controls (Akhtar et al., 2004b, Iqbal and Edyvean, 2005, Akhtar et al., 2003b, Sriharsha et al., 2017). To our knowledge, loofah-based biocomposites have yet to be assessed for gaseous carbon capture applications. Using an iterative screening process, the current work has evaluated the toxicity and effectiveness of latex binder coatings to immobilise industrially relevant live microalgae and cyanobacteria onto loofah to develop stable and inexpensive 3D biocomposites (see Figure 4.1) for carbon capture applications, with an initial target operational longevity exceeding 1000 hours.
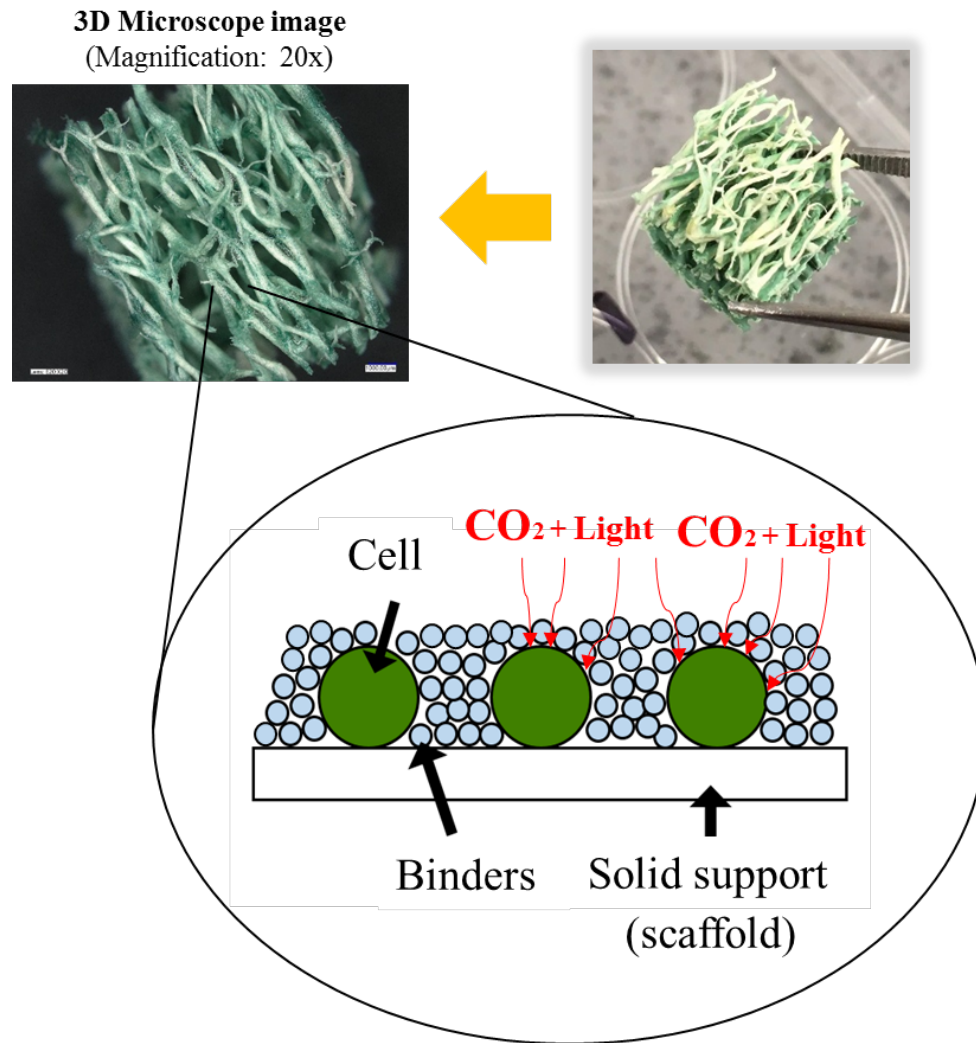
Figure 4.1 Theoretical biofilm arrangement on loofah based biocomposites comprising cells and binder particles on loofah scaffold.

4.2 Materials and methods

4.2.1 Organisms, media and growth conditions

Two cyanobacteria strains (*Synechococcus elongatus* CCAP 1479/1A purchased from Culture Collection of Algae and Protozoa SAMS Limited and PCC 7942 donated from Consejo Superior de Investigaciones Cientificas, Madrid, Spain) were used to produce biocomposites with the bio-based binders. DNA sequencing of *S. elongatus* PCC 7942 was performed after received for confirmation. *S. elongatus* PCC 7942 and CCAP 1479/1A were cultivated in BG11 medium and JM medium respectively. All cultures were grown in 10L polycarbonate carboys (Nalgene), with constant HEPA filtered aeration using an aquarium pump (KOI AIR 50 Blagdon), and maintained at the default conditions of our microalgae growth suite i.e. 18 ± 2 °C with a 16:8 h light:dark cycle with 2,500 lux ($\approx$ 30.5 μmol m^{-2} s^{-1}; (Thimijan and Heins,

1982)) of illumination provided by 30W daylight-type fluorescent tubes (Sylvania Luxline Plus, n = 6).

4.2.2 Latex binders

Six bio-based (plant based; Replebin®) emulsions were purchased from AURO Paint Company, UK (Table 4.1). The pH of all binders was adjusted to within 7.5-6.5 using 0.1 and 0.5 M acetic acid due to initial pH of all binders were basic. Solids content was determined using dry weight by drying at 100 °C overnight and left in the desiccator for 24 hours before re-weighed on a precise five digit digital balance.

Table 4.1 Name, coding and available compositional details of the bio-based latex binders.

Binder name	Binder code	Main components	% Solid
AURO Ecological dispersion wall paint	321	Mineral fillers, water, Replebin, titanium dioxide, cellulose, surfactants made of rapeseed-, castor oil, ammonia and thiazoles	52.85
AURO Ecological dispersion wall paint	320	Mineral fillers, water, Replebin, titanium dioxide, cellulose, surfactants made of rapeseed- castor oil, ammonia and thiazoles	52.57
AURO Clear lacquer glossy	251	Water, colophony glycerol ester with organic acids, mineral fillers, sunflower oil, linseed oil, drying agents (cobalt-free), caster stand oil, surfactants, amino soap, silicic acid, cellulose, fatty acids	29.10
AURO Clear lacquer matt silk	261	Water, colophony glycerol ester with organic acids, mineral fillers, sunflower oil, linseed oil, drying agents (cobalt-free), caster stand oil, surfactants, amino soap, silicic acid, cellulose, fatty acids	19.52
AURO Woodstain transparent	160	Water, linseed oil, colophonium glycerine ester with organic acids, mineral fillers, surfactants, mineral pigments, silicic acids, dryers (cobalt-free), castor stand oil, sunflower seed oil, titanium dioxide, ammonium soaps, cellulose, fatty acids	13.68
AURO Color wash binder	379	Water, ammonium soap, ammonium carbonate, alcohol	9.01

4.2.3 Loofah characterisation

Loofah sponges were purchased from retail outlets. The surface area was determined as follows: a representative sample (approximately 5 × 1 × 1 cm) was embedded in an epoxy resin within a silicon mold and cured for 48 h at 20 °C (100 parts EpoxiCure 2 to 23 parts hardener by weight, containing five drops of black acrylic liquid pigment to enhance contrast). Sections (1 mm thick) were cut using a Buehler IsoMet Low Speed Saw at 100 rpm. Sections were imaged using a digital HD camera (Canon EOS M10 fitted with an EF-M 15-45 mm 1:3.5-6.3 IS STM Canon zoom lens) and the loofah strand perimeter per area (mm mm^{-2}) was determined using ImageJ software.

Light penetration (transmitted photosynthetic active radiation, PAR) through different loofah sections (whole loofah in the vertical orientation, 100.8 ± 0.27 mm height; whole loofah horizontal orientation, 54.63 ± 0.72 mm diameter; half loofah horizontal orientation, 13.01 ± 0.43 mm) was measured using a Skye PAR Quantum Sensor under natural sunlight (1500 hrs BST, July 3rd, 2019, full sunlight) (equation 4.1). The sensor was held within a lightproof tube to prevent peripheral light from distorting the readings. Ambient sunlight PAR (mean ± StDev = 1902 ± 39 μmol m^{-2} s^{-1}) was recorded before and after each loofah sample. All measurements were in triplicate.

$$\% \text{ PAR loss with depth (mm)} = \frac{[\text{transmitted PAR/ambient PAR}]}{\text{Loofah distance}} \qquad (4.1)$$

4.2.4 Contact toxicity test

After pH adjustment, binders were formulated to have 5% w/w solids content using deionised water (dH$_2$O). Approximately 1 ml of each binder was mixed with 1 ml of cell culture in 24-multiwell plates. The cell/binder mixtures were cultured for 7 days (20 °C, 16:8 light:dark photoperiod at 2,500 lux ($\approx$ 30.5 μmol m^{-2} s^{-1}; (Thimijan and Heins, 1982)). After 7 days the samples were diluted by a factor of 20 using sterile dH$_2$O and cell counts were conducted using an improved Neubauer Hawksley haemocytometer relative to suspension controls.

4.2.5 Cell adhesion test

A wet cell paste (WCP) was obtained for each cyanobacterial strain by centrifuging 2 L of culture of known cell density. The centrifugation conditions were 30 mins at 1717 RCF. Loofah

were autoclaved, then dried at 105 °C for 3 h. After drying, they were stored overnight in a desiccator prior to immobilisation. For immobilisation, the loofah was cut into approximately $1 \times 1 \times 1$ cm cubes and placed in 24-multiwell plates. The binder mixtures were formulated as per the contact toxicity test. Each binder was mixed with 2.5% WCP and vortexed for 10 to 20 seconds (Vortex Genie 2, Scientific Industries, Inc.) until uniform. Approximately 1 ml of the cell/binder mixture was pipetted onto each loofah cube and dried at 30 °C for 24 h. The cells in the mixture were counted and dried separately to along with the samples in order to determine number of cells immobilised. Each formed biocomposite was submerged in 2 ml of growth medium and shaken in darkness at 80 rpm for 1, 24, 48 and 72 h. The growth medium was refreshed at each stated time interval and any cells released from the loofah surface were counted using a haemocytometer and converted to a percentage of the cells loaded onto the loofah scaffold. A weighted decision matrix technique (Kosky et al., 2013) was used to identify the most suitable binders for each species based on toxicity and adhesion affinity to the loofah scaffold. Toxicity was given a higher ranking (ratio 3:2) as the maintenance of cell viability was deemed the more important characteristic.

4.2.6   Semi-batch CO_2 fixation test

Six hundred microlitres of cell/binder formulation (2.5% w/v WCP and 2.5% solid binder) was used to make biocomposites. A conservative cell loading strategy was adopted to limit any self-shading effects relative to a comparative biocomposite study (Bernal et al., 2014). Each formulation was carefully pipetted onto one end of dried, autoclaved, pre-weighed loofah strips (dimension 1×5 cm w $\times$ h) and dried for 24 hours at 20°C. It was assumed that all cells added to the WCP were successfully immobilised within the adhesive binder; however, the macroporous structure of the loofah caused some of the formulation to flow to waste, therefore a 100% cell loading efficiency was not achieved. To account for this, the mass of formulation dried onto the loofah was determined and normalised to a reference dried formulation. Abiotic controls comprising loofah, binder and sterile growth medium were similarly established.

For batch CO_2 fixation tests (8 weeks running time), the biocomposites were placed in triplicate into 50 ml glass bottles containing 5 ml of growth medium (Figure 4.2). The bottles were sealed with 20 mm butyl rubber stoppers and crimped using silver aluminium caps. Once sealed, 45 ml of 5% CO_2/air gas mixture was injected with an airtight syringe. Triplicate suspension controls using appropriate growth media were established with a cell density equivalent to the cell loading within the biocomposite. The samples were maintained at 18 ± 2 °C with a 16:8 light:dark photoperiod at 2500 lux. The percentage of CO_2 fixed was determined

every 2 days by extracting the headspace with an airtight syringe and injecting into a GEOTech G100 infrared absorption CO_2 meter. The equivalent volume of CO_2 gas mixture was refreshed.
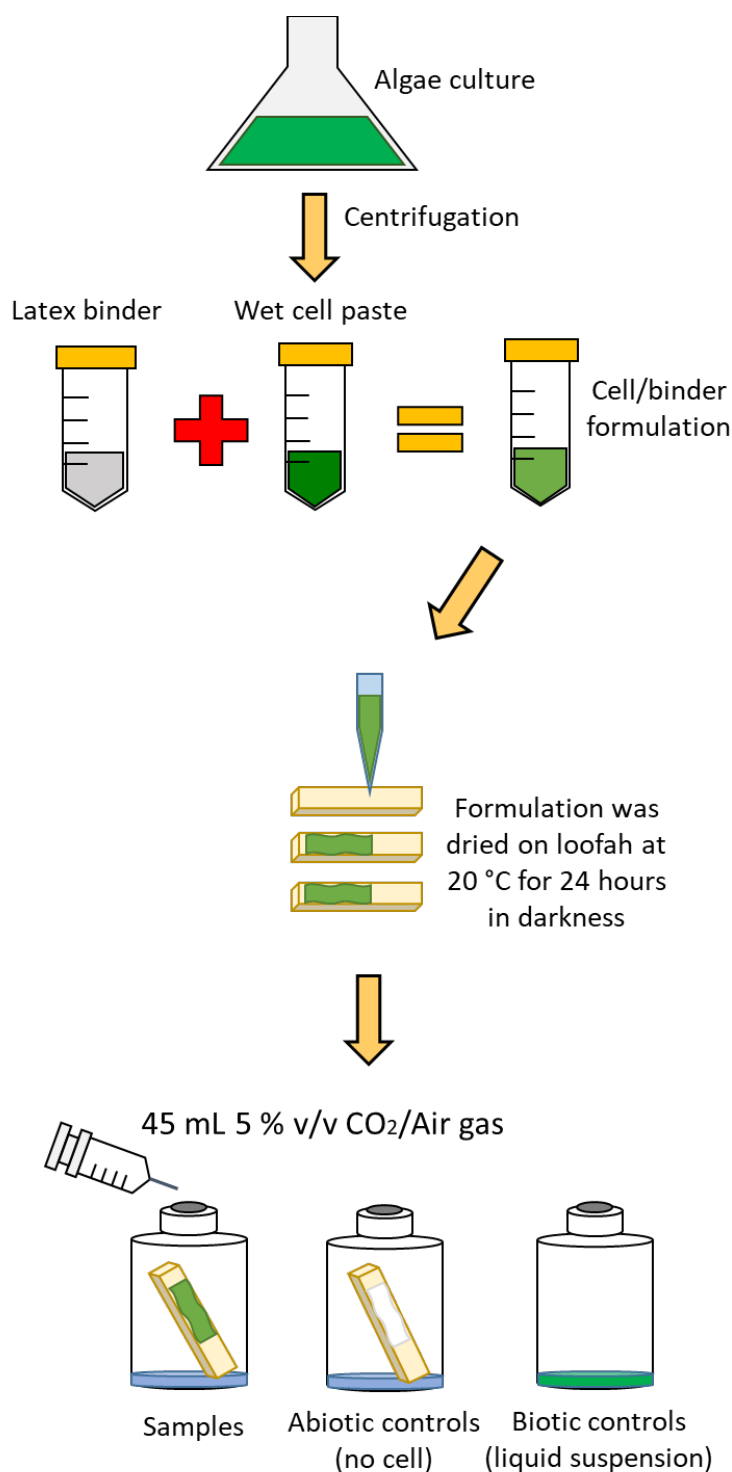
Figure 4.2 A schematic sequence of the process used to immobilise microalgae or cyanobacteria on loofah sponge using latex binders for the batch CO_2 fixation test.

The opacity of the binders, coupled with the 3D structural complexity of the loofah, made direct cell counts impractical, therefore growth was estimated based on mass changes.

The net quantity of CO_2 fixed by the immobilised cells (dry biomass basis) was calculated based on the total immobilised biomass (after normalising to the abiotic and growth medium controls). Biomass was determined based on the difference in weight of the loofah before and after immobilisation after binder density was taken into account. The net CO_2 fixation rate was calculated using equation 4.2, where P is gas pressure (kPa), V is gas volume (l), R is ideal gas constant (J K mol^{-1}), T is temperature (K) and IDW is immobilised dried weight of biomass (g).

$$net\ CO_2\ fixation\ rate\ \left(mol\ CO_2\ g_{biomass}^{-1}\ day^{-1}\right) = \frac{\%\ CO_2\ fixed \times \frac{PV}{RT}}{IDW \times 2\ days} \quad (4.2)$$

To calculate the CO_2 fixation rate per unit surface area, the following assumptions were made: the percentage of void area was the same throughout the structure, i.e. the perimeter to area ratio is equivalent to surface area per volume (mm^{-2} mm^{-3}); loofah does not consume CO_2; the cell/binder formulation was uniformly distributed across the loofah surface; and there was no outgrowth of cells beyond the estimated surface area.

4.2.7 Biocomposite microstructure analysis

Raw loofah was imaged in 3D using a Nikon XTH 225 ST high resolution x-ray computed tomography scanner with a 225 kV UltraFocus Reflection Based Signal and Tungsten Target with a Perkin Elmer 1620 AN3 CS CT detector. The biocomposites were analysed using scanning electron microscopy (SEM) before and after adhesion testing and after the 8 weeks batch net CO_2 fixation test. Samples were dried at 105 °C for 3 h and stored in a desiccator before being attached to 12 mm diameter pin stubs using carbon tape. The instrument was a Hitachi TM 3000 SEM equipped with a backscattered electrons system for digital image acquisition. All coatings were observed in two or more randomised locations using a 5 or 15 kV accelerating voltage. Each location was imaged multiple times using sequential magnifications ranging from 15× to 30,000× to characterise surface topography, cell distribution and available pore space.

4.2.8 Analysis of CO_2 transfer kinetics

The kinetics of CO_2 transport from the gas phase to the cells immobilised with coatings on loofah scaffolds were analysed using the CO_2 absorption rate data from the semi-batch tests and by solving the unsteady state diffusion equation. The rate of CO_2 (R_{CO2}) is given by equation 4.3, where Ka_C is the volumetric transfer coefficient (s^{-1}) and c is the concentration in the gas or liquid phase (mols m^{-3}).

$$R_{CO_2}(mols\ m^3\ s^{-1}) = Ka_C c \qquad (4.3)$$

Equation 4.3 is written for CO_2 transport from the bulk liquid or gas phase to inside the cell assuming that the CO_2 concentration in the cell is zero due to photosynthesis. For the suspension controls, the cells were surrounded by liquid and the volumetric transfer coefficient was calculated by solving equation 4.4, where c^L is the CO_2 concentration in the liquid (mols m^{-3}), $D_{CO_2}^L$ is the diffusivity of CO_2 in the culture medium (1.92 x 10^{-9} m^2 s^{-1}), t is the time (s) and z is the vertical distance in the vial measured from the gas-liquid interface (m).

$$\frac{\partial c^L}{\partial t} = D_{CO_2}^L \frac{\partial^2 c^L}{\partial z^2} - Ka_C c^L \qquad (4.4)$$

Equilibrium was assumed to exist at the interface between the gas and the culture medium. The equilibrium was modelled using Henry's Law. For the biocomposite samples the cells are surrounded by gas and the volumetric transfer coefficient was calculated by solving equation 4.5, where c^G is the CO_2 concentration in the gas (mols m^{-3}), $D_{CO_2}^G$ is the diffusivity of CO_2 in the gas phase (1.6 x 10^{-5} m^2 s^{-1}) and x and y are horizontal distances perpendicular to the vertical axis of the sample vial (m).

$$\frac{\partial c^G}{\partial t} = D_{CO_2}^G \left(\frac{\partial_2 c^G}{\partial x^2} + \frac{\partial_2 c^G}{\partial y^2} \right) - Ka_C c^G \qquad (4.5)$$

Equations 4.4 and 4.5 were solved over the 48 hour period between fresh gas injections ($c_0^G = 2.04$ mols m^{-3}). The value of the transfer coefficient was adjusted until the concentrations predicted by equations 4.4 and 4.5 matched the values measured in the gas at the end of the 48 hours period. Data from day 14 of the semi-batch test onwards were used. Full details about the solution of equations 4.4 and 4.5 are given in the Appendix I (Figure S1-S4, Table S1).

4.2.9 Statistics

Data were statistically analysed using Minitab 17. Toxicity and adhesion data were not normally distributed and were analysed using Kruskal-Wallis tests with Mann-Whitney U-tests. Cumulative net CO_2 fixation data from the batch test were analysed by one-way analysis of variance (ANOVA) with Tukey's Honest Significant Difference post-hoc test at 1104 h (corresponding to the final data obtained from the suspension controls) and at the termination of the experiment (1344 h).

4.3 Results

4.3.1 Loofah characterisation

The loofah had a surface area available for coating equivalent to 947 $m^2\,m^{-3}$ with a void space (for gas exchange and light penetration) of 81.78 ± 4.41 %. The loss in absolute transmitted PAR was greatest in the whole loofah in the horizontal orientation (from 1927 ± 20 to 71 ± 22 μmol $m^{-2}\,s^{-1}$), followed by the whole loofah in the vertical orientation (from 1851 ± 11 to 98 ± 2 μmol $m^{-2}\,s^{-1}$), and the half loofah (from 1930 ± 2 to 146 ± 3 μmol $m^{-2}\,s^{-1}$); however, when converted to the percentage loss in PAR per unit distance the half loofah was the worst performer followed by the horizontal whole loofah then the vertical whole loofah (Table 4.2).

Table 4.2 Loss of photosynthetic active radiation (PAR) per unit depth (mm) for different loofah samples relative to ambient sunlight.

Sample	Thickness (mm) (mean ± Stdev)	PAR loss per unit depth (% loss/mm; mean ± Stdev)
Half loofah	13.01 ± 0.43	7.11 ± 0.02
Whole loofah (horizontal)	54.63 ± 0.72	1.79 ± 0.02
Whole loofah (vertical)	100.8 ± 0.27	0.97 ± 0.03

4.3.2 Latex binder toxicity

Toxicity trials were run for 7 days. As an example, Figure 4.3 shows a comparison between non-toxic (320) and toxic (379) bio-based binders against *S. elongatus* PCC 7942. Only binders 321 and 320 were non-toxic to both strains.
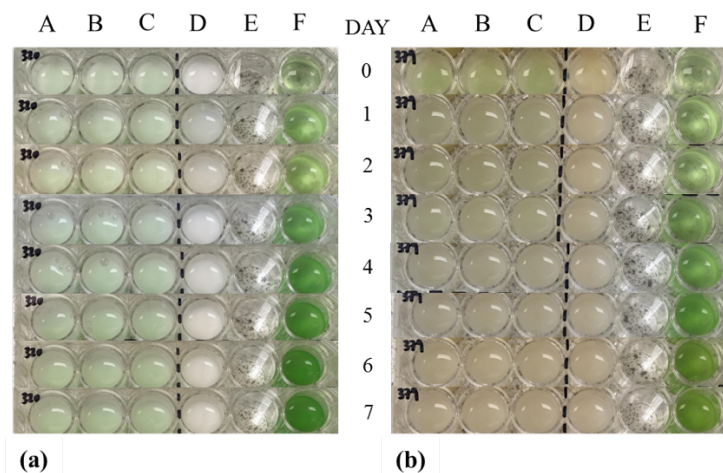
Figure 4.3 A representative 7-day toxicity test using *S. elongatus* CCAP 1479/1A with binders (a) 320 and (b) 379. A-C = binder + growth medium + cells, D = binder + growth medium, E = growth medium, F = growth medium + cells.

Interestingly, binder 320 significantly enhanced the growth of *S. elongatus* CCAP 1479/1A (Kruskal-Wallis, H = 18.11, df = 6, P = 0.006; Mann-Whitney, U = 26 ($n_{1,2}$ = 0.3326), P = 0.0304) and PCC 7942 (Kruskal-Wallis, H = 19.39, df = 6, P = 0.004; 320: Mann-Whitney, U = 26 ($n_{1,2}$ = 1.4571), P = 0.03) by roughly 1.5- and 3-fold respectively (Fig. 5). Binder 321 was equivalent to the control for *S. elongatus* CCAP 1479/1A but supported markedly higher biomass for PCC 7942 (approaching a 6-fold increase relative to the control; Mann-Whitney, U = 26 ($n_{1,2}$ = 2.8172), P = 0.03)). Without complete knowledge of proprietary commercial binder surface chemistry and formulations, it is not possible to determine the relative contribution of each component to the observed toxicity.
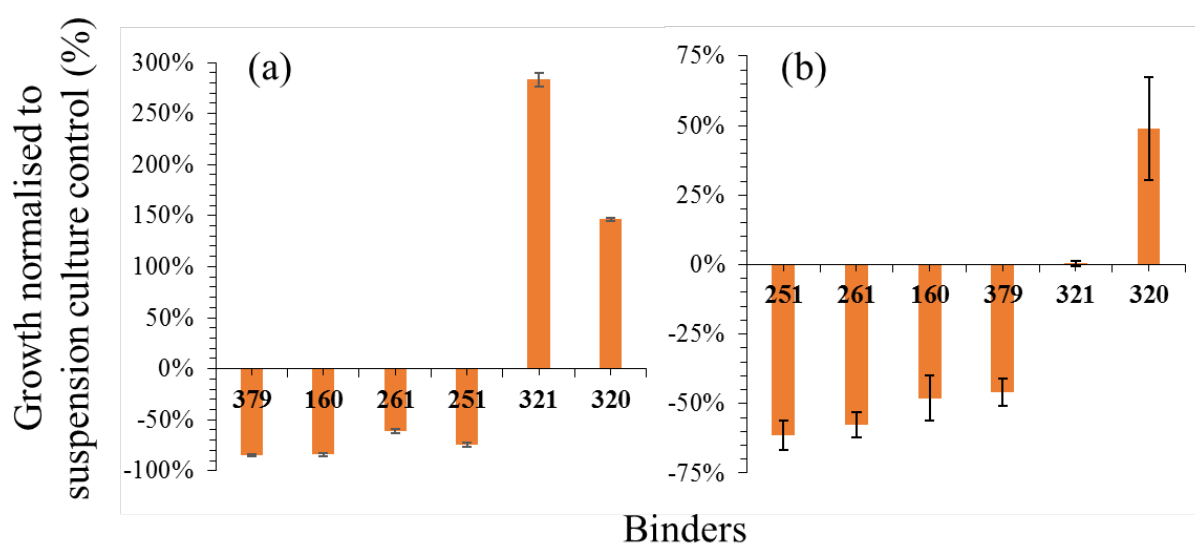
Figure 4.4 Toxicity testing using percentage growth normalised to suspension culture controls for (a) *S. elongatus* PCC 7942 and (b) CCAP 14791/A with bio-based binders.

4.3.3 Cell adhesion testing

The binders exhibited differing adhesion performances (determined as the cumulative release of cells; Kruskal-Wallis, CCAP 1479/1A: H = 15.74, df = 5, P = 0.008; PCC 7942: H = 15.62, df = 5, P = 0.008; Figure 4.5). Binders 251 and 321 were the most adhesive bio-based binders with 0.61% of *S. elongatus* PCC 7942 (Kruskal-Wallis, H = 15.62, df = 5, P = 0.008) and 3.49% of CCAP 1479/1A (Kruskal-Wallis, H = 15.74, df = 5, P = 0.008) cells released.
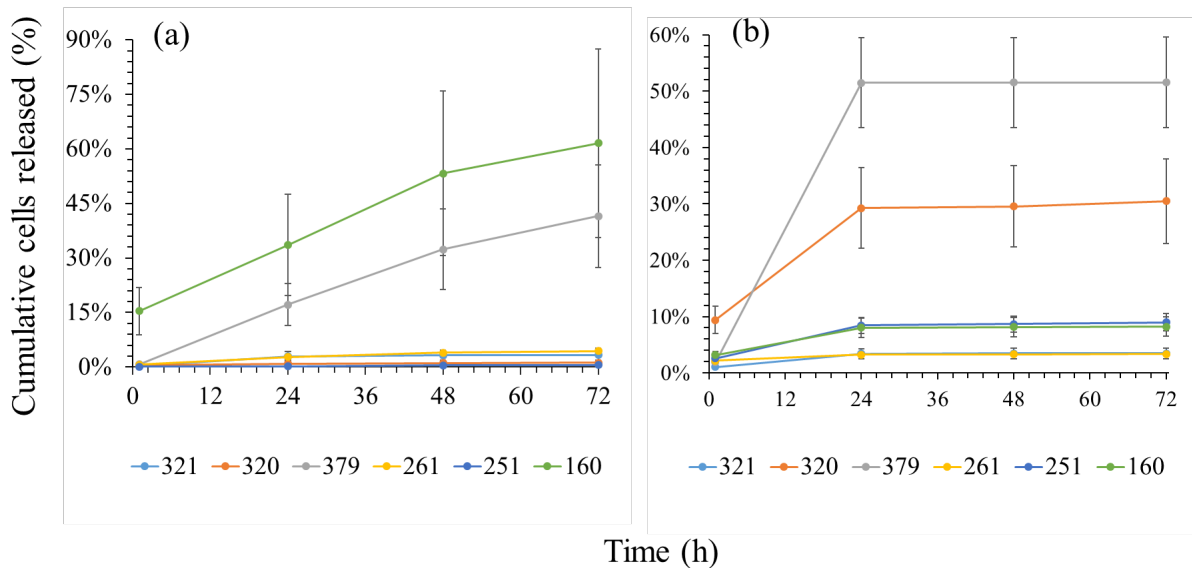
Figure 4.5 Cumulative percentage of cells released from (a) *S. elongatus* PCC 7942 and (b) CCAP 1479/1A biocomposites. Refer to Tables 4.1 for binder details.

SEM analysis of the biocomposite structure was conducted before and after cell immobilisation. In addition to covering the loofah strands, the binders tended to form between the pore spaces potentially reducing the overall porosity of the structure with possible implications for gas exchange and light penetration. Figure 4.6 shows contrasting examples of effective (displaying a smooth surface; Figure 4.6b) and poorly performing binders (cracked during drying; Figure 4.6c). Cracked binders could not adequately retain the cells within the structure as indicated by poor adhesion data.
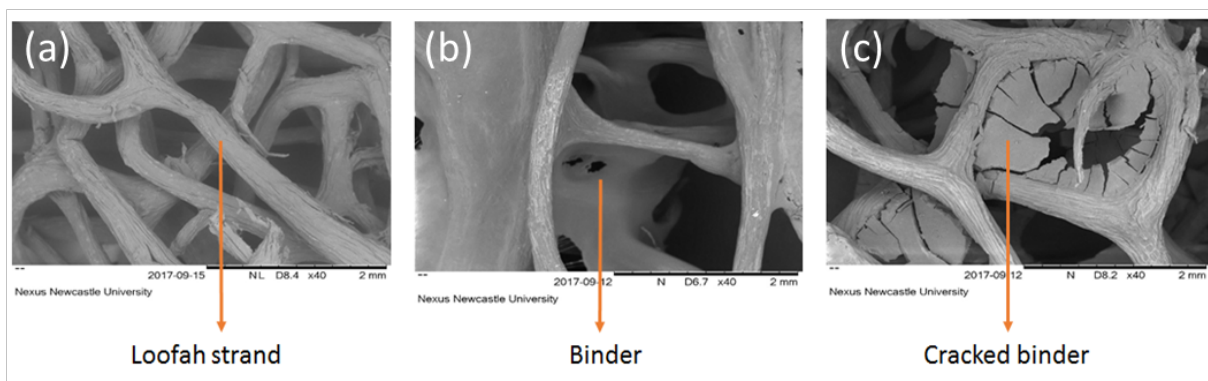
Figure 4.6 SEM images of a representative loofah scaffold (a) before and (b) after cell immobilisation with effective and (c) ineffective synthetic binders. Magnification: 40 ×.

The equivalent *S. elongatus* biocomposites are presented in Figure 4.7 and 4.8. The least effective binders (379 for CCAP 1479/1A; Figure 4.7a-d and 160 for PCC 7942; Figure 4.8a-d) deteriorated rapidly whereas binder 321 (CCAP 1479/1A) (Fig. 4.7e-h) and 251 (PCC 7942)

(Fig. 4.8e-h) retained the cells on the loofah surface in the same form as prior to the adhesion test.
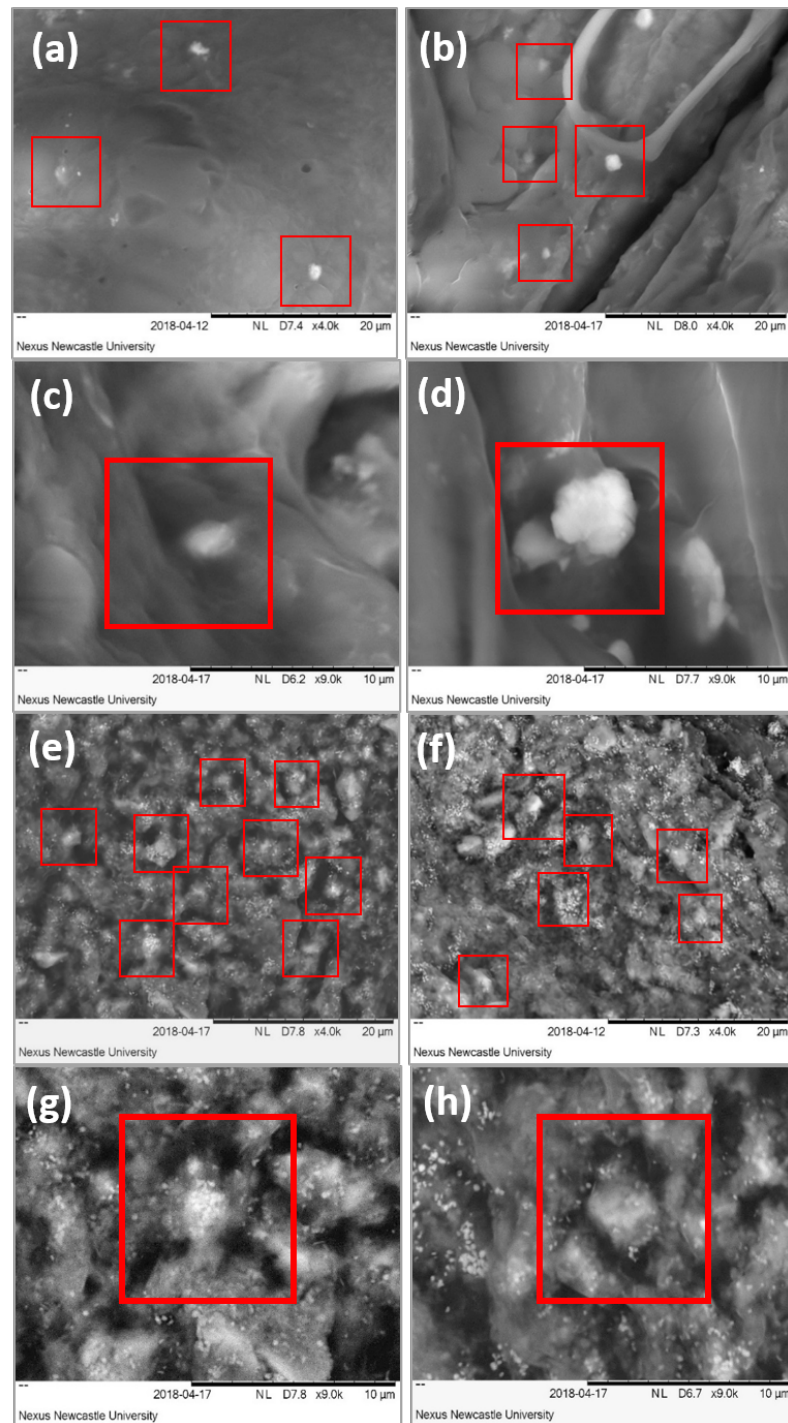
Figure 4.7 SEM images of *S. elongatus* CCAP 1479/1A biocomposites before and after adhesion testing. Binder 379 exhibiting poor cell retention (before = a&c, after = b&d), binder 321 exhibiting good cell retention (before = e&g, after = f&h). Magnification: 4000× (a, b, e, f) and 9000× (c, d, g, h).
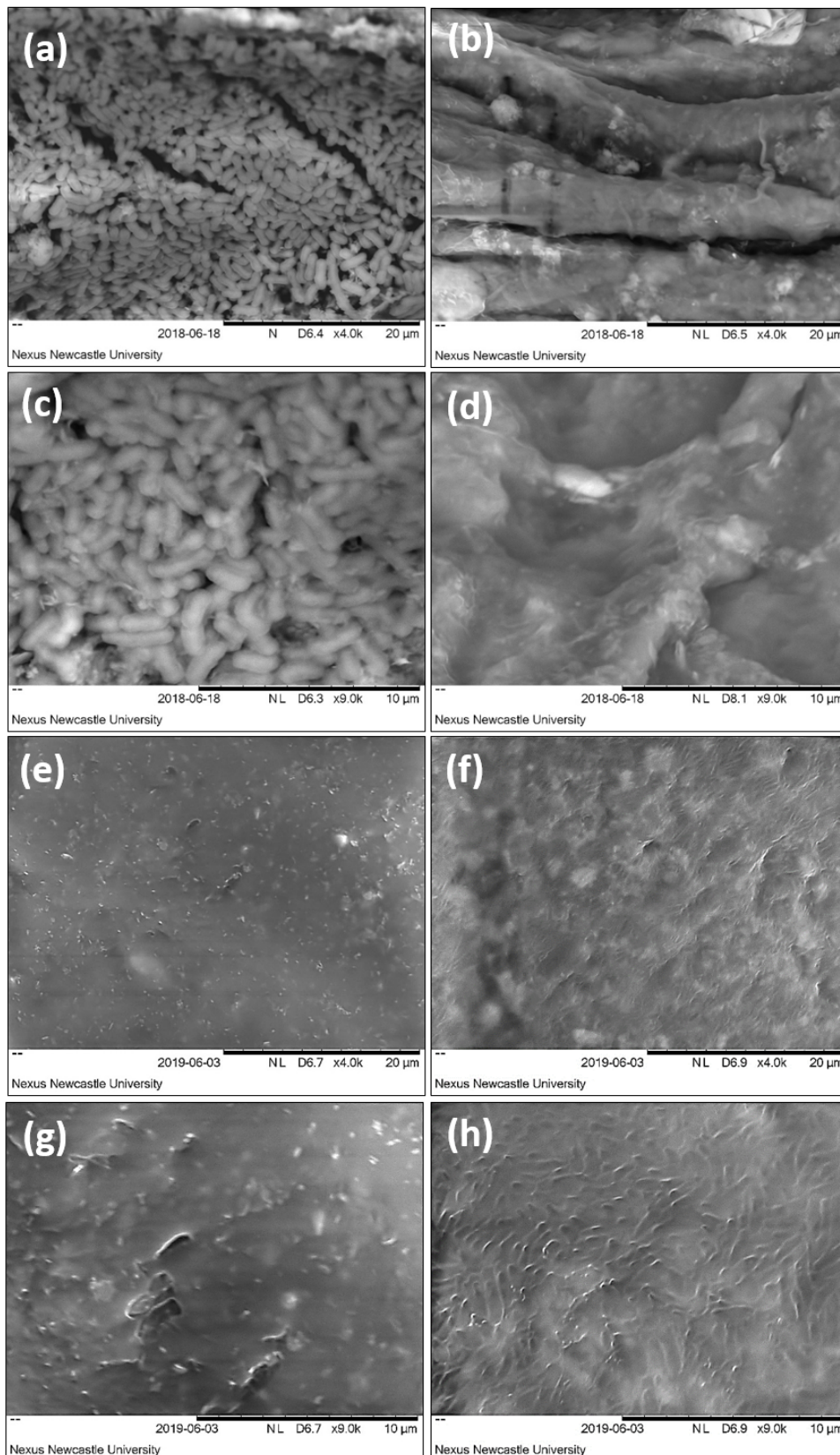
Figure 4.8 SEM images of *S. elongatus* PCC 7942 biocomposites before and after adhesion testing. Binder 160 exhibiting poor cell retention (before = a&c, after = b&d), binder 251 exhibiting good cell retention (before = e&g, after = f&h). Magnification: 4000× (a, b, e, f) and 9000× (c, d, g, h).
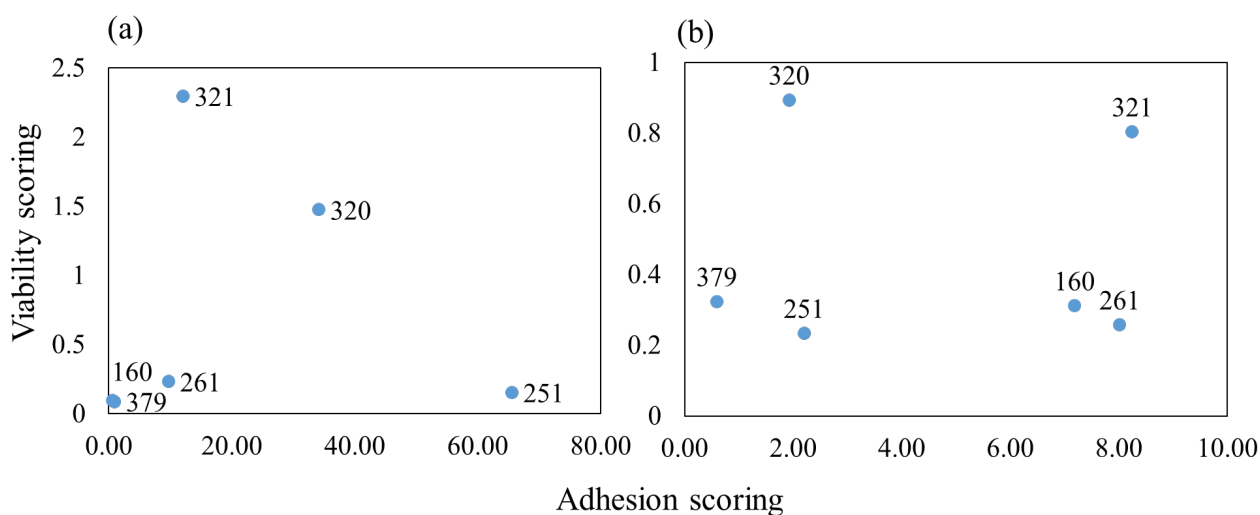
Figure 4.9 Decision matrix derived from toxicity and adhesion data for (a) *S. elongatus* PCC 7942 and (b) CCAP 1479/1A.

A decision matrix based on toxicity and adhesion performance was applied to select the most suitable binders for subsequent net CO_2 fixation tests (Figure 4.9). The bio-based binders were more evenly distributed through the matrix with binder 320 and 321 were ranked on the top right quartile. As a result, binder 320 was selected for *S. elongatus* PCC 7942 and binder 321 for CCAP 1479/1A.

4.3.4   Net CO_2 fixation rates

With excellent pH and temperature tolerances (Ogbonna et al., 1994) loofah may be a useful candidate scaffold for capturing CO_2 from flue gases. A liquid absorption capacity of up to 18.4 g g^{-1} of fibers (Akhtar et al., 2004b) should deliver sufficient hydration and sustenance to bound cells via capillary action over extended periods, in a mechanism similar to a cellulosic sheet biofilm-based photobioreactor described by Hamano and co-workers (Hamano et al., 2017). To test this we utilised batch and continuous CO_2 fixation tests over extended time periods (8 and 6 weeks respectively). Fig. 4.10 shows the cumulative net CO_2 fixation of the biocomposites over the 8-week batch testing period. The cyanobacteria suspension controls were terminated after 1104 h due to culture failure — likely due to a combination of nutrient exhaustion and self-shading, due in part to the initial high inoculum density required to match the biocomposite cell loading. *S. elongatus* CCAP 1479/1A yielded the highest net fixation rate (21.18 ± 6.87 mmol g^{-1} d^{-1}), over ten times higher than its suspension control (2.08 ± 0.13 mmol g^{-1} d^{-1}). The *S. elongatus* PCC 7942 biocomposite was 15.38 ± 4.06 mmol g^{-1} d^{-1}, almost 9-fold higher than its suspension control (1.77 ± 0.12 mmol g^{-1} d^{-1}). There were no significant differences between the biocomposite performances at either time point (Figure 4.10, Table 4.3).

Table 4.3 Net batch CO_2 fixation rates (mean ± StDev) for *S. elongatus* PCC 7942 + 320 and CCAP 1479/1A + 321 biocomposites compared with their suspension culture controls. Data are presented in a range of formats to enable comparison with other published studies. A theoretical scaled CO_2 capture (as tonne CO_2 captured per tonne of biomass per year) from an up-scaled version of the biocomposite system is also presented.

Strain of *S. elongatus*	Net CO_2 fixation rates					Theoretical scaled CO_2 capture (tCO_2 $t^{-1}_{biomass}$ yr^{-1})
	Suspension (mmol CO_2 $g^{-1}_{biomass}$ d^{-1})	Biocomposite (mmol CO_2 $g^{-1}_{biomass}$ d^{-1})	Biocomposite (mmol CO_2 m^{-2} d^{-1})	Biocomposite (g CO_2 m^{-2} d^{-1})	Biocomposite (g CO_2 $g^{-1}_{biomass}$ d^{-1})	
PCC 7942	1.77 ± 0.03	15.38 ± 4.06	7.72 ± 2.04	0.34 ± 0.09	0.68 ± 0.18	246.97 ± 65.20
CCAP 1479/1A	2.08 ± 0.13	21.18 ± 6.87	6.15 ± 2.00	0.27 ± 0.09	0.93 ± 0.30	340.11 ± 110.32
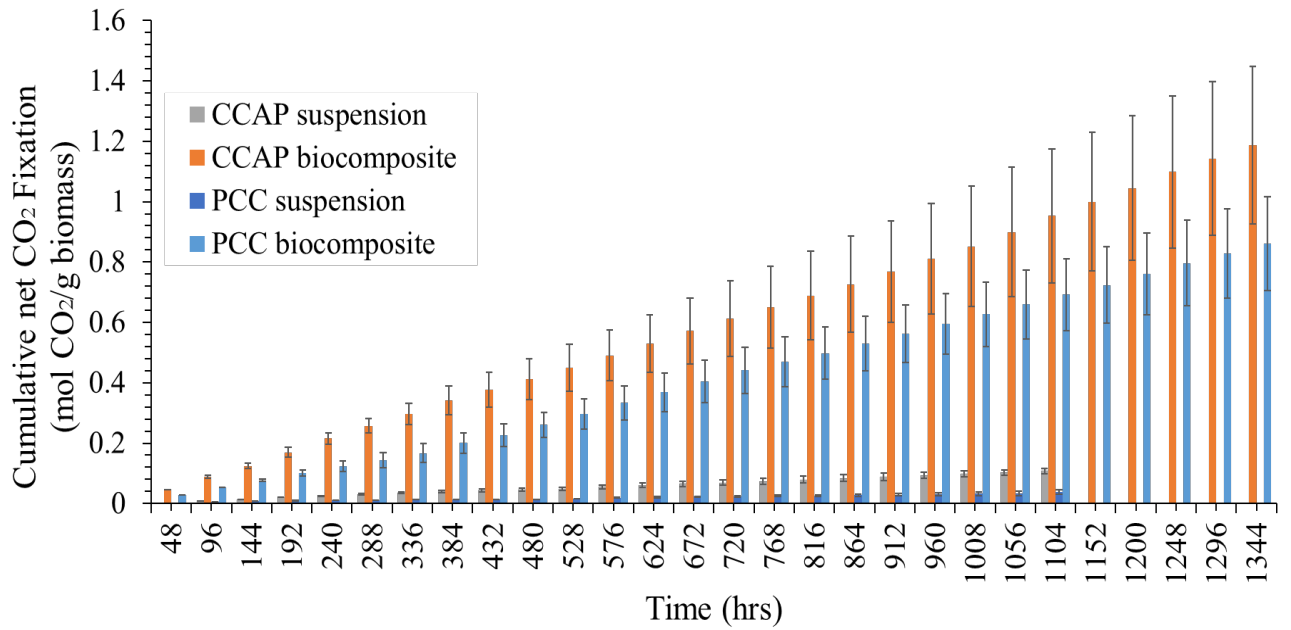
Figure 4.10 Cumulative net CO_2 fixation of *S. elongatus* biocomposites compared with their suspension culture controls from the 8 weeks batch CO_2 fixation test.

4.3.5 CO_2 transfer kinetics

Using the experimental data from the semi-batch tests, the volumetric CO_2 transfer coefficients for the suspended culture controls and the biocomposites were calculated. These data are presented in Table 4.4 and Figure 4.11 and show that the CO_2 transfer coefficient is lower for the biocomposites compared to the suspended cultures. This was expected as by incorporating the cells into the binder an additional transfer resistance has been added.

In an attempt to determine the nature of the mass transfer resistance in the biocoatings, the data in Table 4.5 were analysed in more depth. First, using cell surface areas for the suspended cultures, values of the coefficient for transfer through the cell walls and cell internals were calculated, k_{cell} (mols m^{-2} s^{-1} · (mols m^{-3})$^{-1}$). Next, using cell surface areas for the biocomposites, values of the coefficient for transfer through the binder layer, cell walls and cell internals were calculated, k_{BC}. It was assumed that the resistances due to the cell and the binder were additive as shown in equation 4.6.

$$\frac{1}{k_{BC}} = \frac{1}{k_{binder}} + \frac{1}{k_{cell}} \qquad (4.6)$$

Equation 4.6 was used to calculate values of the transfer coefficient for the binder, k_{binder}. The thickness of the binder layer applied to the loofah was calculated based on the assumption that

the volume of the biocoating formulation in the semi-batch tests (600 μl) was uniformly distributed over the surface of the binder. This gave an average thickness for the binder layer of 26 μm. Being a solid, the resistance of the binder layer is given by equation 4.7. In this equation, δ_B, is the thickness of the binder layer and D_B is the CO_2 diffusivity in the binder layer (m^2 s^{-1}).

$$k_{binder} = \frac{D_B}{\delta_B} \qquad (4.7)$$

Equations 4.6 and 4.7 were used to calculate values for the diffusivity in the binder. The results of these calculations (Table 4.5) show that the CO_2 diffusivities in the binder are of the order of $10^{-15} - 10^{-13}$ m^2 s^{-1}. By comparing these values with the diffusivity of gases in microporous solids ($\sim 10^{-8}$ m^2 s^{-1}) (Liu, 2015), diffusivities of gases in liquids ($\sim 10^{-9}$ m^2 s^{-1}) and the diffusivity of CO_2 in polymer films ($\sim 10^{-13}$ m^2 s^{-1}) (Craster and Jones, 2019), they imply that the cells are covered by a solid layer of polymer, a conclusion which is supported by the SEM images in Figure 4.7 and 4.8.

Table 4.4 Comparison of the volumetric CO_2 transfer coefficients for suspended culture and the biocomposites.

| Phototroph | Cell surface area ($m^2 \times 10^{11}$) | $N_{cell} \times 10^{-7}$ | Suspended culture | | Biocomposite | |
			a_C (m^2 m^{-3})	$K a_C$ ($s^{-1} \times 10^6$)	a_C (m^2 m^{-3})	$K a_C$ ($s^{-1} \times 10^6$)
S. elongatus PCC 7942[a]	2.15	3160	128060	14.6 ± 0.7	135744	5.4 ± 0.5
S. elongatus CCAP 1479/1A[b]	1.26	4490	106458	62.7 ± 1.1	112846	5.9 ± 0.6

a – Calculated from rod-shaped cells with an assumption that all cells had a diameter and length of 2 and 4 μm.

b – Calculated from coccoid cells with an assumption that all cells had a diameter of 2 μm.

Table 4.5 Values of the binder film diffusivity calculated from experimental transfer coefficients.

Phototroph	k_{cell} (m s^{-1} × 10^{10})	k_{BC} (m s^{-1}× 10^{10})	K_{binder} (m s^{-1} × 10^{10})	D_B (m^2 s^{-1} × 10^{15})
S. elongatus PCC 7942	1.1	0.39	0.60	1.6
S. elongatus CCAP 1479/1A	5.9	0.52	0.57	1.5
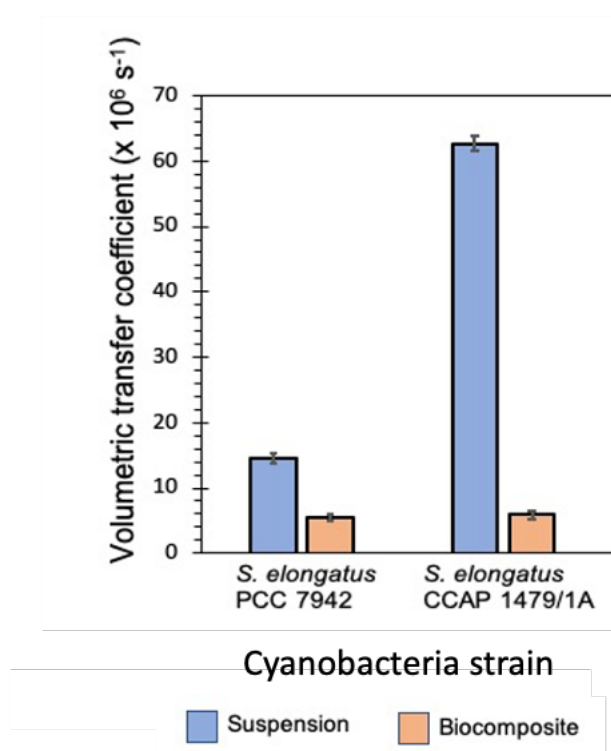
Figure 4.11 Comparison of the volumetric CO_2 transfer coefficients for suspended and biocomposite cultures of cyanobacteria.

4.4 Discussion

Loofah was selected as a candidate 3D scaffold for a low water demand photosynthetic biocomposite for carbon capture applications. Light transmission was not uniform through the loofah, with differences in the percentage loss in PAR affected by the void volumetric space at the centre of the whole loofah allowing greater light penetration per unit depth (Figure 4.12). The half loofah therefore had a greater overall strand density (strands mm^{-3}) relative to the whole loofah in either orientation. It should be noted that these values are based on direct sunlight, whereas the CO_2 fixation tests were conducted under artificial light at a considerably

lower light intensity (30.5 μmol m^{-2} s^{-1}). This approximates to light levels of 19.7 μmol m^{-2} s^{-1} penetrating to the centre of the loofah in the batch test.
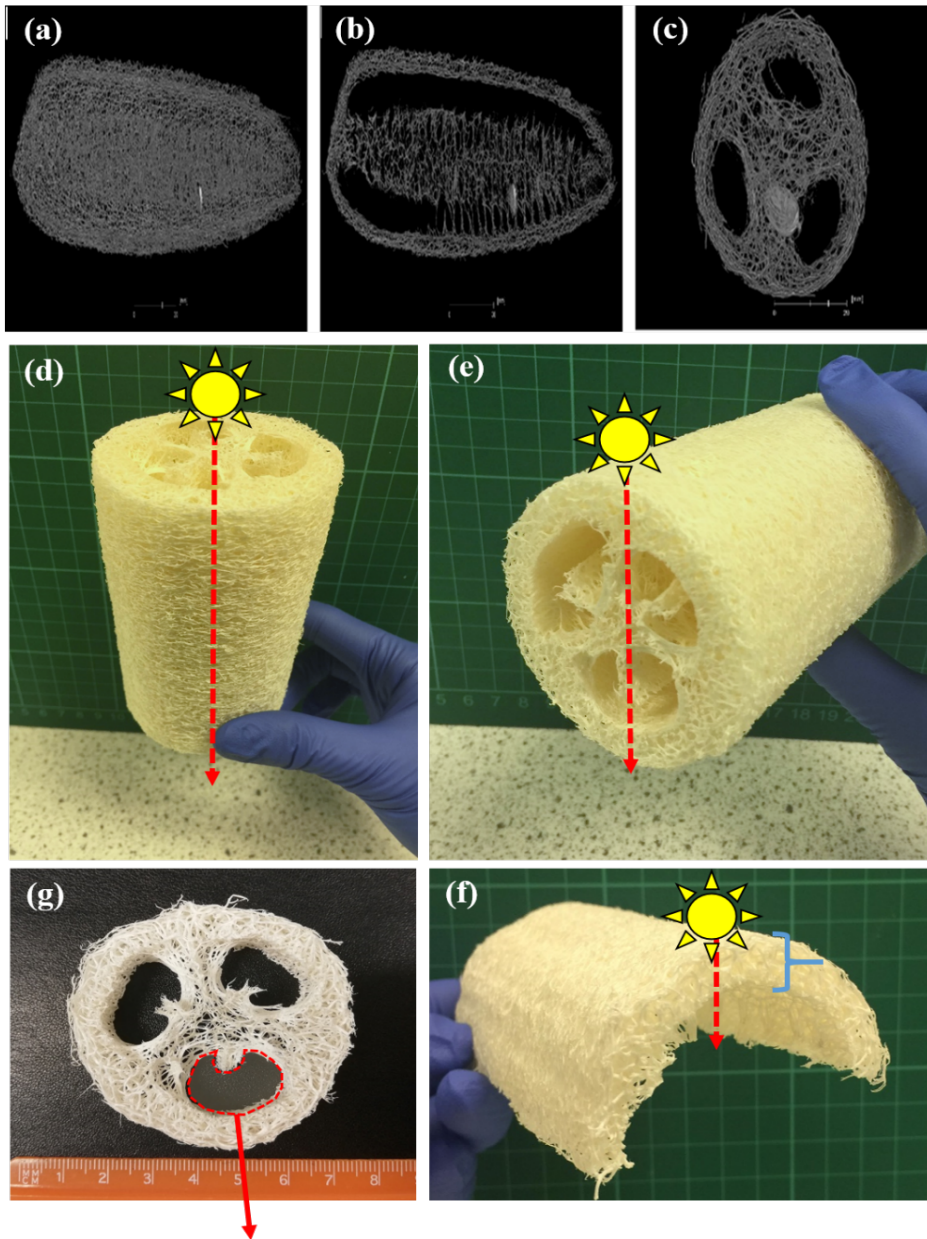
A void space at the
centre of the loofah

Figure 4.12 Illustrating the porosity and orientation of loofah for the light penetration test. CT scans of loofah (a-c): (a) loofah external view in longitudinal orientation, (b) internal view in longitudinal orientation, (c) internal view in transverse section. (d-g) Orientation for light tests. The red line indicates the light path relative to the sun. The PAR sensor was encased in a lightproof tube to prevent peripheral light affecting the readings; (d) whole loofah in vertical orientation, (e) whole loofah in horizontal orientation, (f) half loofah (bracket denotes the loofah thickness), and (g) an example of void spaces within the loofah centre.

The CO_2 absorption rates across the biocomposites were significantly higher than their suspension controls due to a higher CO_2 concentration gradient and loofah surface area compared to suspended cultures. Based on the semi-batch test data, the biocomposites can theoretically capture CO_2 at rates of between 246.97 ± 65.20 to 340.11 ± 110.32 tCO_2 $t^{-1}_{biomass}$ yr^{-1} (Table 4.3). Although biocomposites experienced cell outgrowth, biocomposite performance was stable across treatments as evidenced by the consistent and tight standard deviations. The biocoatings were applied manually, with between replicate variability largely explained by the extent and lack of uniform coverage of the loofah strands, with some pooling of the biocoating on the less illuminated side of the loofah strand—this could partly be ameliorated using spray application. Typically, CO_2 is taken up for photosynthesis by algae and cyanobacteria as bicarbonate (HCO_3^-), although there is evidence of direct CO_2 uptake depending on their environmental parameters, taxonomic features, concentration of carbon sources and pH of culture medium (Kupriyanova et al., 2013, Price et al., 2008). The sorbed water via the thin film of coating in the biocomposites should support a steep CO_2 concentration gradient and rapid solubility of CO_2, allowing efficient uptake by the cells. In contrast, the suspension controls lacked dynamic mixing and relied only on the slow driving force of diffusion which limits mass transfer efficiency as the molecules are required to pass through bulk liquid water before reaching the cells (Farajzadeh R. et al., 2009). A similar scenario will exist for O_2 outgassing (to prevent photorespiration), with the biocomposites presenting a more efficient system (Garcia-Ochoa and Gomez, 2009, Annesini et al., 2017, Kupriyanova et al., 2013). Additionally, as nutrients were not renewed during the tests, increased CO_2 uptake rates could also stem from nutrient limitation (Choi et al., 2016), as the immobilised cells were reliant upon capillary action via loofah to access the growth medium whereas the suspended cells were permanently bathed in nutrients.

It is challenging to compare the current study with other microalgae-based carbon capture technologies due to a lack of standardised conditions between experiments, coupled with variation in the reported metrics (Table 4.6). The majority of studies have been conducted with suspension cultures at various scales, with few using a biocomposite or biofilm approach. Our data compare favourably with studies that report CO_2 fixation as g CO_2 $g^{-1}_{biomass}$ d^{-1}. However, the fixation rates achieved with *S. elongatus* biocomposites were 20 times lower than Bernal et al.'s paper-based acrylate copolymer latex coating biocomposites with immobilised *S. elongatus* PCC 7002 (Bernal et al., 2014). This is likely due to cell loading differences; 2.5

% versus 50 % v/v, i.e. a 20-fold difference. It should be noted that we assume that the binder application is perfectly efficient, i.e. that all cells in the WCP are immobilised to the loofah. In reality, some cells are lost to waste by our current coating technique forming non-uniform coating thickness in the biocomposite structure. Therefore, the CO_2 fixation rates per g biomass will be underestimated. Improvements may therefore be made by increasing cell loading (i.e. using a denser WCP); however, Flickinger et al. (Flickinger et al., 2017) mentioned that a threshold cell loading for latex binders (as yet undefined and likely species and binder specific) should not be exceeded as it may compromise porosity and adhesion. Further, substantially increased cell loading may compromise performance through excessive competition for water, light, nutrients and CO_2. A recent study suggested that it is possible to increase the porosity of the latex to produce stable biocoating using non-toxic non-film forming nanoparticles (Chen et al., 2020); offering a potential route to improve the performance of our biocomposite systems.

Unfortunately, the cells of both cyanobacteria strains grew out of the bio-latex binders after four weeks into the growth medium (see Figure 4.13). Hence, the SEM images could not be obtained at the end of test. The loss of cells to the liquid growth medium in the test would have reduced the overall CO_2 fixation if the released cells reverted to a photosynthetic rate equivalent to the suspension controls.
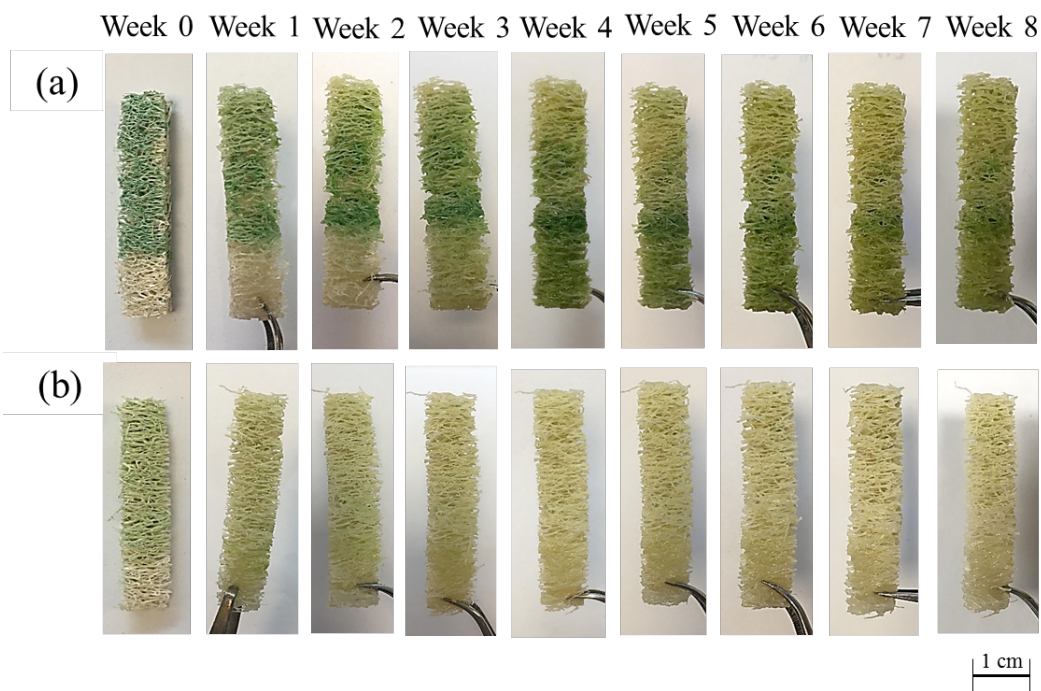
Figure 4.13 Development of representative *S. elongatus* biocomposites during the 8 weeks net CO_2 fixation test (batch); (a) PCC 7942, (b) CCAP 1479/1A cells.

Table 4.6 Comparison of the highest CO_2 fixation rates for batch and continuous tests relative to selected literature values, including the model species *Arabidopsis thaliana* as a reference plant. We made approximate calculations and conversions based on the information available if data were not explicitly stated within a paper in an appropriate form.

Species and strain	Type	System description	CO_2 fixation rate		Ref
			(mmol CO_2 m^{-2} d^{-1})	(g CO_2 g^{-1} $_{biomass}$ d^{-1})	
Arabidopsis thaliana (wild type)	Angiosperm	Open gas exchange chamber (ambient CO_2) at 25 °C; light: 300 μmol m^{-2} s^{-1}	432	0.25	(Eckardt et al., 1997)
Monoraphidium dybowskii LB50	Freshwater chlorophyte	200 m^2 open raceway at ambient temperature and CO_2	750	0.37	(Chen et al., 2018)
Synechococcus PCC7002	Cyanophyte	Paper-based biocomposites with 20% v/v CO_2 at 25 °C; light: 100 μmol m^{-2} s^{-1}	136	0.22	(Bernal et al., 2014)
Oedogonium crispum	Freshwater chlorophyte (macroalgae)	15,000 L culture tank at ambient temperature, CO_2 enriched regulated by culture pH; light: 230 μmol m^{-2} s^{-1}	85	0.45	(Cole et al., 2014)
Chlorella fusca LEB 111	Freshwater chlorophyte	Cultivated on CO_2 adsorbent nanofibers in 0.45 L PBR at 25 °C; light: 41.6 μmol m^{-2} s^{-1}	-	0.27	(Vaz et al., 2019)
C. vulgaris	Freshwater chlorophyte	15 L tubular reactor at 25 °C with continuous 8% v/v CO_2 (100 l h^{-1}); light: >twice daylight	-	0.91	(Adamczyk et al., 2016)
S. elongatus CCAP 1479/1A	Cyanophyte	Binder 321 on loofah at 18 °C; light: 16:8 photoperiod at 30.5 μmol m^{-2} s^{-1} with 5% v/v CO_2 in batch at day 56	6.15	0.93	This study

The exposure conditions may have compromised binder integrity as the biocomposites were continuously exposed to moisture that may have altered their adhesive properties (Dickie, 1994). In addition, the bio-latex appeared to enhance the growth rate as previously observed in the toxicity test (Fig. 4.4), with the growing biomass leading to partial binder failure and release of the cells. This observation poses something of a paradox for mass microalgae/cyanobacteria production systems. Ordinarily, open ponds and PBRs are designed to maximise biomass production by delivering optimised growth conditions; however, rapid biomass production may be suboptimal for immobilised systems. For biocomposites, an unusual 'maintenance of viability' approach is warranted whereby the nutrient system must deliver conditions supportive of active metabolism but sufficiently suboptimal to slow or even eliminate cell division (Flickinger et al., 2017), such as has been achieved for *Escherichia coli* (Lyngberg et al., 1999b), *Rhodopseudomonas palustris* (Gosse et al., 2010) and *Gluconobacter oxydans* (Fidaleo et al., 2006). When combining cells with binders, it appeared to initiate a cell morphology change for *S. elongatus*, transiting from a rod-shaped to a coccoid form (Figure 4.14).
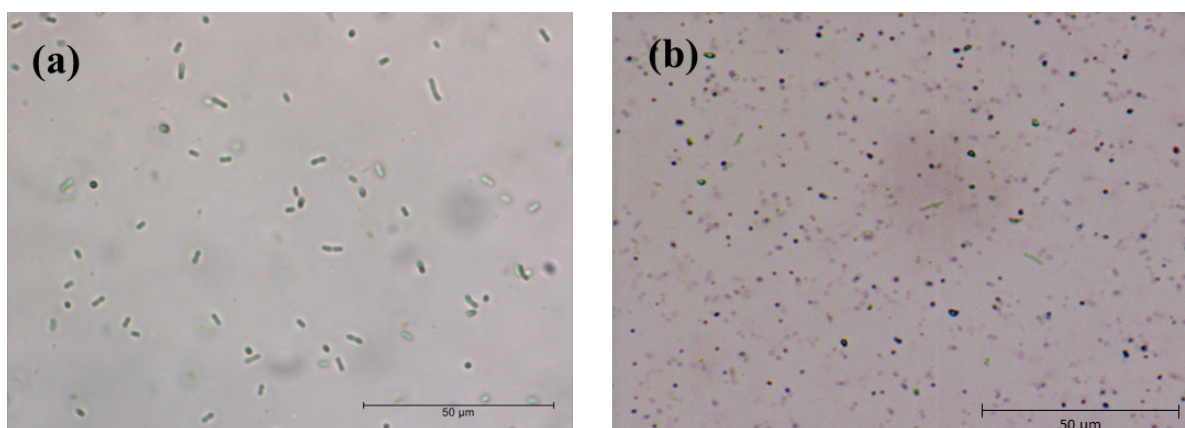
Figure 4.14 Light micrographs of *S. elongatus* PCC 7942 in: (a) BG11 growth medium (suspension control); and, (b) exposed to binder 320 at day 7 of the toxicity test. Control cells had a more rod-like morphology compared with the generally more coccoid morphology of the binder exposed cells.

The implications of this for immobilised cultivation are unknown; however, similar observations have been made for *S. elongatus* and other bacteria with suggestions that the behaviour may regulate photosynthesis and cell division under stress (Chen et al., 2018, MacCready and Vecchiarelli, 2018, Moronta-Barrios et al., 2013). The findings from the semi-batch tests and SEM images appear to show that the cells are covered with a thin polymer layer which protects the cells. The cell retention capabilities of many of the latex binders should

stimulate future biocomposite coating technology exploration, including expanding the use of microalgae 'milking' to recover biochemicals (including lipids) without permanently compromising cell health (Chaudry et al., 2017), and specifically as a platform for the adoption and safe environmental deployment of metabolically engineered microorganisms for industrial and environmental applications (Brenner et al., 2008, Cases and De Lorenzo, 2005). On a similar note, the species assayed in this study are evolved for a planktonic existence (i.e. living in suspension in the water column). The immobilisation process compels the cells to live in a film, i.e. to become benthic — a living state for which they may be genetically ill-equipped. As indicated, the cyanobacteria responded by changing their cell morphology. Options exist to metabolically engineer the organisms whereby the transition from planktonic to benthic lifestyles may be routine as has previously been done for *S. elongatus* (Schatz et al., 2013, Parnasa et al., 2016, Nagar et al., 2017), or they may be engineered for improved adhesive capabilities as reported for *E. coli* (Park et al., 2014, Francisco et al., 1993). Equally, synthetic biology approaches could be used to address resource limitation effects, such as combating self-shading (Melis, 2009). On the theme of entraining planktonic cells to a forced benthic existence, future work may also wish to explore natural biofilm forming species as candidates for biocomposite manufacture, as many such species naturally synthesise extracellular polymeric substances (EPS) that support adhesion and biofilm integrity (Xiao and Zheng, 2016, Schmidt et al., 2016). However, to sound a note of caution, many such species also utilise EPS as a biolubricant to aid gliding motility (c.f. many raphid diatoms) which could act to breakdown the biocomposite. In such instances the need for a robust binder may be even greater, although we have previously observed that a raphid pennate diatom (*Navicula pelliculosa*; In-na and Caldwell, unpublished) readily escapes binders by exploiting EPS to reduce adhesion. Additional complications may arise with natural biofilm formers, as dispersion is an intrinsic part of a biofilm cycle, particularly in response to nutrient stress (Morales-Garcia et al., 2019, Jakubovics et al., 2013). Such a scenario could lead to epidemic biocomposite failure. EPS could also provide a ready substrate for bacterial growth which may compromise the health and longevity of the biocomposite. Whilst the use of planktonic species may seem counterintuitive, there are compelling arguments why they may have fewer operational problems that natural biofilm forming taxa.

4.5 Conclusion

In this study, we developed cyanobacteria based biocomposites for carbon capture over sustained durations, utilising loofah sponge as a cheap and sustainable scaffold. Cell immobilisation greatly enhanced net CO_2 fixation up to 10 folds compared to suspension controls, with most biocomposites showing little or no reduction in performance. However, the cell outgrowth from biocomposites made by the Replebin® based 321 and 320 binders give cause for optimistic further improvements. These 3D coated biocomposites overcome some of the disadvantages of open pond and photobioreactor growth systems, particularly in terms of water consumption. Further optimisation is required to increase CO_2 absorption and stability, for example by increasing binder contend, cell loading and conducting tests under high PAR intensity sunlight rather than low intensity artificial light. With further improvements, including metabolic engineered systems, it may not be unreasonable to predict that living loofah-based cyanobacteria biocomposites could capture in the region of 1000 tCO_2 $t^{-1}_{biomass}$ yr^{-1}.

Chapter 5

Engineered photosynthetic living biocomposites for intensified carbon capture

Abstract

In Chapter 4, loofah-based cyanobacteria biocomposites were developed using commercial bio-based binders, which enhanced the CO_2 absorption rates compared to cyanobacteria suspension controls. From a carbon capture perspective, the biocomposites must have an operational lifespan of several months to be competitive with other carbon capture technologies. However, significant cell outgrowth occurred from the biocomposites during the CO_2 absorption trials. Capacity to interpret this response was limited as the detailed chemical composition of the binders was unknown. Here, the biocomposites were further developed using acrylic latex binders of known chemical composition. The latex binders were polymerised with different styrene/butyl acrylate blends and were further treated with differing concentrations of Texanol™, a coalescence agent to promote film formation. To supplement the established toxicity and adhesion screening endpoints, the photophysiology—maximum photosystem II quantum yield (Fv/Fm) and apparent rate of photosynthesis (PS)—of *Synechococcus elongatus* CCAP 1479/1A and PCC 7942 were investigated in response to exposure to the binders. High styrene content binders decreased cell viability and lowered photosynthetic performance. The glass transition temperature was lowered as the Texanol™ content increased, which improved cell adhesion. All the biocomposites had greater CO_2 uptake rates compared with suspension controls (improvements of 14-20 and 3-8 times for CCAP 1479/1A and PCC 7942 respectively). The CCAP 1479/1A biocomposites lasted up to 12 weeks without additional nutrient addition, with the highest CO_2 absorption rate being 1.57 ± 0.08 g CO_2 g$^{-1}_{biomass}$ d^{-1}, while the PCC 7942 biocomposites experienced cell leaching after four weeks, with the highest CO_2 absorption rate of 1.18 ± 0.29 g CO_2 g$^{-1}_{biomass}$ d^{-1}. The carbohydrate content of both strains peaked midway through the CO_2 absorption tests, being $77.05 \pm 17.03\%$ and $67.88 \pm 3.31\%$ in dried biomass for CCAP 1479/1A and PCC 7942 biocomposites respectively.

Keywords: engineered living biocoating, biological carbon capture, algae latex immobilisation

5.1 Introduction

Biocoatings and/or biocomposites involve a concentrated population of photosynthetic organisms that are encapsulated or immobilised within a thin matrix coating. They have been used for many applications such as bioremediation, wastewater treatment and air purification. At present, most immobilisation technologies are based on hydrogels, which are not mechanically robust for long-term usage, resulting in cell leaching and damage (Webb and Dervakos, 1996). Latex-based binders are alternative adhesive coatings that overcome many of the drawbacks of hydrogels; they are robust, inexpensive, easy to handle, and can be implemented on an industrial scale (Flickinger et al., 2017, Cortez et al., 2017). Microalgae, cyanobacteria and other microorganisms have successfully been immobilised within latex coatings (Gosse et al., 2010, Bernal et al., 2014, Flickinger et al., 2007, Jenkins et al., 2013, Piskorska et al., 2013, Chen et al., 2020).

Cell immobilisation using latex polymers is greatly influenced by latex formulation and the film formation process. Emulsion polymerisation is a heterogeneous polymerisation process which is used to produce a wide range of products including synthetic rubbers, adhesive coatings, sealants, concrete additives, paper and textile coatings, and latex paints (Yamak, 2013). It has several advantages over other polymerisation techniques such as its high reaction rate and conversion efficiency, ease of control over the products, and it being a safe process (Yamak, 2013). The process can be divided into three main intervals: 1) latex particle formation outside or within micelles (a meeting site for free radicals and monomers to react); 2) latex particle growth in size until monomer droplets in the dispersion medium are not presence; and 3) polymer size increases as the concentration of monomer in the latex particles approaches zero (Harkins, 1947).

There are four basic ingredients in a typical emulsion polymerisation formulation; monomers, a dispersion medium, an emulsifier or surfactant, and an initiator. In the current study, water was used as a dispersion medium to create water-borne coatings because it is more environmentally friendly than solvent-based ones (Wang and Chen, 2019). Monomer selection depends on the monomer's hydrophilicity. With multiple monomers (i.e. copolymerisation), latex polymer properties can be altered—including latex particle morphology—by arrangement of different monomers within a polymer chain (Steward et al., 2000). Due to their compatibilities, accessibilities, and inexpensiveness, butyl acrylate and styrene are the most common monomers for acrylic latexes (Anderson and Daniels, 2003), and are used here. A non-toxic combination of these monomers could provide a desirable coating to encapsulate

microalgae and cyanobacteria. The surfactant (Rhodapex® Ab/20 in this case) stabilises the monomer droplets or particles formed by adsorbing at the interface of the droplet/particle and providing a electrostatic repulsion stabilisation mechanism (Anderson and Daniels, 2003). The surfactant also generates micelles once the surfactant concentration exceeds a critical micelle concentration (El-hoshoudy, 2018). An initiator (ammonium persulfate in the current work) promotes polymerisation through the generation of free radicals in the dispersion medium (El-hoshoudy, 2018).

The formation of a latex film over a substrate depends on the drying temperature, which may or may not allow the latex to form a homogeneous continuous film. If the drying temperature is below the minimum film formation temperature (MFFT), the film can take a powdery form with weak mechanical strength (Steward et al., 2000). The MFFT is closely related to the glass transition temperature (Tg). The Tg is an important property for latex polymers that defines the physical property of the latex polymer coating, which can either be in a rubbery (drying above Tg) or glassy state (drying below Tg) (Ebnesajjad, 2016). Tg is influenced by the monomers within the latex polymer as they have their own Tg values. A small addition of a coalescence agent can lower the MFFT of the latexes to enable film formation at ambient or lower temperatures as well as improving the coalescence process (Zohrehvand and Nijenhuis, 2005). Texanol™ (2,2,4 trimethyl-1,3-pentanediol monoisobutyrate; TMPD-MIB) is a common coalescence agent used in latex paints because it is biodegradable, has low toxicity, and its coalescence effectiveness (Corsi and Lin, 2009). To date, there is no literature investigating Texanol™ as a means to improve the latex immobilisation of organisms.

In Chapter 4, commercially available bio-based binders were used to fabricate cyanobacteria loofah-based biocomposites, although the precise chemical composition of the binders were unknown. Further, the biocomposites had a limited capacity to retain the cyanobacteria on the loofah scaffolds during the eight-weeks CO_2 absorption trials. Key design criteria for biocomposites for CO_2 capture include: 1) coatings must be non-toxic; 2) coatings must support long-term adhesion of cells to the structural scaffold; 3) coatings must be robust with a long service life; and 4) coatings should be porous to facilitate effective CO_2 mass transfer and O_2 off-gassing. In this chapter, acrylic latex binders of known chemical composition were investigated with the aims of: 1) determining monomer ratios (styrene and butyl acrylate) that are non-toxic to cyanobacteria, 2) determining whether Texanol™ affects cell viability and adhesion affinity, and, 3) determining effective latex formulation as

biocomposites for CO_2 absorption, and 4) quantifying the carbohydrate content of cyanobacteria within the biocomposites as a measure of biomass utilisation potential.

5.2 Materials and methods

5.2.1 Cyanobacteria cultivation and loofah preparation

Synechococcus elongatus CCAP 1479/1A and PCC 7942 (freshwater cyanobacteria) were cultivated under the same conditions as described in section 4.2.1 of Chapter 4. Loofah were prepared as described in section 4.2.5 of Chapter 4.

5.2.2 Latex binders

Acrylic latex polymer binders were prepared by the Department of Applied Sciences, Northumbria University, using monomer mixtures (styrene (St), butyl acrylate (BA), and acrylic acid (AA)) and adjusted to pH 7 using 0.1 M sodium hydroxide (Table 5.1). With those monomers, the polymers formed were poly (butyl acrylate-co-styrene-co-acrylic acid) as shown in Figure 5.1. St and BA were the main monomers, while the AA was added to maintain the suspension of the latex particles in the emulsion (Reynhout et al., 2005). The hardness of latex binders was defined by the glass transition temperature (Tg) which was controlled by altering the ratio of St and BA, which offer hard and soft characteristics respectively (Wang and Chen, 2019). A typical acrylic latex polymer consists of 50:50 St:BA (Anderson and Daniels, 2003); hence, the binders used in this Chapter with that ratio were termed 'normal' latex binders, those with more St than BA were termed 'hard' binders and those with less St than BA were termed 'soft' binders. The Tg values were measured using differential scanning colorimetry (Koshy et al., 2017).
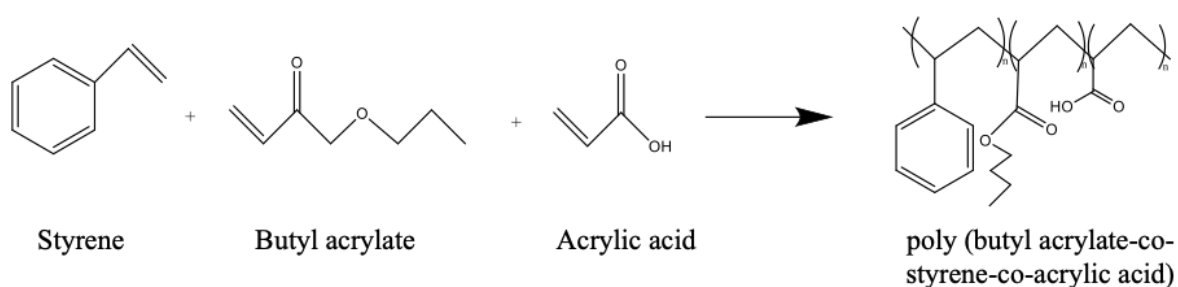
Figure 5.1 Latex polymerisation of styrene, butyl acrylate and acrylic acid as monomers.

To begin the polymerisation process, a solution of all the monomers (150 ml h^{-1}) was added dropwise into an inert aqueous phase (i.e. sterile dH$_2$O) along with an initiator solution made of ammonium persulfate (3 g per 100 mL). Rhodapex® Ab/20 was used as a surfactant and was then added into the mixture (35 g per 1 L). After the latex particles were formed,

Texanol™ was added into the latex mixture as a coalescence agent to promote film formation during the drying stage (Corsi and Lin, 2009). Three levels of Texanol™ were selected (0, 4, 12% v/v) because they offered good viscosity and consistency to the latex binders. The percentage solid binder was determined by oven drying 100 μL of each binder in a pre-weighed aluminium foil cup for 24 h at 100 °C.

Table 5.1 Latex binder code, compositions of monomers, coalescence agent (Texanol™), and latex characteristics.

Type of latex	Latex code	Texanol™ (% v/v)	Glass transition temperature (°C)	Styrene (St) (g; mol)	Butyl acrylate (BA) (g; mol)	Acrylic acid (g; mol)	% solid binder (w/w)
Hard (St/BA 75:25)	0H	0	55.1 ± 0.5	375; 3.6	120; 0.94	10; 0.14	40.9 ± 0.4
	4H	4	46.5 ± 0.5	375; 3.6	120; 0.94	10; 0.14	42.2 ± 0.3
	12H	12	30.4 ± 2.6	375; 3.6	120; 0.94	10; 0.14	43.7 ± 0.6
Normal (St/BA 50:50)	0N	0	20.3 ± 0.8	250; 2.4	240; 1.87	10; 0.14	39.3 ± 0.3
	4N	4	17.6 ± 0.9	250; 2.4	240; 1.87	10; 0.14	39.9 ± 0.4
	12N	12	12.6 ± 0.8	250; 2.4	240; 1.87	10; 0.14	40.7 ± 0.2
Soft (St/BA 25:75)	0S	0	-13.1 ± 0.2	125; 1.2	360; 2.81	10; 0.14	41.8 ± 0.1
	4S	4	-17.9 ± 0.7	125; 1.2	360; 2.81	10; 0.14	42.3 ± 0.2
	12S	12	-21.1 ± 0.5	125; 1.2	360; 2.81	10; 0.14	44.8 ± 0.7

5.2.3 Contact toxicity and cell adhesion tests

Contact toxicity and adhesion tests followed the same procedures as outlined in section 4.2.4 and 4.2.5 of Chapter 4. A weighted decision matrix method was performed based on the obtained toxicity and adhesion data with a weighted ratio of toxicity to adhesion (3:2).

5.2.4 Photosynthetic response analysis using Imaging-PAM

An imaging pulse amplitude modulated-fluorometer (Imaging-PAM M-Series MAXI Version; Walz GmbH) is an instrument used for analysing photosynthetic metabolic responses through

quantification of chlorophyll fluorescence levels (GmbH, 2019). The purpose of the analysis was to determine photosynthetic responses of cyanobacteria exposed to different latex binders. For each sample, 1 mL of the polymer emulsion mixture was combined with 1 mL of concentrated cell mixture to form a biocoating (2.5% v/v cells/ sterile dH_2O) in individual wells (n = 3) of a 24-multiwell plate. The corresponding abiotic controls (latex only) were run in the same well plate. The samples were monitored daily for seven days, during which the samples were gently mixed using forward and reverse pipetting and left to adapt in darkness for 30 mins before each record. To mitigate for the high phycocyanin pigment content in cyanobacteria, the IPAM settings were adjusted to the gain values of 20 to 25 depending on the base intensity and a low saturation pulse intensity of 1. These settings were determined experimentally prior to the assays. The maximum photosystem II (PSII) quantum yield (Fv/Fm) was determined from the dark fluorescence yield (Fo) and maximum fluorescence yield (Fm) using Equation 5.1 (GmbH, 2019). The apparent rate of photosynthesis (PS) was calculated from the measured effective PSII quantum yield (Y(II)), the incident photon flux density (PAR) which was fixed at 370 μmol photon m^{-2} s^{-1}, and the measured absorptivity (Abs.) using Equation 5.2 (GmbH, 2019). For the calculation of PS, 50% of the absorbed PAR was assumed to be distributed to PSII (GmbH, 2019).

$$\frac{F_v}{F_m} = \frac{F_m - F_o}{F_m} \qquad (5.1)$$

$$PS = 0.5 \times Y(II) \times PAR \times Abs. \qquad (5.2)$$

5.2.5 Semi-batch CO₂ absorption test

Loofah were cut into strips of approximately 1 × 1 × 5 cm. Each strip was pre-weighed and labelled. From the decision matrices, the two best performing polymer emulsions for each species were 4S and 12S for *S. elongatus* CCAP 1479/1A, while 4N and 12N were better for *S. elongatus* PCC 7942 (Figure 5.5). Six hundred μL of biocoating was pipetted onto each replicate loofah strip, covering approximately 1 × 1 × 3 cm and oven dry at 20 °C for 24 h in darkness. Each biocomposite was tested using the same procedure and conditions as detailed in section 4.2.6 of Chapter 4 including abiotic and biotic controls.

5.2.6 Biocomposite microstructure analysis

Biocomposites were analysed before and after the CO_2 absorption tests using scanning electron microscopy (Tescan Vega 3LMU) with a voltage of 8 kV. Biocomposites were dried at 105 °C for 3 h, stored in a desiccator for at least 24 h, and attached to 12 mm diameter pin stubs using carbon tape. Prior to the analysis, each sample was gold coated to protect the structure from

bombarded electron beams and to increase the conductivity of the samples. A 5000×
magnification was used.

5.2.7 Total carbohydrate extraction

The total carbohydrate extraction was modified from Moheimani et al. (2013). Prior to
extraction, the biocomposites from the semi-batch CO_2 absorption tests were frozen at -20 °C,
freeze-dried (Martin Christ 1-4 LD Plus) for 48 h, and ground (Cookworks Coffee and Herb
Grinder). Each sample was homogenised with 1 mL of 1M H_2SO_4 in a 45 mL acid resistant
centrifuge tube then 10 mL of the same solution was added. The samples were incubated in a
water bath at 100 °C for 1 h and left to cool to ambient temperature (20 °C). The samples were
isolated from the acid solution by centrifugation (Sigma Laboratory Centrifuges, 3K18 C) at
2000 RCF (3333 RPM) for 10 mins. For each sample, 2 mL was carefully transferred into a
new centrifuge tube without disturbing the solid residue. The isolated extract was mixed with
1 mL of phenol solution (50 g L^{-1} in concentration) before 5 mL concentrated H_2SO_4 (>95%
concentration) was added, and both solutions were vortexed for 10 to 20 sec (Vortex Genie 2,
Scientific Industries, Inc.). The mixture was left to cool to ambient temperature (20 °C) before
1 mL was placed into a 1.5 mL cuvette and analysed in a UV-Vis spectrometer (Cary 100 Bio
UV-Visible Spectrometer) at a wavelength of 485 nm. A standard calibration curve of known
glucose concentrations was used to calculate the total carbohydrate content in the
biocomposites. The samples were sacrificially analysed for carbohydrate content at weeks 2, 4,
6, and 12 of the CO_2 absorption tests (n = 3 for each treatment). The carbohydrate extraction
was also conducted on abiotic controls (i.e. loofah scaffold with latex only) to normalise the
biocomposites, and presented as a percentage of the total carbohydrate content in immobilised
dried weight biomass.

5.2.8 Statistical analysis

Minitab 18 and Microsoft Excel with RealStatistics Add-in were used for statistical analysis.
Normality was tested with the Anderson-Darling test and equality of variance tested using the
Levene's test. Data that met these assumptions were analysed using two-way analysis of
variance (ANOVA) with Tukey's test as a post-hoc analysis. Two factor data that did not meet
the assumptions of normality and equality of variance were analysed using the Scheirer-Ray-
Hare test, followed by the Mann-Whitney U test to identify significance between treatments. A
Generalised Linear Mixed (GLM) model was used for non-normal data with three factors, in
which the data were transformed using a Johnson transformation (Smith, 2018). A Pearson's
product-moment correlation was conducted to assess relationship between Texanol™
concentration, Tg of latex binders, toxicity, and adhesion data.

5.3 Results

5.3.1 Toxicity and adhesion screening

Nine latex binders with three polymer particle blends (H - Hard, N - Normal, S - Soft) and three levels of Texanol™ (0, 4, 12% v/v) were tested for toxicity and adhesion with two cyanobacterial strains. Binder type significantly influenced cell growth for *S. elongatus* PCC 7942 (Scheirer-Ray-Hare test, Binder: DF = 2, H = 23.157, P = <0.001) and CCAP 1479/1A (Two-way ANOVA, Binder: DF = 2, F = 103.93, P = <0.001) (Figure 5.2). There was no significant effect of Texanol™ concentration on *S. elongatus* PCC 7942 cell growth; only the N-latex binders were non-toxic (Figure 5.2a), with 0N and 4N supporting increased cell growth of 26 and 35% respectively (Mann-Whitney U, 0N vs. 4N: W = 13.50, P = 0.245; 0N vs. control: W = 25.0, P = 0.061; 4N vs. control: W = 25.0, P = 0.061), and 12N sustaining growth that was comparable to the biotic controls (Mann-Whitney U, 12N vs. control: W = 17.0, P = 0.885). For *S. elongatus* CCAP 1479/1A, binder blend and Texanol™ concentration were both significant factors, with a significant interaction between the two (Two-way ANOVA, Binder: DF = 2, F = 103.93, P = <0.001, Texanol: DF = 2, F = 5.96, P = 0.01, Binder*Texanol: DF = 4, F = 3.41, P = 0.03). The 0N binder and all of the soft latex binders enhanced cell growth (Figure 5.2b). There was a trend of improved growth as the styrene composition decreased.

In most cases, cell viability decreased as the Texanol™ concentration increased. However, a Pearson's product-moment correlation suggested that there was no statistical linear relationship between the Texanol™ concentration and growth of both cyanobacteria strains (CCAP 1479/1A: DF = 25, r = -0.208, P = 0.299; PCC 7942: DF = 25, r = -0.127, P = 0.527). Figure 5.3 presents the relationship between cell growth and the binder's glass transition temperature (Tg). With each type of latex binder, there was a strong negative correlation between the Texanol™ concentration and Tg values (H binder: DF = 7, r = -0.989, P = < 0.001; N binder: DF = 7, r = -0.964, P = < 0.001; S binder: DF = 7, r = -0.946, P =< 0.001). The data indicate an optimal Tg for cell growth for *S. elongatus* PCC 7942 of approximately 17 °C (Figure 5.3a), whereas *S. elongatus* CCAP 1479/1A cell growth had a linear relationship that favoured a Tg of below 0 °C (Figure 5.3b). There was a strong negative correlation between the Tg and toxicity data of *S. elongatus* CCAP 1479/1A (DF = 25, r = -0.857, P =< 0.001), while there was no statistical linear correlation for the other strain (PCC 7942: DF = 25, r = -0.197, P = 0.325).

All of the latex binders had good adhesive affinity, with none of the replicates releasing more than 1% of cells after 72 h of testing (Figure 5.4). There were no statistically significant

differences between latex binders for either *S. elongatus* strain (PCC 7942: Scheirer-Ray-Hare test, Binder*Texanol, DF = 4, H = 0.903; P = 0.924; CCAP 1479/1A: Scheirer-Ray-Hare test, Binder*Texanol, DF = 4, H = 3.277, P = 0.513). As the Texanol™ concentration increased more cells were released (Figure 5.5). There was a stronger negative correlation between Texanol™ concentration and cell adhesion affinity for *S. elongatus* CCAP 1479/1A (DF = 25, r = -0.428, P = 0.026) than for *S. elongatus* PCC 7942 (DF = 25, r = -0.660, P = <0.001). Furthermore, there was no statistical relationship between the Tg and the cell adhesion data for either strain (PCC 7942: DF = 25, r = 0.301, P = 0.127; CCAP 1479/1A: DF = 25, r = 0.287, P = 0.147).
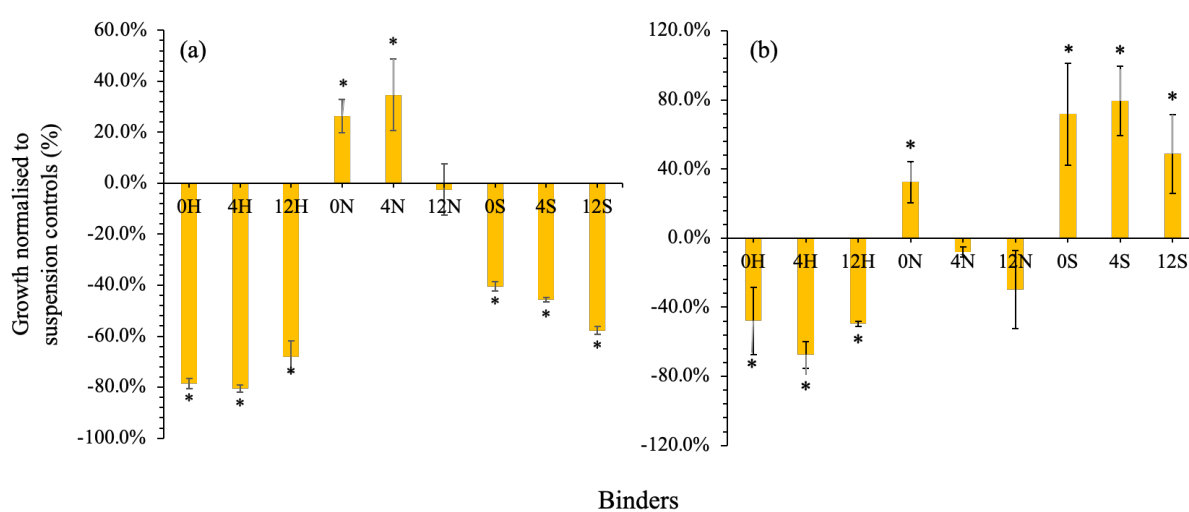
Figure 5.2 Toxicity testing using percentage growth normalised to suspension culture controls for (a) *S. elongatus* PCC 7942 and (b) CCAP 1479/1A. (Mean ± StDev; n = 3). Treatments marked with * were significantly different from the controls.
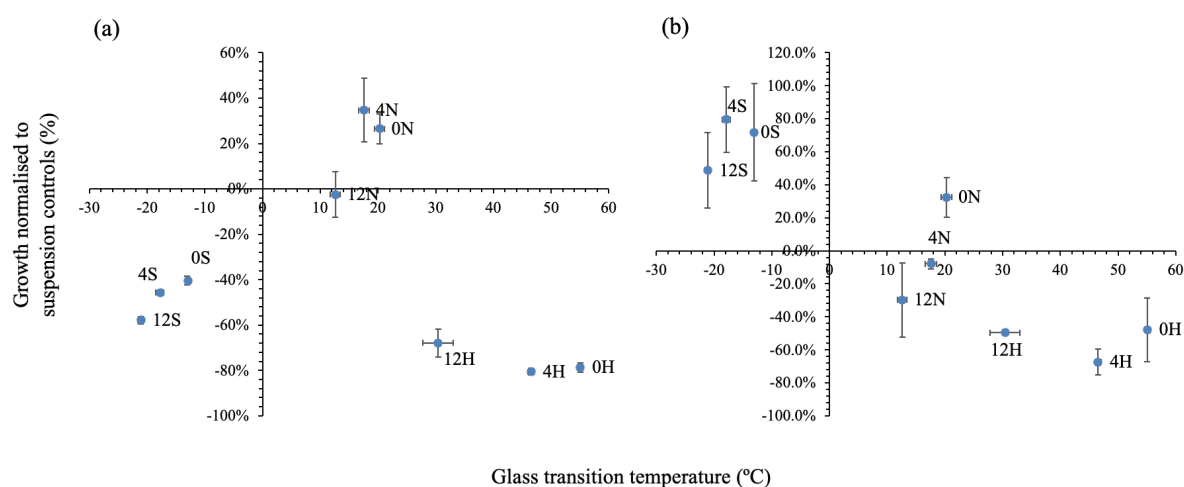
Figure 5.3 Growth data plotted against the glass transition temperature (Tg) of latex binders for *S. elongatus* (a) PCC 7942 and (b) CCAP 1479/1A. (Mean ± StDev; n = 3).
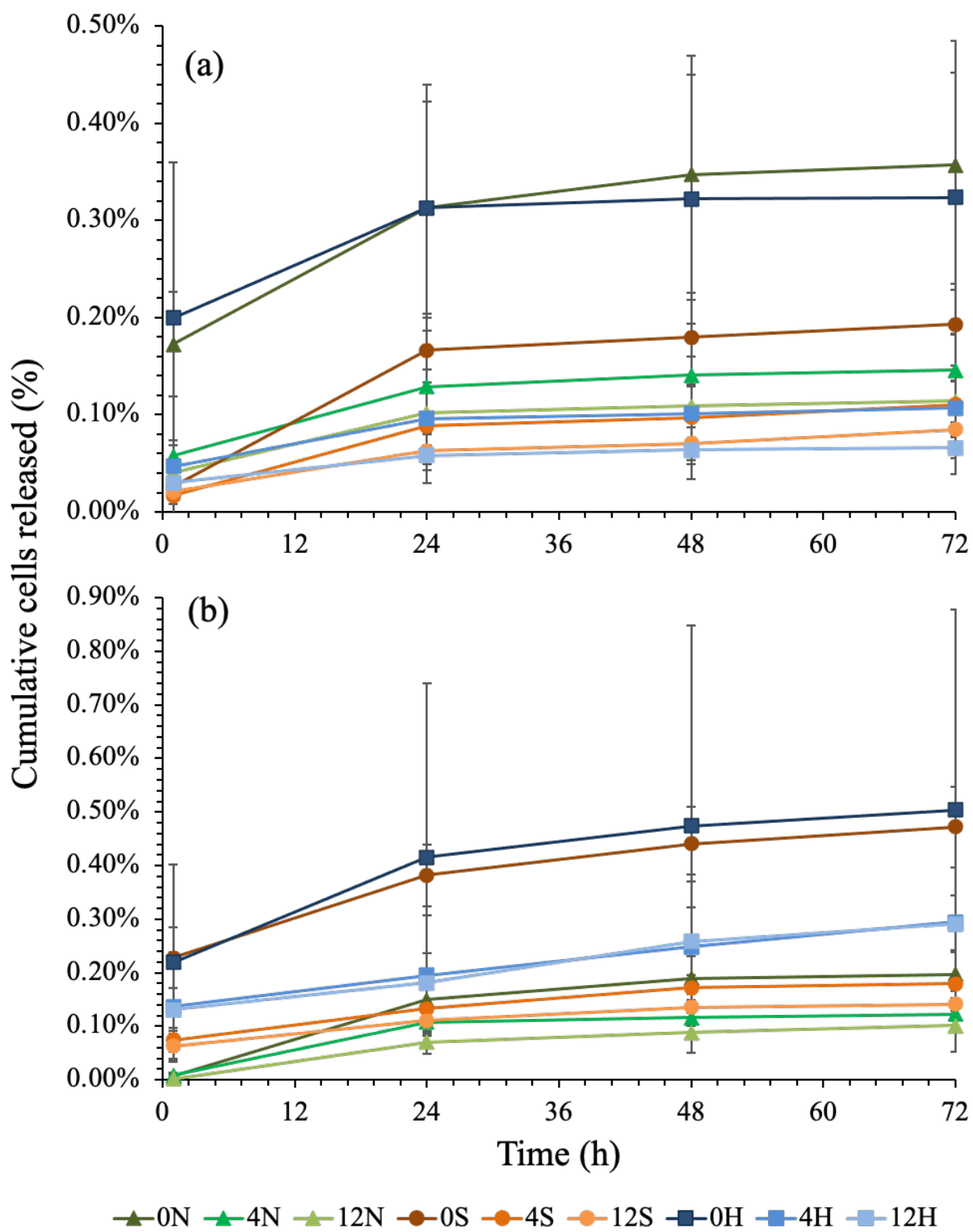
Figure 5.4 Cumulative cells released from adhesion testing of biocomposites for *S. elongatus* (a) PCC 7942 and (b) CCAP 1479/1A. (Mean ± StDev; n = 3).
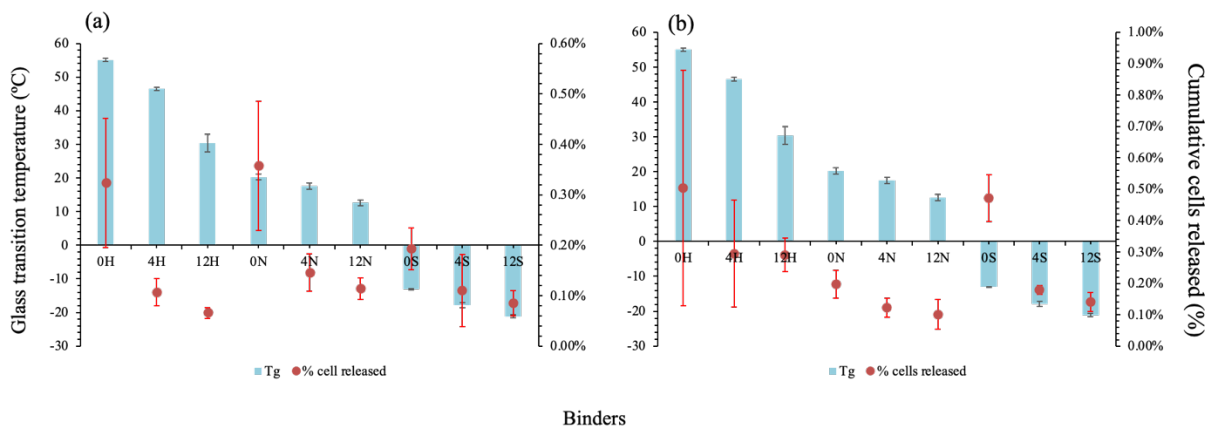
Figure 5.5 Adhesion data plotted against the glass transition temperature (Tg) of latex binders for *S. elongatus* (a) PCC 7942 and (b) CCAP 1479/1A. (Mean ± StDev; n = 3).

For both *S. elongatus* strains the hard latex binders, 0H and 4H in particular, performed poorly. In contrast, 4N and 12N were the best performing binders for *S. elongatus* PCC 7942, while 4S and 12S were the top binders for CCAP 1479/1A (Figure 5.6). These binders were taken forward for semi-batch net CO_2 absorption tests.
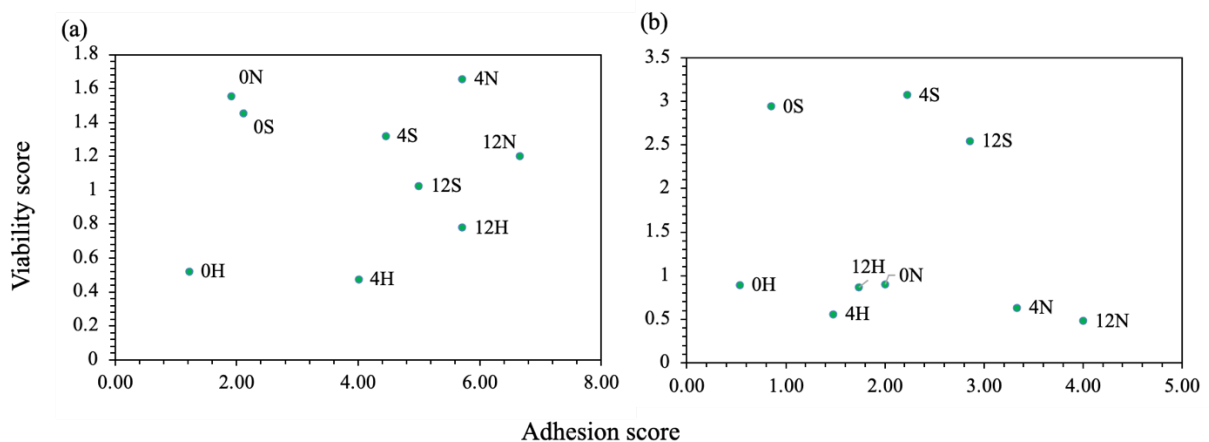
Figure 5.6 Decision matrix derived from toxicity and adhesion data for (a) *S. elongatus* PCC 7942 and (b) CCAP 1479/1A.

5.3.2   Photosynthetic responses to latex binders

I-PAM analyses were conducted over seven days using cells suspended in the aqueous latex formulations. In general, both the apparent rate of photosynthesis (PS) and the maximum PSII quantum yield (Fv/Fm) decreased over time, although the decreases were not uniform and a number of the PS datasets displayed a bi-phasic response indicating a partial, albeit short-lived

recovery of PS activity with time (Figure 5.7 and 5.9). The biphasic response was less pronounced for Fv/Fm (Figure 5.8 and 5.10).

PCC 7942 cells suspended in 12H binder had the lowest mean PS and F_v/F_m values (Figures 5.7 and Figure 5.8), indicating that the binder was more toxic. There were no significant differences in PS values between binders over time (GLM model, Binder*Texanol*Time, DF = 28, F = 1.49, P = 0.07). The type of binders had a significant effect on the PS data over time (GLM model, Binder*Time, DF = 14, F = 3.14, P =< 0.001), while Texanol™ concentration did not have a significant effect over time (GLM model, Texanol*Time, DF = 14, F = 1.63, P = 0.078). For the F_v/F_m dataset, there were significant differences between binders over time (GLM model, Binder*Texanol*Time, DF = 28, F = 4.54, P =< 0.001).

For CCAP 1479/1A cells, there were significant differences between binders over time for PS dataset (GLM model, Binder*Texanol*Time, DF = 28, F = 2.75, P =<0.001). Similar to PCC 7942 cells, the type of binders had a significant effect on the PS data over time (GLM model, Binder*Time, DF = 14; F = 6.38; P =< 0.001) but Texanol™ concentration did not affect the PS data (GLM model, Texanol*Time, DF = 14, F = 1.26, P = 0.239). The 0S and 4S soft binders supported PS performance levels slightly higher than the suspension controls and supported improved performance of F_v/F_m (Figure 5.10) indicating an enhancement of photon transport into photosystem II. For the F_v/F_m values of CCAP 1479/1A cells, there were significance differences between binders over time (GLM model, Binder*Texanol*Time, DF = 28, F = 6.00, P =<0.001).

Figures 5.11 and 5.12 plot the mean PS and Fv/Fm values over the seven days period against the cell growth data for each strain. There were no clear patterns for the *S. elongatus* PCC 7942 data (Figure 5.11); however, the CCAP 1479/1A data indicated a parabolic relationship for PS and Fv/Fm values with the cell growth broadly following the change in the styrene and butyl acrylate ratio (Figure 5.12).
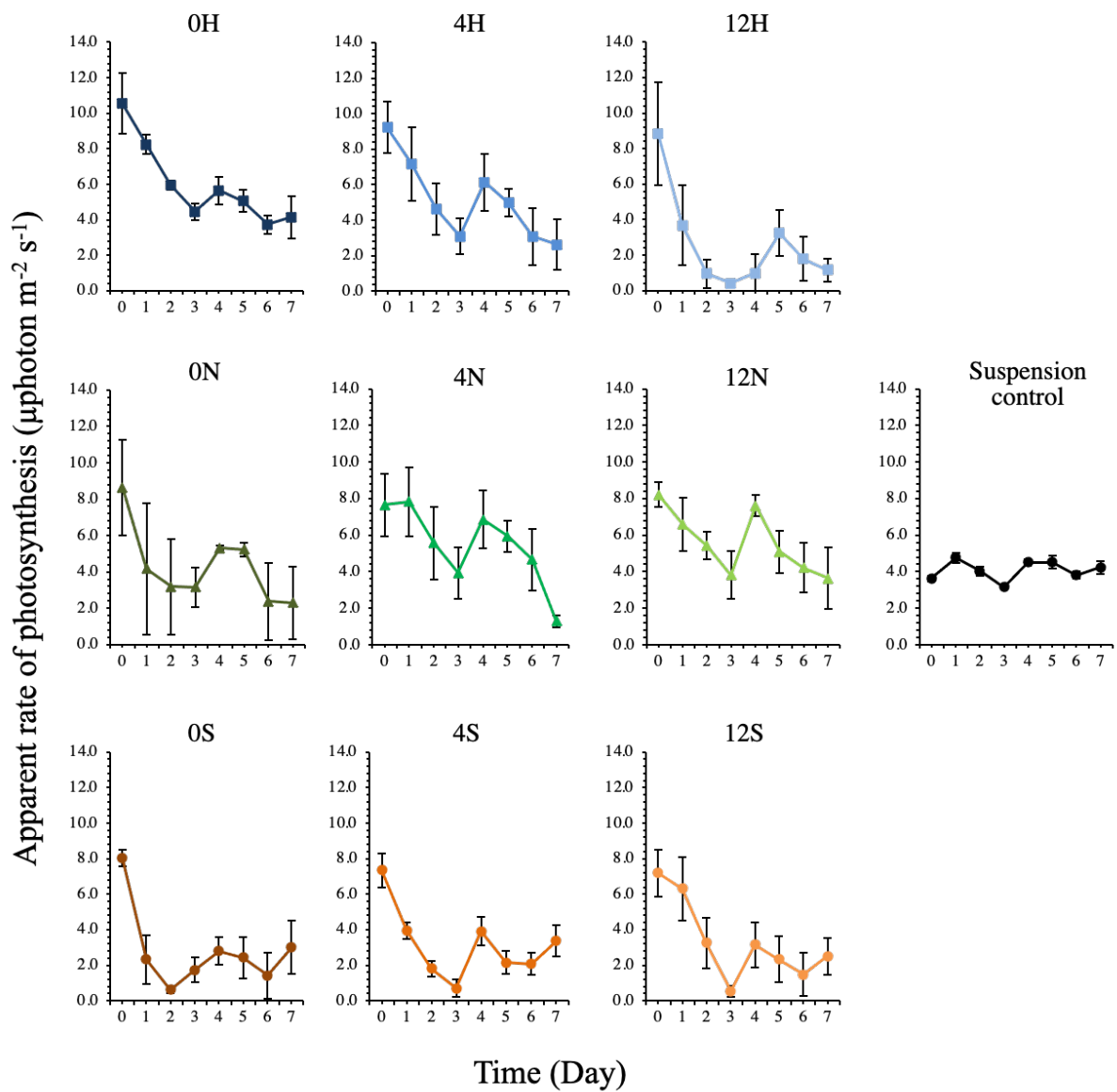
Figure 5.7 Apparent rate of photosynthesis of *S. elongatus* PCC 7942 in response to latex binders compared to suspension culture controls over a seven day period. (Mean ± StDev).
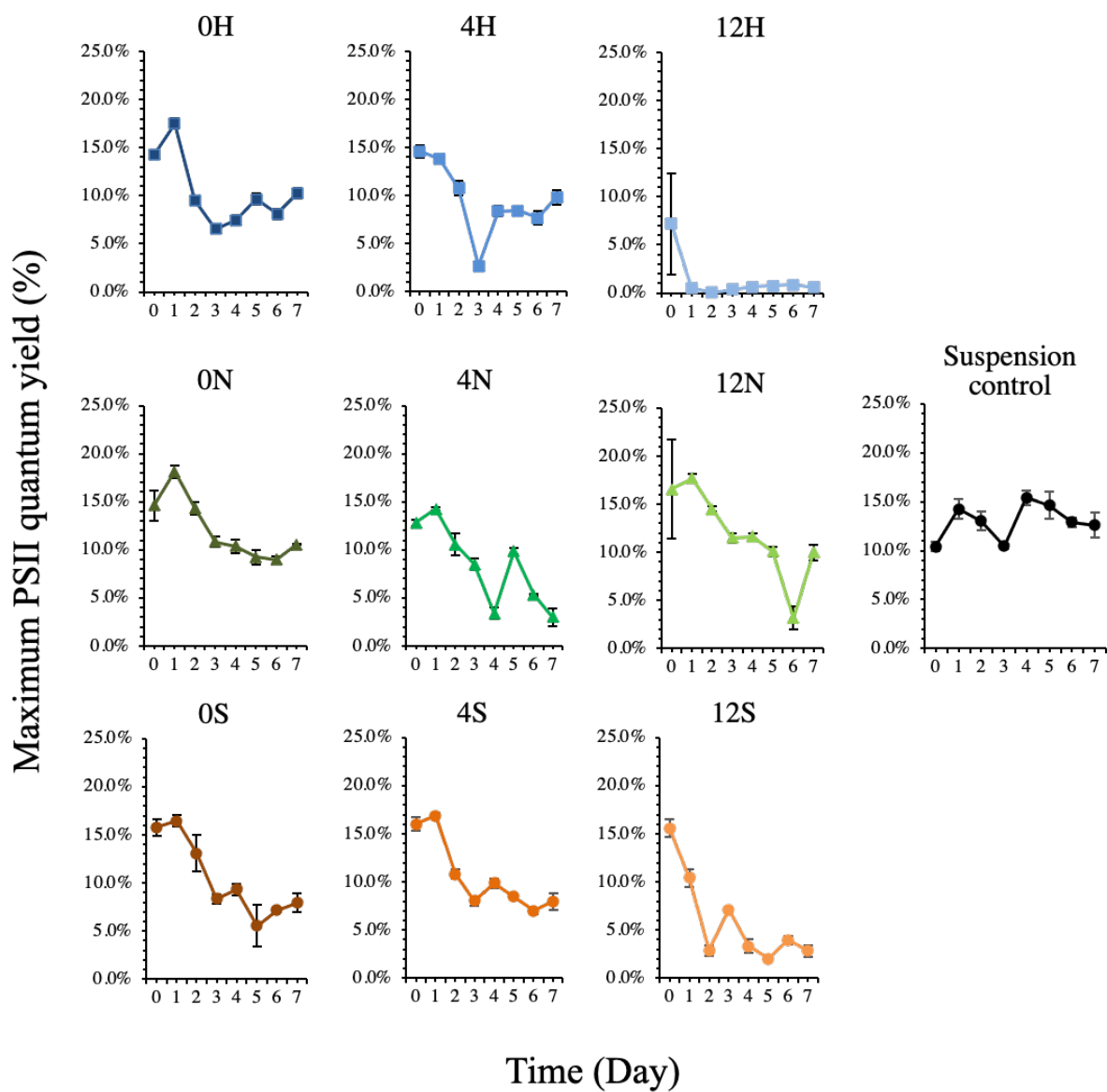
Figure 5.8 Maximum PSII quantum yield of *S. elongatus* PCC 7942 in response to latex binders compared to suspension culture controls over a seven day period. (Mean ± StDev).
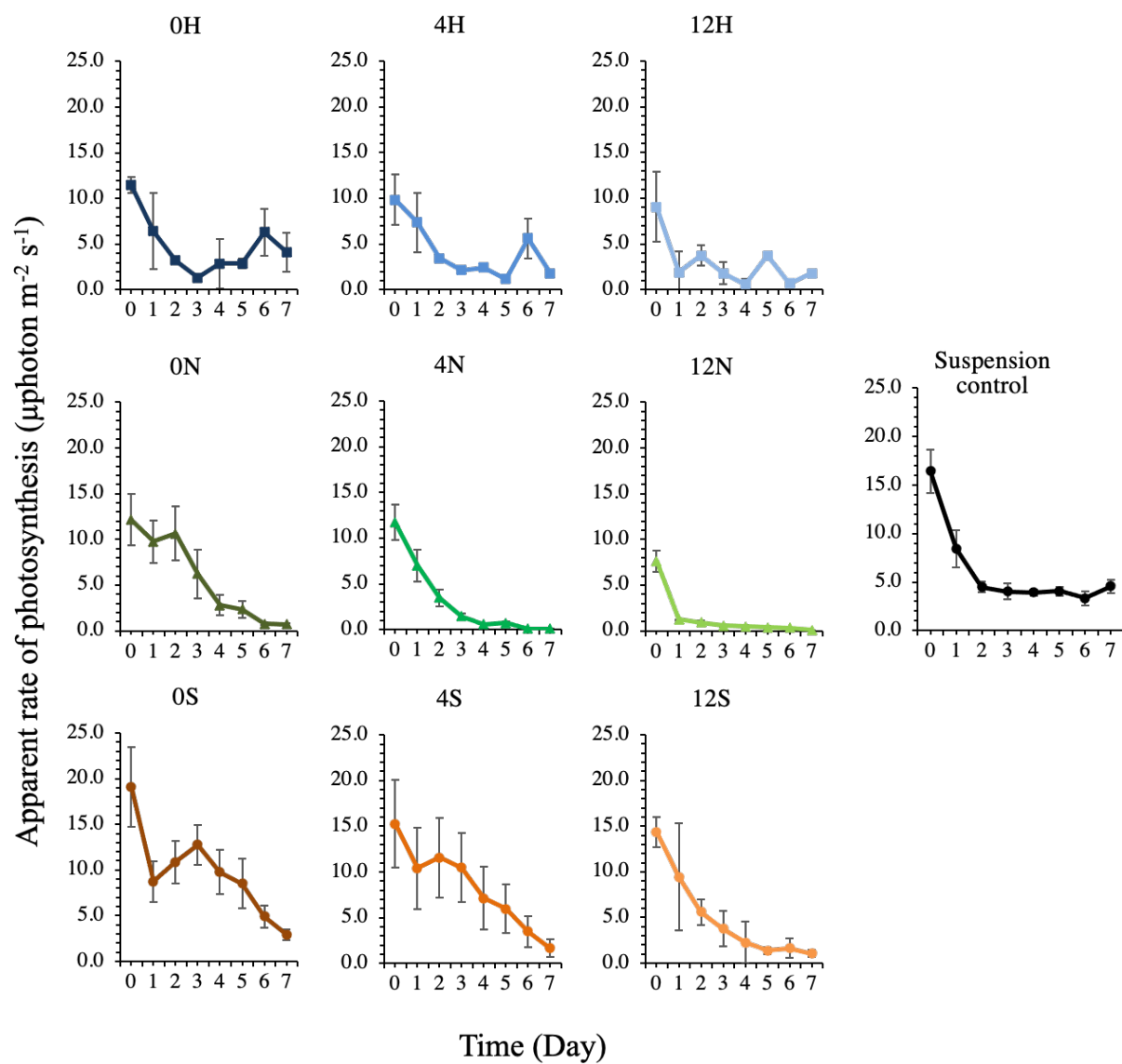
Figure 5.9 Apparent rate of photosynthesis of *S. elongatus* CCAP 1479/1A in response to latex binders compared to suspension culture controls over a seven day period. (Mean ± StDev).
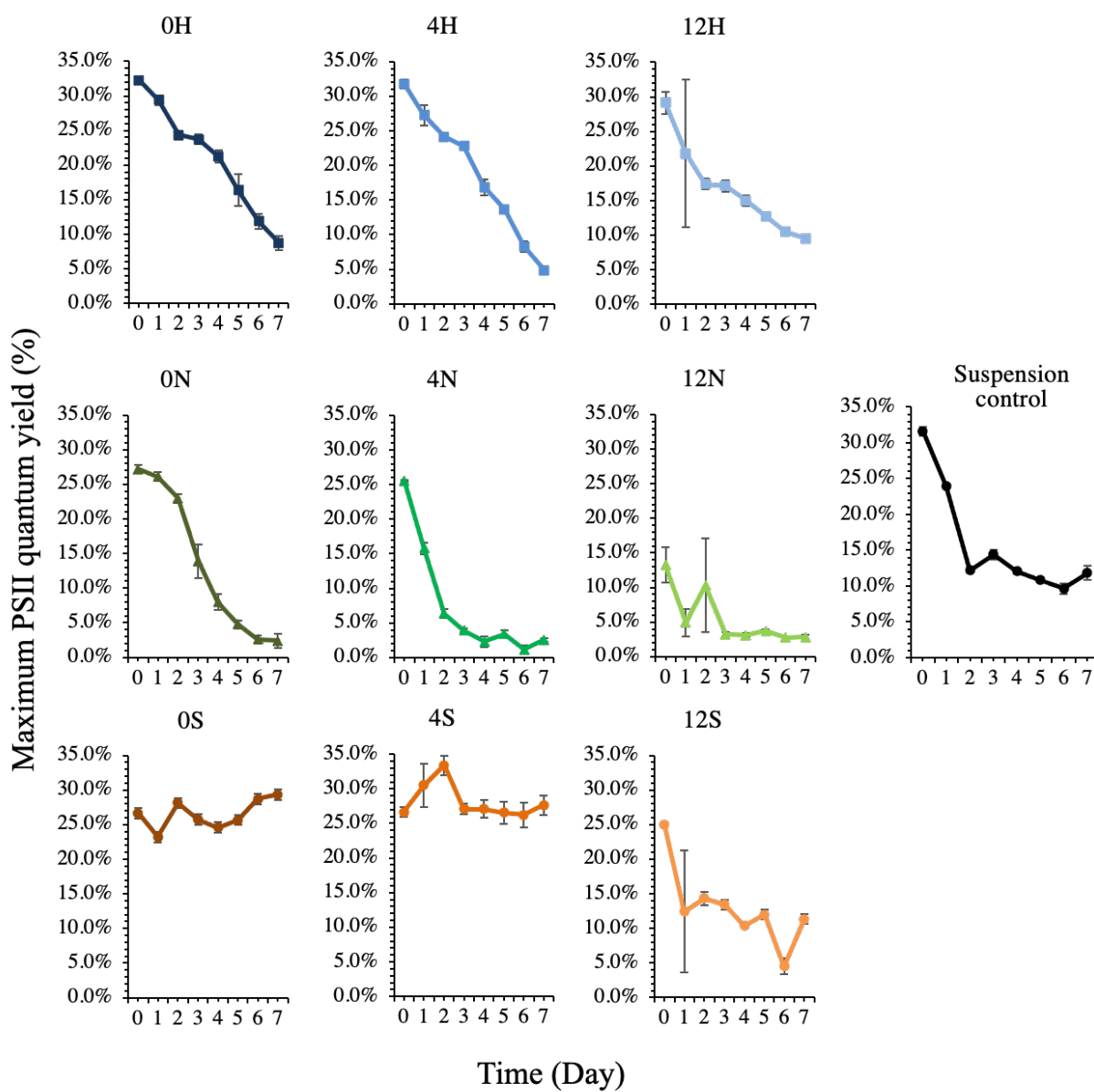
Figure 5.10 Maximum PSII quantum yield of *S. elongatus* CCAP 1479/1A in response to latex binders compared to suspension culture controls over a seven day period. (Mean ± StDev).
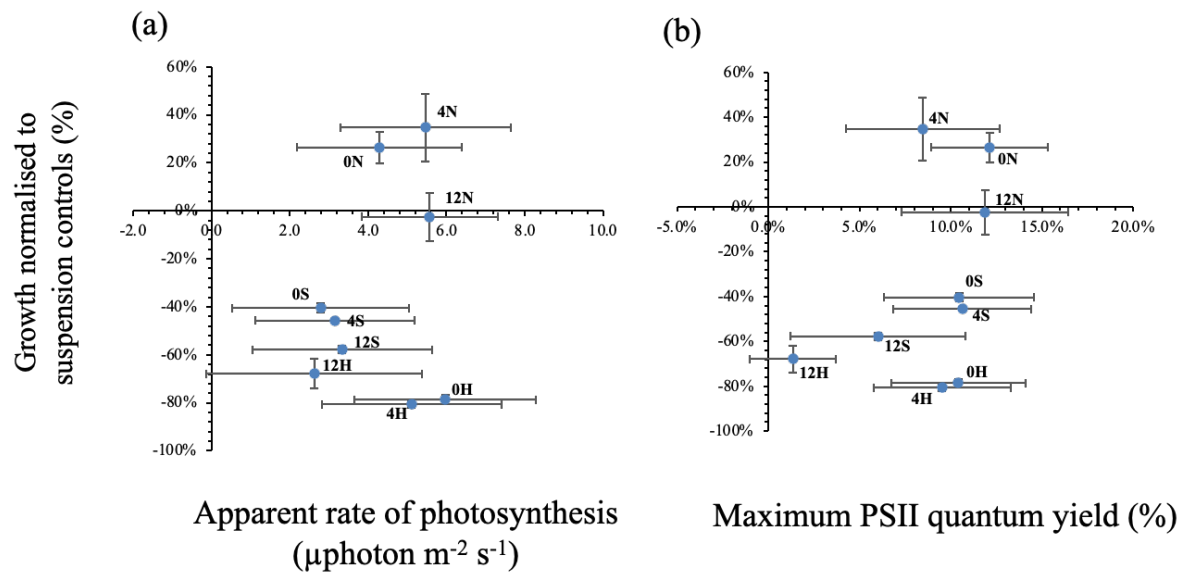
Figure 5.11 Toxicity data vs. (a) apparent rate of photosynthesis and (b) maximum PSII quantum yield of *S. elongatus* PCC 7942 in response to latex binders. (Mean ± StDev).
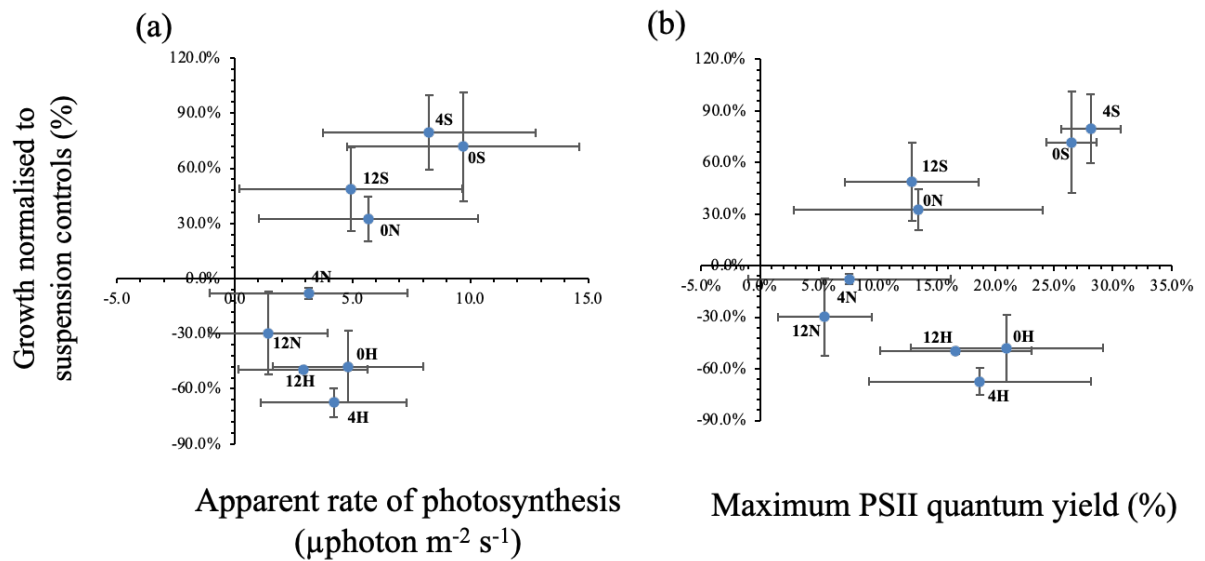
Figure 5.12 Toxicity data vs. (a) apparent rate of photosynthesis and (b) maximum PSII quantum yield of *S. elongatus* CCAP 1479/1A in response to latex binders. (Mean ± StDev).

5.3.3 Net CO$_2$ fixation rates

The PCC 7942 biocomposites had limited effectiveness in retaining cells, with considerable cell leaching within the first four weeks (Figure 5.13a). After an initial CO$_2$ absorption phase, cells immobilised with the 12N binder began to release CO$_2$, maintaining this pattern between days 4 to 14 (Figure 5.13b). These data correspond to observations of pigment bleaching. Net CO$_2$ absorption commenced again from day 18. Despite the release of cells (Figure 5.13a), the PCC 7942 12N biocomposites still accumulated more CO$_2$ than the suspension controls across the 28 days, although not significantly so (Mann-Whitney U test, W = 2275.5; P = 0.066). The CO$_2$ absorption rates with the 12N and 4N binders were 0.51 ± 0.34 and 1.18 ± 0.29 g CO$_2$ g$^{-1}_{biomass}$ d^{-1}. There were statistically significant differences between treatment and time levels (Scheirer-Ray-Hare test, Treatment: DF = 2, H = 70.62, P = <0.001 Time: DF = 13, H = 23.63, P = 0.034) but there was no significant interaction between treatment and time (Scheirer-Ray-Hare test, Time*Treatment: DF = 26, H = 8.70, P = 0.999).

Cell retention was much improved for the CCAP 1479/1A strain with binders 4S and 12S, despite the pigments slowly discolouring with time (Figure 5.15a). Both CCAP 1479/1A biocomposites absorbed CO$_2$ for the full 84 days (12 weeks) without additional nutrient supplementation. SEM analysis (Figure 5.16) supported the visual observation of little cell detachment. Initially, the cells were embedded within the latex coatings (Figures 5.16a and 5.16c) and, despite cell growth, the integrity of the binders held (Figures 5.16b and 5.16d). The CO$_2$ absorption rates were significantly higher than the suspension controls (Scheirer-Ray-Hare test, Treatment: DF = 2; H = 240.59; P = <0.001, Time: DF = 42; H = 112; P = <0.001) (Figure 5.15b). The 12S biocomposites achieved the highest CO$_2$ absorption rate (1.57 ± 0.08 g CO$_2$ g$^{-1}_{biomass}$ d^{-1}), with the 4S binder being 1.13 ± 0.41 g CO$_2$ g$^{-1}_{biomass}$ d^{-1}, but they were not significantly different (Mann-Whitney U test, W = 1507.50; P = 0.07) and there was no significant interaction between treatment and time (Scheirer-Ray-Hare test, Time*Treatment: DF = 82; H = 10.37; P = 1.000).
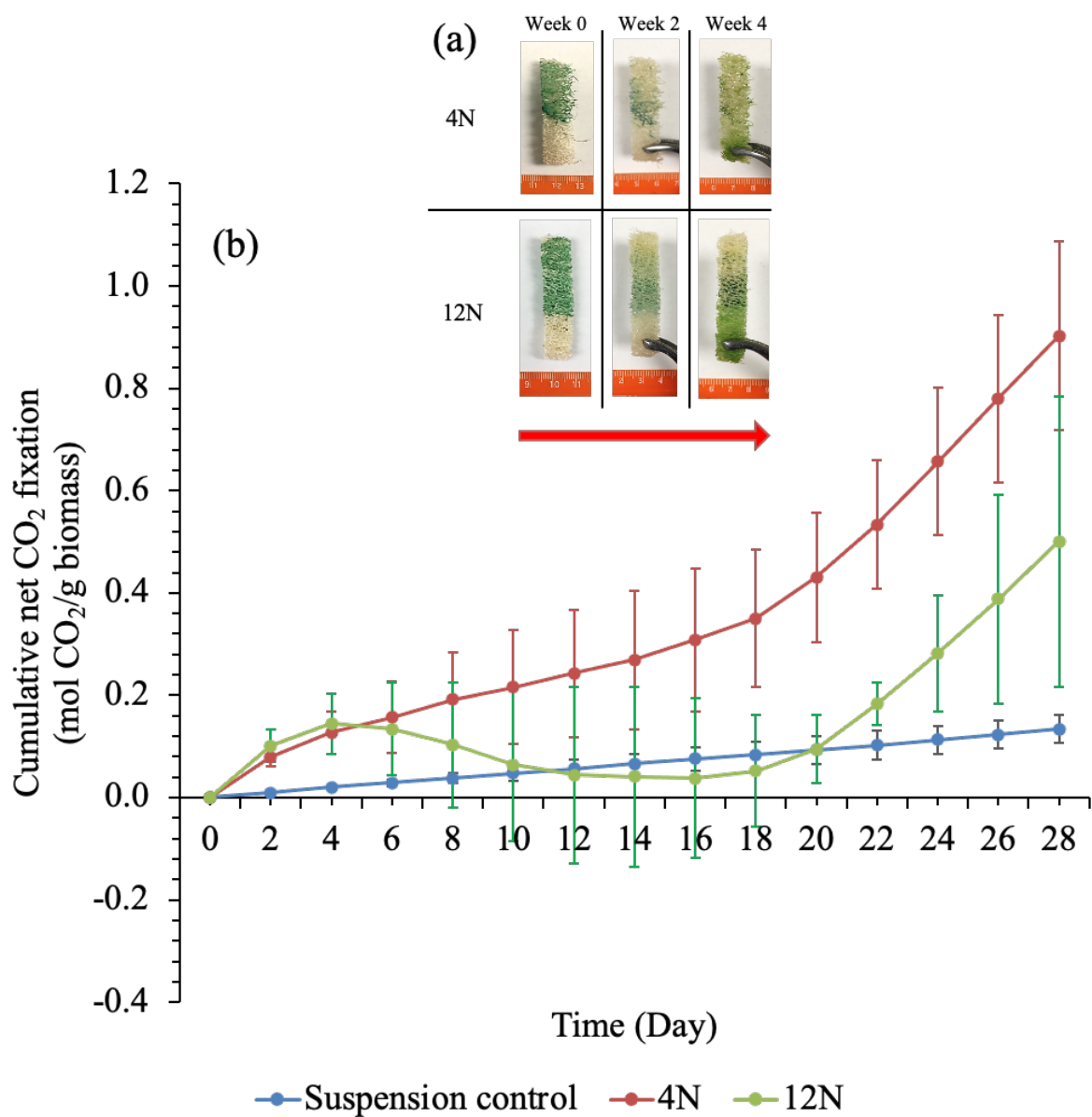
Figure 5.13 Semi-batch CO_2 absorption tests on (a) *S. elongatus* PCC 7942 biocomposites with the 4N and 12N latex binders. (a) Images demonstrating cell release and pigment bleaching; (b) cumulative net CO_2 absorption over the four weeks period. (Mean ± StDev; n = 3).
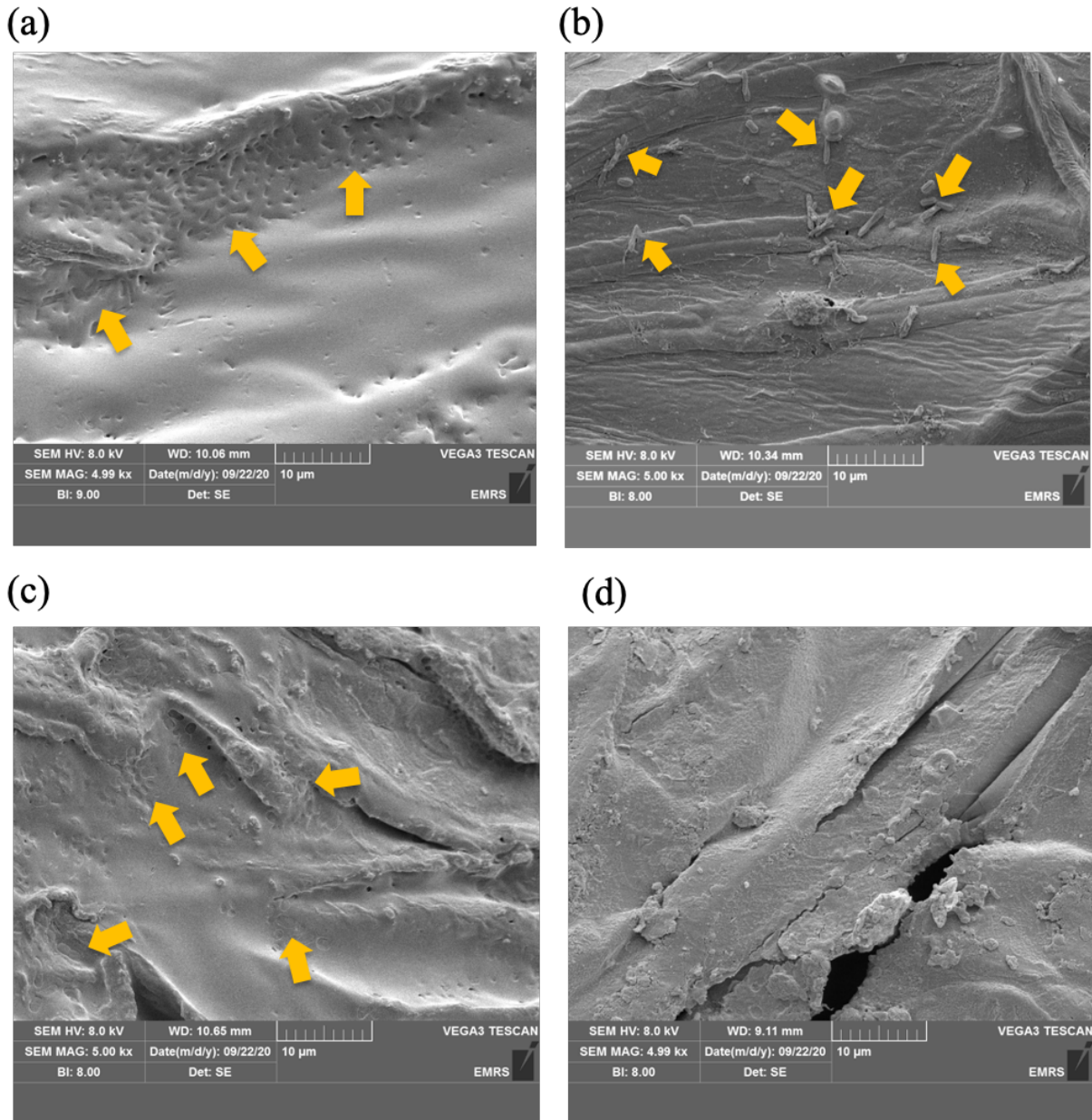
Figure 5.14 SEM images of *S. elongatus* PCC 7942 biocomposites before (a = 4N, c = 12N) and after (b = 4N, d = 12N) semi-batch CO_2 absorption tests. Arrows indicate where cells were deposited on the biocomposites.
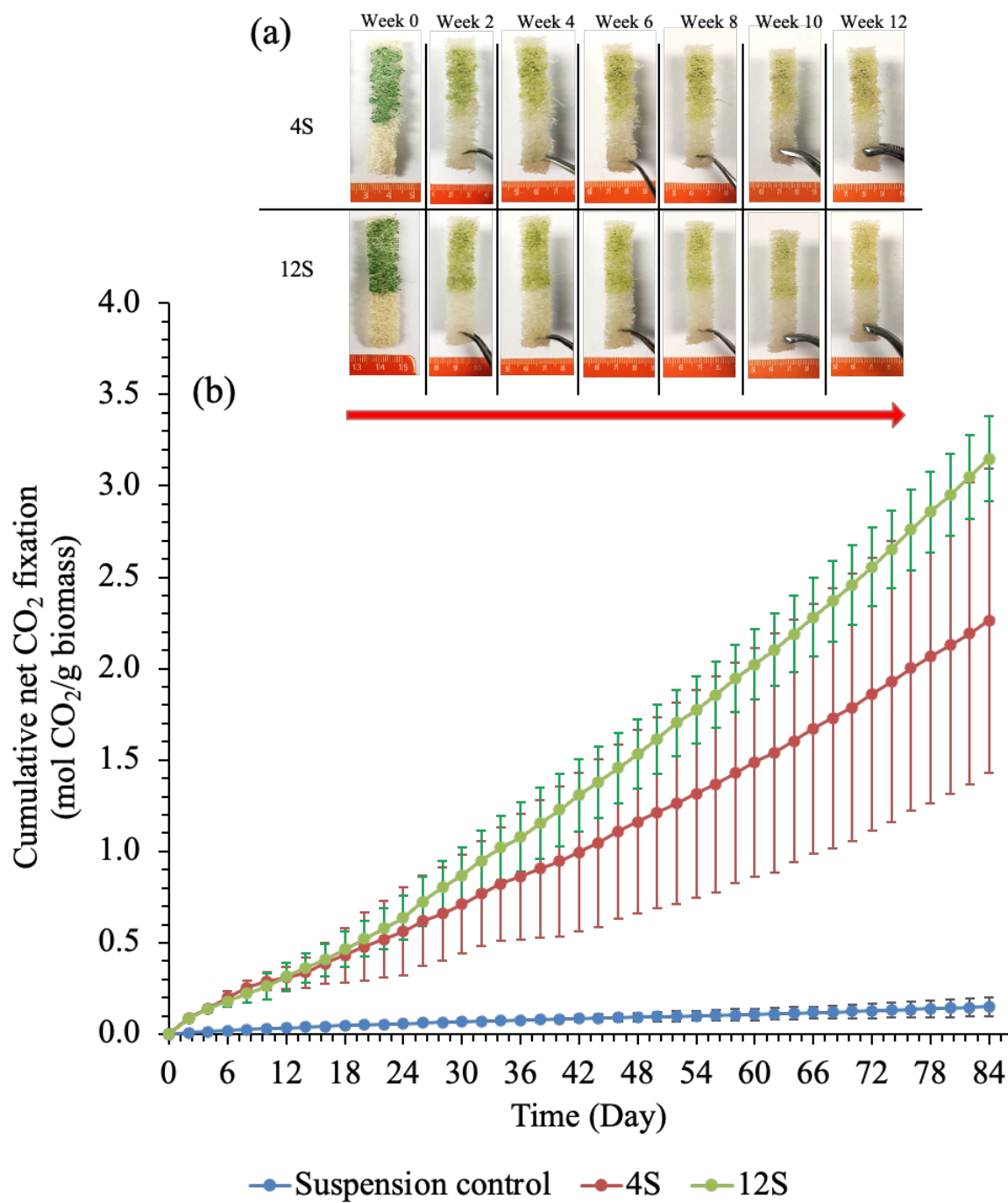
Figure 5.15 Semi-batch CO$_2$ absorption tests on (a) *S. elongatus* CCAP 1479/1A biocomposites with the 4S and 12S latex binders. (a) Images demonstrating pigment bleaching but little cell release; (b) cumulative net CO$_2$ absorption over the 12 weeks period. (Mean ± StDev; n = 3).
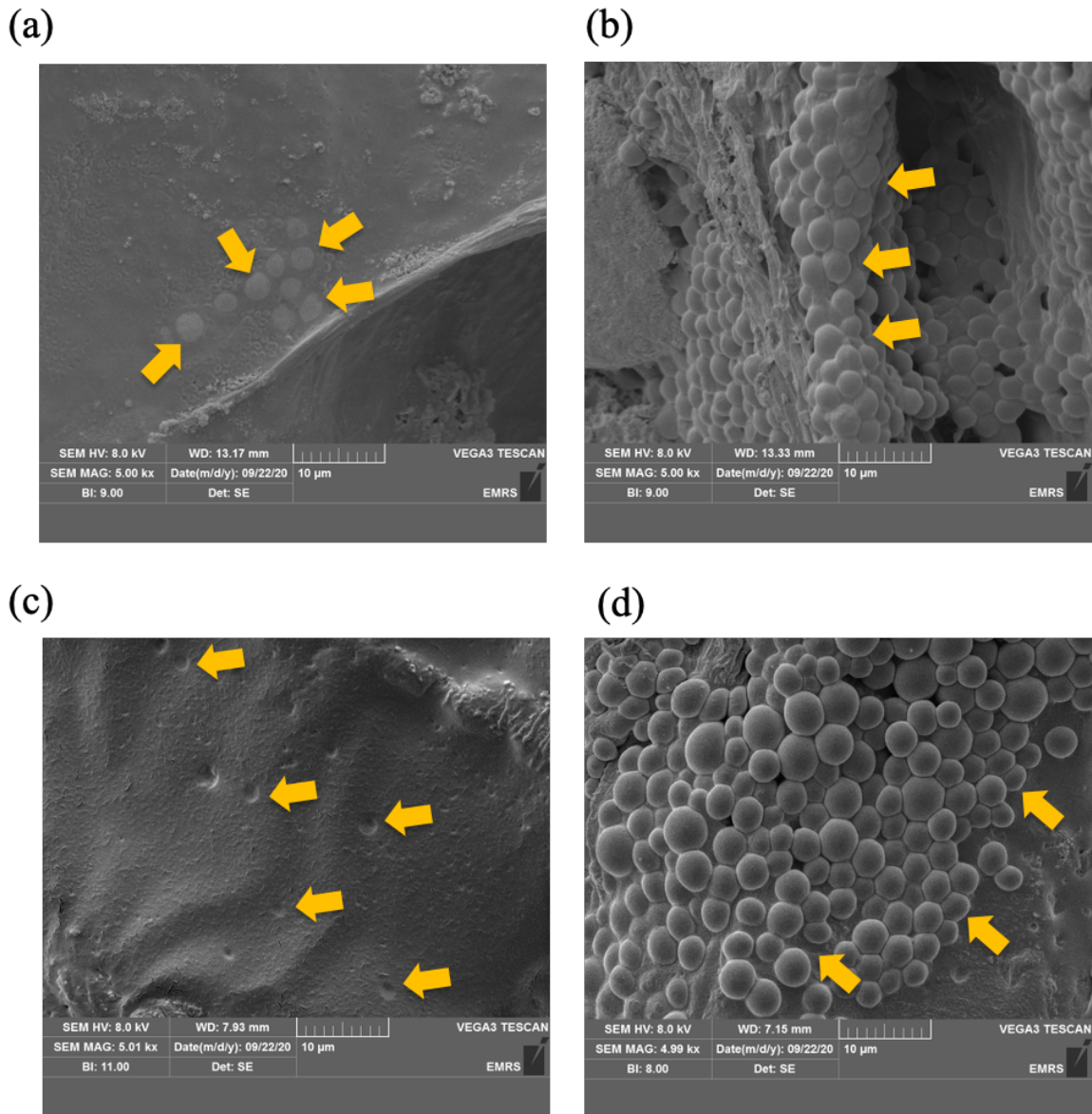
Figure 5.16 SEM images of *S. elongatus* CCAP 1479/1A biocomposites before (a = 4S, c = 12S) and after (b = 4S, d = 12S) semi-batch CO_2 absorption tests. Arrows indicate where cells were deposited on the biocomposites.

5.3.4 Carbohydrate production in biocomposites

Figure 5.17 shows the carbohydrate content of the dried cyanobacteria biomass of the biocomposites (normalised to the carbohydrate content of the loofah scaffolds with binders) and the suspension controls following the CO_2 absorption tests. There were no significance differences for either PCC 7942 (Scheirer-Ray-Hare test, Time*Treatment: DF = 4, H = 3.243, P = 0.518) and CCAP 1479/1A biocomposites (two-way ANOVA, Time*Treatment: DF = 8, F = 1.79, P = 0.119). Carbohydrate content was highest by week 2 in the PCC 7942 biocomposites (4N = 59.4 ± 22.5% w/w, 12N = 67.9 ± 3.3% w/w) (Figure 5.17a), whereas the carbohydrate content of the suspension control was highest by week 4 (Control = 59.6 ± 2.84%

w/w) (Figure 5.17a). Apart from at the start of the trial, the total carbohydrate content of the CCAP 1479/1A biocomposites was generally equivalent to the suspension controls, with some variation in the 12S binder on week 4 (Figure 5.17b). The highest biocomposite values were $51.9 \pm 9.6\%$ w/w for 4S and $77.1 \pm 17.0\%$ w/w for 12S.
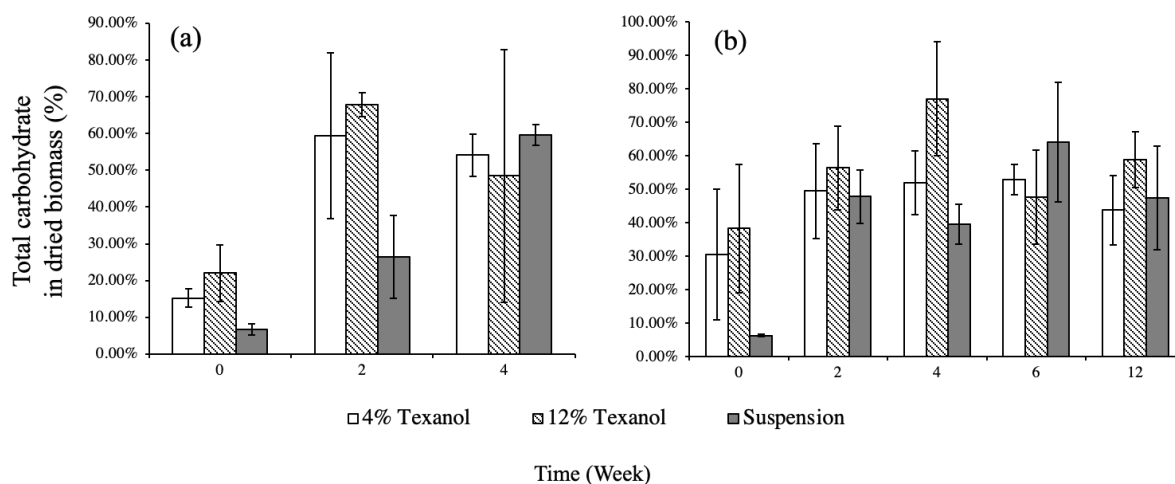
Figure 5.17 Total carbohydrate content extracted from (a) *S. elongatus* PCC 7942 + normal binder biocomposites and (b) CCAP 1479/1A + soft binder biocomposites during the CO_2 absorption test. (Mean $\pm$ StDev, n = 3).

5.4 Discussion

In Chapter 4, latex binder selection was highlighted as a vital stage for the further development of loofah biocomposites. Acrylic latex binders are easily formulated and widely used in the coatings, textiles and adhesives industries (Anderson and Daniels, 2003). Here, cyanobacteria combined with water-borne acrylic latex polymer emulsions polymerised from known ratios of styrene/butyl acrylate particles and differing Texanol™ concentrations were tested. Styrene and butyl acrylate, which are hard and soft polymer particles, were chosen to manipulate surface physical properties, particularly the flexibility of the coating. Styrene is frequently used as a co-monomer with butyl acrylate because of its accessibility and compatibility (Anderson and Daniels, 2003). However, the toxicity data indicated that hard latex binders with a high styrene concentration were unfavourable for the survival of both cyanobacteria strains (Figure 5.2). Styrene is recognised as having certain ecological impacts on aquatic life and is highly toxic to algae (Cushman et al., 1997). Butyl acrylate is not known to be toxic to algae growth (McGowan et al., 2013), likely due to its low bioaccumulation potential (Rocha et al., 2016). Although the two cyanobacteria strains belong to the same species, they responded quite differently to the latex binders. For *S. elongatus* PCC 7942, there seemed to be an optimal Tg

(Figure 5.3a), whereas *S. elongatus* CCAP 1479/1A had a negative linear relationship with the Tg (Figure 5.3b). This indicates that factors other than nutrient media and cell morphology may influence the observed outcome.

Texanol™ is a widely used coalescence additive for most latex paints, with an annual mass production of up to 98,000 metric tons (Lin and Corsi, 2007). It has desirable properties including a slow evaporation rate, efficient coalescence, low water solubility, a low flammability rate, and is biodegradable (Corsi and Lin, 2009). Texanol™ promotes film formation by softening the polymer particles via absorption into polymer particles causing complete fusion during the drying stage (Corsi and Lin, 2009). With this physio-chemical property, as the increased concentration of Texanol™ in the latex binders, the Tg of the binders was reduced, potentially decreasing the film porosity and resulting in better cell adhesion (Figure 5.5).

The Tg also controls the final film morphology of coatings and can be adjusted by altering the composition of the monomers (Elizalde et al., 2020). As the biocomposites were dried at ambient temperature (~18-20 ℃), the Tg of the hard latex binders (30 to 55 ℃) were higher than the drying temperature, ensuring that the polymer was still in a glassy state (i.e. brittle) (Anderson and Daniels, 2003), ultimately resulting in greater cell leaching from the coatings. On the other hand, film formation in the normal and soft latex binders would had achieved the rubbery state as their Tg was close to (normal blend: 12 to 20 ℃) or well below (soft blend: -21 to -13 ℃) the ambient temperature (Anderson and Daniels, 2003) – potentially providing better cell retention. The surface charge of the binders is likely to influence the adhesion affinity, but further data are needed to provide meaningful insights. Nevertheless, all of the latex binders were effective at retain the cells, releasing less than 1% from the biocomposites.

In terms of biological responses, the apparent photosynthesis rate (PS) and maximum PSII quantum yield (Fv/Fm) showed that photosynthetic performances decreased over time in most cases for both cyanobacteria strains. These results agree with previous studies that exposed microalgae to polystyrene nanoparticles, which reduced chlorophyll *a* concentration and photosynthetic performance over time (Besseling et al., 2014, Bhattacharya et al., 2010, Hazeem et al., 2020). Feng et al. (2019) tested the metabolic activity of *S. elongatus* PCC 7942 following short-term exposure (48 h) to polystyrene nanoparticles, observing membrane destruction and oxidative stress, which corresponded well with the decline in PS and Fv/Fm

values in this chapter. The Fv/Fm values of *S. elongatus* CCAP 1479/1A exposed to 0S and 4S binders were enhanced almost two-fold compared to the suspension controls (Figure 5.10), which corresponded well with the CO_2 absorption rates achieved in the CCAP 1479/1A biocomposites using the 4S binder (Figure 5.15b), regardless of their low average PS values. The higher Fv/Fm values infer that the electron transport to PSII can deliver more photons for photosynthesis reactions (Beer et al., 1998) potentially leading to higher CO_2 uptake rates. However, it should be noted that the biological data were obtained from cells suspended in the aqueous latex solution and may not be directly compared with the cells in the biocomposites, which were embedded within dry latex coatings.

The causes of biological stress on the cyanobacteria could also be explained by light shading from nanoparticles, and/or the latex presenting a physical barrier to nutrient uptake and/or CO_2 gas flow (Bhattacharya et al., 2010). An analysis of reactive oxygen species (ROS) production would have been useful to provide data to corroborate the PS and Fv/Fm values. ROS are found in plant and algae cells at higher concentrations in response to environmental stress such as photoinhibition, drought, heavy metal exposure, and extreme temperatures (Mallick and Mohn, 2000, Rezayian et al., 2019). ROS react with biomolecules and can influence their biochemical reactivities.

The net CO_2 absorption rates of the biocomposites were higher than the suspension controls, by 14-20 and 3-8 times for *S. elongatus* CCAP 1479/1A and PCC 7942 (Figure 5.13 and 5.15). The CCAP 1479/1A biocomposites lasted up to 84 days without nutrient refreshment or noticeable biomass loss, which overcame the outgrowth issues described in Chapter 4. The SEM images showed that the cells were retained within the coatings, despite cell division having taken place (Figure 5.16d). This is evidence that the flexibility of the soft latex binders were able to accommodate the tension imposed by a growing population of cells. Elizalde et al. (2020) reported that acrylic film coatings made from butyl acrylate at concentrations lower than 50% by weight resulted in poor mechanical properties (too glassy and brittle to handle). In this study, the soft latex binders had around 70% by weight, which is well above the reported concentration and likely to result in flexible film coatings after drying. In addition, cell growth was less (by 1.5 to 3-fold) with the soft latex binders (Figure 5.2b) than observed with the AURO plant-based binders (See Chapter 4, Figure 4.4).

The CO_2 uptake performance of the *S. elongatus* PCC 7942 4N biocomposites was better than with the 12N binder. The toxicity data provide a plausible explanation as a 40% increase in cell growth was obtained from 4N, whereas the 12N binder supported no increased growth compared to the suspension controls (Figure 5.2a). It could be explained by the toxicity data (Figure 5.2a), which indicated that the 12N binder did not promote cell viability, but had favourable adhesion scores (Figure 5.6a). The depigmentation of the cells was likely due to a chlorosis process that acted as a response to nitrogen starvation to enable long term survival (dormant-like state), which may assist the cells to reinitiate growth once sufficient nitrogen accumulation is reached (Sauer et al., 2001). This phenomenon may explain the cell outgrowth as seen from Figure 5.14.

Table 5.2 lists all net CO_2 absorption rates of all the biocomposites and the operational period without cell growth. Theoretically, the best performing biocomposites could capture up to 574.08 ± 30.19 tCO$_2$ t^{-1} $_{biomass}$ yr^{-1}, assuming the performances of the biocomposites were still the same at a larger scale. This value is higher than the biocomposites developed in Chapter 4. Although the biocomposites made from the AURO plant-based binders were tested for eight weeks (56 days), cell outgrowth was spotted at day 28 (See Chapter 4, Figure 4.13). Similarly, the *S. elongatus* PCC 7942 4N and 12N biocomposites also lasted 28 days before cell detachment. This may be explained by latex degradation due to the constant moisture exposure (Lambert et al., 2013a, Lambert et al., 2013b) and/or a regain in cell division after sufficient nitrogen accumulation is met (Sauer et al., 2001).

To overcome this, non-film forming particles could be introduced into the latex formulations to provide nano spacing to the immobilised cyanobacteria. Recently, Chen et al. (2020) explored halloysite – rigid tubular nanoclays with non-toxic latex particles to increase porosity in biocoatings for *Escherichia coli* encapsulation. The resulting nanovoids increased coating permeability, and supported higher metabolic activities. However, to use this approach the non-film forming particles must be non-toxic and be smaller in size than the cyanobacteria but larger than the latex film particles (Cortez et al., 2017). In addition, the cost of biocomposites production would increase because of the additional materials. Alternating chemical composition during latex polymerisation to increase porosity may be a better option. For instance, Reyes-Mercado et al. (2008) found that increases in acrylic acid concentration in the poly(styrene-co-butyl acrylate) latex films resulted in higher water uptake and permeability. All of the latex binders used in this Chapter had acrylic acid as one of the chemical components,

but its effect has not been explored. It would be another idea to vary acrylic acid concentration for future optimisation of the biocomposites' robustness.

It is difficult to make fair comparisons between the current study and other microalgae for carbon capture applications due to a lack of standardised cultivation conditions. In Chapter 4, comparison of the biocomposites were made against various scales of suspension cultures (See section 4.4, Table 4.6). Here, the performance of the new biocomposites are compared with recent studies that have developed algae biocomposites using different microalgae and cyanobacteria species (Table 5.3). The CO_2 absorption data compared favourably when using g CO_2 g^{-1} $_{biomass}$ d^{-1} as a metric. However, the new biocomposites had 12- and 14-times lower CO_2 fixation rates than Ekins-Coward et al.'s *C. vulgaris* biocomposites (Ekins-Coward et al., 2019) and Bernal et al.'s paper-based *Synechococcus* PCC 7002 biocomposite (Bernal et al., 2014) when compared on a per area (m^2) basis. This is likely due to both studies used cell loading of 50% v/v, while the current work used 2.5% v/v. This could be improved by increasing the cell loading but excessive cell loading could lead to compromised coating porosity and adhesion as well as increased competition for water, nutrient, light and CO_2. The current cyanobacteria biocomposites had slightly higher CO_2 fixation rates than the *C. vulgaris* and *D. salina* biocomposites developed by Umar (2018), which would likely be due to a longer testing period for CO_2 to accumulate and different CO_2 concentrating mechanisms between microalgae and cyanobacteria (Beardall and Raven, 2017).

Table 5.2 Comparison of the net CO_2 fixation rates (Mean ± StDev) of cyanobacteria loofah biocomposites from Chapter 4 and the current study. An annual theoretical scaled CO_2 capture for each biocomposite and tested period without cell outgrowth or failure are also presented.

Phototroph + binder	Net CO_2 fixation rates				Tested period without cell outgrowth/failure (Day)	Theoretical scaled CO_2 capture (tCO_2 t^{-1} biomass yr^{-1})
	mmol CO_2 g^{-1} biomass d^{-1}	mmol CO_2 m^{-2} d^{-1}	g CO_2 m^{-2} d^{-1}	g CO_2 g^{-1} biomass d^{-1}		
S. elongatus PCC 7942 + AURO 320	15.38 ± 4.06	7.72 ± 2.04	0.34 ± 0.09	0.68 ± 0.18	28	246.97 ± 65.20
S. elongatus CCAP 1479/1A + AURO 321	21.18 ± 6.87	6.15 ± 2.00	0.27 ± 0.09	0.93 ± 0.30	28	340.11 ± 110.32
S. elongatus PCC 7942 + 4N	26.77 ± 6.26	8.84 ± 2.81	0.39 ± 0.12	1.18 ± 0.29	28	429.87 ± 100.52
S. elongatus PCC 7942 + 12N	11.54 ± 7.81	2.40 ± 1.62	0.11 ± 0.07	0.51 ± 0.34	28	185.31 ± 125.41
S. elongatus CCAP 1479/1A + 4S	25.76 ± 9.35	6.91 ± 3.59	0.30 ± 0.16	1.13 ± 0.41	84	413.66 ± 150.14
S. elongatus CCAP 1479/1A + 12S	35.75 ± 1.88	9.57 ± 1.10	0.42 ± 0.05	1.57 ± 0.08	84	574.08 ± 30.19

Table 5.3 Comparison of the highest CO_2 absorption rates relative to selected literature values. The approximate calculation was used to convert the metrices based on the information available if the data were not reported.

Species and strain	Type	System description	CO$_2$ fixation rate		References
			(mmol CO_2 m^{-2} d^{-1})	(g CO_2 g^{-1} $_{biomass}$ d^{-1})	
Synechococcus PCC 7002	Cyanophyte	Paper-based biocomposites with 20% v/v CO_2 at 25 ºC; light: 100 μmol m^{-2} s^{-1} in batch for 500 h	136	0.22	(Bernal et al., 2014)
Chlorella vulgaris	Freshwater chlorophyte	Biopolymer porous paper pulp in microfiber cellulose mixed with chitosan matrix in BG11 and fixed onto spinning disk reactor for 15 h at 300 rpm with 5% v/v CO_2	110.64	1.38	(Ekins-Coward et al., 2019)
Chlorella vulgaris	Freshwater chlorophyte	Immobilised with binder S3 on loofah at 18 ºC; light: 16:8 photoperiod at 30.5 μmol m^{-2} s^{-1} with continuous 5% v/v CO_2 at day 42	2.38	0.17	(Umar, 2018)
Dunaliella salina	Marine chlorophyte	Immobilised with binder S11 on loofah at 18 ºC; light: 16:8 photoperiod at 30.5 μmol m^{-2} s^{-1} with continuous 5% v/v CO_2 at day 42	3.44	0.25	(Umar, 2018)
S. elongatus CCAP 1479/1A	Cyanophyte	Immobilised with binder AURO 321 (Replebin®) on loofah at 18 ºC; light: 16:8 photoperiod at 30.5 μmol m^{-2} s^{-1} with 5% v/v CO_2 in semi-batch at day 56	6.15	0.93	Chapter 4
S. elongatus CCAP 1479/1A	Cyanophyte	Immobilised with binder 12S on loofah at 18 ºC; light: 16:8 photoperiod at 30.5 μmol m^{-2} s^{-1} with 5% v/v CO_2 in semi-batch at day 84	9.57	1.57	This study

Cyanobacteria have certain advantages over eukaryotic microalgae for biomass utilisation. For example, cyanobacteria have a less complex cell wall than microalgae, which can be broken more easily to extract their carbohydrate compounds e.g. glycogen to be used in fermentation processes (Möllers et al., 2014, Aikawa et al., 2014). The percentage content of carbohydrate obtained from the biocomposites compared favourably to other studies that have reported carbohydrate compounds from cyanobacteria such as *Synechococcus* and *Spirulina* under nitrogen depletion, ranging from 55 to 74% dry weight biomass (Depraetere et al., 2015, Philippis et al., 1992, Möllers et al., 2014, Sassano et al., 2010). Choi et al. (2016) found that metabolic activity, particularly of genes that relate to carbon uptake, of *S. elongatus* PCC 7942 were upregulated when the cells were exposed to a nitrogen depleted environment. As the cyanobacteria were entrapped within biocomposites and the nutrient medium was only delivered through loofah capillary action, the cells would be under nutrient limitation and would likely have accumulated more carbohydrate compounds. However, extracting carbohydrates from the cells in the biocomposites would result in cell destruction and would be counterintuitive for long-term carbon capture applications. An approach called "milking technique" that maintains the cell's metabolic activities (Chaudry et al., 2017) could be applied to extract the products, while letting the biocomposites continuously absorb CO_2.

5.5   Conclusion

This study has shown that the chemical composition of latex binders affects cyanobacteria photosynthetic performance, growth and CO_2 absorption. Hard latex binders made with a high styrene concentration were unfavourable for cell viability. As Texanol™ concentration increased, the cell adhesion affinity to loofah was improved because of its characteristic of promoting latex film formation and lowering Tg of latex binders. All of the biocomposites had significantly higher net CO_2 absorption rates than the suspension controls. The biocomposites with *S. elongatus* CCAP 1479/1A using the soft latex binder with 4% v/v Texanol™ had the best CO_2 capture performance that functioned up to 84 days without additional nutrients and could theoretically capture around 570 tCO_2 $t^{-1}_{biomass}$ yr^{-1}. In addition, carbohydrates accumulated within the cells in the biocomposites at up to 77% by dry weight. Further optimisation with polymerisation of highly porous latex binders and tests on the biocomposites using other biological analysis related to photosynthetic efficiency are still required to enhance biocomposite robustness and enable the technology to scale up to commercial levels.

Chapter 6

Preliminary techno-economic analysis of living biocomposites for carbon capture from breweries

Abstract

The brewing sector is trialling a range of sustainability strategies in an attempt to reduce its carbon footprint, including utilising algae for CO_2 capture and wastewater treatment. In this thesis, loofah-based biocomposites were developed to intensify biological CO_2 capture as a direct replacement for conventional suspension cultures. This chapter presents a simplified techno-economic analysis of the biocomposites under predicted (exposed to natural solar light intensity: 467.59 μmol m^{-2} s^{-1}) and experimental (used laboratorial data, which exposed to low light intensity: 30.5 μmol m^{-2} s^{-1}) scenarios, and compared against three established algal cultivation systems—open raceways, flat panel photobioreactors (PBR) and biofilm PBRs— for capturing CO_2 emitted from beer fermentation. The techno-economic analysis consisted of: 1) sizing algal cultivation systems to achieve 90% CO_2 removal; 2) estimating annual water and energy consumption; and, 3) calculating the overall capital and operating costs. The CO_2 avoidance costs were estimated using an annualisation method to evaluate biocomposites against other algae carbon capture and storage technologies. The biocomposites significantly decreased the water and energy required per unit culture volume compared to other algae systems. The biocomposite CO_2 avoidance costs were estimated 120 - 140 US\$ t$^{-1}_{CO2\ avoided}$ t$^{-1}_{biomass}$ yr^{-1} for the experimental scenario and 90 - 110 US\$ t$^{-1}_{CO2\ avoided}$ t$^{-1}_{biomass}$ yr^{-1} for the predicted scenario, which compares favourably with the best performing established algae culture system (80 - 100 US\$ t$^{-1}_{CO2\ avoided}$ t$^{-1}_{biomass}$ yr^{-1} for the biofilm PBR). The CO_2 avoidance costs of the biocomposites in the experimental scenario were higher due to lower light exposure resulting in less CO_2 captured. Compared to the other culture systems, the quantity of algae biomass present in the biocomposites was small; thus, extraction of high value biochemicals should be targeted instead of selling algae biomass. Overall, this preliminary techno-economic analysis provided an interesting insight to the feasibility of the biocomposites for the brewing industry.

Keywords: Intensified carbon capture, economic assessment, algae biocomposites, algae carbon capture and utilisation, CO_2 avoidance cost

6.1 Introduction

A 1 °C rise in average global temperatures from pre-industrial levels (Kirtman et al., 2018) is primarily due to the amount of greenhouse gas (GHG) emissions to the atmosphere. The Paris Climate Agreement, ratified in 2016, aimed to limit global temperature increase to 1.5 °C (Shepard, 2016). The main GHG contributor is CO_2, mainly emitted from the energy, transport, and industrial sectors (including food and drink industries) (Fischedick M. et al., 2014). Around 0.7% of global GHG emissions were estimated to be from alcoholic beverages when the whole product lifecycle is considered (Cimini and Moresi, 2016). Consequently, the brewing industry has started to address its carbon footprint (BIER, 2012).

Beer is the world's fifth most consumed beverage (Shin and Searcy, 2018). In the UK, Amienyo and Azapagic (2016) conducted a life cycle assessment (LCA) of beer production, in which the system boundary included raw material production, beer manufacturing, packaging, retail and consumption. It was found that the annual beer consumption emitted 2.61 million tonnes of CO_2 equivalent (i.e. 0.85% of UK emissions). From the craft beer industry, the total GHG sources consisted of: 46.4% from barley agriculture, malted barley transportation, and bottle production; 38.7% from energy consumption; and 14.9% from direct emissions from beer fermentation (Shin and Searcy, 2018). Most efforts in the beer industry to reduce the carbon footprint have been focused on using renewable energy sources, sustainable packaging and greener transportation fuels (BIER, 2012, Hansi et al., 2017), which neglects the direct emissions. Hence, more studies (including carbon capture) are needed to lower the CO_2 emissions at the beer production stage.

Carbon capture technologies can be divided into carbon capture and sequestration (CCS), and carbon capture and utilisation (CCU). CCS technologies prevent or remove CO_2 emissions at source, mostly prior to entering the atmosphere, using various techniques such as chemical/physical absorption, adsorption, cryogenics, and membrane separation (Salvi and Jindal, 2019). However, most CCS technologies are economically unfeasible due to complex infrastructure and high capital costs (Rubin et al., 2007). CCU is deemed more attractive from an economic point of view as the carbon can be converted into valuable products to potentially generate an additional business income.

Microbiological algae systems (including cyanobacteria) are candidates for CCU, as algae biomass can be converted to various bioproducts such as biofuels, biofertilisers, medicines, and food additives (Bleakley and Hayes, 2017, Markou et al., 2012). Microalgae

and cyanobacteria have different tolerances for temperature and CO_2 concentration (Salih, 2011). In this study, a cyanobacteria species (*Synechococcus elongatus*) was chosen because of its tolerance to high temperatures (up to 60 °C) and CO_2 levels (60% v/v) (Miyairi, 1995); this would minimise additional energy cost from diluting the concentrated CO_2 gas stream. The CO_2 off-gas from the active beer fermentation can be evolved at up to 100% v/v (Finne, 2001). A number of studies have used algae cultivation systems for wastewater purification from breweries, with all reporting positive outcomes for converting CO_2 into high valuable compounds (Song et al., 2020, Ferreira et al., 2017, Chagas et al., 2015, Choi, 2016, Papadopoulos et al., 2020, Marchão et al., 2017, Gaigher et al., 1985, Zheng et al., 2018, Subramaniyam et al., 2016) (Table 6.1). Amenorfenyo et al. (2019) argued that microalgae-based methods have more promise compared with current wastewater treatments used for the brewing industry.

Table 6.1 Summary of previous microalgae studies related to brewery wastewater and CO_2 treatments.

Species	Process	Results	References
Scenedesmus sp. 336 and *Chlorella* sp. UTEX1602	Investigated both wastewater and CO_2 fixation tests in 250 mL Erlenmeyer flask suspension culture containing 200 mL medium with exposure to 15% v/v CO_2/air at a flow rate of 0.1 vvm for 9 h daily for 10 days. The culture was maintained at 25 ± 1 °C using 6000 lux light intensity and a photoperiod of 24:0 (light/dark) cycle.	*Scenedesmus* sp. 336 had 89.99% NH_3–N, 75.96% total nitrogen (TN), 95.71% total phosphorous (TP) and 73.66% chemical oxygen demand (COD) uptakes. *Chlorella* sp. UTEX1602 had 84.22% NH_3–N, 81.43% TN, 97.54% TP and 44.97% COD uptakes.	(Song et al., 2020)
Scenedesmus obliquus ACOI 204/07	5 L cylindrical PBR (14 × 40 cm diameter × height) fed continuously by 10% v/v CO_2/air at 23–25 °C and brewery wastewater for 17 days. Biomass was harvested and went through pyrolysis to extract bioenergy products. Light intensity was 3200 lux with photoperiod of 24:0 (light/dark) cycle.	Obtained 64% bio-oil, 30% bio-char and 6% bio-gas content based on dry weight biomass.	(Ferreira et al., 2017)

Dunaliella tertiolecta BE 003	2.4 L flat-panel airlift PBRs connected directly to 2L beer fermenter to continuously feed CO_2. Cultured with f/2 medium and fed by air at 1L min^{-1} at 28 °C for six days. Light intensity was 5800 lux with photoperiod of 24:0 (light/dark) cycle.	Obtained biomass productivity, carotenoids, carotenoids productivity and lipids were 0.18 ± 0.01 g L^{-1} d^{-1}, carotenoids 4.74 ± 0.59 mg g$^{-1}_{dry biomass}$, 0.86 ± 0.06 mg L^{-1} d^{-1} and 135 ± 4 mg g$^{-1}_{dry biomass}$ respectively.	(Chagas et al., 2015)
Chlorella vulgaris	100 mL of *C. vulgaris* in JM medium was mixed with 1 L brewery wastewater effluent in a flask culture. The culture pH was maintained at 7.3 ± 0.4 at 28–32 °C for 15 days and shaken at a rate of 80 rpm. Effect of light (with and without) at 200–220 µmol photons m^{-2} s^{-1} with 16:8 (light/dark) cycle and aeration rate (with and without) at 0.5 L min^{-1} were investigated.	Achieved the maximum dry biomass of 0.917 g L^{-1} and obtained the highest amount of unsaturated fatty acids at 83.22% dry weight under darkness with aeration. The maximum reduction of biochemical oxygen demand (BOD) and COD were 91.43 and 83.11% respectively.	(Choi, 2016)
Closterium	A series of pilot scale 2-4.5 m^3 plastic pools under a 240 m^2 plastic tunnel of photosynthetic purple nonsulfur bacteria (*Rhodopseudomonas*), algae (*Closterium*), fish (*Oreochromis mossambicus*), and macrophytes (*Aponogeton distachyos*) were operated for 10 months to treat sorghum beer brewery effluent.	Total suspended solids concentration decreased significantly when the fish pond was fed directly from the algae pond. The phosphate concentration was reduced by >80% over the whole system. For every 3 g of dry algae biomass and 60 g of COD added into the fish pond, around 1 g of fish was obtained.	(Gaigher et al., 1985)
Scenedesmus obliquus ACOI 204/07	5 L and 6 L PET bottles were used as bubble column PBRs with 14 × 34 cm and 14 × 40 cm (d × h) in batch and continuous modes. The culture was supplied with continuous light intensity of 43.2 µmol photons m^{-2} s^{-1}, maintained at 25 °C.	Maximum biomass productivity was 0.2 g ash-free dry weight per day. TN and COD removal rates were 97 and 74% respectively.	(Marchão et al., 2017)

Leptolyngbya sp.	1 L PBR with continuous magnetic stirring at 24–25 °C with a pre-treated brewery effluent from electrocoagulation harvesting. Continuous average light intensity of 2000 lux for 15 days.	Total biomass concentration reached 525.0 and 740 mg L^{-1} after 15 days for aluminium and iron-pre-treated brewery wastewater respectively. The whole process removed 89.1% nitrate, 100% ammonium, 89.4% TN, 98.5% TP, and 91.6% COD.	(Papadopoulos et al., 2020)
C. vulgaris FACHB-31	1 L flask culture with a working volume of 750 mL (1:5 v/v ratio of microalgae: wastewater) was used for cultivation at 25 °C with light intensity of 200 µmol photons m^{-2} s^{-1} and a 12:12 (light/dark) photoperiod. The cultivation cycle was 7 days.	The biomass concentration of 2.85 g L^{-1} was obtained when using the mixed piggery-brewery (1:5) wastewater at pH 7. 100% ammonia, 96% of TN, 90% of TP, and 93% COD in the wastewater were removed.	(Zheng et al., 2018)
Chlorella sp. MM3	500 mL flask cultures were used for cultivation with brewery wastewater under continuous light intensity of 200 µmol photons m^{-2} s^{-1} at 25 °C.	Complete removal of TN, TP and total organic carbon concentrations were found.	(Subramaniyam et al., 2016)

Around 70% of the world's commercial algae biomass production takes place in open ponds/raceways (Ullah et al., 2015). Raceways suffer from issues such as poor CO_2 mass transfer, they have intensive energy demands for mixing, and require large land and water usage. Further, their open nature makes the cultures vulnerable to contamination from pathogens, grazers, or competitor algae (Seyed Hosseini et al., 2018). Closed photobioreactors (PBRs) (such as airlift, membrane, bubble, and flat panel reactors) have many advantages over raceways, although capital costs are high and water usage is still significant (Carvalho et al., 2006, Ho et al., 2011). There is emerging interest in biofilm technologies, e.g. rotating algal biofilm (RAB) ((Gross and Wen, 2014, Gross et al., 2013)), rope-based rotating drum (Christenson and Sims, 2012), and biofilm capillary membrane PBRs (Gao et al., 2015, Hamano et al., 2017, Xu et al., 2017), mostly focused on wastewater treatment (Kesaano and Sims, 2014). However most biofilm technologies have a short life cycle for capturing CO_2 and still suffer from bacterial contamination (Gross et al., 2015).

Loofah biocomposites (developed in Chapters 4 and 5) go beyond biofilm PBRs, where the algae are immobilised on hydrophilic solid scaffolds (i.e. loofah/luffa sponge), increasing the surface area available for colonisation, providing a barrier (i.e. thin layer binder) to foreign microorganisms, prolonging the cultivation period (up to 12 weeks), and enhancing CO_2 mass transfer (In-na et al., 2020). Umar (2018) attempted a brief economic assessment of loofah biocomposites for CO_2 fixation from a power plant, finding that biocomposites significantly reduced water and land consumption compared to raceway and PBR systems; however, a more detailed techno-economic analysis is required.

In this Chapter, a simplified techno-economic analysis is demonstrated for loofah biocomposites, with a specification to remove up to 90% of CO_2 from off-gas from a beer fermentation process. Performance was compared against a model open raceway, a flat panel PBR, and a biofilm PBR. The cost of CO_2 avoidance was determined using an annualisation method comparing biocomposites with the other algae cultivating systems and with other CCS technologies.

6.2 Methodology

6.2.1 Sizing cultivation units

Three contrasting algae cultivating systems; 1) an open raceway, 2) a flat panel suspension PBR, and 3) a biofilm PBR were compared against loofah biocomposites (Figure 6.1).

The systems were assumed to be located in a tropical region (i.e. Thailand) to minimise seasonal effects and enable a total operational time of 8000 h yearly. To be applicable to the brewing industry, each process was designed to have a minimal culture volume to reach 90% CO_2 removal from the off-gas from a 625 L fermenter offered by STUBrew at Newcastle University, Newcastle upon Tyne, UK. The evolved CO_2 was previously measured to be 2000 L_{CO2} by Singleton (2019) for a 625 L brewing vessel over a 108 h fermentation, with no further CO_2 produced afterwards (See Figure 6.2).

(a)

Paddlewheel

Gas inlet

- Suspension culture.
- Used a paddlewheel for mixing culture.
- Pond depth was 0.25 m.

(b)

Culture inlet

Culture outlet

Gas inlet

- Suspension culture.
- Used an aeration system for mixing culture.
- Flat panel depth was 2.5 cm.

(c)

Nutrient dripping system

Nutrient sedimentation

Peristaltic pump

- Biofilm grown on concrete with a wooden sheet support.
- Used a dripping system for water circulation with a peristaltic pump.
- A polytunnel structure was used to cover the system with CO_2 gas inlet and outlet.

(d)

Nutrient tank with microporous sheet

Gas inlet

Gas outlet

Peristaltic pump

- Used a microporous sheet for water circulation installed at the top of biocomposites.
- A polytunnel structure was used as reactor vessel to contain biocomposites.
- Depth of biocomposite was 2 cm.

Figure 6.1 Configuration of a) an open paddlewheel raceway pond (Henrikson, 2013), b) a flat panel suspension PBR (Henrikson, 2013), c) a biofilm-based PBR (Ozkan et al., 2012), and d) loofah biocomposites integrated into a beer fermentation process for the techno-economic analysis.
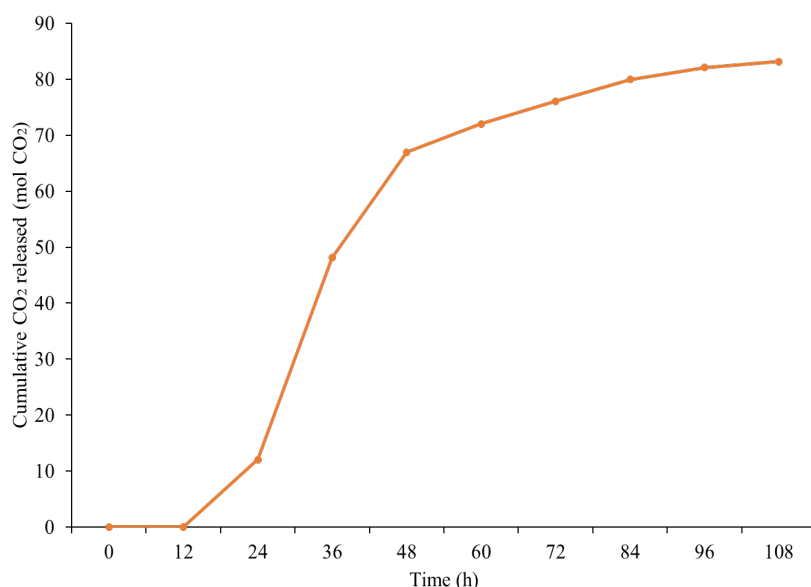
Figure 6.2 Cumulative CO_2 released from 625 L brewing vessel over a 108 h fermentation (Singleton, 2019).

A 50 mL airtight gasbag was attached to the fermenter outlet to collect the gas sample over successive 24 h periods. The CO_2 concentration was analysed by gas chromatography with a thermal conductivity detector. From the gas spectrometry spectra, the CO_2 concentration released from the fermenter was 95.51% v/v CO_2/air gas mixture with minor contributions from oxygen and nitrogen (Table 6.2). The remaining % mol content was assumed to be H_2O vapour (BIER, 2012).

Table 6.2 Gas chromatogram data of gas exhausted from the brewing fermenter.

Index	Name	Time (min)	Quantity (% mol)	Height (μV)	Area (μV.min)	Peak area (%)
1	CO_2	0.80	95.51	469507.1	116644.5	97.84
2	O_2	3.78	0.34	10200.8	721.7	0.605
3	N_2	4.33	1.40	17767.6	1848.9	1.55
		Total	97.25	497475.5	119215.1	100

The gas stream was diluted with air to 60% v/v reaching the maximum CO_2 concentration tolerance for *S. elongatus* (Salih, 2011) before entering into each cultivation system as shown in Figure 6.3.
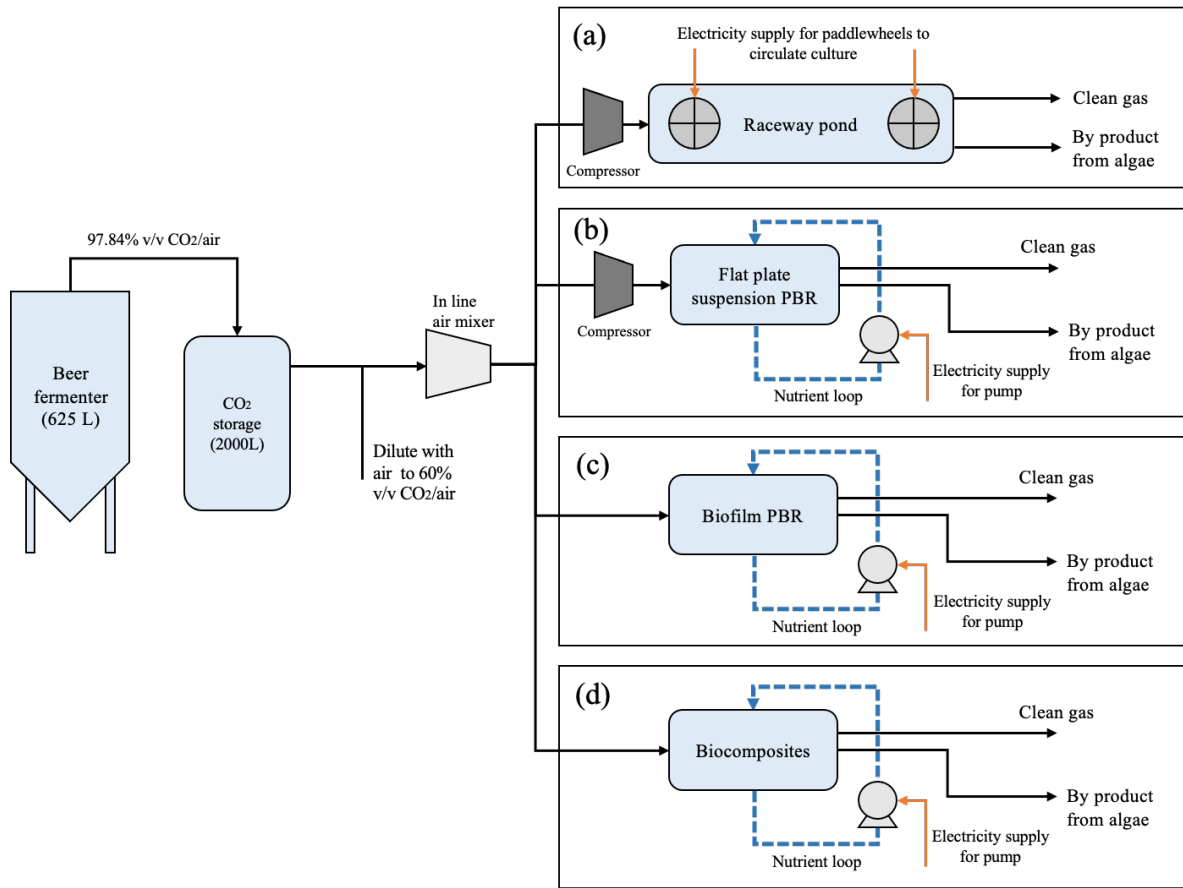
Figure 6.3 Process flow diagram to integrate (a) an open raceway pond, (b) a flat panel PBR, (c) a biofilm-based PBR, and (d) loofah biocomposites into the beer fermenter system.

A generic method correlation (see Equation 6.1) from Rezvani et al. (2016) was used to predict a CO_2 fixation rate (X; mol CO_2 m$^{-3}_{culture}$ d^{-1}), which is a function of daily solar radiation (I; MJ m^{-2} d^{-1}), net photosynthetic efficiency (η_{ph}, %), surface to volume ratio (SV, m$^2_{culture}$ m$^{-3}_{culture}$), and the amount of energy required to convert a mole of CO_2 to glucose (E = 0.48 MJ mol^{-1} CO_2). The equation was not species specific and the method was based on an assumption that the net photosynthetic efficiency represents all parameters affecting the CO_2 fixation rates such as nutrients balance, biomass concentration, light cycle, oxygen concentration and water quality. In addition, it was assumed that the majority of CO_2 was converted into glucose molecules to make the equation valid.

$$X = \frac{I \cdot \eta_{ph} \cdot SV}{E} \qquad (6.1)$$

According to Rezvani et al. (2016), open raceways and PBRs both obtained optimal economic scenarios for capturing CO_2 from a power plant when the SV ratios were 4 and 40 m$^2_{culture}$ m$^{-3}_{culture}$ respectively, at a solar radiation of 20 MJ m^{-2} d^{-1} (equivalent to 467.59 μmol m^{-2} s^{-1} (Reis and Ribeiro, 2020)) and 4% net photosynthetic efficiency. Ozkan et al. (2012)

developed a biofilm PBR system for harvesting a green algae, *Botryococcus braunii* (LB 272), that reduced water consumption by 45% and the energy required for dewatering by 99.7% compared with raceways. Since the system was developed to reduce water usage, it should be a good comparator to the biocomposites, which have low water-low maintenance characteristics.

The total working volume of the system was reported to be 0.6 $L_{culture}$ with the total system area of 0.275 $m^2_{culture}$, which was equivalent to a SV ratio of 458 $m^2_{culture}$ $m^{-3}_{culture}$. For the biocomposites, the SV ratio was 947 $m^2_{culture}$ $m^{-3}_{culture}$ because of the highly macroporous loofah scaffolds. To use this SV ratio, the following assumptions were made: 1) the surface of the loofah scaffolds were uniformly covered by the biocoating; and, 2) all immobilised cells were equally exposed to light.

For a fair comparison, it was assumed that all the systems were exposed to the same light intensities (i.e. 20 MJ m^{-2} d^{-1}) and maintained the same net photosynthetic efficiency at 4%. Table 6.3 summarises the SV ratios used to estimate CO_2 fixation rates using Equation 6.1. The associated amount of algae in the system for those CO_2 fixation rates were reported from the studies except for the biocomposites, which were extrapolated from the experimental data.

Table 6.3 SV ratios, algae in system and calculated CO_2 fixation rates.

System	Surface to volume ratio (m^2 m^{-3})	Algae in system (kg dried biomass m^{-3} d^{-1})	CO_2 fixation rates (kg CO_2 m^{-3} d^{-1})
Raceway[a]	4	0.16	0.29
PBR[a]	40	1.58	2.93
Biofilm PBR[b]	458	11.42	33.59
Biocomposite (predicted)	947	0.75	69.46
Biocomposite (experimental)	947	0.75	0.26

a – values were obtained from Rezvani et al. (2016)

b – values were calculated from Ozkan et al. (2012)

With algae systems, a gas flow rate changes along the system because CO_2 in the gas mixture is being consumed by the algae. Mass balances were used to calculate a minimal culture

volume required to reach 90% CO_2 removal with respect to the estimated CO_2 fixation rates. Equation 6.2 and 6.3 express CO_2 and overall mass balances changing with reactor length (z). They were numerically integrated to solve for the reactor length. The assumptions for the mass balance calculations were: 1) the gas mixture was an ideal gas and there were no gas leaks from any system; 2) CO_2 was absorbed in one direction for all systems; and, 3) CO_2 fixation rates were constant along the system length.

$$\frac{\partial c^G}{\partial z} = \left(\frac{A}{Q}\right)\left(\frac{c^G RT}{P} - 1\right) K \, a_C \, c^G \qquad (6.2)$$

$$\frac{\partial Q}{\partial z} = -\frac{RTA}{P} K \, a_C \, c^G \qquad (6.3)$$

Where c^G – CO_2 concentration in a gas mixture (mol $_{CO2}$ m^{-3})

z – Length of reactor (m)

A – Cross-sectional surface area of reactor system (m^2)

Q – Gas flow rate (m^3 h^{-1})

R – Ideal gas constant (8.314 J K^{-1} mol^{-1})

P – System pressure (Pa)

$K \, a_C \, c^G$ – Rate of CO_2 removal by microalgae (mol $_{CO2}$ s^{-1} m^{-3})

Due to the porous structure of the biocomposites, the Ergun equation (Equation 6.4) was used to check for a pressure drop that may cause potential backpressure to the fermenter. Due to a slow gas flow rate the pressure drop was negligible (less than 1 Pa per m). The biocomposite in the experimental case also used Equation 6.2 – 6.4 to determine the size required.

$$\frac{\partial P}{\partial z} = -4.17\frac{(1-\varepsilon)^2}{\varepsilon^3} a_P^2 \, \mu \, V - 0.29\frac{(1-\varepsilon)}{\varepsilon^3} a_P \rho |V| V \qquad (6.4)$$

Where P – System pressure (Pa)

z – Length of reactor (m)

ε – Void space ratio (decimal unit); $= 0.8178$ for loofah.

a_P – Surface area of packed bed/loofah substrate in this case (m^2 m^{-3}); $= 947$ m^2 m^{-3} for loofah.

μ – Viscosity of CO_2 gas (kg m^{-1} s^{-1})

ρ – Density of CO_2 gas (kg m^{-3})

V – Volume of system (m^3)

6.2.2 Reactor vessel costs of biocomposite and biofilm PBRs

The total cost of the biocomposites consisted of loofah, binder, plastic reactor vessel and wet algae biomass. The price of loofah was quoted at 1.50 US$ kg_{loofah} (Alibaba.com, 2020b) and loofah density was measured in the lab to be 54.9 kg_{loofah} m^{-3}_{loofah}. By dividing the loofah price with density, the specific loofah price was calculated as 82.35 US$ $m^{-3}_{culture}$. The binder cost was quoted as 10.87 US$ L^{-1}_{binder} based on the commercial price of the AURO 321 White Natural Emulsion (Sustainables, 2020). From the experiment (Chapter 5), 200 $\mu L_{formulation}$ was used to fully cover a 1 cm^3 of loofah scaffold for producing biocomposite samples. Thus, the specific amount of formulation required to produce the biocomposite was 200 L m^{-3}_{loofah}, in which only 2.5% g $_{binder}$ L^{-1} $_{formulation}$ was used. The density of binder was 1.4 g $_{binder}$ mL^{-1}_{binder}. With this information the specific binder price was calculated by equation 6.5. being 0.039 US$ $m^{-3}_{culture}$.

$$Specific\ binder\ price = \frac{Specific\ amount\ of\ formulation\ volume\ \times\ \%\ weight\ binder}{Binder\ density\ \times\ V_{culture}} \quad (6.5)$$

The specific amount of inoculating biomass required for the biocomposites was 5 kg_{WCP} m^{-3} $_{loofah}$ when using 2.5% v/v WCP/formulation. Since the algae cultivation systems were assumed to be located in Thailand, the price of *S. elongatus* was assumed to be the same as *Arthrospira platensis* (*Spirulina*), which is a well-known cyanobacterium grown in the country. EnerGaia Ltd sold biomass in both wet and dry forms for 1866.67 and 5000 THB $kg^{-1}_{biomass}$ respectively (Energaia, 2019). To estimate wet biomass prices from other companies, it was assumed that the drying technology in all the companies was the same as EnerGaia Ltd. Hence, the conversion cost was 2.68 from dry to wet biomass. Table 6.4 lists all the companies in Thailand that sell *Spirulina* with dry and wet biomass prices giving the biomass prices for low, medium and high operating cost scenarios were 22.17, 31.84 and 56.86 US $ $kg^{-1}_{wet\ biomass}$.

Table 6.4 Dry and wet *Spirulina* biomass prices in Thailand (exchange rate: 1 US $=32.8 THB).

Company	Dry biomass price (US $ $kg^{-1}_{dry\ biomass}$)	Wet biomass price (US $ $kg^{-1}_{wet\ biomass}$)	References
EnerGaia Ltd	152.30	56.9	(Energaia, 2019)
Health Food Thailand Co. Ltd	117.27	43.8	(Ltd., 2020)
Organic Lover (Thailand) Co. Ltd	85.29	31.8	(Infotech., 2020)
Organic Seeds	60.92	22.7	(Organicseedsthailand.com, 2020)
Organicthailand.com	59.40	22.2	(MakeWebEasy.com, 2020)

An inexpensive polytunnel configuration was used to house the biocomposites with prices ranging from 7.45 to 5.07 US $ m^{-3}_{tunnel} (Alibaba.com, 2020c). These prices included both shipping from China to Thailand as well as manufacturing costs.

During the retrofitting of the cultivation system onsite, a factorial Lang method was applied to include equipment erection costs (Towler and Sinnott, 2013a); the installation factors are given in Table 6.5

Table 6.5 Installation factors for calculating specific reactor cost for biocomposites (Towler and Sinnott, 2013a).

Major equipment for installation	Symbol	Factors
Equipment erection	f_{er}	0.3
Piping	f_p	0.8
Instrumentation and control	f_i	0.3
Electrical	f_{el}	0.2
Civil	f_c	0.3
Structures and buildings	f_s	0.2
Lagging	f_l	0.1
Plastic material	f_m	0.014

A specific cultivation cost of biocomposite PBR can be determined from Equation 6.6 (Towler and Sinnott, 2013a).

$$Specific\ cultivation\ cost = \frac{C_{total}[(1 + f_p)f_m + (f_{er} + f_{el} + f_i + f_c + f_s + f_l)]}{V_{PBR}} \quad (6.6)$$

Where C_{total} is the sum of loofah, binder, wet biomass and plastic reactor vessel and V_{PBR} is volume of PBR.

Table 6.6 summarises the specific cost for each part of the biocomposite. For the biofilm PBR, the specific cost was calculated based on the information provided from Ozkan et al. (Ozkan et al., 2012). Their system was made of a concrete substrate (0.275 m² with 8 mm in thickness) to grow biofilm with a wooden sheet support (0.275 m²). The prices used for concrete and wooden sheet were 0.015 US$ $m^{-3}_{concrete}$ (Aggregates, 2018) and 2.64 US $ m^{-2}_{sheet} (Alibaba.com, 2020a). Only 0.5 kg $m^{-3}_{culture}$ algae wet biomass were used to inoculate the culture (Ozkan et al., 2012). To make a fair estimation of capital costs for the biofilm PBR, the same approach as the biocomposites was used under the assumptions: 1) the system was cultivated

within the same polytunnel setting; 2) the wet algae biomass used for inoculation was the same price; and, 3) all installation factors were the same. As a result, the specific reactor costs of the biofilm PBR were estimated to be 520, 500, and 490 US$ $m^{-3}_{culture}$ for high, medium and low scenarios. The specific costs of the biofilm PBR is shown in Table 6.7.

Table 6.6 Specific costs of each part of the biocomposite system.

Part of biocomposite system	Specific cost per unit culture volume (US$ $m^{-3}_{culture}$)		
	High	Medium	Low
Loofah scaffold		82	
Binder		0.04	
Reactor vessel	7.5	6.3	5.1
Wet algae biomass	284	159	111
Specific total capital cost [a]	**550**	**350**	**280**

a – The values included installation costs, which calculated using Equation 6.6 and Equation 6.7

Table 6.7 Specific costs of each part of the biofilm PBR.

Part of biofilm PBR	Specific cost of system (US$ $m^{-3}_{culture}$)		
	High	Medium	Low
Concrete substrate and wooden support		330	
Biomass for inoculation	28.4	15.9	11.1
Reactor vessel	7.5	6.3	5.1
Specific total capital cost [a]	**520**	**500**	**490**

A – The values included installation costs, were calculated using Equation 6.6 and Equation 6.7

6.2.3   Installation cost of the cultivation systems

Equation 6.7 provides an estimation of the establishment of microalgae cultivation systems integrated onto an industrial site for carbon capture (Rezvani et al., 2016). The previous calculation (Section 2.2) for the biofilm PBR and biocomposites did not take into account the costs associated with contingency, land use, and owner's costs as well as the CO_2 fixation rates. Hence, the following calculation is used on those systems for a fair comparison with the raceway and flat panel PBR. The assumptions were made for this calculation: 1) A daily amount of CO_2 released into algae system during sun shines is consistent throughout the cultivation lifetime. 2) The CO_2 fixation rates of the overall algae system are constant. 3) The depths of algae systems are consistent throughout the system. According to Rezvani et al. (2016), the

specific cultivation costs of raceways and PBRs ranged from 150 to 300 US\$ $m^{-3}_{culture}$ and 2000 to 4000 US\$ $m^{-3}_{culture}$ respectively. The equation considered the amount of CO_2 captured from exhausted gas, occupied land area, contingency, and owner's costs. The contingency (ϱ) and owner's costs (ω) for installing microalgae systems were assumed to be 30% of the capital cost (Rezvani et al., 2016). In this study the cost of land was 108.51 US\$ m^{-2}_{land} (Wakefield, 2019), which was based on the specific land cost for industrial use in Thailand (conversion rate: 1 US \$ = 32.8 THB). An equivalent cultivation depth (d_R; m) was calculated from the SV ratios. The CO_2 flow from the brewery (m_{in}) was calculated to be 0.8131 kg CO_2 d^{-1} from the data of the evolved CO_2 gas over time (108 h) from the 625 L fermenter at Newcastle University (Figure 6.2). All variables used in the calculation are summarised in Table 6.8.

$$I_{MC} = \left(\frac{m_{in}}{X} \times \left(\frac{SC_L}{d_R} + SC_R \right) \right) (\rho + \omega + 1) \quad (6.7)$$

Where I_{MC} – Total capital cost for microalgae cultivation (US \$), m_{in} – CO_2 flow rate from the industry (kg CO_2 d^{-1}), X – CO_2 fixation rate (kg CO_2 d^{-1}), SC_L – Specific land cost (US \$ m^{-2}_{land}), d_R – Equivalent cultivation depth (m), SC_R – Specific reactor/pond cost (US \$ $m^{-3}_{culture}$), ϱ – contingency cost (decimal unit), ω – owner's cost (decimal unit)

Table 6.8 Parameters used in Equation 6.8 for calculating capital costs for the raceway and flat panel PBR to integrate for carbon capture.

System	Equivalent culture depth (m)	CO_2 fixation rate (kg CO_2 $m^{-3}_{culture}$ d^{-1})	Specific cost of system (US \$ $m^{-3}_{culture}$)		
			High	Medium	Low
Raceway	0.25	0.29	300	225	150
Flat panel PBR	0.025	2.93	4000	3000	2000
Biofilm PBR	0.0022	33.59	520	500	490
Biocomposite (Predicted)	0.0011	69.46	550	350	280
Biocomposite (Experimental)	0.0011	0.26	550	350	280

6.2.4 Estimating water consumption

To determine annual water consumption, all the systems were assumed to operate for 8000 h yearly. This calculation focused only on the cultivation process and excluded water used for supporting an inoculating system and effluent storage. Murphy and Allen (2011) identified that a raceway with 0.3 m depth required 0.8 m^3_{water} $m^{-2}_{culture}$ to fill up. For the raceway, the cultivation

depth associated with 4 $m^2_{culture}$ $m^{-3}_{culture}$ SV ratio was 0.25 m. Under an assumed linear relationship, the water required for the raceway would be 0.67 m^3_{water} $m^{-2}_{culture}$. In Thailand, an average water evaporation per year from reservoirs was approximated to be 8.8% of storage (Rittima et al., 2013), which was equivalent to 0.024% daily water loss assuming that the evaporation rate was constant over one year. With the 28 days cultivation cycle, the amount of water loss replacement per inoculation was calculated being 0.0045 m^3_{water} $m^{-2}_{culture}$ by multiplying 0.024% and 28 days with 0.67 m^3_{water} $m^{-2}_{culture}$. Hence, the total amount of water required per inoculation would be 0.6745 m^3_{water} $m^{-2}_{culture}$.

Nogueira et al. (Nogueira Junior et al., 2018) reported that the volume of water required to produce one kg of wet algae biomass was 0.372 m^3_{water} for a flat panel PBR. However, this value did not include water losses from the system through gas saturation. Martins et al. (Martins et al., 2018) analysed the water footprint of a flat panel PBR system and found that the system required 10% water makeup of total culture volume over a four weeks period to maintain its volume. Hence, 0.372 m^3_{water} $kg^{-1}_{dry\ biomass}$ was adjusted to 0.409 m^3_{water} $kg^{-1}_{dry\ biomass}$ by multiplying by 110%. Since the flat panel PBR in this case produced 1.58 kg m^{-3} d^{-1}, the water required was 0.647 m^3_{water} $m^{-3}_{culture}$ d^{-1} by multiplying the produced biomass with the adjusted water needed per 1 kg of biomass.

Ozkan et al. (Ozkan et al., 2012) published their water use, operation time, reactor dimensions, and evaporation loss from their biofilm PBR. From those details, the water requirement can be calculated as 0.0804 m^3_{water} $m^{-3}_{culture}$ d^{-1}. For the biocomposites, a linear relationship of nutrient enriched water (medium) was assumed from the batch experiment (see Chapter 5) to the scaled up system. The amount of medium used was 5 mL for 3 cm^3 of biocomposite. With an assumption of 84 days (12 weeks) between refreshing the medium, the calculated water requirement was 0.020 m^3_{water} $m^{-3}_{culture}$ d^{-1}. To take into account of the continuous exposure of gas flow from the beer fermenter, the water requirement was increased by 10% to be 0.022 m^3_{water} $m^{-3}_{culture}$ d^{-1}. With all determined daily water requirements (W_{daily}), the annual water consumption was calculated using Equation 6.8.

$$Annual\ water\ consumption = W_{daily} \times \frac{operation\ time\ (h)}{24\ h} \qquad (6.8)$$

6.2.5   Energy requirement for water circulation

In this study, only the energy required for water circulation within the cultivation systems was considered. Jorquera et al. (Jorquera et al., 2010) conducted a techno-economic analysis on raceways with paddle wheels and a flat panel PBR with air pumps, for which the specific power consumption was 4 and 55 W m$^{-3}_{culture}$ respectively. These values were used to estimate the power required for the raceway and flat panel PBR scenarios used in this chapter. For the biofilm PBR, Ozkan et al. (Ozkan et al., 2012) used a peristaltic pump with a dripping nozzle to recirculate the nutrient medium back into the system. They reported their total energy consumed was 32.29 kJ with 70% pump efficiency, a continuous flow rate of 150 mL min^{-1}, and a total operation time of 35 days. Under those conditions, the specific power consumption over that period would be 1.19 W m$^{-3}_{culture}$. For the biocomposite, a flow rate of circulating water was calculated to be 0.035 m$^3_{culture}$ h^{-1} by multiplying the water requirement of 0.020 m$^3_{water}$ m$^{-3}_{culture}$ d^{-1} with the culture volume of 42.7 m$^3_{culture}$ and dividing by 24 h. This calculation is based on the assumption that water continuously circulates for 24 h throughout the system during operation. It was also assumed that the head difference for a water irrigation system on top of the biocomposites was 0.1 m with 70% pump efficiency. Based on these assumptions, the power required for pumping can be calculated using Equation 6.9 (Moran, 2016), where ϱ is assumed as the water density (996 kg$_{water}$ m$^{-3}_{water}$ at 30 °C) and g is gravity (9.81 m s^{-1}). Due to the low water flow rate, the specific power consumed was 1.16 W m$^{-3}_{culture}$.

$$P = \frac{Q\rho g H}{\eta} \quad (6.9)$$

Where *P* – Power consumption of pump (W)

Q – Water flow rate (m$^3_{culture}$ h^{-1})

ρ – Density of water (996 kg$_{water}$ m$^{-3}_{water}$ at 30 °C)

g – Gravity (9.81 m s^{-1})

H – Head difference (m)

η – Pump efficiency (%)

Equation 6.10 was used to calculate the annual power consumption of the pump for water circulation. In this case it was assumed that all the systems were operated annually for 8000 h. Table 6.9 lists the specific power consumption and type of pumps for each system.

$$Annual\ power\ required = \frac{V_{culture} \times Specific\ power \times 3600\ secs}{3.6 \times 10^6\ secs} \times T_{operation}\ (h) \quad (6.10)$$

Table 6.9 Pump specifications and specific power consumption used in the estimations.

System	Pump specifications for water circulation	Specific power consumption for pump (W m^{-3})	References
Raceway	Paddle wheel	4	(Jorquera et al., 2010)
Flat panel PBR	Air pump	55	(Jorquera et al., 2010)
Biofilm PBR	Peristaltic pump with dripping nozzle	1.19	(Ozkan et al., 2012)
Biocomposites	Centrifugal pump with 100 cm head	1.27	this study

6.2.6 Operating cost

The annual operating cost consisted of water, energy cost for water circulation, algae biomass for inoculation, maintenance, property taxes, insurance, and labour costs. Here, the operating cost was based on the assumption that all systems operate for 8000 h yearly.

6.2.6.1 Water and energy costs

With different cultivation systems, harvesting cycles vary greatly because of different configurations and culturing techniques. To be more sustainable, it was assumed that 90% of water was reused after the dewatering stage for raceway and flat panel PBR because cells were cultivated in suspension. Since the biomass in both biofilm PBR and biocomposites were not submerged in water, the amount of water recovered from the drying stage would be negligible and would be difficult to recycle. The price of freshwater in Thailand (0.48 US$ m^{-3} (investment, 2019)) was used to calculate an annual total cost of water using Equation 6.11.

$Annual\ water\ cost$

$$= W_{daily} \times V_{culture} \times T_{operation}\ (day) \times cost\ of\ water\ per\ m^3 \quad (6.11)$$

After the total annual energy required was calculated (Equation 6.10), it was multiplied by the power cost. The cost of power was based on Thai prices in 2020 (i.e. 0.13 US$ per kWh) (investment, 2019).

6.2.6.2 Algae cost for inoculation

A long-lasting period of cultivation is preferable in CCS applications to absorb and accumulate CO_2 from the emitting sources. Generally, algae biomass in suspension culture from raceways and flat panel PBRs are harvested after 3-4 weeks (Marshall et al., 2018). Hence, the inoculation cycle for the two systems was assumed to be every 28 days. This was equivalent to the cultures being refreshed 12 times yr^{-1}. For the biofilm PBR, inoculation happened after 35 days (Ozkan et al., 2012) corresponding to 9.5 times yr^{-1}. Assuming that the biocomposite PBR had a cultivation cycle of 84 days (based on semi-batch experiments), this would only require water renewal four times per year. In every re-cultivation, a given number of algae cells are used for inoculation. Table 6.10 summarises the required amount of wet biomass needed to inoculate and the annual harvesting cycle number for all the systems. The algae biomass required in the biocomposite PBR was significantly higher than the others because of the starting high cell density immobilised onto loofah scaffolds. The annual algae biomass cost was calculated from Equation 6.12. The biomass prices used were 22.17 (low), 31.84 (medium), 56.86 (high) US\$ $kg_{wet\ biomass}$ as used in Section 6.2.2.

$$Annual\ algae\ biomass\ cost\ = wet\ biomass\ price\ \times\ no.\ of\ innoculation\ per\ year$$
$$\times\ biomass\ concentration\ \times\ V_{culture}\quad(6.12)$$

Table 6.10 Biomass concentration for inoculation and number of inoculations per year.

System	Cultivation time (day)	No. of inoculations per year	Biomass concentration ($kg_{wet\ biomass}\ m^{-3}_{culture}$)	References
Raceway	28	12	0.3	(Henrikson, 2013)
Flat panel PBR	28	12	0.3	(Henrikson, 2013)
Biofilm PBR	35	10	0.5	(Ozkan et al., 2012)
Biocomposite	84	4	5.0	This study

6.2.6.3 Labour cost and others

Preliminary estimations for labour costs and other factors such as maintenance, direct overhead, property taxes and insurance were based on Towler and Sinnott (2013b) and Clippinger and Davis (2019). A typical approximation for the maintenance cost is 3-5% of the capital cost, while the property taxes plus insurance are 1-2% of the capital cost. A supervision cost is typically 25% of the total operating labour cost. A salary for site engineers and

technicians in Thailand costs around 15,000 US$ yr^{-1} (investment, 2019). Direct salary overhead costs can vary between 40 to 60% of the labour plus supervision costs.

It was assumed that at least one technician/engineer is on site for the daily check up on algae cultivation to prevent culture from crashing by contamination. According to Clippinger and Davis (2019), number of labours required was estimated for different algae cultivations including algae raceway pond and flat plate PBR. It was estimated that 100 workers were needed annually for the algae pond of 5,000 acres of cultivation area (0.02 people acre^{-1}). For the flat plate PBR, 273 workers were required for cultivation area of 2428 acres (0.11 people acre^{-1}). Since the cultivation volumes were known (Table 6.12), the cultivation areas were approximated by cultivation volume divided by the culture depths. In most cases, the raceway pond requires less manpower because of less maintenance requirement than the closed PBRs, which need replacing and servicing (Clippinger and Davis, 2019). Table 6.11 summarises the parameters used to calculate labour cost and other associated factors. The estimation of labour force was based on the following assumptions:

- Reactor structure of flat plate PBR was replaced every year due to one year lifespan of plastic material used. The replacement took two hours and required one person for each vessel.
- Our raceway and flat plate PBR had the same structure as in Clippinger and Davis (2019).
- Operators for dewatering and inoculating the systems were counted.
- Inoculation numbers and cultivation cycles were the same as this study.
- Number of manpower required per cultivation area of biofilm PBR and biocomposites were treated the same as flat plate PBR (0.11 people acre^{-1}).

Table 6.11 Values of operating factors used in calculating operating labour costs.

Factors	Values	Units
Maintenance	3-5	% of fixed capital cost
Property taxes plus insurance	1-2	% of fixed capital cost
Salary per shift position	15,000	US$ yr^{-1}
Minimal shift position	1	-
Supervision	25	% of labour cost
Direct salary overhead	40-60	% of labour + supervision costs
Algae system	Cultivation area (m²)	Total number of manpower
Raceway	26480	1.13
Flat panel PBR	2648	1.07
Biofilm PBR	0.126	1.00
Biocomposite (Predicted)	0.045	1.00
Biocomposite (Experimental)	0.004	1.00

6.2.7 CO$_2$ avoidance cost

One of the key metrics to compare carbon capture technologies is the CO$_2$ avoidance cost, which is the minimal CO$_2$ tax required for emitting anthropogenic CO$_2$ into the atmosphere (Simbeck and Beecy, 2011). There are several methods to calculate this metric based on different assumptions. In this case, the annualisation method was used to calculate the CO$_2$ avoidance costs as shown in Equation 6.13 and 6.14 (Roussanaly, 2019). This approach has an advantage of evaluating CCS technology to be retrofitted without knowledge of technical data of the industrial plant, which is suitable for various breweries.

$$CO_2 \text{ avoidance cost} = \frac{\begin{array}{c}\text{Annualised investment due to CCS implementation} \\ + \text{ Annual operating cost due to CCS implementation}\end{array}}{\text{Annual amount of } CO_2 \text{ emissions avoided}} \quad (6.13)$$

$$\text{Annualised investment due to CCS implementation} = \frac{\sum^i \frac{TCR_{CCS}(i)}{(1+d)^i}}{\sum_i \frac{1}{(1+d)^i}} \quad (6.14)$$

With the annualisation method, the following assumptions (Roussanaly, 2019) were made:

1) the production of the brewery plant is not affected by CCS implementation.

2) extra costs and CO_2 emissions avoided due to CCS technology were separately assessed from the main industrial plant.

3) Annual operating costs and CO_2 emissions avoided were constant over the project lifetime.

4) CO_2 emissions during construction of microalgae cultivation systems were negligible

5) CO_2 emitted from downstream processing of algae harvesting were excluded.

All the cultivation systems were assumed to have a discount cash flow rate of 8% and an operating lifetime of 10 years. An influence of specific algae selling price was taken into account, varying by up to 1000 US$ using Equation 6.15. With this integration, it is necessary to assume that the total amount of algae is consistently produced yearly.

$$CO_2 \; avoidance \; cost = \frac{\begin{matrix} Annualised \; investment \; due \; to \; CCS \; implementation \\ + \; Annual \; operating \; cost \; due \; to \; CCS \; implementation \\ - \; (Specifc \; algae \; selling \; price \; \times \; Annual \; algae \; produced) \end{matrix}}{Annual \; amount \; of \; CO_2 \; emissions \; avoided} \quad (6.15)$$

6.3 Results and discussion

6.3.1 Culture volumes, water, and power consumption

Minimal required algae culture volumes mainly depended on the rate of CO_2 uptake and the SV ratio of the specific systems. The raceway required the highest culture volume of 6620 $m^3_{culture}$ because it had the lowest SV ratio and CO_2 fixation rates compared to other systems (Table 6.12). The flat panel PBR reduced the culture volume of the raceway by tenfold, being 662 $m^3_{culutre}$ due to the higher SV ratio. Theoretically, the flat panel PBRs were expected to be designed as thin panels for achieving high SV ratios and could be built vertically to minimise land use (Carvalho et al., 2006). For the biofilm PBR, the culture volume (57.8 m^3) was slightly larger than the culture volume of biocomposite in the predicted scenario (42.7 m^3). The biocomposite from the experimental scenario had a significantly lower culture volume (3.5 m^3) likely due to the predicted CO_2 fixation rate (Equation 6.1) did not take into account the enhanced CO_2 mass transfer via the cell immobilisation technique. The equation was largely dependent on the net photosynthetic efficiency and SV ratio, while there are other parameters (such as system arrangement, culture mixing rates, humidity etc.) that in reality can affect the CO_2 fixation rate. In addition, the reaction kinetics of CO_2 value (Kac) used in the estimation was obtained from the biocomposites' experimental data conducted under low light intensity

and 5% v/v CO_2/air mixture as a semi-batch condition. Increasing exposure of both light and CO_2 concentration should greatly influence the CO_2 fixation rates leading to further reduced culture volume to achieve the desirable CO_2 removal efficiency.

Table 6.12 Culture volume required to achieve 90% CO_2 removal from the fermenter.

System	Volume required for 90% CO_2 removal ($m^3_{culture}$)
Raceway	6620
Flat panel PBR	662
Biofilm PBR	57.8
Biocomposite (Predicted)	42.7
Biocomposite (Experimental)	3.5

The water requirement for the raceway and flat panel PBR were both significantly higher than the biofilm PBR and biocomposites (Table 6.13). This was due to the former two systems being operated as suspension cultures unlike the latter two systems. The flat panel PBR required lower water consumption than the raceway because it was a closed system leading to lower water evaporation loss (Nogueira Junior et al., 2018). The biocomposites consumed less water than the biofilm PBR by almost nine times if compared on a per surface area basis. The significant water reduction resulted from the continuous operational period of 84 days without water or nutrient refreshment combined with probable water retention within the hydrophilic loofah scaffold. In contrast, the biofilm PBR required daily water makeup to maintain its moisture from evaporative loss and varying water nutrient gradient through an increasing biomass thickness (Gross et al., 2015).

Table 6.13 Specific daily and annual water consumption for all cultivation systems.

System	Specific daily water consumption		Specific annual water consumption		Number of inoculations per year
	$m^3_{water}\ m^{-3}_{culture}\ d^{-1}$	$m^3_{water}\ m^{-2}_{culture}\ d^{-1}$	$m^3_{water}\ m^{-3}_{culture}\ yr^{-1}$	$m^3_{water}\ m^{-2}_{culture}\ yr^{-1}$	
Raceway	0.096	0.024	31.96	7.99	12
Flat panel PBR	0.65	0.016	215.51	5.38	12
Biofilm PBR	0.080	0.00018	26.81	0.059	10
Biocomposite	0.022	0.000023	7.28	0.0077	4

Table 6.14 Specific power consumption for pumps, annual power consumption and its cost.

System	Annual power consumed (kWh yr^{-1})	Annual power cost (US\$ yr^{-1})
Raceway	211,840	27,539
Flat panel PBR	291,280	37,866
Biofilm PBR	548	71
Biocomposite (Predicted)	395	51
Biocomposite (Experimental)	32	4

Even though the raceway system required a large amount of water, the power consumption of the raceway (211,840 kWh yr^{-1}) was estimated to be lower than the power required for the flat panel PBR (291,280 kWh yr^{-1}) due to the lower power supply required for paddlewheels (Jorquera et al., 2010) (Table 6.14). Typically, the flat panel PBR uses an airlift aeration system installed at the bottom of the reactor to circulate the water, requiring a higher energy supply than the paddlewheel mixing configuration (Carvalho et al., 2006). The power consumption of 55 W m$^{-3}_{culture}$ used in this techno-economic analysis was considerably lower compared to other enclosed PBR systems (e.g. helical and horizontal tubular PBRs), for which the specific power consumption can range up to 2000 to 3400 W m$^{-3}_{culture}$ (Sierra et al., 2008). On the other hand, the biocomposites required a significantly lower power supply (i.e. 395 and 32 kWh yr^{-1} for both predicted and experimental scenarios) compared to the biofilm PBR (548.4 kWh yr^{-1}) as water was retained in the loofah scaffold and delivered through loofah capillary action. The biofilm PBR required a constant flow of water to compensate for the evaporation loss and that consumed by the biofilm, which resulted in a specific power consumption being 1.19 W m$^{-3}_{culture}$ based on the information given in Ozkan et al. (2012). However, the specific power consumption of the biocomposites would increase when scaling up the process as the water circulation through the capillary network can be affected by gravity. Thus, the arrangement of the biocomposites (particularly the height) should be cautiously considered during reactor design and implementation.

6.3.2   Capital and operating costs

Most commercial algae systems are open raceways because of their lower capital cost than enclosed PBR systems, plus raceways can be made from inexpensive materials and with low construction cost (Jorquera et al., 2010, Rezvani et al., 2016). The total capital cost of the raceway pond ranged from 2590-3260 US $, while the cost of the flat panel PBR ranged from 2810-3700 US $ (Table 6.15). The predicted biocomposites (1930–1940 US $) had slightly lower total investment than the biofilm PBR (1940–1950 US$) because of a similar culture volume required to achieve 90% CO_2 removal. The experimental scenario biocomposites had the lowest total capital investment among other systems ranging from 520-530 US $, which would likely be due to the lowest volume required to remove CO_2 being 3.5 m^3.

Table 6.15 Total capital costs for all algae systems.

System	Total capital cost (US$)		
	Low	Medium	High
Raceway [a]	2590	2920	3260
Flat panel PBR [a]	2810	3260	3700
Biofilm PBR	1940	1940	1950
Biocomposite (Predict)	1930	1930	1940
Biocomposite (Experimental)	520	530	530

a – based on assumption of 90% water reuse from the dewatering stage of algae harvesting.

In all annual operation cost scenarios, the open raceway had the highest annual operating cost ranging from 591,750 to 1,416,410 US$ yr^{-1} from while other systems were all below 250,000 US$ yr^{-1} (Table 6.16). Algae cost was the main factor, contributed more than 80% for all cost scenarios of the raceway system (even with 90% water reuse) (Figure 6.4a). The high algae cost was due to the fact that the inoculation algae biomass has to be brought at mature state for carbon capture purpose unlike typical algae raceway pond that aims to produce maximum amount of biomass from an initial low cell density culture. In practice, most open raceways use either seawater or wastewater (in this case from the brewery) to compensate the water cost and reduce additional water usage (Murphy and Allen, 2011). Algae species have proven to tolerate harsh conditions from those water sources (Table 6.1). This suggests that the concentrated algae biomass required to produce biocomposites should be purchased lower than 22.17 US$ kg$^{-1}_{biomass}$ to be economically comparable to the biofilm PBR.

The biocomposites (Chapter 5) lasted for 84 days (i.e. 3 months) of continuous operation without additional nutrients. If further optimisation can be made to increase the operational time to 6 or 12 months, the annual operation costs could potentially be reduced by 32-47% in the predicted scenario (Figure 6.5a) due to a decrease in algae cost from a lower number of inoculations required per year. For the experimental biocomposite scenario, the longer operational period would cause around 4-9% reduction in the annual operation cost (Figure 6.5b). Furthermore, the labour cost would vary depending on the number of maintenance cycles and hours required (Clippinger and Davis, 2019), which could further reduce the overall operation cost of the biocomposites.
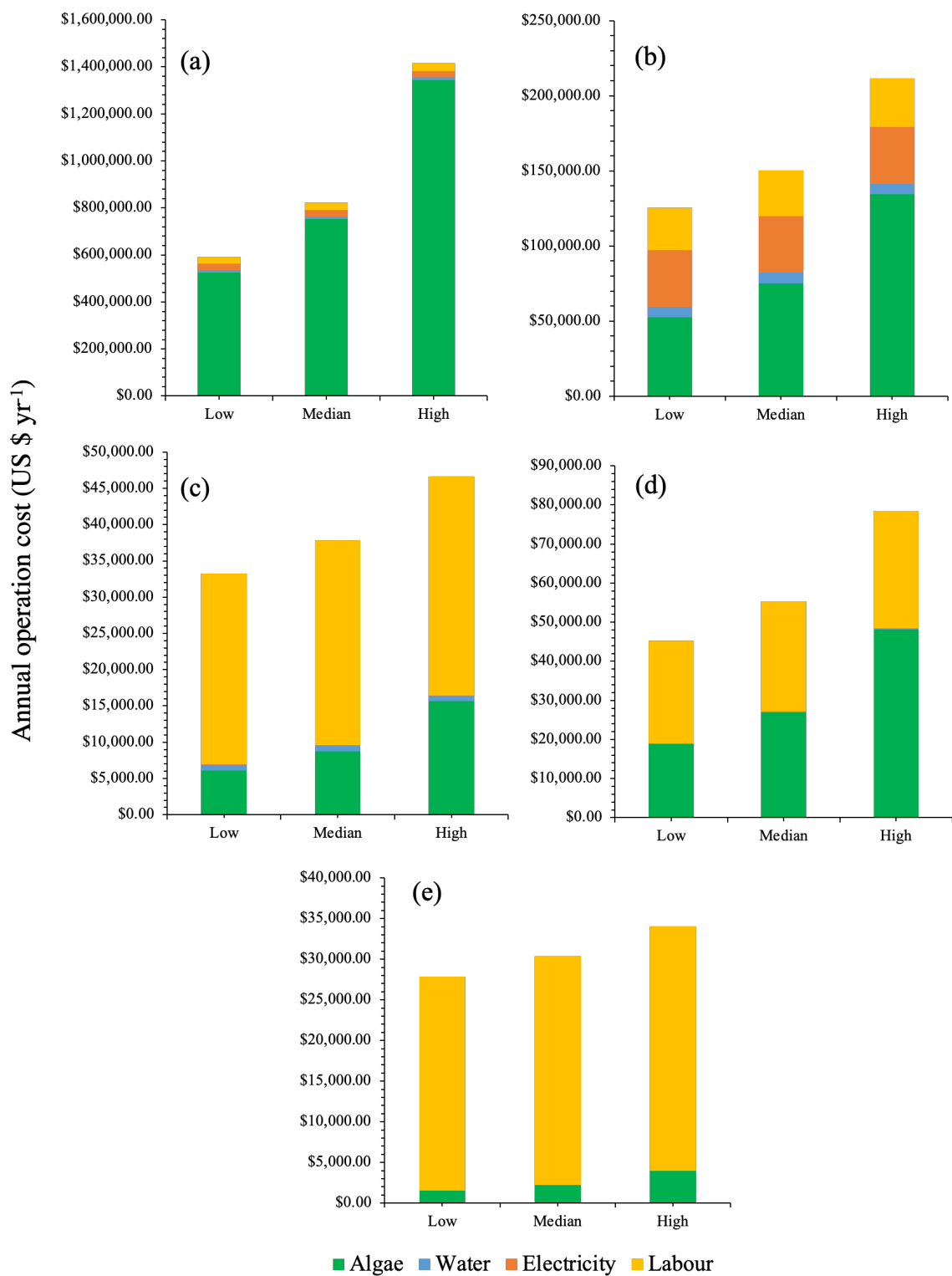
Figure 6.4 A breakdown of annual operating costs for (a) open raceway pond, (b) flat panel PBR, (c) biofilm PBR, (d) predicted and (e) experimental biocomposite scenarios in low, medium and high cost scenarios.

Table 6.16 Annual operation costs for all algae systems.

System	Total annual operation cost (US$ yr⁻¹)		
	Low	Medium	High
Raceway [a]	591,750	822,650	1,416,410
Flat panel PBR [a]	125,500	150,360	211,830
Biofilm PBR	33,320	37,920	46,740
Biocomposite (Predicted)	67,540	69,470	92,600
Biocomposite (Experimental)	28,990	31,550	35,180

a – based on assumption of 90% water reuse from dewatering stage of algae harvesting.
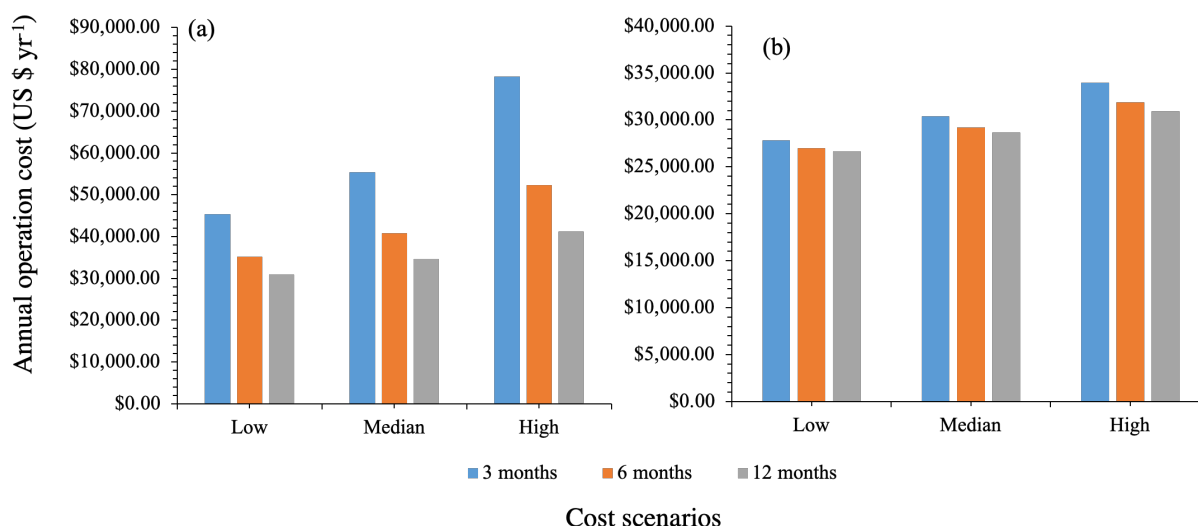
Figure 6.5 Effect of operation time of the biocomposites on the annual operation cost in (a) predicted and (b) experimental scenarios.

6.3.3 CO₂ avoidance cost

The cost of CO_2 avoided assists industries to evaluate different CCS processes and decide the most effective option for reducing CO_2 emissions (Adam II et al., 2017). Lower CO_2 avoidance costs are preferable as they indicate that small CCS investments can be made for a large CO_2 reduction (Simbeck and Beecy, 2011).

This study attempted to estimate the CO_2 avoidance costs using the annualisation method, which focused on the costs to retrofit the algae cultivating systems with the beer fermentation process. Despite the similar annual amount of CO_2 captured and yearly algae

156

biomass production, the raceway had a higher range of CO_2 avoidance costs (960 - 2240 US$ $t^{-1}_{CO2\ avoided}\ yr^{-1}$) than the flat panel PBR (240 – 390 US$ $t^{-1}_{CO2\ avoided}\ yr^{-1}$) (Table 6.17). The lower algae and water costs of the flat panel reduced the CO_2 avoidance costs from the raceway system. The CO_2 avoidance costs estimated from the predicted biocomposite scenario had slightly higher CO_2 avoidance costs (90 - 110 US$ $t^{-1}_{CO2\ avoided}\ yr^{-1}$) than the ones of biofilm PBR (80 – 100 US$ $t^{-1}_{CO2\ avoided}\ yr^{-1}$).

Due to lower annual CO_2 uptake rate of the experimental scenario biocomposite, the CO_2 avoidance costs (120 – 140 US$ $t^{-1}_{CO2\ avoided}\ yr^{-1}$) were higher than the predicted scenario biocomposite. If the light exposures were equivalent to the predicted case, the CO_2 uptake rate could be enhanced because of higher light energy input into photosynthesis reaction. In reality, the CO_2 removal efficiency of the biocomposites would be affected once scaled up and exposed to higher light intensity and CO_2 concentration in the gas stream. In future work, to increase the accuracy of this techno-economic analysis, the assessment should be based from the pilot scale of the biocomposites data rather than the lab scale data. In addition, analysis of all the CCS algae cultivation systems with a baseline scenario (i.e. no CCS implementation) could be performed based on the rigorous complexity of full physical models including detailed process flow sheets, mass balances, and heat transfer with the targeted integrated industry. This would provide a more comprehensive techno-economic analysis and identify the degree of uncertainty on the biocomposites. The current techno-economic analysis would be classified as a simplified techno-economic analysis because most of the values were based on previous literature (van der Spek et al., 2020).

Table 6.17 Annual amount of CO_2 captured, algae biomass produced and CO_2 avoidance costs.

System	Annual amount of CO_2 captured (t CO_2 yr^{-1})	Annual algae biomass harvest (t yr^{-1})	CO_2 avoidance cost (US$ $t^{-1}_{CO2\ avoided}\ yr^{-1}$)		
			Low	Medium	High
Raceway [a]	646.79	352.71	960	1320	2240
Flat panel PBR [a]	646.79	348.30	240	280	390
Biofilm PBR	646.60	219.81	80	90	100
Biocomposite (Predict)	987.69	10.66 [c]	90	90	110
Biocomposite (Experimental)	298.01 [b]	0.87 [c]	120	120	140

a – based on assumption of 90% water reuse from dewatering stage.

b – Value was based from 3.5 m³ of CCAP biocomposites; exposed to lower light intensity.

c – Low biomass value because of no biomass accumulation.

One advantage of algae CCS technologies to many businesses is that algae biomass can be sold and utilised in various products to reduce the costs of CO_2 capture. With an increase of the specific algae selling price, the cost of avoiding CO_2 emissions decreased for the raceway, flat panel and biofilm PBR in all scenarios (Figure 6.6). For the latter two systems, the analysis suggests that it is possible to generate profit from selling algae biomass if they were sold at more than 500 and 300 US$ $t^{-1}_{biomass}$ for the flat panel and biofilm PBRs respectively.

On the other hand, there were only small changes in the CO_2 avoidance costs for the biocomposites. This was due to the small amount of algae biomass being produced (only 10.66 and 0.87 t yr^{-1} for the predicted and experimental scenarios) compared to other algal processes (Table 6.18). This suggests that high value algae products such as astaxanthin that can be sold at 2,500 US$ kg^{-1} (Lorenz and Cysewski, 2000) to 100,000 US$ kg^{-1} for nutraceutical grade (Olaizola, 2003a) should be targeted instead of selling algae biomass. A microalgae "milking" recovery technique (Chaudry et al., 2017) can also be applied to frequently extract the high value biochemicals without breaking through the latex binders, whilst still keeping the cells to continuously capture CO_2 in the biocomposites.
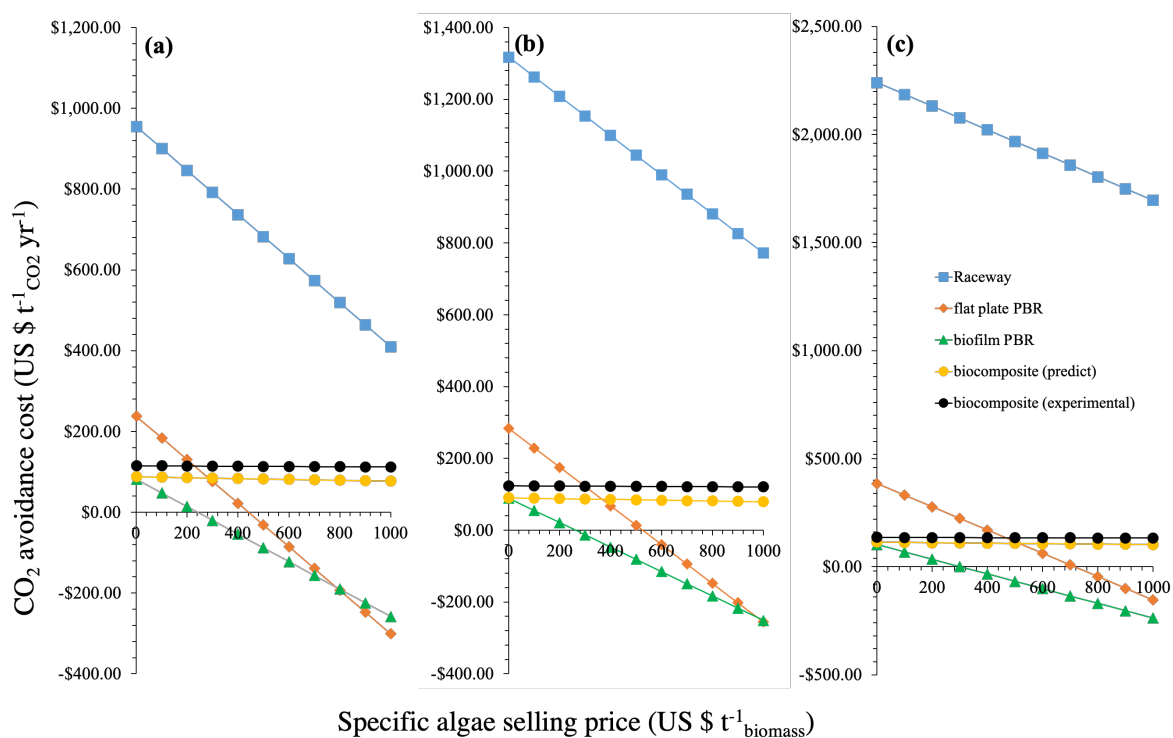
Figure 6.6 Scenarios of (a) low, (b) medium and (c) high CO_2 avoidance costs vs. specific algae selling prices

It is challenging to compare the biocomposites with other CCS technologies. Table 6.18 lists the costs of CO_2 avoided and descriptions of different CCS technologies including amine CCS, direct air capture (DAC), bio-energy with CCS (BECCS), and algae bio-energy with CCS (ABECCS). An amine scrubbing process has been known to be the most mature CO_2 removal system invented since 1930 (Bottoms, 1930). With the well-established full-scale installations, Rochelle (2009) reported that the cost of CO_2 avoided was 52 US\$ $t^{-1}_{CO2\ avoided}$ when the system was employed on a 450-MW plant using 30% w/w MEA solution with efficient energy integration. Power supply was a key factor influencing the cost of CO_2 removal for the amine scrubbing, which would be specific to the local power grid. Zeman (2014) conducted a techno-economic analysis and reported an optimal CO_2 avoidance cost to be 309 US\$ $t^{-1}_{CO2\ avoided}$ when the DAC system was made from plastic packing materials with aqueous NaOH solution and retrofitted onsite of a natural gas combined cycle (NGCC) facility with combined heat integration. Although, Sanz-Perez et al. (Sanz-Perez et al., 2016) reviewed that the costs of many DAC systems could range from 30 to 1000 US\$ $t^{-1}_{CO2\ avoided}$ depending on the specifications and assumptions made for the cost estimations. Under similar circumstances, the CO_2 avoidance costs of biocomposites would be affected under different assumptions. In addition, it should be noted that the reported CO_2 avoidance costs for DAC and amine-based CCS only considered the costs of capture and compression operations, while the biocomposites also included storage cost in the algae cells until they were burnt for fuel combustion or converted into long-term carbon products. Hence, the cost for amine-based CCS could be higher once the storage stage is taken into account and the biocomposites could compare favourably.

Several BECCS technologies have been considered based on biomass feedstock and type of fuel produced. The CO_2 avoidance costs of BECSS can vary from 15 to 400 US\$ $t^{-1}_{CO2\ avoided}$ and they greatly depend on the fuel conversion sectors (Fuss et al., 2018). For example, BECCS using biomass for combustion had a range of CO_2 avoidance costs between 88 to 288 US\$ $t^{-1}_{CO2\ avoided}$ while biomass used for producing pulp and paper mills had a lower cost penalty (20 to 70 US\$ $t^{-1}_{CO2\ avoided}$). Beal et al. (2018) tried to evaluate ABECCS aiming to avoid stress on food security from BECCS by integrating with an algae high protein feed production. In their study, the algae cultivation was integrated with BECCS and it was reported that the CO_2 avoidance cost of 278 US\$ $t^{-1}_{CO2\ avoided}$ could be achieved if the algal biomass were sold at 600 US\$ $t^{-1}_{CO2\ avoided}$ for soybean replacement under the electricity supply at 0.07 US\$ kWh^{-1}. However, the system model showed a significant water footprint compared to other CCS technologies because of the large algae raceways (up to 114,000 m^3). By far, the CO_2 avoidance

costs of the biocomposites in both scenarios compared favourably within the range of the BECCS technologies. They were estimated to be lower than DAC and ABECCS.

Apart from the CCS system itself, many parameters such as choice of integrated industries (CO_2 sources), countries, fuel costs, energy supply, plant geographical locations, carbon transport and storage can greatly affect the CO_2 avoidance cost. Irlam (2017) found that the CO_2 avoidance costs of the post combustion amine technology had a relatively small variance (20 to 27 US\$ $t^{-1}_{CO2\ avoided}$) when the system was integrated with natural gas processing, fertiliser and bio-ethanol production across various countries. However, the costs could range much wider for cement (104 to 194 US\$ $t^{-1}_{CO2\ avoided}$), and iron and steel (71 to 119 US\$ $t^{-1}_{CO2\ avoided}$) industries with the same CCS technology. In the current work, the location was assumed to be based in Thailand and the system boundary was focused only on CO_2 capture and storage. In addition, a life cycle analysis (LCA) on the biocomposites technology would be a good measure to assess other sustainable aspects including social and environmental impacts beyond the boundary of the cultivation stage with a suitable database. The LCA would help to convince the brewery business and ease a questionable public image about CCS technologies.

Table 6.18 Comparison of CO_2 avoidance costs with other CCS technologies.

CCS technology	Description and source of integration	CO_2 avoidance cost (US\$/$t_{CO2\ avoided}$)	Scope of reported costs	References
Direct air capture (DAC)	Onsite NGCC facility with DAC combined with heat integration. The system is made of plastic packing material with aqueous NaOH solution.	309	Capture and compression	(Zeman, 2014)
Amine CCS	MEA scrubbing installed on a 450-MW plant with 30% w/w MEA solution under power used at 80 US\$ MWh^{-1} $t^{-1}_{CO2\ removed}$.	52	Capture and compression	(Rochelle, 2009)
BECCS	Combustion	88-288	Capture, transport and storage	(Fuss et al., 2018)
	Ethanol	20-175		
	Pulp and paper mills	20-70		
	Biomass gasification	30-76		

160

ABECCS	114,000 m^3 raceways integrated with eucalyptus production; electricity price of 0.07 US$ kWh^{-1}; and selling algae biomass for 600 US$ t$^{-1}_{biomass}$ for soymeal replacement.	278	Capture, transport and storage	(Beal et al., 2018)
Biocomposite (Predicted scenario)	Integrated with brewery in Thailand; culture volume of 42.7 m^3 for 90% CO_2 removal; no selling algae biomass.	90 - 110	Capture and storage	This study
Biocomposite (Experimental scenario)	Integrated with brewery in Thailand; culture volume of 3.5 m^3 for 90% CO_2 removal; no selling algae biomass.	120 - 140	Capture and storage	This study

6.4 Conclusions

This techno-economic analysis indicated that both water and algae biomass were the main factors influencing the CO_2 avoidance costs for the algae systems. The biocomposites had the lowest CO_2 avoidance costs because of significant reductions in culture volume, water and energy consumption compared to the other processes. To be competitive with the biofilm PBR, the algal biomass for inoculation of the biocomposites must be cheap, lowering the overall annual operating costs. The analysis also showed that selling algae biomass produced from the biocomposite did not have a large impact on the CO_2 avoidance costs, which recommend that high value biochemical products should be a target for the end use of the biocomposites. In future work, simulations based on pilot scale data and a LCA should be performed to provide a realistic scenario for the biocomposites and inform investment decisions for the brewing industry.

Chapter 7

Conclusions, scaling up, and future vision

7.1   Conclusions

In this thesis, the journey of biocomposite development began with the novel application of hydrogel as a topcoat—instead of the typical random mixing of cells into hydrogel solution—for immobilising microalgae (*Chlorella vulgaris*) onto cotton and polyester textile blends (Chapter 3). The textile biocomposites significantly enhanced CO_2 capture compared with suspension culture controls over a four-week period. The topcoat aided the retention of cells onto the textiles. Textile biocomposites functioned well under low water usage and without nutrient refreshment, offering a "low-water low-maintenance" system that overcomes many issues in conventional open pond or suspension based photobioreactor (PBR) systems. Hence, the system can tackle both CO_2 emissions as well as address water shortage issues. However, the textiles and gel topcoat degraded during the trials, likely due to constant moisture exposure, indicating the subsequent biocomposites needed to be more robust. Since the textile biocomposites had a short lifespan, their application should aim for capturing short term concentrated CO_2 emissions. Furthermore, this study gave rise to the idea of utilising waste textiles from the fashion industry as biocomposites, adding both economic and environmentally friendly attributes to end-of-life clothing recycling.

The deliver this, commercial latex bio-based binders were used to immobilise two strains of cyanobacteria (*Synechococcus elongatus* CCAP 1479/1A and PCC 7942) onto loofah sponge as the solid scaffold to create 3D living biocomposites (Chapter 4). Simple and effective protocols were established that other stakeholders can easily replicate, involving toxicity tests, adhesion tests, binder evaluation, and semi-batch CO_2 absorption tests. The biocomposites significantly outperformed the suspension culture controls, and were predicted to capture 340.11 ± 110 tCO_2 $t^{-1}_{biomass}$ yr^{-1} once scaled up. SEM imaging in combination with modelling of CO_2 absorption kinetics indicated that the cyanobacteria were embedded within a polymer film that had high mass transfer resistance coefficients suggesting that the high CO_2 concentration gradient in the gas phase was the main driving force for intensified CO_2 fixation rates. Despite the high CO_2 uptake, the loofah biocomposites began to release cells mid-way through the CO_2 absorption trials. The root cause could not be determined as the chemical composition of the commercial binders were not publicly available.

In Chapter 5, in collaboration with Northumbria University, different acrylic latex formulations of known composition were made by altering monomer blends (creating hard, normal and soft latexes) and levels of a commercial coalescence agent (Texanol™). The photosynthetic responses of cyanobacteria were also investigated as additional toxicity/stress endpoints using imaging pulse amplitude fluorometry. Hard binders made with a high styrene content were unfavourable for cell viability. Texanol™ improved cell adhesion because of its characteristic of promoting latex film formation and lowering the glass transition temperature of latex binders. The biocomposites had significantly higher net CO_2 absorption rates than suspension culture controls, with the best performing biocomposite being *S. elongatus* CCAP 1479/1A with the soft latex and 4% v/v Texanol™, which functioned for up to 84 days without additional nutrients and could theoretically capture around 570 tCO_2 $t^{-1}_{biomass}$ yr^{-1}. In addition, carbohydrates were accumulated within the cells up to 77% by dry weight.

Finally, a preliminary techno-economic analysis was conducted on the best performing biocomposites with respect to other algae cultivation technologies, i.e. raceway ponds, flat panel PBRs, and biofilm-based PBRs for capturing CO_2 from the brewing industry. Predicted and experimental scenarios were performed in which the former scenario was based on a predicted CO_2 fixation rate with high light exposure and the latter was based on the experimental data from low light exposure. The CO_2 avoidance costs were calculated using an annualisation method to compare the algae technologies with other CCS technologies. The biocomposites had the lowest CO_2 avoidance costs because of significant reductions in culture volume, water and energy consumption among the algal technologies. The CO_2 avoidance costs of the biocomposites in both scenarios also compared favourably within the range of the BECCS technologies. They were estimated to be lower than DAC and ABECCS based on the assumptions made. The predicted biocomposite scenario had the lowest CO_2 avoidance costs (90 - 110 US\$ $t^{-1}_{CO2\ avoided}$ $t^{-1}_{biomass}$ yr^{-1}). The experimental biocomposite scenario had higher estimated CO_2 avoidance costs (120 - 140 US\$ $t^{-1}_{CO2\ avoided}$ $t^{-1}_{biomass}$ yr^{-1}) likely because of lower light exposure resulting in less CO_2 captured. To be competitive with the biofilm PBR, the algae biomass for biocomposite inoculation must be cheap, lowering the overall annual operating costs. It should be noted that the biocomposites were designed with the aim of maximising CO_2 uptake rates instead of maximising algae biomass production; hence, unlike other culture systems the quantity of algae biomass in the biocomposites was small. The analysis showed that selling the biomass from biocomposites had a minor impact on the CO_2 avoidance costs, favouring high value biochemical products as end targets.

Table 7.1 All textile *Chlorella vulgaris* biocomposites with their CO_2 absorption rates (mean ± StDev).

Treatment	Net CO_2 fixation rates		Theoretical scaled CO_2 capture (tCO_2 $t^{-1}_{biomass}$ yr^{-1})
	g CO_2 $g^{-1}_{biomass}$ day^{-1}	g CO_2 m^{-2} day^{-1}	
Coated cotton	1.82 ± 0.10	4.70 ± 0.25	664.3 ± 36.5
Uncoated cotton	1.55 ± 0.27	4.00 ± 0.69	565.75 ± 98.6
Coated polyester	0.49 ± 0.04	4.03 ± 0.31	178.85 ± 14.6
Uncoated polyester	0.42 ± 0.03	3.47 ± 0.26	153.3 ± 11.0

Table 7.2 All loofah biocomposites with their CO_2 absorption rates (mean ± StDev) and their operational lifespan without nutrient renewal.

Phototroph + binder	Net CO_2 fixation rates		Tested period without failure (Day)	Theoretical scaled CO_2 capture (tCO_2 $t^{-1}_{biomass}$ yr^{-1})
	g CO_2 m^{-2} d^{-1}	g CO_2 $g^{-1}_{biomass}$ d^{-1}		
S. elongatus PCC 7942 + AURO 320	0.34 ± 0.09	0.68 ± 0.18	28	246.97 ± 65.20
S. elongatus CCAP 1479/1A + AURO 321	0.27 ± 0.09	0.93 ± 0.30	28	340.11 ± 110.32
S. elongatus PCC 7942 + 4N	0.39 ± 0.12	1.18 ± 0.29	28	429.87 ± 100.52
S. elongatus PCC 7942 + 12N	0.11 ± 0.07	0.51 ± 0.34	28	185.31 ± 125.41
S. elongatus CCAP 1479/1A + 4S	0.30 ± 0.16	1.13 ± 0.41	84	413.66 ± 150.14
S. elongatus CCAP 1479/1A + 12S	0.42 ± 0.05	1.57 ± 0.08	84	574.08 ± 30.19

This thesis has delivered a range of living biocomposites made from inexpensive supporting materials that have been trialled successfully for intensified carbon capture. Tables 7.1 and 7.2 summarise their CO_2 absorption rates and their theoretical annual rates of scaled CO_2 capture. In all cases, the biocomposites significantly increased CO_2 absorption compared to suspension culture controls. The textile- and loofah-based biocomposites were suitable for short-term and longer-term carbon capture respectively. It can be concluded that the biomimetic concept that inspired the development of the biocomposites has contributed to enhancing CO_2 capture by microalgae and cyanobacteria with a suitable fusion of **non-toxic adhesive materials**, **robust solid supports**, and **highly porous substrates** with **sufficient gas, light and liquid transfers**.

7.2   Future work

This section outlines design criteria, potential challenges, proposed design, and possible improvements that should be considered for scaling up the loofah-based biocomposites for pilot-scale CCS applications. The intention of this section is to provide guidelines in designing the biocomposites for future work beyond the constraints in Chapter 6.

7.2.1   Design criteria of the pilot-scale biocomposites

Design criteria for large-scale and longer-term use of biocomposites should consider the following key points:

1) The need for a biologically safe coating method that delivers a uniform coating throughout the loofah scaffold;

2) The spatial arrangement of the biocomposite should not hinder light penetration to the cells that lie in the inner parts of the biocomposites;

3) The need for a nutrient delivery system that assists/augments the capillary action of loofah without compromising the structural integrity of the binder;

4) The containment infrastructure for the biocomposites should be cheap but robust enough to support long term operation as well as provide transparency for light penetration.

7.2.2   Potential challenges upon scaling up

A drawback of the loofah-based biocomposites was the non-uniform latex coating caused by a random fibrous network of the loofah structure. During lab manufacture any excess latex formulation flowed through the loofah pores instead of adhering to the strands. This potentially

could be solved with an inkjet coating sprayer to deposit the coating mixture via fine droplets and precisely coat the targeted area even with a three-dimensional structure (Carey et al., 2018). This technique has been widely used in commercial vehicle and paper coatings.

Another issue that arises from the random fibrous network is variation in pore size and strand diameter, which causes non-uniform light penetration to the cells deeper within the biocomposite structure, resulting in lower photosynthetic performance and CO_2 uptake. The use of optical fibres integrated within the biocomposite structure as internal light sources could potentially overcome this obstacle and increase biomass productivity (Xue et al., 2013, Wondraczek et al., 2019). However, this would increase capital and operating costs and introduce complexity into the manufacturing process. Hence, the depth of containment is important and should be designed as a panel with a small width (ideally around 1-2 cm).

7.2.3   Case studies of pilot-scale algal biofilm systems

Case studies are used to identify good practice to inform the design of a pilot-scale biocomposite system. Three algae biofilm systems were selected because the biofilm concept is more similar to the biocomposites than suspension-based processes (Figure 7.1). The first system was previously selected for techno-economic analysis in Chapter 6 (Ozkan et al., 2012). Ozkan et al.'s system required large land areas because cultivation was arranged horizontally, and the use of artificial light would increase capital cost and energy consumption (Figure 7.1a); however, they employed an effective low energy gravity fed nutrient recirculation system.

The second system is a revolving algal biofilm (RAB) design built within an inexpensive greenhouse made from transparent polycarbonate plastic sheets (Gross and Wen, 2014), which reduces land demand by rotating the biofilm between liquid and gas phases (Figure 7.1b), and enabling homogenous light distribution throughout the biofilm. However, this arrangement is unsuitable for biocomposites as the constant motion can potentially disturb the binders and compromise cell adhesion.

The third case study—a laminar PBR (Martín-Girela et al., 2017) (Figure 7.1c)—was also built within a greenhouse. The vertical arrangement of the PBRs further reduced the land requirement compared to the other two systems. A more sophisticated gravity fed nutrient circulation system was used than in Ozkan et al.'s system.
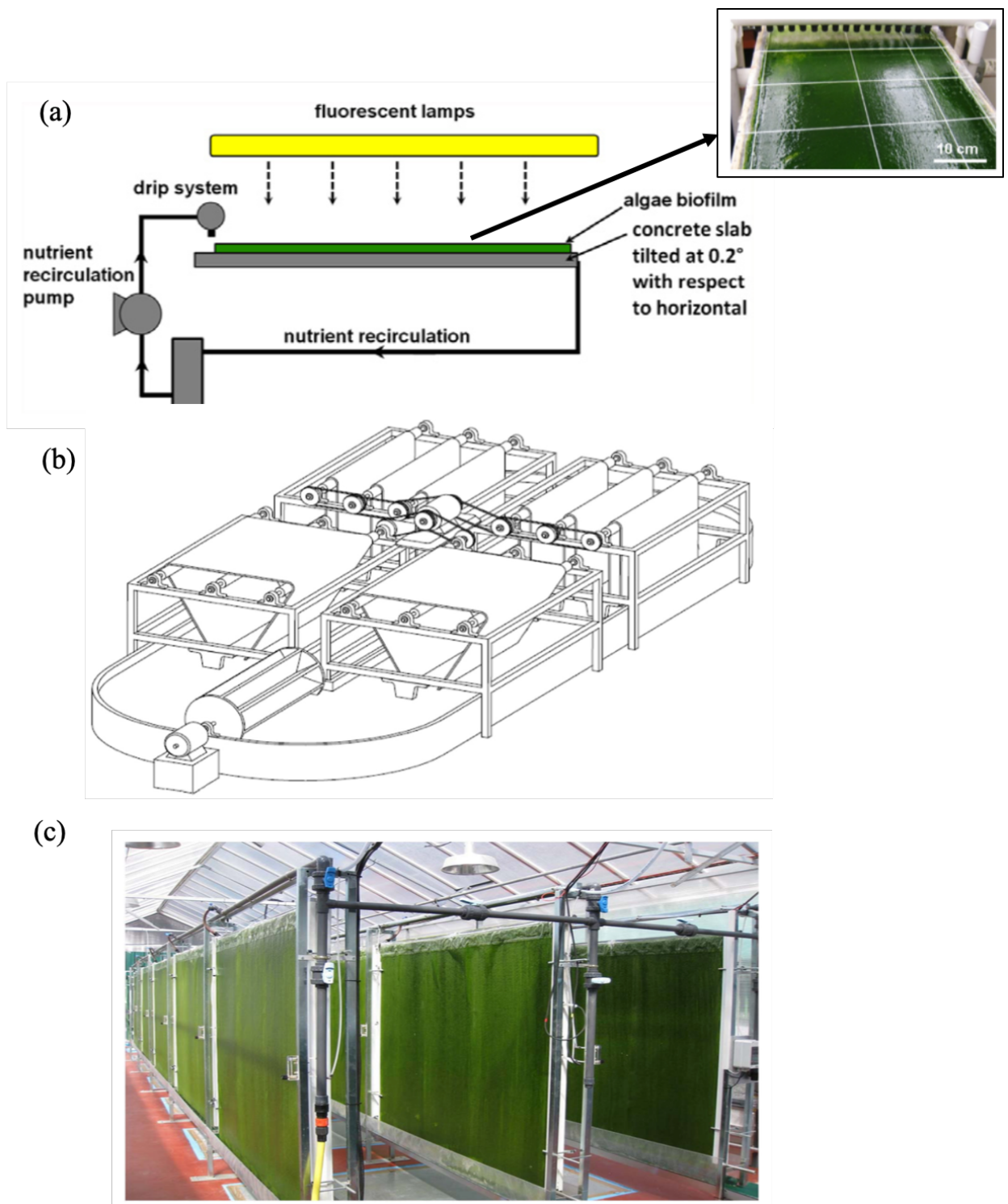
Figure 7.1 Configurations of algae biofilm systems: (a) A concrete slab PBR (Ozkan et al., 2012), (b) a revolving algal biofilm PBR (Gross and Wen, 2014), and (c) laminar PBRs (Martín-Girela et al., 2017).

Table 7.3 Selected studies of pilot-scale algae biofilm systems for case studies to inform the design of a pilot-scale biocomposite system.

Study	Algal species	Operation description	Light source	Irrigation system
(Ozkan et al., 2012)	*Botryococcus braunii* (LB 572)	A biofilm PBR with a cultivation area of 0.275 m^2 constructed from a concrete slab (8 mm thick layer) and a wooden support plate. The system was implemented horizontally with a tilted of 0.2 °.	Four 32 W fluorescent lamps	Dripping nozzles located above the concrete surface were used to deliver nutrient medium. The medium was collected at the end of the growth surface and delivered to reservoir by gravity before being pumped back to the nozzles using a peristaltic pump.
(Gross and Wen, 2014)	*Chlorella vulgaris* (UTEX #265)	Rotating biofilm cultivation designed in a triangular configuration with vertical orientation. The supporting material was flexible cotton duct fabric. Rotation was motor driven. The biofilm moved between liquid and gas phases i.e. alternate exposure between nutrient medium and CO_2. The system was placed in a polycarbonate walled greenhouse.	Natural lighting	Nutrient medium was supplied by rotation of the biofilm into a medium reservoir placed at the bottom of the system.
(Martín-Girela et al., 2017)	*Chlorella* sp. and *Scenedesmus* sp.	Biofilms were cultivated on 1.5 × 2 × 0.1 m (h × l × w) polypropylene geo-textile sheets as a part of the vertical laminar PBRs. The sheets were hung from narrow and hallow chambers. The system was placed in a polycarbonate walled greenhouse.	Natural lighting	A water recirculation system was integrated into laminar PBRs and connected to a water mixing tank and nutrient storage. The nutrient medium flow was pumped and delivered via a perforated pipeline (trickle system) located along the top of the PBR system.

7.2.4 Proposed design of a pilot-scale biocomposite system

A pilot-scale biocomposite CCS system (Figure 7.2) is proposed that combines good practice from the three case studies. The system would be built within an inexpensive polytunnel made from transparent polycarbonate sheets with CO_2 gas inlets and outlets flowing through the facility. The polytunnel enables biocomposites to gather natural light to maintain low running costs. Each containment unit would be built vertically from affordable materials like fine mesh netting that are attached to transparent plastic frame supports. The reason for selecting these materials is because the immobilised cells are already protected by latex coatings, thus eliminating the need for solid plastic structures. A nutrient system with fine mist distributors or a humidifier would be integrated at the top of each unit to circulate nutrients via gravity (with minimal shear stress), thereby reducing nutrient gradients and preventing mechanical damage to the binder. The nutrient system would be installed with smart sensors to detect the system humidity level and responsively trigger nutrient supply. Valves would also be integrated with the nutrient system to prevent gas escape. One access door is required for an operator to access the facility for maintenance and would be positioned on the same side as the gas outlet.
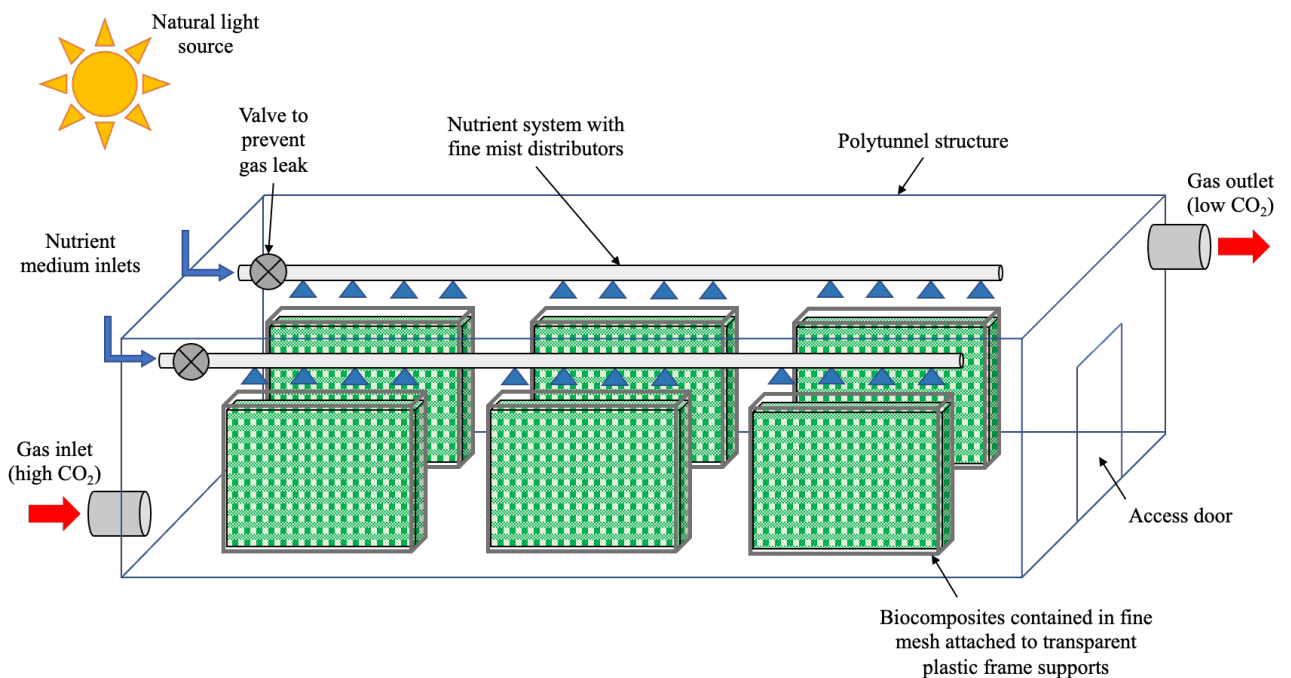
Figure 7.2 Schematic of a proposed design for a pilot-scale biocomposite system. Biocomposites are housed within a transparent polycarbonate polytunnel, with a door for operator access. The biocomposites are contained within flexible plastic fine mesh attached to vertical transparent plastic frame supports. An automatic nutrient system with fine mist distributors is installed at the top of each biocomposite unit.

7.2.5   Improvements on the biocomposites

Several improvements can be made to increase the carbon capture performance of the biocomposites. From an engineering aspect, as mentioned in Chapter 5, further study on latex formulations can be used to optimise cell viability, gas mass transfer and photosynthetic performance. Parameters such as cell loading, total solid binder, light intensity, light cycle, and nutrient concentration can greatly influence CO_2 uptake but have not been explored. For example, increasing cell loading can lead to higher competition for nutrients meaning nutrient concentration has to be increased. Another approach is to introduce non-film forming particles into the latex formulations to increase the porosity of the coatings. However, this may increase the total capital cost of the biocomposites and risks secondary pollution if non-biodegradable additives are used, e.g. microplastics.

From a biological perspective, metabolic engineering could be used to modify and improve genes that are related to RuBisCo kinetics or that favour biofilm formation. CRISPR (clustered regularly interspaced short palindromic repeats) technology is a precise, simple, and fast approach to target and edit the desired genes, that has revolutionised genetic engineering. The CRISPR method involves proteins found in bacteria, in which the Cas9 protein is the most commonly used by researchers. The protein is injected into a cell along with a piece of guide RNA. They attach together and move along the DNA strand to the specific point where RNA and DNA sequences match. The protein then cut off those DNA parts.

However, in order to effectively utilise metabolic engineering, biological responses of cells in confined spaces within the biocomposites should be understood. Recently, Moore et al. (2020) found that cyanobacteria (*Synechococcus* sp. PCC 7002) grew in the confined environment showed increased fluorescence compared to the ones without confinement. The cells in the confinement responded by generated fluorescence in the thylakoid membrane areas and propagated to the interior cell compartments. The observation indicated that cell-cell and cell-substrate interactions can greatly influence photosynthesis and these mechanical regulations could be the key to unlock photosynthesis potential in immobilised cells of the biocomposites.

7.3 Future vision

To envision the potential of our biocomposite technology, one question has to be asked:

"How much biocomposite would be required to capture the total amount of anthropogenic
CO$_2$ emissions?"

Recently, Wang et al. (2020) showed that the global CO$_2$ fertilisation effect – enhancement in vegetation productivity driven by increased CO$_2$ source in air - has decreased in most terrestrial regions likely due to changes in key soil nutrients (N and P) and water sources. This means that terrestrial photosynthesis may not result in increased CO$_2$ uptake, despite rising CO$_2$ concentration in air. With this scenario, climate mitigation strategies that are land-based such as BECCS would be unlikely to solve the global warming issue and reach climate targets. Hence, if this global phenomenon holds true, our biocomposites would be a valuable asset to combat global warming by turning aquatic photosynthetic unicellular microorganisms into 'terrestrial proxies', i.e. aquatic algae/cyanobacteria engineered to behave as lichens and leaves. With different CO$_2$ harness systems between terrestrial plants (mostly are C3 plants – CO$_2$ gather through stomata and adapt well in cool environment (Medrano et al., 2002)) and cyanobacteria (gather CO$_2$ through CCM, which help them to adapt in harsh environment to maintain their photosynthesis ability (Kupriyanova et al., 2013)), the CO$_2$ fertilisation effect may not be applicable with the biocomposites. This vision may seem radical, but nature has already evolved its own natural biocomposites – lichen (a terrestrial composite organism comprising algae/cyanobacteria and fungus). Around 8% of the Earth's surface is covered by lichen and its habitat can be extreme, with minimal water and nutrient availability (Asplund and Wardle, 2016). If the biocomposites are implemented as a means to assist the global ecosystem and restabilise the global carbon cycle, this would be equivalent to undoing excess anthropogenic pollution without working against nature. This vision is not without precedent as it was cyanobacteria that drove the "Great Oxygenation Event" 2.5 billion years ago, which was responsible for producing massive quantities of oxygen via photosynthesis (Ligrone, 2019). Clearly, the timescales involved is a fundamental difference between these scenarios (tens of millions of years versus tens of years), but the rationale still stands.

According to Luderer et al. (2018), it was found that 640 to 950 of GtCO$_2$ must be removed from the atmosphere before 2100 to limit temperature rise to 1.5 °C. Counting from 2020, this means that 8 to 12 GtCO$_2$ must be removed per year. With the best performing loofah-based biocomposites (574.08 ± 30.19 tCO$_2$ t^{-1} $_{biomass}$ yr^{-1}), we would need 5.5×10^{10} to 8.2×10^{10}

m^3 of biocomposites assuming that the photosynthesis efficiency was maintained. The total amount of latex binder required would be 196 – 292 million litres. If we assume that 1 m^3 of biocomposite covers a 1 m^2 area, the required area to absorb the total annual global CO_2 would range between 5.5 to 8.17 million hectares (equivalent to only 0.18 – 0.27% of habitable land in the tropics). With these estimated areas, the biocomposites could reduce the land requirement of BECCS (0.4 – 12 billion hectares) by 98 – 99%. It should be noted that the theoretical scaled capture was based on the CO_2 absorption rates recorded under low light exposure. Once the biocomposites are exposed to natural light, which is high light intensity, the CO_2 uptake rates should be increased, which will decrease the land requirement even further. However, implementation location would need to be equatorial in order to obtain high consistently light intensity.

Furthermore, unlike terrestrial plants, implemented of the biocomposite strategy is not restricted only to certain types of land—an enormous benefit of the "low-water low-maintenance" characteristics of the biocomposites. This would facilitate their deployment to hitherto unforeseen places or even in urban settings. For example, most high-rise building rooftops are 'unused' areas upon which biocomposites could be built, with plentiful natural light and water from rainfall. Another idea would be to deploy biocomposites next roads to capture the CO_2 produced by traffic. By integrating biocomposites into urban settings the air quality could be improved and, as a result, uplift the quality of human lives.

7.4   Biocomposites for other applications

Apart from CCS and biofuel applications, the concept of biocomposites or cell immobilisation have been widely used in wastewater treatment. Loofah-based cyanobacteria biocomposites have characteristics compatible with wastewater treatment and bioremediation, such as good mechanical strength, prevention of microbial attack, and high porosity for good gas and liquid diffusion.

Microbial fuel cells (MFC) are another area that loofah-based biocomposites could be integrated. A typical MFC consists of anode (bacteria live in solution) and cathode sides. The bacteria produce electrons by reacting with the substrate solution through which electricity is being generated. The anode attracts those electron and transfers them to the cathode react with protons via reduction of oxygen to create water molecules (Ezziat et al., 2019). The process could potentially be intensified by changing the immobilised species from cyanobacteria to electrogenic bacteria. There are a number of studies that tried to use algae to assist cathode

performance, as algae can substitute the need for aeration for the cathode by producing oxygen from photosynthesis (González del Campo et al., 2013, Pandit and Das, 2015, Kusmayadi et al., 2020).

Microalgae-based biosensors are also another emerging application for environmental and pollution monitoring (Antonacci and Scognamiglio, 2020). Biosensors are divided into two parts i.e., bioreceptor element (a biological sensing element and transducer) that detects biochemical signals then transforms them to either electrical or optical data. Microalgae can use whole cells and their photosynthetic subcomponents as bioreceptors. Current immobilisation techniques used in the development of microalgae-based biosensors are mostly hydrogel based, which have poor stability and result in short operational lives. Loofah-based biocomposites can overcome this issue.

One radical idea is that biocomposites can be used as sustainable living materials that integrate into interior settings to design living buildings. Urban buildings have isolated humanity from nature. There is an emerging trend of integrating nature processes within the built environment through developing living building materials to establish a more balanced environment and bring society closer to nature (Biloria and Thakkar, 2020). With the photosynthetic ability of microalgae (provide O_2 rich air), there is a possibility to implement these microorganisms into ceiling tiles or wall fixtures and reduce the need for ventilation. Loofah-based biocomposites could potentially be utilised as living walls, living coatings, living paints, or living inks. The latex binders provide a protective barrier between microalgae and humans. Loofah would require less space in the interior settings because of its 3D porous structure enabling high cell density. In addition, the biocomposites can make use of wastewater from buildings potentially reducing waste.

To reiterate, microalgae and cyanobacteria biocomposites have been successfully developed for intensified carbon capture. Apart from providing a promising solution to CO_2 capture, this technology can potentially be implemented in a wide range of applications such as wastewater, biosensors, and living materials. They can be integrated into existing society and business infrastructures seamlessly as "heroes behind the scene" to sustainably improve human lives.

Appendix I

Simulation of control vial and biocomposite experiments to estimate mass transfer resistances

1.0 Control vial model

In this section the simulation of diffusion in the control vials, filled with gas and a suspended microalgae or cyanobacteria culture, is described. The purpose of this work was to establish a rate constant for the removal of CO_2 by the cells suspended in culture medium. The removal of CO_2 by the cells is assumed to be a first order process.

$$\text{rate of } CO_2 \text{ removal by cells} = K\, a_C\, c_{CO2}$$

This assumes that either mass dominates or that the reaction consuming CO_2 is first order. The diffusion model in conjunction with experimental data were used to determine values for the volumetric transfer coefficient $K\, a_C$. A second diffusion model was used to simulate vials with biocomposite and the values of the volumetric transfer coefficient were compared.

1.1 Differential mass balances

In the gas phase we assume diffusion is the only mass transfer mechanism. A mass balance and the application of Fick's first law leads to equation 1.1.

$$\frac{\partial c^G}{\partial t} = D^G_{CO_2} \frac{\partial^2 c^G}{\partial z^2} \quad (1.1)$$

Assuming that:

there is no mixing in the liquid phase and that diffusion is the only mass transfer mechanism. Diffusion flux is in the axial direction; and CO_2 removal by the cells is represented by a reaction that is first order with respect to the concentration of CO_2 in the liquid phase.

Using these assumptions, a mass balance in the liquid phase leads to equation 1.2.

$$\frac{\partial c^L}{\partial t} = D^L_{CO_2} \frac{\partial^2 c^L}{\partial z^2} - K a_C c^L \quad (1.2)$$

To solve these equations we have to spatially discretize them and solve the resulting set of ordinary differential equations. The vial is split into slices as shown in Fig. S4.

Since diffusion is the only transport mechanism for the CO_2, the second order differentials in equations 1.1 and 1.2 can be represented using second order central differences. Equations 1.1 and 1.2 are discretized to give equation 1.3 and 1.4.

$$\frac{\partial c_i^G}{\partial t} = D_{CO_2}^G \left(\frac{c_{i+1}^G - 2c_i^G + c_{i-1}^G}{\Delta z^2} \right) \quad (1.3)$$

$$\frac{\partial c_j^L}{\partial t} = D_{CO_2}^L \left(\frac{c_{j+1}^L - 2c_j^L + c_{j-1}^L}{\Delta z^2} \right) - K a_c c_i^L \quad (1.4)$$
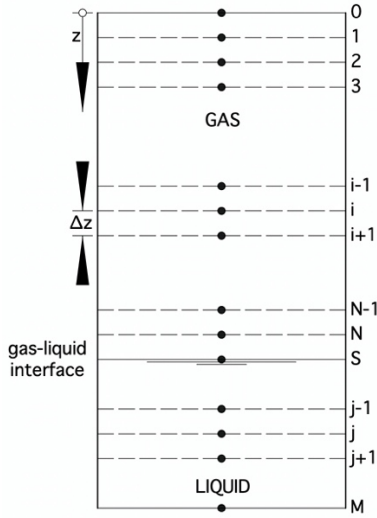
Figure S1 The vial compartmentalised into a numerical grid.

1.2 Boundary conditions

There are three boundaries within the vial; the top of the vial, the gas-liquid interface, and the base of the vial.

1.2.1 Top and bottom of the vial

At the top and bottom of the vial, the wall prevents diffusion so the diffusion flux is zero. We used a forward difference at the top of the vial and a backwards difference at the bottom of the vial to represent the concentration gradient as shown in equations 1.5 and 1.6.

$$J_0^G = -D_{CO_2}^G \left. \frac{\partial c^G}{\partial z} \right|_0 = 0 = -D_{CO_2}^G \left(\frac{-3c_0^G + 4c_1^G - c_2^G}{2\Delta z} \right) \quad (1.5)$$

$$J_M^L = -D_{CO_2}^L \left. \frac{\partial c^L}{\partial z} \right|_M = 0 = -D_{CO_2}^L \left(\frac{c_{M-2}^L - 4c_{M-1}^L + 3c_M^L}{2\Delta z} \right) \quad (1.6)$$

Equations 1.5 and 1.6 were solved for the gas concentration at the top of the vial (c_0^G) and the liquid concentration at the base of the vial (c_M^L), as given by equations 1.7 and 1.8.

$$c_0^G = \tfrac{4}{3}c_1^G - \tfrac{1}{3}c_2^G \quad (1.7)$$

$$c_M^L = \tfrac{4}{3}c_{M-1}^L - \tfrac{1}{3}c_{M-2}^L \quad (1.8)$$

1.2.2 Interface between gas and liquid

At the interface between the gas and the liquid (surface S in Fig. S4) we assume that equilibrium exists between the phases. In this case the equilibrium is given by Dalton's law and Henry's law, as given by equation 1.7.

$$y_S P = c_S^G RT = Hc_S^L \quad (1.7)$$

Mass balances for the cell above the interface in the gas phase (eqn. 1.8) and the cell below the interface in the liquid phase (eqn. 1.9) are written in terms of the flux of CO_2 instead of the concentration gradient.

$$\frac{\partial c_N^G}{\partial t} = \frac{J_N^G - J_i}{\Delta z_G} \quad (1.8)$$

$$\frac{\partial c_1^L}{\partial t} = \frac{J_i - J_1^L}{\Delta z_L} \quad (1.9)$$

The diffusion fluxes in the gas (J_N^G) and liquid (J_1^L) phases are estimated using Fick's law with second order differences, as given by equations 1.10 and 1.11.

$$J_N^G = -D_{CO_2}^G \left.\frac{\partial c^G}{\partial z}\right|_N = -D_{CO_2}^G \left(\frac{c_{N-2}^G - 4c_{N-1}^G + 3c_N^G}{2\Delta z_G}\right) \quad (1.10)$$

$$J_1^L = -D_{CO_2}^L \left.\frac{\partial c^L}{\partial z}\right|_1 = -D_{CO_2}^L \left(\frac{-3c_1^L + 4c_2^L - c_3^L}{2\Delta z_L}\right) \quad (1.11)$$

The flux crossing the interface is calculated by applying two film theory around the interface so that the concentrations at point N in the gas phase and point 1 in the liquid phase can be used instead of interfacial concentrations. The flux is given by equation 1.12.

$$J_i = K_{ov}\left(\frac{c_N^G RT}{H} - c_1^L\right) \quad (1.12)$$

The overall mass transfer coefficient, K_{ov}, is given by equation 1.13.

$$\frac{1}{K_{ov}} = \left(\frac{\Delta z_L}{D_{CO_2}^L} + \frac{\Delta z_G}{D_{CO_2}^G}\frac{RT}{H}\right) \quad (1.13)$$

Substituting from equations 1.10, 1.11 and 1.12 into equations 1.8 and 1.9 leads to equations 1.14 and 1.15 which describe the way the CO_2 concentration in the cells next to the interface change with time.

$$\frac{\partial c_N^G}{\partial t} = \frac{1}{\Delta z_G}\left[D_{CO_2}^G\left(\frac{-c_{N-2}^G+4c_{N-1}^G-3c_N^G}{2\Delta z_G}\right) - K_{ov}\left(\frac{c_N^G RT}{H} - c_1^L\right)\right] \quad (1.14)$$

$$\frac{\partial c_1^L}{\partial t} = \frac{1}{\Delta z_L}\left[K_{ov}\left(\frac{c_N^G RT}{H} - c_1^L\right) - D_{CO_2}^L\left(\frac{3c_1^L-4c_2^L+c_3^L}{2\Delta z_L}\right)\right] - a_c k c_1^L \quad (1.15)$$

1.3 Making the equations dimensionless

Defining the following characteristic variables

$$\bar{c} = \frac{c}{c_0} \qquad \bar{t} = \frac{t}{\tau} \qquad \text{where} \ \ \tau = \frac{\Delta z_0\, z_0}{D_0} \qquad \bar{z} = \frac{z}{z_0} \qquad \Delta z_0 = \frac{z_0}{N+1+M}$$

The mass balances in the gas and liquid phases are transformed using dimensionless variables. The mass balances are given for the first cell in the gas layer, the cells in the middle of the gas layer, cell N in the gas layer, cell 1 in the liquid layer and cell M-1 in the liquid layer.

Point 1 in the gas layer

$$\frac{\partial \bar{c}_i^G}{\partial \bar{t}} = \frac{2}{3}\frac{\Delta z_0}{z_0}\frac{D_{CO_2}^G}{D_0}\left(\frac{\bar{c}_2^G-\bar{c}_1^G}{\overline{\Delta z}_G^2}\right) \quad (1.16)$$

Points 2 to N-1 in the gas layer

$$\frac{\partial \bar{c}_i^G}{\partial \bar{t}} = \frac{\Delta z_0}{z_0}\frac{D_{CO_2}^G}{D_0}\left(\frac{\bar{c}_{i+1}^G-2\bar{c}_i^G+\bar{c}_{i-1}^G}{\overline{\Delta z}_G^2}\right) \quad (1.17)$$

Point N in the gas layer

$$\frac{\partial \bar{c}_N^G}{\partial \bar{t}} = \frac{\Delta z_0}{z_0}\frac{1}{\overline{\Delta z}_G}\left[\left(\frac{D_{CO_2}^G}{D_0}\right)\left(\frac{-\bar{c}_{N-2}^G+4\bar{c}_{N-1}^G-3\bar{c}_N^G}{2\overline{\Delta z}_G}\right) - \left(\frac{z_0}{D_0}\right)K_{ov}\left(\frac{\bar{c}_N^G RT}{H} - \bar{c}_1^L\right)\right] \quad (1.18)$$

Point 1 in the liquid layer

$$\frac{\partial \bar{c}_1^L}{\partial t} = \frac{\Delta z_0}{z_0}\frac{1}{\overline{\Delta z}_L}\left[\left(\frac{z_0}{D_0}\right)K_{ov}\left(\frac{\bar{c}_N^G RT}{H} - \bar{c}_1^L\right) - \left(\frac{D_{CO_2}^L}{D_0}\right)\left(\frac{3\bar{c}_1^L-4\bar{c}_2^L+\bar{c}_3^L}{2\overline{\Delta z}_L}\right)\right] - \left(\frac{z_0 \Delta z_0}{D_o}\right)K a_c \bar{c}_1^L \quad (1.19)$$

Points 2 to M-2 in the liquid layer

$$\frac{\partial \bar{c}_j^L}{\partial \bar{t}} = \frac{\Delta z_0}{z_0}\frac{D_{CO_2}^L}{D_0}\left(\frac{\bar{c}_{j+1}^L-2\bar{c}_j^L+\bar{c}_{j-1}^L}{\overline{\Delta z}_L^2}\right) - \left(\frac{z_0 \Delta z_0}{D_0}\right)K a_c \bar{c}_j^L \quad (1.20)$$

Point M-1 in the liquid layer

$$\frac{\partial \bar{c}_{M-1}^L}{\partial \bar{t}} = \frac{2}{3} \frac{\Delta z_0}{z_0} \frac{D_{CO_2}^L}{D_0} \left(\frac{\bar{c}_{M-2}^L - \bar{c}_{M-1}^L}{\overline{\Delta z}_L^2} \right) - \left(\frac{z_0 \, \Delta z_0}{D_0} \right) Ka_c \bar{c}_{M-1}^L \quad (1.21)$$

1.4 Solving the equations

Equations were set up and solved by numerical integration using Mathematica version 12. The following protocol was adopted to ensure that the models represented the experimental situation.

Saturating the liquid with CO_2

Run 1, saturate the liquid with CO_2 at atmospheric concentrations of CO_2. Runs 2-4, put initial gas concentration up 5 mol%. Final gas and liquid compositions were the same between runs 3 and 4.

Implementing the light dark cycles.

A piecewise function was used to simulate the light-dark cycles of the growth room. It was assumed that the gas in the vial was changed at 15:00 and that the lights were switched off at 21:00 for eight hours. The schedule is given in Table S3.

Table S1 Lighting schedule during the trial.

Day	Time	Hours	Lights on/off
1	15:00	0	on
1	21:00	6	off
2	05:00	14	on
2	21:00	30	off
3	05:00	38	on

These are based on assumptions: 1) one dimensional diffusion in the vial, 2) all vials contain the same number of cells, and 3) all biocomposite samples contain the same number of cells as the suspended cultures in control vials

2.0 Diffusion model for vials containing biocomposite

2.1 Mass balance equations and discretization

In the gas surrounding the biocomposite sample a mass balance on an element with dimensions $\Delta x \, \Delta y \, \Delta z \,(\Delta z = 1)$ leads to equation 2.1.

$$\frac{\partial c^G}{\partial t} = -\frac{\partial J_x}{\partial x} - \frac{\partial J_y}{\partial x} \quad (2.1)$$

In the gas within the biocomposite sample, a mass balance on an element with dimensions $\Delta x \, \Delta y \, \Delta z \,(\Delta z = 1)$, including diffusion and CO_2 consumption due to photosynthesis leads to equation 2.2.

$$\frac{\partial c^G}{\partial t} = -\frac{\partial J_x}{\partial x} - \frac{\partial J_y}{\partial x} - a_{BC}kc^G \quad (2.2)$$

Using Fick's first law of diffusion to replace the diffusion fluxes in equations 2.1 and 2.2 leads to equations 2.3 and 2.4.

$$\frac{\partial c^G}{\partial t} = D^G_{CO_2}\left(\frac{\partial_2 c^G}{\partial x^2} + \frac{\partial_2 c^G}{\partial y^2}\right) \quad (2.3)$$

$$\frac{\partial c^G}{\partial t} = D^G_{CO_2}\left(\frac{\partial_2 c^G}{\partial x^2} + \frac{\partial_2 c^G}{\partial y^2}\right) - a_{BC}kc^G \quad (2.4)$$

Equations 2.3 and 2.4 are solved by discretizing the spatial derivatives on the numerical grid shown in Fig. S5. Due to rotational symmetry only a quarter of the vial and biocomposite sample have to be simulated. In Fig. S5 the black lines represent the biocomposite sample, within these lines equation 2.4 is used for simulation. Outside the black lines equation 2.3 is used. The yellow lines represent symmetry boundaries and the green lines the wall of the vial. Using second order central second differences to replace the concentration gradients in equations 2.3 and 2.4 leads to equations 2.5 and 2.6.

$$\frac{\partial c^G_{i,j}}{\partial t} = D^G_{CO_2}\left(\frac{c^G_{i+1,j}-2c^G_{i,j}+c^G_{i-1,j}}{\Delta x^2} + \frac{c^G_{i,j+1}-2c^G_{i,j}+c^G_{i,j-1}}{\Delta y^2}\right) \quad (2.5)$$

$$\frac{\partial c^G_{i,j}}{\partial t} = D^G_{CO_2}\left(\frac{c^G_{i+1,j}-2c^G_{i,j}+c^G_{i-1,j}}{\Delta x^2} + \frac{c^G_{i,j+1}-2c^G_{i,j}+c^G_{i,j-1}}{\Delta y^2}\right) - a_{BC}kc^G_{i,j} \quad (2.6)$$

Figure S2 The numerical grid.

Equation 2.3 or 2.4 is written for every point on the numerical grid within the green boundary. This leads to a set of ordinary differential equations that are solved over time to follow the evolution of CO_2 concentration.

2.2 Boundary conditions

There are two boundary conditions that are applied at the boundaries of the numerical grid.

At the symmetry boundaries: $\qquad \dfrac{\partial c^G}{\partial n} = 0$

At the vial wall: $\qquad J_x = J_y = 0$

The remainder of this section with deal with the application of these boundary condition to the numerical grid shown in Fig. S5.

Symmetry boundaries

Along the x-axis symmetry boundary, diffusion in the y-direction is normal to the boundary, and on the y-axis symmetry boundary diffusion in the x-direction is normal to the boundary. Therefore we can write that:

$$\left.\frac{\partial c^G}{\partial y}\right|_{y=0} = 0 \quad \Rightarrow \quad \left.\frac{\partial^2 c^G}{\partial y^2}\right|_{y=0} = 0$$

$$\left.\frac{\partial c^G}{\partial x}\right|_{x=0} = 0 \quad \Rightarrow \quad \left.\frac{\partial^2 c^G}{\partial x^2}\right|_{x=0} = 0$$

This simplifies the mass balance equations as follows. At the x-axis symmetry boundary equations 2.7 and 2.8 are used, depending on whether the point is inside or outside the biocomposite sample.

$$\frac{\partial c_{i,j}^G}{\partial t} = D_{CO_2}^G \left(\frac{c_{i+1,j}^G - 2c_{i,j}^G + c_{i-1,j}^G}{\Delta x^2}\right) \quad (2.7)$$

$$\frac{\partial c_{i,j}^G}{\partial t} = D_{CO_2}^G \left(\frac{c_{i+1,j}^G - 2c_{i,j}^G + c_{i-1,j}^G}{\Delta x^2}\right) - a_{BC} k c_{i,j}^G \quad (2.8)$$

At the y-axis symmetry boundary, equations 2.9 and 2.10 are used, depending on whether the point is inside or outside the biocomposite sample.

$$\frac{\partial c_{i,j}^G}{\partial t} = D_{CO_2}^G \left(\frac{c_{i,j+1}^G - 2c_{i,j}^G + c_{i,j-1}^G}{\Delta y^2}\right) \quad (2.9)$$

$$\frac{\partial c_{i,j}^G}{\partial t} = D_{CO_2}^G \left(\frac{c_{i,j+1}^G - 2c_{i,j}^G + c_{i,j-1}^G}{\Delta y^2}\right) - a_{BC} k c_{i,j}^G \quad (2.10)$$

At the centre of the vial and the biocomposite sample there are two symmetry boundaries. At this single point there are no concentration gradients in the x or y direction and the mass balances simplifies to give equation (2.11).

$$\frac{\partial c_{i,j}^G}{\partial t} = -a_{BC} k c_{i,j}^G \quad (2.11)$$

(a)   (b)   (c)
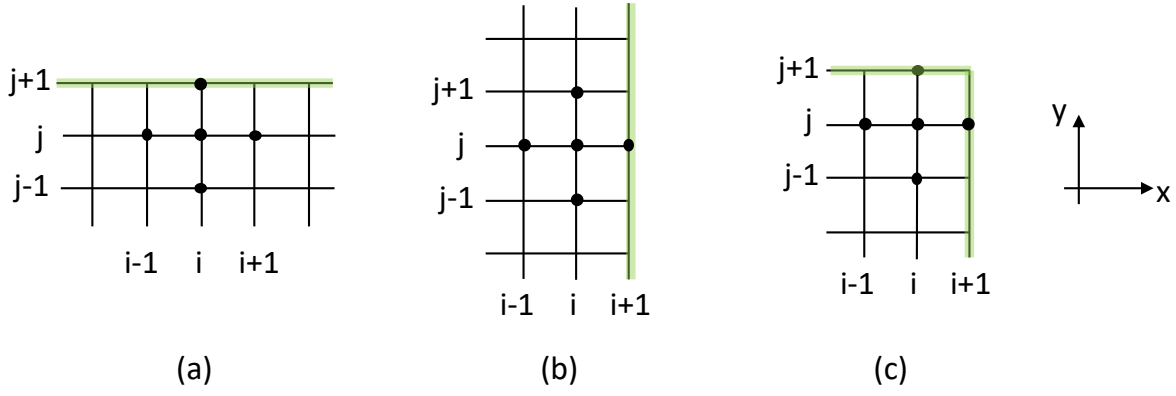
Figure S3 Vial wall boundaries.

Vial boundaries

The different types of vial wall boundary cells in the numerical grid are shown in Fig. S6. These are horizontal wall Fig. S6(a), vertical wall Fig. S6(b) and a corner Fig. S6(c).

For the horizontal wall the flux normal to the wall is in the y-direction. The boundary condition at the wall is

$$J_{i,j+1} = -D_{CO_2}^L \frac{\partial c^G}{\partial y}\Big|_{i,j+1} = 0 = -D_{CO_2}^G \left(\frac{c_{i,j-1}^G - 4c_{i,j}^G + 3c_{i,j+1}^G}{2\Delta z} \right) \quad (2.12)$$

solving equation 2.12 for $c_{i,j+1}^G$ gives $c_{i,j+1}^G = \frac{4}{3}c_{i,j}^G - \frac{1}{3}c_{i,j-1}^G$. Substituting this into equation 2.3 leads to equation 2.13.

$$\frac{\partial c_{i,j}^G}{\partial t} = D_{CO_2}^G \left(\frac{c_{i+1,j}^G - 2c_{i,j}^G + c_{i-1,j}^G}{\Delta x^2} + \frac{2}{3}\left[\frac{c_{i,j-1}^G - c_{i,j}^G}{\Delta y^2} \right] \right) \quad (2.13)$$

For the vertical wall the flux normal to the wall is in the x-direction. The boundary condition at the wall is

$$J_{i+1,j} = -D_{CO_2}^L \frac{\partial c^G}{\partial y}\Big|_{i+1,j} = 0 = -D_{CO_2}^G \left(\frac{c_{i-1,j}^G - 4c_{i,j}^G + 3c_{i+1,j}^G}{2\Delta z} \right) \quad (2.14)$$

solving equation 2.14 for $c_{i+1,j}^G$ gives $c_{i+1,j}^G = \frac{4}{3}c_{i,j}^G - \frac{1}{3}c_{i-1,j}^G$. Substituting this into equation 2.3 leads to equation 2.15.

$$\frac{\partial c_{i,j}^G}{\partial t} = D_{CO_2}^G \left(\frac{2}{3}\left[\frac{c_{i-1,j}^G - c_{i,j}^G}{\Delta x^2} \right] + \frac{c_{i,j+1}^G - 2c_{i,j}^G + c_{i,j-1}^G}{\Delta y^2} \right) \quad (2.15)$$

182

For a corner, the flux in the y-direction at point (i,j+1) and the flux in the x-direction at point (i+1,j) are both zero. Solving equations 2.12 and 2.14 and substituting the results into equation 2.3 leads to equation 2.16.

$$\frac{\partial c_{i,j}^G}{\partial t} = \frac{2D_{CO_2}^G}{3}\left(\frac{c_{i-1,j}^G - c_{i,j}^G}{\Delta x^2} + \frac{c_{i,j-1}^G - c_{i,j}^G}{\Delta y^2}\right) \quad (2.16)$$

There are a further two types of wall point, those which lie on the symmetry boundaries. If a wall point lies on the x-axis symmetry boundary then equation 2.17 is used and if it lies on the y-axis then equation 2.18 is used.

$$\frac{\partial c_{i,j}^G}{\partial t} = \frac{2}{3}D_{CO_2}^G\left(\frac{c_{i-1,j}^G - c_{i,j}^G}{\Delta x^2}\right) \quad (2.17)$$

$$\frac{\partial c_{i,j}^G}{\partial t} = \frac{2}{3}D_{CO_2}^G\left(\frac{c_{i,j-1}^G - c_{i,j}^G}{\Delta y^2}\right) \quad (2.18)$$

2.3 Making the equations dimensionless

Defining the following characteristic variables

$$\bar{c} = \frac{c}{c_0} \qquad \bar{t} = \frac{t}{\tau} \qquad \bar{x} = \frac{x}{r_0} \qquad \bar{y} = \frac{y}{r_0}$$

where

$$\tau = \frac{\Delta r_0\, r_0}{D_0} \qquad\qquad \Delta r_0 = \min\left[\Delta x, \Delta y\right]$$

According to whether biocomposite is present and applying the boundary conditions, equations 2.3, 2.4, 2.5, 2.6, 2.7, 2.8, 2.9, 2.11, 2.13, 2.14, 2.15 and 2.16 are the mass balances that will be made dimensionless using these characteristic variables. The dimensionless mass balances (equations 2.19-28) were solved to give the concentration in the vial as a function of time.

Gas only – type "G"

$$\frac{\partial \bar{c}_{i,j}^G}{\partial \bar{t}} = \frac{D_{CO_2}^G}{D_0}\frac{\Delta r_0}{r_0}\left(\frac{\bar{c}_{i+1,j}^G - 2\bar{c}_{i,j}^G + \bar{c}_{i-1,j}^G}{\overline{\Delta x}^2} + \frac{\bar{c}_{i,j+1}^G - 2\bar{c}_{i,j}^G + \bar{c}_{i,j-1}^G}{\overline{\Delta y}^2}\right) \quad (2.19)$$

Biocomposite present – type "B"

$$\frac{\partial \bar{c}_{i,j}^G}{\partial \bar{t}} = \frac{D_{CO_2}^G}{D_0}\frac{\Delta r_0}{r_0}\left(\frac{\bar{c}_{i+1,j}^G - 2\bar{c}_{i,j}^G + \bar{c}_{i-1,j}^G}{\overline{\Delta x}^2} + \frac{\bar{c}_{i,j+1}^G - 2\bar{c}_{i,j}^G + \bar{c}_{i,j-1}^G}{\overline{\Delta y}^2}\right) - \left(\frac{\Delta r_0\, r_0}{D_0}\right)a_{BC}k\bar{c}_{i,j}^G \quad (2.20)$$

Symmetry boundary (x-axis) gas only – type "GSX"

$$\frac{\partial \bar{c}_{i,j}^G}{\partial \bar{t}} = \frac{D_{CO_2}^G}{D_0} \frac{\Delta r_0}{r_0} \left(\frac{\bar{c}_{i+1,j}^G - 2\bar{c}_{i,j}^G + \bar{c}_{i-1,j}^G}{\overline{\Delta x}^2} \right) \quad (2.21)$$

Symmetry boundary (x-axis) biocomposite present – type "BSX"

$$\frac{\partial \bar{c}_{i,j}^G}{\partial \bar{t}} = \frac{D_{CO_2}^G}{D_0} \frac{\Delta r_0}{r_0} \left(\frac{\bar{c}_{i+1,j}^G - 2\bar{c}_{i,j}^G + \bar{c}_{i-1,j}^G}{\overline{\Delta x}^2} \right) - \left(\frac{\Delta r_0 \, r_0}{D_0} \right) a_{BC} k \bar{c}_{i,j}^G \quad (2.22)$$

Symmetry boundary (y-axis) gas only – type "GSY"

$$\frac{\partial \bar{c}_{i,j}^G}{\partial \bar{t}} = \frac{D_{CO_2}^G}{D_0} \frac{\Delta r_0}{r_0} \left(\frac{\bar{c}_{i,j+1}^G - 2\bar{c}_{i,j}^G + \bar{c}_{i,j-1}^G}{\overline{\Delta y}^2} \right) \quad (2.23)$$

Symmetry boundary (y-axis) biocomposite present – type "BSY"

$$\frac{\partial \bar{c}_{i,j}^G}{\partial \bar{t}} = \frac{D_{CO_2}^G}{D_0} \frac{\Delta r_0}{r_0} \left(\frac{\bar{c}_{i,j+1}^G - 2\bar{c}_{i,j}^G + \bar{c}_{i,j-1}^G}{\overline{\Delta y}^2} \right) - \left(\frac{\Delta r_0 \, r_0}{D_0} \right) a_{BC} k \bar{c}_{i,j}^G \quad (2.24)$$

Symmetry boundary centre of the vial with biocomposite present – type "CS"

$$\frac{\partial \bar{c}_{i,j}^G}{\partial \bar{t}} = - \left(\frac{\Delta r_0 \, r_0}{D_0} \right) a_{BC} k \bar{c}_{i,j}^G \quad (2.25)$$

Horizontal vial wall – type "WH"

$$\frac{\partial \bar{c}_{i,j}^G}{\partial \bar{t}} = \frac{D_{CO_2}^G}{D_0} \frac{\Delta r_0}{r_0} \left(\frac{\bar{c}_{i+1,j}^G - 2\bar{c}_{i,j}^G + \bar{c}_{i-1,j}^G}{\overline{\Delta x}^2} + \frac{2}{3} \left[\frac{\bar{c}_{i,j-1}^G - \bar{c}_{i,j}^G}{\overline{\Delta y}^2} \right] \right) \quad (2.26)$$

Vertical vial wall – type "WV"

$$\frac{\partial \bar{c}_{i,j}^G}{\partial \bar{t}} = \frac{D_{CO_2}^G}{D_0} \frac{\Delta r_0}{r_0} \left(\frac{2}{3} \left[\frac{\bar{c}_{i-1,j}^G - \bar{c}_{i,j}^G}{\overline{\Delta x}^2} \right] + \frac{\bar{c}_{i,j+1}^G - 2\bar{c}_{i,j}^G + \bar{c}_{i,j-1}^G}{\overline{\Delta y}^2} \right) \quad (2.27)$$

Corner vial wall – type "WC"

$$\frac{\partial \bar{c}_{i,j}^G}{\partial \bar{t}} = \frac{2}{3} \frac{D_{CO_2}^G}{D_0} \frac{\Delta r_0}{r_0} \left(\frac{\bar{c}_{i-1,j}^G - \bar{c}_{i,j}^G}{\overline{\Delta x}^2} + \frac{\bar{c}_{i,j-1}^G - \bar{c}_{i,j}^G}{\overline{\Delta y}^2} \right) \quad (2.28)$$

Symmetry boundary (x-axis) at the wall – type "WSX"

$$\frac{\partial \bar{c}_{i,j}^G}{\partial t} = \frac{2}{3} \frac{D_{CO_2}^G}{D_0} \frac{\Delta r_0}{r_0} \left(\frac{\bar{c}_{i-1,j}^G - \bar{c}_{i,j}^G}{\overline{\Delta x}^2} \right) \quad (2.29)$$

Symmetry boundary (y-axis) at the wall – type "WSY"

$$\frac{\partial \bar{c}_{i,j}^G}{\partial t} = \frac{2}{3} \frac{D_{CO_2}^G}{D_0} \frac{\Delta r_0}{r_0} \left(\frac{\bar{c}_{i,j-1}^G - \bar{c}_{i,j}^G}{\overline{\Delta y}^2} \right) \quad (2.30)$$

2.4 Solution
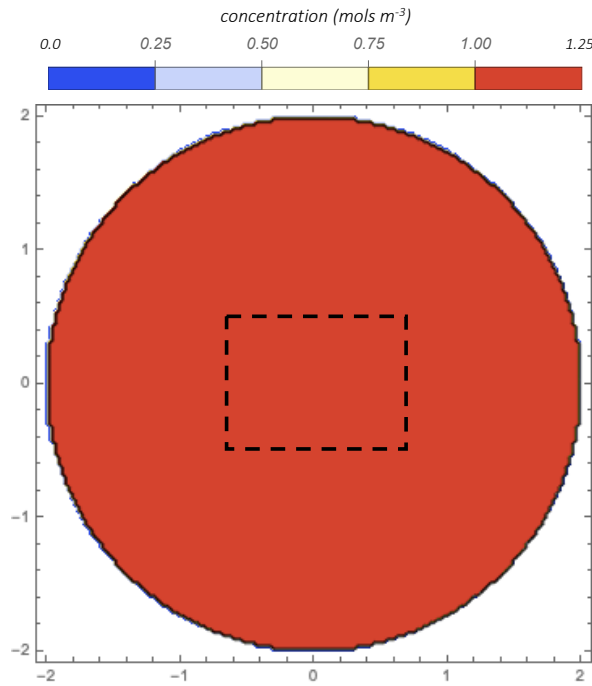
Figure S4 Contour plot of the gas phase composition after 48 hours for CCAP 1479/1A biocomposite. Initial CO_2 concentration = 2.05 mols m^{-3} (5 mol% CO_2), light:dark ratio 16:8. The transfer coefficient for the cells in the suspension controls in the vial is 5 x 10^{-9} m s^{-1}. The characteristic time for diffusion across the vial is much shorter than the characteristic time for transfer through the biocomposite. There are three options for the diffusion of CO_2 through the latex coating.

1. The coating is a porous structure that CO_2 gas diffuses through. The DVS experiments gave the value of diffusivity for this as approximately 10^{-8} m^2 s^{-1}.

2. The coating is a porous structure saturated with water. In this case the diffusivity will be approximately that for CO_2 in water (10^{-9} m^2 s^{-1}).

3. The coating is a polymer film which the CO_2 has to dissolve into the film and diffuse through it. The diffusivity for CO_2 in polymer films is of the order of 10^{-13} m^2 s^{-1}.

The mass transfer coefficient for the biocomposite is given by the following equation.

$$a_C \left(\frac{1}{K a_C} \right)_{exp} = \frac{1}{K_{exp}} = \frac{1}{k_{cell}} + \frac{1}{k_{film}}$$

In this equation k_{cell} is the mass transfer coefficient for the cell in suspended culture. Using ranges of the surface area given in Table S4 we can calculate values for k_{film}.

$$k_{film} = \frac{D_{film}}{\Delta z_{film}}$$

The change in the mass transfer coefficient indicates that the CO_2 is having to diffuse through a solid polymer film to reach the cells.

Nomenclature

a_C – specific surface area of cell interface (m^2 m^{-3})

c^G – concentration of CO_2 in the gas phase (mols m^{-3}).

c^L – concentration of CO_2 in the liquid phase (mols m^{-3}).

c_0 – characteristic concentration (mols m^{-3}).

$D_{CO_2}^G$ – diffusivity of CO_2 in the gas phase (m^2 s^{-1}).

$D_{CO_2}^L$ – diffusivity of CO_2 in the liquid phase (m^2 s^{-1}).

D_0 – characteristic diffusivity (m^2 s^{-1}).

K – transfer coefficient across the cell membrane incorporating the rate of CO_2 consumption by the cell (m s^{-1}).

K_{ov} – mass transfer coefficient for CO_2 transport across the air-water interface (m s^{-1}).

N – number of cells in the gas layer.

M – number of cells in the liquid layer.

t – time (s).

z – axial distance in the vial (m).

z_0 – characteristic height (m).

t – characteristic time ($\Delta z_0 \, z_0 / D_0$) (s).

Data

Diffusivity of CO_2 in air = 1.6 x 10^{-5} m^2 s^{-1}

Diffusivity of CO_2 in water = 1.92 x 10^{-9} m^2 s^{-1}

Henry's constant for CO_2 in water at 25°C = 2938 m^3 mol^{-1} Pa

Sample Vials

<u>Cyanobacteria:</u>

OD = 4.0 cm, height = 7.3 cm.

Height of straight section = 4.8 cm, wall thickness = 0.13 cm, base thickness = 0.28 cm.

Curved section is 1.3 cm tall and diameter goes from 4. 0 cm to 1.4 cm.

Top straight section has wall thickness of 2.2 mm and height of 8 mm.

Volume of straight section at the bottom = ¼ π $(4.0 – 2 \times 0.13)^2$ x (4.8 – 0.28) = 49.7 ml

Volume of curved section = $\frac{2}{3} \times \pi \times 0.5 \times (4.0 - 0.26) \times 1.3^2$ = 6.6 ml

Volume of straight section at the top = ¼ π $(1.4 – 2 \times 0.22)^2$ x 0.8 = 0.6 ml

Total volume = 56.9 ml

Equivalent vial with an OD of 4.0 cm, wall thickness = 0.13 cm and a height of 5.2 cm.

References

AATCC, C. 2007. pH of the water-extract from wet processed textiles. AATCC Technical Manual American Association of Textile Chemists and Colorists.

ABERNATHY, M. H., YU, J., MA, F., LIBERTON, M., UNGERER, J., HOLLINSHEAD, W. D., GOPALAKRISHNAN, S., HE, L., MARANAS, C. D., PAKRASI, H. B., ALLEN, D. K. & TANG, Y. J. 2017. Deciphering cyanobacterial phenotypes for fast photoautotrophic growth via isotopically nonstationary metabolic flux analysis. *Biotechnol. Biofuels,* 10**,** 1-13.

ACOSTA-RUBÍ, S., CAMPOCOSIO, A. T., MONTES-HORCASITAS, M. D. C., QUINTANAR-VERA, L., ESPARZA-GARCÍA, F. & RODRÍGUEZ-VÁZQUEZ, R. 2017. Production of a halotolerant biofilm from green coffee beans immobilized on loofah fiber (*Luffa cylindrica*) and its effect on phenanthrene degradation in seawater. *J. Environ. Sci. Heal. A.,* 52**,** 632-640.

ADAM II, T. A., HOSEINZADE, L., MADABHUSHI, P. B. & OKEKE, I. J. 2017. Comparison of CO_2 capture approaches for fossil-based power generation: review and meta-study. *Processes,* 5**,** 44-81.

ADAMCZYK, M., LASEK, J. & SKAWINSKA, A. 2016. CO_2 biofixation and growth kinetics of *Chlorella vulgaris* and *Nannochloropsis gaditana. Appl. Biochem. Biotechnol.,* 179**,** 1248-1261.

ADAMS, E. E. & CALDEIRA, K. 2008. Ocean storage of CO_2. *Elements,* 4**,** 319-324.

AGGREGATES, O. 2018. Orkney Aggregates Price List.

AGUILAR-MAY, B., DEL PILAR SÁNCHEZ-SAAVEDRA, M., LIZARDI, J. & VOLTOLINA, D. 2007. Growth of *Synechococcus sp.* immobilized in chitosan with different times of contact with NaOH. *J. Appl. Phycol.,* 19**,** 181-183.

AIKAWA, S., NISHIDA, A., HO, S. H., CHANG, J. S., HASUNUMA, T. & KONDON, A. 2014. Glycogen production for biofuels by the euryhaline cyanobacteria *Synechococcus* sp. strain PCC 7002 from an oceanic environment. *Biotechnol. Biofuels,* 7**,** 88-96.

AKHTAR, N., IQBAL, J. & IQBAL, M. 2003a. Microalgal-luffa sponge immobilized disc: a new efficient biosorbent for the removal of Ni(II) from aqueous solution. *Lett. Appl. Microbiol.,* 37**,** 149-153.

AKHTAR, N., IQBAL, J. & IQBAL, M. 2004a. Enhancement of Lead(II) Biosorption by Microalgal Biomass Immobilized onto Loofa (*Luffa cylindrica*) Sponge. *Eng. Life Sci.,* 4**,** 171-178.

AKHTAR, N., IQBAL, J. & IQBAL, M. 2004b. Removal and recovery of nickel(II) from aqueous solution by loofa sponge-immobilized biomass of *Chlorella sorokiniana*: Characterization studies. *J. Hazard,* 108**,** 85-94.

AKHTAR, N., IQBAL, M., ZAFAR, S. I. & IQBAL, J. 2008. Biosorption characteristics of unicellular green alga *Chlorella sorokiniana* immobilized in loofa sponge for removal of Cr(III). *J. Environ. Sci.,* 20**,** 231-239.

AKHTAR, N., SAEED, A. & IQBAL, M. 2003b. *Chlorella sorokiniana* immobilized on the biomatrix of vegetable sponge of *Luffa cylindrica*: A new system to remove cadmium from contaminated aqueous medium. *Bioresour. Technol.,* 88**,** 163-165.

ALIBABA.COM. 2020a. *Factory price 2mm bamboo wood sheet for surfboard manufacturer* [Online]. Available: https://www.alibaba.com/product-detail/Factory-price-2mm-bamboo-wood-sheet_60819882383.html?spm=a2700.7724857.normalList.105.1fcd6d52YgbdyL [Accessed 30/09/2020].

ALIBABA.COM. 2020b. *Organic loofah spa exfoliating scrubber natural luffa body wash sponge* [Online]. Available: https://www.alibaba.com/product-detail/Organic-Loofahs-Loofah-Spa-Exfoliating-

Scrubber_62349262044.html?spm=a2700.7724857.normalList.87.39e062920qD0fC [Accessed].

ALIBABA.COM. 2020c. *Polytunnel garden, tunnel, greenhouse* [Online]. Available: https://thai.alibaba.com/product-detail/garden-polytunnel-tunnel-greenhouse-368571104.html [Accessed 30/09/2020].

ALKARAWI, M. A. S., CALDWELL, G. S. & LEE, J. G. M. 2018. Continuous harvesting of microalgae biomass using foam flotation. *Algal Res.,* 36, 125-138.

AMENORFENYO, D. K., HUANG, X., ZHANG, Y., ZENG, Q., ZHANG, N., REN, J. & HUANG, Q. 2019. Microalgae brewery wastewater treatment: potentials, benefits and the challenges. *Int. J. Environ. Res. Public Health,* 16.

AMIENYO, D. & AZAPAGIC, A. 2016. Life cycle environmental impacts and costs of beer production and consumption in the UK. *Int. J. Life Cycle Assess.,* 21, 492-509.

ANDERSON, C. D. & DANIELS, E. S. 2003. Emulsion polymerisation and latex applications.

ANNESINI, M. C., MARRELLI, L., PIEMONTE, V. & TURCHETTI, L. 2017. Mass transfer coefficient. *Artificial Organ Engineering.* 23-31.

ANTONACCI, A. & SCOGNAMIGLIO, V. 2020. Biotechnological advances in the design of algae-based biosensors. *Trends Biotechnol.,* 38, 334-347.

ARASHIRO, L. T., BOTO-ORDONEZ, M., VAN HULLE, S. W. H., FERRER, I., GARFI, M. & ROUSSEAU, D. P. L. 2020. Natural pigments from microalgae grown in industrial wastewater. *Bioresour. Technol.,* 303, 122894-122905.

ASPLUND, J. & WARDLE, A. D. 2016. How lichens impact on terrestrial community and ecosystem properties. *Biol. Rev. Camb. Philos. Soc.,* 92, 1720-1738.

BAENA-MORENO, F. M., RODRÍGUEZ-GALÁN, M., VEGA, F., ALONSO-FARIÑAS, B., VILCHES ARENAS, L. F. & NAVARRETE, B. 2018. Carbon capture and utilization technologies: a literature review and recent advances. *Energ. Source Part A.,* 41, 1403-1433.

BARKA, A. & BLECKER, C. 2016. Microalgae as a potential source of single-cell proteins. A review. *Biotechnol. Agron. Soc. Environ.,* 20, 427-436.

BASHAN, Y. 1986. Alginate beads as synthetic inoculant carriers for slow release of bacteria that affect plant growth. *Appl. Environ. Microbiol. ,* 51, 1089-1098.

BEAL, C. M., ARCHIBALD, I., HUNTLEY, M. E., GREENE, C. H. & JOHNSON, Z. I. 2018. Integrating algae with bioenergy carbon capture and storage (ABECCS) increases sustainability. *Earth's Future,* 6, 524-542.

BEARDALL, J. & RAVEN, J. A. 2017. Cyanobacteria vs green algae: which group has the edge? *J. Exp. Bot.,* 68, 3697-3699.

BECKER, E. W. 2007. Microalgae as a source of protein. *Biotechnol. Adv.,* 25, 207-210.

BEER, S., VILENKIN, B., WEIL, A., VESTE, M., SUSEL, L. & ESHEL, A. 1998. Measuring photosynthetic rates in seagrasses by pulse amplitude modulated (PAM) fluorometry. *Mar. Ecol. Prog. Ser.,* 174, 293 - 300.

BELLERA, C. A., JULIEN, M. & HANLEY, J. A. 2017. Normal approximations to the distributions of the Wilcoxon statistics: accurate to what *N*? Graphical insights. *J. Stat. Educ.,* 18, 1-17.

BERGER, R. G. 2009. Biotechnology of flavours—the next generation. *Biotechnol. Lett.,* 31, 1651–1659.

BERNAL, O. I., BHARTI, B., FLICKINGER, M. C. & VELEV, O. D. 2017. Fabrication of photoreactive biocomposite coatings via electric field-assisted assembly of cyanobacteria. *Langmuir,* 33, 5304-5313.

BERNAL, O. I., MOONEY, C. B. & FLICKINGER, M. C. 2014. Specific photosynthetic rate enhancement by cyanobacteria coated onto paper enables engineering of highly reactive cellular biocomposite "leaves". *Biotechnol. Bioeng.,* 111, 1993-2008.

BERNER, F., HEIMANN, K. & SHEEHAN, M. 2014. Microalgal biofilms for biomass production. *J. Appl. Phycol.,* 27, 1793-1804.

BESSELING, E., WANG, B., LURLING, M. & KOELMANS, A. A. 2014. Nanoplastic affects growth of *S. obliquus* and reproduction of *D. magna*. *Environ. Sci. Technol.*, 48, 12336-12343.

BHATTACHARYA, P., LIN, S., TURNER, J. P. & KE, P. C. 2010. Physical adsorption of chared plastic nanoparticles affects algal photosynthesis. *J. Phys. Chem.*, 114, 16556-16561.

BIER 2012. Research on the carbon footprint of beer. Beverage Industry Environmental Roundtable.

BILORIA, N. & THAKKAR, Y. 2020. Integrating algae building technology in the built environment: A cost and benefit perspective. *Front. Archit. Res.*, 9, 370-384.

BLEAKLEY, S. & HAYES, M. 2017. Algal proteins: extraction, application, and challenges concerning production. *Foods*, 6, 1-34.

BOROWITZKA, M. A. 1999. Commercial production of microalgae: ponds, tanks, tubes and fermenters. *J. Biotechnol.*, 70, 313-321.

BOTTOMS, R. R. 1930. *Process for separating acidic gases*.

BRANYIKOVA, I., MARSALKOVA, B., DOUCHA, J., BRANYIK, T., BISOVA, K., ZACHLEDER, V. & VITOVA, M. 2011. Microalgae-novel highly efficient starch producers. *Biotechnol. Bioeng.*, 108, 766-776.

BRENNER, K., YOU, L. & ARNOLD, F. H. 2008. Engineering microbial consortia: A new frontier in synthetic biology. *Trends Biotechnol.*, 26, 483-489.

BRUNETTI, A., SCURA, F., BARBIERI, G. & DRIOLI, E. 2010. Membrane technologies for CO_2 separation. *J. Membr. Sci.*, 359, 115-125.

BUNGARTZ, F., ROSENTRETER, R. & NASH III, T. H. 2002. Field guide to common epiphytic macrolichens in Arizona.

BUNNING, T. J., LAWTON, C. W., KLEI, H. E. & SUNDSTROM, D. W. 1991. Physical property improvements of a pellicular biocatalyst. *Bioprocess Eng.*, 7, 71-75.

CABRAL, R. P., BUI, M. & MAC DOWELL, N. 2019. A synergistic approach for the simultaneous decarbonisation of power and industry via bioenergy with carbon capture and storage (BECCS). *Int. J. Greenh. Gas Control.*, 87, 221-237.

CARBALLEIRA, J. D., QUEZADA, M. A., HOYOS, P., SIMEÓ, Y., HERNAIZ, M. J., ALCANTARA, A. R. & SINISTERRA, J. V. 2009. Microbial cells as catalysts for stereoselective redox reactions. *Biotechnol. Adv.*, 27, 686-714.

CAREY, T., JONES, C., LE MOAL, F., DEGANELLO, D. & TORRISI, F. 2018. Spray-coating thin films on three-dimensional surfaces for a semitransparent capacitive-touch device. *ACS Appl. Mater. Interfaces*, 10, 19948-19956.

CARVALHO, P. A., MEIRELES, A. L. & MATCATA, X. F. 2006. Microalgal reactors: a review of enclosed system designs and performances. *Biotechnol. Prog.*, 22, 1490-1506.

CASES, I. & DE LORENZO, V. 2005. Genetically modified organisms for the environment: Stories of success and failure and what we have learned from them. *Int. J. Microbiol.*, 8, 213-222.

CASSIDY, M. B., LEE, H. & TREVORS, J. T. 1996. Environmental applications of immobilized microbial cells: a review. *J. Ind. Microbiol.*, 16, 79-101.

CHAFFEE, A. L., KNOWLES, G. P., LIANG, Z., ZHANG, J., XIAO, P. & WEBLEY, P. A. 2007. CO_2 capture by adsorption: Materials and process development. *Int. J. Greenh. Gas Control.*, 1, 11-18.

CHAGAS, A. L., RIOS, A. O., JARENKOW, A., MARCÍLIO, N. R., AYUB, M. A. Z. & RECH, R. 2015. Production of carotenoids and lipids by *Dunaliella tertiolecta* using CO_2 from beer fermentation. *Process Biochem.*, 50, 981-988.

CHAIWONG, C., KOOTTATEP, T. & POLPRASERT, C. 2020. Comparative study on attached-growth photobioreactors under blue and red lights for treatment of septic tank effluent. *J. Environ. Manage.*, 260, 110134-110144.

CHAUDRY, S., BAHRI, P. A. & MOHEIMANI, N. R. 2017. Potential of milking of microalgae grown on biofilm photobioreactor for renewable hydrocarbon production. *Comput. Aided Chem. Eng.*, 40**,** 2497-2502.

CHEAH, W. Y., SHOW, P. L., CHANG, J. S., LING, T. C. & JUAN, J. C. 2015. Biosequestration of atmospheric CO_2 and flue gas-containing CO_2 by microalgae. *Bioresour. Technol.*, 184**,** 190-201.

CHEN, B. Y., CHEN, C. Y., GUO, W. Q., CHANG, H. W., CHEN, W. M., LEE, D. J., HUANG, C. C., REN, N. Q. & CHANG, J. S. 2014. Fixed-bed biosorption of cadmium using immobilized Scenedesmus obliquus CNW-N cells on loofa (*Luffa cylindrica*) sponge. *Bioresour. Technol.*, 160**,** 175-181.

CHEN, P. C. & LIN, S.-Z. 2018. Optimization in the absorption and desorption of CO_2 using sodium glycinate solution. *Applied Sciences,* 8**,** 2041-2061.

CHEN, Y., KRINGS, S., BOOTH, J. R., BON, S. A. F., HINGLEY-WILSON, S. & KEDDIE, J. L. 2020. Introducing porosity in colloidal biocoatings to increase bacterial viability. *Biomacromolecules***,** 4545–4558.

CHEN, Y., SU, N., ZHANG, K., ZHU, S., ZHU, Z., QIN, W., YANG, Y., SHI, Y., FAN, S., WANG, Z. & GUO, Y. 2018. Effect of fiber surface treatment on structure, moisture absorption and mechanical properties of luffa sponge fiber bundles. *Ind. Crop. Prod.*, 123**,** 341-352.

CHENG, J., HUANG, Y., FENG, J., SUN, J., ZHOU, J. & CEN, K. 2013. Improving CO_2 fixation efficiency by optimizing *Chlorella* PY-ZU1 culture conditions in sequential bioreactors. *Bioresour. Technol.*, 144**,** 321-327.

CHEVALIER, P. & NOUE, J. D. L. 1985. Wastewater nutrient removal with microalgae immobilized in carrageenan. *Enzyme Microb. Technol.*, 7**,** 621-624.

CHIU, S. Y., KAO, C. Y., CHEN, C. H., KUAN, T. C., ONG, S. C. & LIN, C. S. 2008. Reduction of CO_2 by a high-density culture of *Chlorella* sp. in a semicontinuous photobioreactor. *Bioresour. Technol.*, 99**,** 3389-3396.

CHIU, S. Y., KAO, C. Y., TSAI, M. T., ONG, S. C., CHEN, C. H. & LIN, C. S. 2009a. Lipid accumulation and CO_2 utilization of *Nannochloropsis oculata* in response to CO_2 aeration. *Bioresour. Technol.*, 100**,** 833-838.

CHIU, S. Y., TSAI, M. T., KAO, C. Y., ONG, S. C. & LIN, C. S. 2009b. The air-lift photobioreactors with flow patterning for high-density cultures of microalgae and carbon dioxide removal. *Eng. Life Sci.*, 9**,** 254-260.

CHOI, H.-J. 2016. Parametric study of brewery wastewater effluent treatment using *Chlorella vulgaris* microalgae. *Environ. Eng. Res.*, 21**,** 401-408.

CHOI, S. Y., PARK, B., CHOI, I. G., SIM, S. J., LEE, S. M., UM, Y. & WOO, H. M. 2016. Transcriptome landscape of *Synechococcus elongatus* PCC 7942 for nitrogen starvation responses using RNA-seq. *Sci. Rep.*, 6**,** 30584-30594.

CHOI, Y. Y., PATEL, A. K., HONG, M. E., CHANG, W. S. & SIM, S. J. 2019. Microalgae bioenergy with carbon capture and storage (BECCS): An emerging sustainable bioprocess for reduced CO_2 emission and biofuel production. *Bioresour. Technol. Rep. ,* 7**,** 100270-100284.

CHRISTENSON, L. & SIMS, R. 2011. Production and harvesting of microalgae for wastewater treatment, biofuels, and bioproducts. *Biotechnol. Adv.*, 29**,** 686-702.

CHRISTENSON, L. B. & SIMS, R. C. 2012. Rotating algal biofilm reactor and spool harvester for wastewater treatment with biofuels by-products. *Biotechnol. Bioeng.*, 109**,** 1674-1684.

CIMINI, A. & MORESI, M. 2016. Carbon footprint of a pale lager packed in different formats: Assessment and sensitivity analysis based on transparent data. *J. Clean. Prod.*, 112**,** 4196-4213.

CLÉMENT-LAROSIÈRE, B., LOPES, F., GONÇALVES, A., TAIDI, B., BENEDETTI, M., MINIER, M. & PAREAU, D. 2014. Carbon dioxide biofixation by *Chlorella vulgaris* at different CO_2 concentrations and light intensities. *Eng. Life Sci.,* 14**,** 509-519.

CLIPPINGER, J. & DAVIS, R. 2019. Techno-economic analysis for the production of algal biomass via closed photobioreactors: future cost potential evaluated across a range of cultivation system designs. NREL.

COHAN, Y. 2001. Biofiltration - the treatment of fluids by microorganisms immobilized into the filter bedding material: a review. *Bioresour. Technol.,* 77**,** 257-274.

COLE, A. J., MATA, L., PAUL, N. A. & DE NYS, R. 2014. Using CO_2 to enhance carbon capture and biomass applications of freshwater macroalgae. *GCB BioEnergy,* 6**,** 637-645.

COLLINS, M. & KNUTTI, R. 2014. Long-term climate change: projections, commitments and irreversibility. IPCC.

CORSI, R. L. & LIN, C.-C. 2009. Emissions of 2,2,4-Trimethyl-1,3-Pentanediol Monoisobutyrate (TMPD-MIB) from latex paint: A critical review. *Crit. Rev. Env. Sci. Tec.,* 39**,** 1052-1080.

CORTEZ, S., NICOLAU, A., FLICKINGER, M. C. & MOTA, M. 2017. Biocoatings: A new challenge for environmental biotechnology. *Biochem. Eng. J.,* 121**,** 25-37.

CRASTER, B. & JONES, T. G. J. 2019. Permeation of a range of species through polymer layers under varying conditions of temperature and pressure: In Situ measurement methods. *Polymers,* 11**,** 1056-1077.

CUÉLLAR-FRANCA, R. M. & AZAPAGIC, A. 2015. Carbon capture, storage and utilisation technologies: A critical analysis and comparison of their life cycle environmental impacts. *J. CO_2 Util.,* 9**,** 82-102.

CUSHMAN, J. R., RAUSINA, G. A., CRUZAN, G., GILBERT, J., WILLIAMS, E., HARRASS, M. C., SOUSA, J. V., PUTT, A. E., GARVEY, N. A., LAURENT, J. P. S., HOBERG, J. R. & MACHADO, M. W. 1997. Ecotoxicity hazard assessment of styrene. *Ecotoxicol. Environ. Saf. ,* 37**,** 173-180.

DE GODOS, I., MENDOZA, J. L., ACIEN, F. G., MOLINA, E., BANKS, C. J., HEAVEN, S. & ROGALLA, F. 2014. Evaluation of carbon dioxide mass transfer in raceway reactors for microalgae culture using flue gases. *Bioresour. Technol.,* 153**,** 307-14.

DE-BASHAN, L. E. & BASHAN, Y. 2010. Immobilized microalgae for removing pollutants: Review of practical aspects. *Bioresour. Technol.,* 101**,** 1611-1627.

DEMAIN, A. L. 2009. Biosolutions to the energy problem. *J. Ind. Microbiol. Biotechnol.,* 36**,** 319-332.

DENG, X., LI, Y. & FEI, X. 2009. Microalgae: A promising feedstock for biodiesel. *Afr. J. Microbiol. Res.,* 3**,** 1008-1014.

DEPRAETERE, O., DESCHOENMAEKER, F., BADRI, H., MONSIEURS, P., FOUBERT, I., LEYS, N., WATTIEZ, R. & MUYLAERT, K. 2015. Trade-off between growth and carbohydrate accumulation in nutrient-limited *Arthrospira* sp. PCC 8005 studied by integrating transcriptomic and proteomic approaches. *PLoS One,* 10**,** 1-19.

DICKIE, R. A. 1994. Paint adhesion, corrosion protection and interfacial chemistry. *Prog. Org. Coat.,* 25**,** 3-22.

DOE, U. 1985. Review and evaluation of immobilized algae systems for the production of fuels from microalgae. Solar Energy Research Institute.

DOUSKOVA, I., DOUCHA, J., LIVANSKY, K., MACHAT, J., NOVAK, P., UMYSOVA, D., ZACHLEDER, V. & VITOVA, M. 2009. Simultaneous flue gas bioremediation and reduction of microalgal biomass production costs. *Appl. Microbiol. Biot.,* 82**,** 179-185.

DRAGONE, G., FERNANDES, B. D., ABREU, A. P., VICENTE, A. A. & TEIXEIRA, J. A. 2011. Nutrient limitation as a strategy for increasing starch accumulation in microalgae. *Applied Energy,* 88**,** 3331-3335.

DUQUE SCHUMACHER, A. G., PEQUITO, S. & PAZOUR, J. 2020. Industrial hemp fiber: A sustainable and economical alternative to cotton. *J. Clean. Prod.,* 268.

DURALL, C. & LINDBLAD, P. 2015. Mechanisms of carbon fixation and engineering for increased carbon fixation in cyanobacteria. *Algal Res.,* 11, 263-270.

DUTCHER, B., FAN, M. & RUSSELL, A. G. 2015. Amine-based CO_2 capture technology development from the beginning of 2013-a review. *ACS Appl. Mater. Interfaces,* 7, 2137-2148.

E. BAJAMUNDI, C. J., KOPONEN, J., RUUSKANEN, V., ELFVING, J., KOSONEN, A., KAUPPINEN, J. & AHOLA, J. 2019. Capturing CO_2 from air: Technical performance and process control improvement. *J. CO2 Util.,* 30, 232-239.

EBNESAJJAD, S. 2016. Introduction to plastics. *Chemical Resistance of Commodity Thermoplastics.* xiii-xxv.

ECKARDT, N. A., SNYDER, G. W., PORTIS, A. R. & OGREN, W. L. 1997. Growth and photosynthesis under high and low irradiance of *Arabidopsis thaliana* antisense mutants with reduced ribulose-1, 5-bisphosphate carboxylase/oxygenase activase content. *Plant Physiol.,* 113, 575-586.

EKINS-COWARD, T., BOODHOO, K. V. K., VELASQUEZ-ORTA, S., CALDWELL, G., WALLACE, A., BARTON, R. & FLICKINGER, M. C. 2019. A microalgae biocomposite-integrated spinning disk bioreactor (SDBR): Toward a scalable engineering approach for bioprocess intensification in light-driven CO_2 absorption applications. *Ind. Eng. Chem. Res.,* 58, 5936-5949.

EL-HOSHOUDY, A. N. M. B. 2018. Emulsion polymerization mechanism. *Recent research in polymerization.* 3-14.

ELIZALDE, L. E., MENDOZA, J. J., LEDEZMA-RODRÍGUEZ, R., TREVIÑO, M. E. & MONDRAGON, M. 2020. Synthesis of butyl acrylate–styrene–TMI latexes and their application as water-based coatings. *J. Coat. Technol. Res.,* 17, 911-919.

ELLIS, A. L., MILLS, T. B., NORTON, I. T. & NORTON-WELCH, A. B. 2019. The hydrophobic modification of kappa carrageenan microgel particles for the stabilisation of foams. *J. Colloid Interface Sci. ,* 538, 165-173.

END, N. & SCHÖNING, K.-U. 2004. Immobilized biocatalysts in industrial research and production. *In:* KIRSCHNING, A. (ed.) *Immobilized Catalysts: Solid Phases, Immobilization and Applications.* Berlin, Heidelberg: Springer Berlin Heidelberg. 273-317.

ENERGAIA. 2019. *About Energaia* [Online]. Available: https://www.dugongconservation.org/media/2019/03/Day1_5.Incentives_EnerGaia.pdf [Accessed].

ERIKSEN, N. T., POULSEN, B. R. & IVERSEN, J. J. L. 1998. Dual sparging laboratory-scale photobioreactor for continuous production of microalgae. *J. Appl. Phycol.,* 10, 377-382.

EROGLU, E., SMITH, S. M. & RASTON, C. L. 2015. Application of various immobilization techniques for algal bioprocesses. *In:* MOHEIMANI, N., MCHENRY, M., DE BOER, K. & BAHRI, P. (eds.) *Biomass and Biofuels from Microalgae. Biofuel and Biorefinery Technologies.* Cham: Springer. 19-44.

ESTEVE-TURRILLAS, F. A. & DE LA GUARDIA, M. 2017. Environmental impact of recover cotton in textile industry. *Resour. Conserv. Recy.,* 116, 107-115.

EZZIAT, L., ELABED, A., IBNSOUDA, S. & EL ABED, S. 2019. Challenges of microbial fuel cell architecture on heavy metal recovery and removal from wastewater. *Front. Energy,* 7, 1-13.

FAAFENG, B. A., DONK, V. E. & KALLQVIST, S. T. 1994. In situ measurement of algal growth potential in aquatic ecosystems by immobilized algae. *J. Appl. Phycol.,* 6, 301-308.

FAJARDY, M., KOBERLE, A., DOWELL, N. M. & FANTUZZI, A. 2019. BECCS deploment: a reality check. Imperial College London: Grantham Institute.

FAN, L.-H., ZHANG, Y.-T., ZHANG, L. & CHEN, H.-L. 2008. Evaluation of a membrane-sparged helical tubular photobioreactor for carbon dioxide biofixation by *Chlorella vulgaris*. *J. Membr. Sci.* , 325**,** 336-345.

FARAJZADEH R., ZITHA P. L. J. & J., B. 2009. Enhanced mass transfer of CO_2 into Water: Experiment and Modeling. *Ind. Eng. Chem. Res.*, 48**,** 6423-6431.

FENG, L.-J., LI, J.-W., XU, E. G., SUN, X.-D., ZHU, F.-P., DING, Z., TIAN, H., DONG, S.-S., XIA, P.-F. & YUAN, X.-Z. 2019. Short-term exposure to positively charged polystyrene nanoparticles causes oxidative stress and membrane destruction in cyanobacteria. *Environ. Sci. Nano,* 6**,** 3072-3079.

FERNANDES, B. D., MOTA, A., FERREIRA, A., DRAGONE, G., TEIXEIRA, J. A. & VICENTE, A. A. 2014. Characterization of split cylinder airlift photobioreactors for efficient microalgae cultivation. *Chem. Eng. Sci.,* 117**,** 445-454.

FERREIRA, A., RIBEIRO, B., MARQUES, P. A. S. S., FERREIRA, A. F., DIAS, A. P., PINHEIRO, H. M., REIS, A. & GOUVEIA, L. 2017. *Scenedesmus obliquus* mediated brewery wastewater remediation and CO_2 biofixation for green energy purposes. *J. Clean. Prod.,* 165**,** 1316-1327.

FIDALEO, M., CHARANIYA, S., SOLHEID, C., DIEL, U., LAUDON, M., GE, H., SCRIVEN, L. E. & FLICKINGER, M. C. 2006. A model system for increasing the intensity of whole-cell biocatalysis: investigation of the rate of oxidation of D-sorbitol to L-sorbose by thin bi-layer latex coatings of non-growing *Gluconobacter oxydans*. *Biotechnol. Bioeng.,* 95**,** 446-458.

FINNE, M. 2001. CO_2 measurements in breweries and wineries. *Vaisala news*.

FISCHEDICK M., J. ROY, A. ABDEL-AZIZ, A. ACQUAYE, J.M. ALLWOOD, J.-P. CERON, Y. GENG, H. KHESHGI, A. LANZA, D. PERCZYK, L. PRICE, E. SANTALLA, C. SHEINBAUM & TANAKA, K. 2014. Industry. In: Climate Change 2014: mitigation of climate change. Contribution of working group III to the fifth assessment report of the Intergovernmental Panel on Climate Change. *In:* O. EDENHOFER, R. PICHS-MADRUGA, Y. SOKONA, E. FARAHANI, S. KADNER, K. SEYBOTH, A. ADLER, I. BAUM, S. BRUNNER, P. EICKEMEIER, B. KRIEMANN, J. SAVOLAINEN, S. SCHLÖMER, C. VON STECHOW, ZWICKEL, T. & MINX, J. C. (eds.). Cambridge, United Kingdom,

New York, NY, USA: IPCC.

FLICKINGER, M. C., BERNAL, O. I., SCHULTE, M. J., BROGLIE, J. J., DURAN, C. J., WALLACE, A., MOONEY, C. B. & VELEV, O. D. 2017. Biocoatings: challenges to expanding the functionality of waterborne latex coatings by incorporating concentrated living microorganisms. *J. Coat. Technol. Res.,* 14**,** 791-808.

FLICKINGER, M. C., FIDALEO, M., GOSSE, J., POLZIN, K., CHARANIYA, S., SOLHEID, C., LYNGBERG, O. K., LAUDON, M., GE, H. & SCHOTTEL, J. L. 2009. Engineering nanoporous bioactive smart coatings containing microorganisms: fundamentals and emerging applications. *ACS Symp. Ser.*,**** 52-94.

FLICKINGER, M. C., SCHOTTEL, J. L., BOND, D. R., AKSAN, A. & SCRIVEN, L. E. 2007. Painting and printing living bacteria: Engineering nanoporous biocatalytic coatings to preserve microbial viability and intensify reactivity. *Biotechnol. Prog.,* 23**,** 2-17.

FRANCISCO, J. A., STATHOPOULOS, C., WARREN, R. A. J., KILBURN, D. G. & GEORGIOU, G. 1993. Specific adhesion and hydrolysis of cellulose by intact *Escherichia coli* expressing surface anchored cellulase or cellulose binding domains. *Nat. Biotechnol.,* 11**,** 491-495.

FU, J., HUANG, Y., LIAO, Q., XIA, A., FU, Q. & ZHU, X. 2019. Photo-bioreactor design for microalgae: A review from the aspect of CO_2 transfer and conversion. *Bioresour. Technol.,* 292**,** 121947-121959.

FUSS, S., LAMB, F. W., CALLAGHAN, W. M., HILAIRE, J., CREUTZIG, F., AMANN, T., BERINGER, T., OLIVEIRA GARCIA, D. W., HARTMANN, J., KHANNA, T.,

LUDERER, G., NEMET, G. F., ROGELJ, J., SMITH, P., VICENTE VICENTE, L. J., WILCOX, J., DOMINGUEZ, Z. M. D. M. & MINX, C. J. 2018. Negative emissions—part 2: costs, potentials and side effects. *Environ. Res. Lett.,* 13, 1-47.

GABRIELLI, P., GAZZANI, M. & MAZZOTTI, M. 2020. The role of carbon capture and utilization, carbon capture and storage, and biomass to enable a net-zero-CO_2 emissions chemical industry. *Ind. Eng. Chem. Res.,* 59, 7033-7045.

GAIGHER, I. G., TOERIEN, D. F. & GROBBELAAE, J. U. 1985. Preliminary studies on the treatment of Sorghum beer brewery effluent in an integrated baterial/algal/fish/macrophyte culture system. *Agric. Wastes,* 12, 207-224.

GALVITA, V. V., POELMAN, H., BLIZNUK, V., DETAVERNIER, C. & MARIN, G. B. 2013. CeO_2-modified Fe_2O_3 for CO_2 utilization via chemical looping. *Ind. Eng. Chem. Res.,* 52, 8416-8426.

GAMBHIR, A. & TAVONI, M. 2019. Direct air carbon capture and sequestration: How it works and how it could contribute to climate change mitigation. *One Earth,* 1, 405-409.

GAO, F., YANG, Z. H., LI, C., ZENG, G. M., MA, D. H. & ZHOU, L. 2015. A novel algal biofilm membrane photobioreactor for attached microalgae growth and nutrients removal from secondary effluent. *Bioresour. Technol.,* 179, 8-12.

GAO, T., SELINGER, J. L. & ROCHELLE, G. T. 2019. Demonstration of 99% CO_2 removal from coal flue gas by amine scrubbing. *Int. J. Greenh. Gas Control.,* 83, 236-244.

GARCIA-OCHOA, F. & GOMEZ, E. 2009. Bioreactor scale-up and oxygen transfer rate in microbial processes: an overview. *Biotechnol. Adv.,* 27, 153-176.

GMBH, H. W. 2019. Imaging-PAM M-series chlorophyll fluorometer: Instruction description and information for users. Germany.

GONZÁLEZ DEL CAMPO, A., CAÑIZARES, P., RODRIGO, M. A., FERNÁNDEZ, F. J. & LOBATO, J. 2013. Microbial fuel cell with an algae-assisted cathode: A preliminary assessment. *J. Power Sources,* 242, 638-645.

GOSSE, J., L., ENGEL BRIAN, J., HUI JEREMY, C. H., HARWOOD CAROLINE, S. & FLICKINGER MICHAEL, C. 2010. Progress toward a biomimetic leaf: 4,000 h of hydrogen production by coating-stabilized nongrowing photosynthetic *Rhodopseudomonas palustris. Biotechnol. Prog.,* 26, 907-918.

GOSSE, J. L., ENGEL, B. J., REY, F. E., HARWOOD, C. S., SCRIVEN, L. E. & FLICKINGER, M. C. 2007. Hydrogen production by photoreactive nanoporous latex coatings of nongrowing *Rhodopseudomonas palustris* CGA009. *Biotechnol. Prog.,* 23, 124-130.

GOU, Y., YANG, J., FANG, F., GUO, J. & MA, H. 2020. Feasibility of using a novel algal-bacterial biofilm reactor for efficient domestic wastewater treatment. *Environ. Technol.,* 41, 400-410.

GRANCARIC A.M., TARBUK, A. & PUSIC, T. 2005. Electrokinetic properties of textile fabrics. *Color. Technol.,* 121, 221-227.

GROSS, M., HENRY, W., MICHAEL, C. & WEN, Z. 2013. Development of a rotating algal biofilm growth system for attached microalgae growth with in situ biomass harvest. *Bioresour. Technol.,* 150, 195-201.

GROSS, M., JARBOE, D. & WEN, Z. 2015. Biofilm-based algal cultivation systems. *Appl. Microbiol. Biotechnol.,* 99, 5781-5789.

GROSS, M. & WEN, Z. 2014. Yearlong evaluation of performance and durability of a pilot-scale Revolving Algal Biofilm (RAB) cultivation system. *Bioresour Technol,* 171, 50-8.

GUIMARAES, C., MATOS, C., AZEREDO, J., MOTA, M. & OLIVERIA, R. 2002. The importance of the morphology and hydrophobicity of different carriers on the immobilization and sugar refinery effluent degradation activity of *Phanerochaete chrysosporium. Biotechnol. Lett.,* 24, 795-800.

HAMANO, H., NAKAMURA, S., HAYAKAWA, J., MIYASHITA, H. & HARAYAMA, S. 2017. Biofilm-based photobioreactor absorbing water and nutrients by capillary action. *Bioresour. Technol.,* 223**,** 307-311.

HAMEED A.S.M. & O., E. H. 2007. Review biotechnological potential uses of immobilized algae. *Int. J. Agric. Biol.,* 9**,** 183-192.

HANAGATA, N., TAKEUCHI, T., FUKUJU, Y., BARNES, D. J. & KARUBE, I. 1992. Tolerance of microalgae to high CO_2 and high temperature. *Phytochemistry,* 31**,** 3345-3348.

HANN, M. A. & THOMAS, B. G. 2005. *Patterns of culture - decorative weaving techniques*, University of Leeds International Textiles Archive (ULITA).

HANSI, L., XIONGWEN, Z. & XUNMIN, O. 2017. Life cycle analysis of distributed energy system projects' energy consumption and GHG emission – A case of beer brewery auxiliary power supply in China. *Energy Procedia,* 105**,** 3456-3463.

HARKINS, W. D. 1947. A general theory of the mechanism of emulsion polymerization. *J. Am. Chem. Soc.,* 69**,** 1428-1444.

HARPER, A. B., POWELL, T., COX, P. M., HOUSE, J., HUNTINGFORD, C., LENTON, T. M., SITCH, S., BURKE, E., CHADBURN, S. E., COLLINS, W. J., COMYN-PLATT, E., DAIOGLOU, V., DOELMAN, J. C., HAYMAN, G., ROBERTSON, E., VAN VUUREN, D., WILTSHIRE, A., WEBBER, C. P., BASTOS, A., BOYSEN, L., CIAIS, P., DEVARAJU, N., JAIN, A. K., KRAUSE, A., POULTER, B. & SHU, S. 2018. Land-use emissions play a critical role in land-based mitigation for Paris climate targets. *Nat. Commun.,* 9**,** 2938-2951.

HART, A. & GNANENDRAN, N. 2009. Cryogenic CO_2 capture in natural gas. *Energy Procedia,* 1**,** 697-706.

HASHEMI, A., PAJOUM SHARIATI, F., SOHANI, E., AZIZI, S., HOSSEINIFAR, S. Z. & DELAVARI AMREI, H. 2020. CO_2 biofixation by *Synechococcus elongatus* from the power plant flue gas under various light–dark cycles. *Clean Technol. Environ. Policy,* 22**,** 1735-1743.

HASZELDINE, R. S. 2009. Carbon capture and storage: how green can black be? *Science,* 325**,** 1647-1652.

HAZEEM, L. J., YESILAY, G., BOUOUDINA, M., PERNA, S., CETIN, D., SULUDERE, Z., BARRAS, A. & BOUKHERROUB, R. 2020. Investigation of the toxic effects of different polystyrene micro-and nanoplastics on microalgae *Chlorella vulgaris* by analysis of cell viability, pigment content, oxidative stress and ultrastructural changes. *Mar. Pollut. Bull.,* 156**,** 111278-111288.

HENRIKSON, R. 2013. *Algae microfarms for home, school, community and urband gardens, rooftop, mobile, and vertical farms and living buildings*, Ronore Enterprises, Inc.

HENRIQUES, M., SILVA, A. & J., R. 2007. Extraction and quantification of pigments from a marine microalga: a simple and reproducible method. *Commun. Current Res. Edu. Topics Trends Appl. Microbiol.,* 586-593.

HETTI, R. K., KARUNATHILAKE, H., CHHIPI-SHRESTHA, G., SADIQ, R. & HEWAGE, K. 2020. Prospects of integrating carbon capturing into community scale energy systems. *Renew. Sustain. Energy Rev.,* 133**,** 110193-110210.

HO, S.-H., CHEN, C.-Y., LEE, D.-J. & CHANG, J.-S. 2011. Perspectives on microalgal CO_2-emission mitigation systems — A review. *Biotechnol. Adv.,* 29**,** 189-198.

HO, S. H., CHEN, C. Y. & CHANG, J. S. 2012. Effect of light intensity and nitrogen starvation on CO_2 fixation and lipid/carbohydrate production of an indigenous microalga *Scenedesmus obliquus* CNW-N. *Bioresour. Technol.,* 113**,** 244-252.

HOLMES, S. A. & RYAN, M. J. 1982. *Cryogenic distillative separation of acid gases from methane*.

HONEGGER, R. 2009. Lichen-forming fungi and their photobionts. *The Mycota.* 307-333.

HOUSE, K. Z., BACLIG, A. C., RANJAN, M., VAN NIEROP, E. A., WILCOX, J. & HERZOG, H. J. 2011. Economic and energetic analysis of capturing CO_2 from ambient air. *Proc. Natl. Acad. Sci. USA,* 108, 20428-20433.

HU, Q., GUTERMAN, H. & RICHMOND, A. 1996. A flat inclined modular photobioreactor for outdoor mass cultivation of photoautotrophs. *Biotechnol. Bioeng.,* 51, 51-60.

HUANG, Q., JIANG, F., WANG, L. & YANG, C. 2017. Design of photobioreactors for mass cultivation of photosynthetic organisms. *Engineering,* 3, 318-329.

IN-NA, P., UMAR, A. A., WALLACE, A. D., FLICKINGER, M. C., CALDWELL, G. S. & LEE, J. G. M. 2020. Loofah-based microalgae and cyanobacteria biocomposites for intensifying carbon dioxide capture. *J. CO_2 Util.,* 42, 101348-101362.

INFOTECH., T. 2020. *Spirulina powder organic 1 kg* [Online]. Available: http://organicloverthailand.com/super-food/402-spirulina-powder-100-gram.html [Accessed 8/26/2020].

INVESTMENT, T. B. O. 2019. Cost of doing business in Thailand 2019. Thailand board of investment.

IQBAL, M. & EDYVEAN, R. G. J. 2005. Loofa sponge immobilized fungal biosorbent: A robust system for cadmium and other dissolved metal removal from aqueous solution. *Chemosphere,* 61, 510-518.

IQBAL, M. & ZAFAR, S. I. 1993a. Bioactivity of immobilized microalgal cells: application potential of vegetable sponge in microbial biotechnology. *Lett. Appl. Microbiol.,* 17, 289-291.

IQBAL, M. & ZAFAR, S. I. 1993b. The use of fibrous network of matured dried fruit of *Luffa aegyptica* as immobilizing agent. *Biotechnol. Tech.,* 7, 15-18.

IRLAM, L. 2017. Global costs of carbon capture and storage. Global CCS Institute.

ISSA, A. A., ABD-ALLA, H. M. & OHYAMA, T. 2014. Nitrogen fixing cyanobacteria: Future prospect. *Advances in Biology and Ecology of Nitrogen Fixation.*

JAKUBOVICS, N. S., SHIELDS, R. C., RAJARAJAN, N. & BURGESS, J. G. 2013. Life after death: the critical role of extracellular DNA in microbial biofilms. *Lett. Appl. Microbiol.,* 57, 467-475.

JASSIM, M. S., ROCHELLE, G. T., EIMER, D. & RAMSHAW, C. 2007. Carbon dioxide absorption and desorption in aqueous monoethanolamine solutions in a rotating packed bed. *Ind. Eng. Chem. Res.,* 46, 2823-2833.

JENKINS, J. S. 2013. *Engineering multifunctional living paints: Thin, convectively-assembled biocomposite coatings of live cells and colloidal latex particles deposited by continuous convective-sedimentation assembly.* PhD PhD, North Carolina State University.

JENKINS, J. S., FLICKINGER, M. C. & VELEV, O. D. 2012. Deposition of composite coatings from particle-particle and particle-yeast blends by convective-sedimentation assembly. *J. Colloid Interface Sci.,* 380, 192-200.

JENKINS, J. S., FLICKINGER, M. C. & VELEV, O. D. 2013. Engineering cellular photocomposite materials using convective assembly. *Materials (Basel),* 6, 1803-1825.

JI, G. & ZHAO, M. 2017. Membrane separation technology in carbon capture. *Recent advances in carbon capture and storage.*

JIANG, L., GONZALEZ-DIAZ, A., LING-CHIN, J., ROSKILLY, A. P. & SMALLBONE, A. J. 2019. Post-combustion CO_2 capture from a natural gas combined cycle power plant using activated carbon adsorption. *Appl. Energy,* 245, 1-15.

JIANG, Y., ZHANG, W., WANG, J., CHEN, Y., SHEN, S. & LIU, T. 2013. Utilization of simulated flue gas for cultivation of *Scenedesmus dimorphus*. *Bioresour. Technol.,* 128, 359-364.

JIMÉNEZ, C., COSSÍO, B. R., LABELLA, D. & NIELL, F. X. 2003. The feasibility of industrial production of Spirulina (*Arthrospira*) in Southern Spain. *Aquaculture,* 217, 179-190.

JOHNSON, M. P. 2016. Photosynthesis. *Essays Biochem.,* 60, 255-273.

JORQUERA, O., KIPERSTOK, A., SALES, E. A., EMBIRUCU, M. & GHIRARDI, M. L. 2010. Comparative energy life-cycle analyses of microalgal biomass production in open ponds and photobioreactors. *Bioresour. Technol.,* 101, 1406-1413.

KAJIWARA, S., TAMADA, H., OHKUNI, N. & OHTAGUCHI, K. 1997. Design of the bioreactor for carbon dioxide fixation by *Synechococcus* PCC 7942. *Energy Convers. Mgmt.,* 38, S529-S532.

KALAJI, H. M., SCHANSKER, G., BRESTIC, M., BUSSOTTI, F., CALATAYUD, A., FERRONI, L., GOLTSEV, V., GUIDI, L., JAJOO, A., LI, P., LOSCIALE, P., MISHRA, V. K., MISRA, A. N., NEBAUER, S. G., PANCALDI, S., PENELLA, C., POLLASTRINI, M., SURESH, K., TAMBUSSI, E., YANNICCARI, M., ZIVCAK, M., CETNER, M. D., SAMBORSKA, I. A., STIRBET, A., OLSOVSKA, K., KUNDERLIKOVA, K., SHELONZEK, H., RUSINOWSKI, S. & BABA, W. 2017. Frequently asked questions about chlorophyll fluorescence, the sequel. *Photosynth. Res.,* 132, 13-66.

KAMENNAYA, N., AJO-FRANKLIN, C., NORTHEN, T. & JANSSON, C. 2012. Cyanobacteria as biocatalysts for carbonate mineralization. *Minerals,* 2, 338-364.

KEFFER, J. E. & KLEINHEINZ, G. T. 2002. Use of *Chlorella vulgaris* for CO_2 mitigation in a photobioreactor. *J. Ind. Microbiol. Biotechnol.,* 29, 275-280.

KEMPER, J. 2015. Biomass and carbon dioxide capture and storage: A review. *Int. J. Greenh. Gas Control.,* 40, 401-430.

KESAANO, M. & SIMS, R. C. 2014. Algal biofilm based technology for wastewater treatment. *Algal Res.,* 5, 231-240.

KESHAVARZ, A., SARVESTANI, E. M. & RAHIMPOUR, R. M. 2019. Cryogenic CO_2 Capture. *Sustainable Agriculture Reviews.* Switzerland AG: Springer Nature.

KHANRA, S., MONDAL, M., HALDER, G., TIWARI, O. N., GAYEN, K. & BHOWMICK, T. K. 2018. Downstream processing of microalgae for pigments, protein and carbohydrate in industrial application: A review. *Food Bioprod. Process.,* 110, 60-84.

KIRTMAN, B., STOCKER, T. F., QIN, D., TIGNOR, M., ALLEN, S. K. & BOSCHUNG, J. 2018. Long-term climate change: Projections, commitments and irreversibility. *Climate Change 2013: The Physical Science Basis. Contribution of Working Group I to the Fifth Assessment Report of the Intergovernmental Panel on Climate Change.* Cambridge, UK; New Yor, USA.

KLINTHONG, W. 2015. A review: Microalgae and their applications in CO_2 capture and renewable energy. *Aerosol Air Qual. Res.,* 712–742.

KLOK, A. J., LAMERS, P. P., MARTENS, D. E., DRAAISMA, R. B. & WIJFFELS, R. H. 2014. Edible oils from microalgae: insights in TAG accumulation. *Trends Biotechnol.,* 32, 521-528.

KOSHY, O., SUBRAMANIAN, L. & THOMAS, S. 2017. Differential scanning calorimetry in nanoscience and nanotechnology. *Thermal and rheological measurement techniques for nanomaterials characterization.* Elsevier. 109-122.

KOSKY, P., BALMER, R., KEAT, W. & WISE, G. 2013. Chapter 20 - Design Step 3. Evaluation of Alternatives and Selection of a Concept. *In:* KOSKY, P., BALMER, R., KEAT, W. & WISE, G. (eds.) *Exploring engineering.* Third ed. Boston: Academic Press. 383-396.

KUMAR, K., DASGUPTA, C. N., NAYAK, B., LINDBLAD, P. & DAS, D. 2011. Development of suitable photobioreactors for CO_2 sequestration addressing global warming using green algae and cyanobacteria. *Bioresour. Technol.,* 102, 4945-4953.

KUMAR, P. 2011. Capture of CO_2 emissions using algae. Oilgae.

KUMORO, A. C., PRASETYANINGRUM, A., JOS, B., DHARMAWAN, Y., OCTAVIANI, R. V., RATNAWATI, R., HADIYANTO, ROCES, S. A., YUNG, L., RONG, X., LOTHONGKUM, A. W., PHONG, M. T., HUSSAIN, M. A., DAUD, W. R. W. &

NAM, P. T. S. 2018. Chemical and spectral characterization of the ozonation products of ϰ-carrageenan. *MATEC Web Conf.*, 156, 1-4.

KUPRIYANOVA, E. V., SINETOVA, M. A., CHO, S. M., PARK, Y. I., LOS, D. A. & PRONINA, N. A. 2013. CO_2-concentrating mechanism in cyanobacterial photosynthesis: Organization, physiological role, and evolutionary origin. *Photosynth. Res.*, 117, 133-146.

KUSMAYADI, A., LEONG, Y. K., YEN, H. W., HUANG, C. Y., DONG, C. D. & CHANG, J. S. 2020. Microalgae-microbial fuel cell (mMFC): an integrated process for electricity generation, wastewater treatment, CO_2 sequestration and biomass production. *Int. J. Energy Res.*, 44, 9254-9265.

KUU, W. Y. & POLACK, J. A. 1983. Improving immobilized biocatalysts by gel phase polymerization. *Biotechnol. Bioeng.*, 25, 1995-2006.

LACKNER, K., ZIOCK, H. & GRIMES, P. 1999. Carbon dioxide extraction from air: Is it an option? . Los Alamos National Laboratory.

LACKNER, K. S. 2009. Capture of carbon dioxide from ambient air. *Eur. Phys. J. Spec. Top.*, 176, 93-106.

LAM, M. K., LEE, K. T. & MOHAMED, A. R. 2012. Current status and challenges on microalgae-based carbon capture. *Int. J. Greenh. Gas Control.*, 10, 456-469.

LAMBERT, S., SINCLAIR, C. J., BRADLEY, E. L. & BOXALL, A. B. 2013a. Effects of environmental conditions on latex degradation in aquatic systems. *Sci. Total Environ.*, 447, 225-234.

LAMBERT, S., SINCLAIR, C. J., BRADLEY, E. L. & BOXALL, A. B. 2013b. Environmental fate of processed natural rubber latex. *Environ. Sci. Process Impacts*, 15, 1359-1368.

LAU, P. S., TAM, N. F. Y. & WONG, Y. S. 1997. Wastewater nutrients (N and P) removal by carrageenan and alginate immobilized *Chlorella vulgaris*. *Environ. Technol.*, 18, 945-951.

LEE, D. B., APEL, A. W. & WALTON, R. M. 2004. Screening of cyanobacterial species for calcification. *Biotechnol. Prog.*, 20, 1345-1351.

LEE, J., KOLAWOLE, T. & ATTIDEKOU, P. 2017. Carbon capture from a simulated flue gas using a rotating packed bed adsorber and mono ethanol amine (MEA). *Energy Procedia*, 114, 1834-1840.

LEEHAM, C. & ALLEN, M. 2013. *Human-induced warming* [Online]. Environmental Change Institute. Available: https://globalwarmingindex.org/ [Accessed 09/10/2020 2020].

LEUNG, D. Y. C., CARAMANNA, G. & MAROTO-VALER, M. M. 2014. An overview of current status of carbon dioxide capture and storage technologies. *Renew. Sustain. Energy Rev.*, 39, 426-443.

LI, S., LUO, S. & GUO, R. 2013. Efficiency of CO_2 fixation by microalgae in a closed raceway pond. *Bioresour. Technol.*, 136, 267-272.

LI, W., CHOI, S., DRESE, J. H., HORNBOSTEL, M., KRISHNAN, G., EISENBERGER, P. M. & JONES, C. W. 2010. Steam-stripping for regeneration of supported amine-based CO_2 adsorbents. *ChemSusChem*, 3, 899-903.

LIANG, F., LINDBERG, P. & LINDBLAD, P. 2018. Engineering photoautotrophic carbon fixation for enhanced growth and productivity. *Sustain. Energ. Fuels*, 2, 2583-2600.

LIGRONE, R. 2019. The great oxygenation event. *Biological innovations that built the world*. Springer, Cham. 129-154.

LIN, C. C. & CORSI, R. L. 2007. Texanol® ester alcohol emissions from latex paints: Temporal variations and multi-component recoveries. *Atmos. Environ.*, 41, 3225-3234.

LIU, Y. 2015. *Water transport and sorption in primary and secondary emulsion polymer films*. University of Surrey.

LODE, A., KRUJATZ, F., BRÜGGEMEIER, S., QUADE, M., SCHÜTZ, K., KNAACK, S., WEBER, J., BLEY, T. & GELINSKY, M. 2015. Green bioprinting: Fabrication of

photosynthetic algae-laden hydrogel scaffolds for biotechnological and medical applications. *Eng Life Sci,* 15**,** 177-183.

LORENZ, T. R. & CYSEWSKI, R. G. 2000. Commercial potential for *Haematococcus* microalgae as a natural source of astaxanthin. *Trends Biotechnol.,* 18**,** 160-167.

LTD., H. F. T. C. 2020. *Spirulina organic - health food store Thailand* [Online]. Available: https://healthfoodthailand.com/en/new-items/273-spirulina-organic-100-grams-powder.html [Accessed 8/26/2020].

LU, W., ASRAFUL ALAM, M., LIU, S., XU, J. & SALDIVAR, P. R. 2020. Critical processes and variables in microalgae biomass production coupled with bioremediation of nutrients and CO_2 from livestock farms: A review. *Sci. Total Environ.,* 716**,** 1-16.

LUDERER, G., VRONTISI, Z., BERTRAM, C., EDELENBOSCH, O. Y., PIETZCKER, R. C., ROGELJ, J., DE BOER, H. S., DROUET, L., EMMERLING, J., FRICKO, O., FUJIMORI, S., HAVLÍK, P., IYER, G., KERAMIDAS, K., KITOUS, A., PEHL, M., KREY, V., RIAHI, K., SAVEYN, B., TAVONI, M., VAN VUUREN, D. P. & KRIEGLER, E. 2018. Residual fossil CO_2 emissions in 1.5–2 °C pathways. *Nat. Clim. Change,* 8**,** 626-633.

LUIS, P., VAN GERVEN, T. & VAN DER BRUGGEN, B. 2012. Recent developments in membrane-based technologies for CO_2 capture. *Prog. Energy Combust. Sci.,* 38**,** 419-448.

LUXBACHER, T., PUSIC, T., BUKSEK, H. & PETRINIC, I. The zeta potential of textile fabrics: A review. 8th International textile, clothing & design conference - Magic world of textiles, October 2-5 2016 Dubrovnik, Croatia. 1-6.

LYNGBERG, O. K., NG, C. P., THIAGARAJAN, V., SCRIVEN, L. E. & FLICKINGER, M. C. 2001. Engineering the microstructure and permeability of thin multilayer latex biocatalytic coatings containing *E.coli. Biotechnol. Prog.,* 17**,** 1169-1179.

LYNGBERG, O. K., STEMKE, D. J., SCHOTTEL, J. L. & FLICKINGER, M. C. 1999a. A single-use luciferase-based mercury biosensor using *Escherichia coli* HB101 immobilized in a latex copolymer film. *J. Ind. Microbiol. Biotechnol.,* 23**,** 668-676.

LYNGBERG, O. K., THIAGARAJAN, V., STEMKE, D. J., SCHOTTEL, J. L., SCRIVEN, L. E. & FLICKINGER, M. C. 1999b. A patch coating method for preparing biocatalytic films of *Escherichia coli. Biotechnol. Bioeng.,* 62**,** 44-55.

MACCREADY, J. S. & VECCHIARELLI, A. G. 2018. In long bacterial cells, the min system can act off-center. *Mol. Microbiol.,* 109**,** 268-272.

MADAN, G. L., DAVE, A. M., DAS, T. K. & SARMA, T. S. 1978. Hydrophilicity of textile fibers. *Text. Res. J.,* 48**,** 662-663.

MAGDELDIN, S. & MOSER, A. 2012. *Affinity chromatography: principles and applications,* Croatia, InTech.

MAKEWEBEASY.COM. 2020. *Spirulina Powder 1kg - Organicthailand* [Online]. Available: https://www.organicthailand.com/en/product/19102/spirulina-powder-1kg [Accessed].

MALLICK, N. 2002. Biotechnological potential of immobilized algae for wastewater N, P and metal removal: A review. *Biometals,* 15**,** 377-390.

MALLICK, N. & MOHN, F. H. 2000. Reactive oxygen species: Response of algal cells. *J. Plant Physiol.,* 157**,** 183-193.

MALLICK, N. & RAI, L. C. 1992. Removal and assessment of toxicity of Cu and Fe to *Anabaena doliolum* and *Chloreila vulgaris* using free and immobilized cells. *World J. Microbiol. Biotechnol.,* 8**,** 110-114.

MANGAN, N. & BRENNER, M. 2014. Systems analysis of the CO_2 concentrating mechanism in cyanobacteria. *Elife***,** e02043.

MANTZOROU, A. & VERVERIDIS, F. 2019. Microalgal biofilms: A further step over current microalgal cultivation techniques. *Sci. Total Environ.,* 651**,** 3187-3201.

MARCHÃO, L., DA SILVA, T. L., GOUVEIA, L. & REIS, A. 2017. Microalgae-mediated brewery wastewater treatment: effect of dilution rate on nutrient removal rates, biomass biochemical composition, and cell physiology. *J. Appl. Phycol.*, 30, 1583-1595.

MARKEWITZ, P., KUCKSHINRICHS, W., LEITNER, W., LINSSEN, J., ZAPP, P., BONGARTZ, R., SCHREIBER, A. & MÜLLER, T. E. 2012. Worldwide innovations in the development of carbon capture technologies and the utilization of CO_2. *Energy Environ. Sci.*, 5, 7281-7305.

MARKOU, G., ANGELIDAKI, I. & GEORGAKAKIS, D. 2012. Microalgal carbohydrates: an overview of the factors influencing carbohydrates production, and of main bioconversion technologies for production of biofuels. *Appl. Microbiol. Biotechnol.*, 96, 631-645.

MARRION, A. & GUY, A. 2004. The science and art of paint formulation. *The chemistry and physics of coatings*. 317-346.

MARSHALL, D. J., LAWTON, R. J., MONRO, K. & PAUL, N. A. 2018. Biochemical evolution in response to intensive harvesting in algae: Evolution of quality and quantity. *Evol. Appl.*, 11, 1389-1400.

MARTENS, N. & HALL, E. A. H. 1994. Immobilisation of photosynthetic cells based on film-forming emulsion polymers. *Anal. Chim. Acta*, 292, 49-63.

MARTÍN-GIRELA, I., CURT, M. D. & FERNÁNDEZ, J. 2017. Flashing light effects on CO_2 absorption by microalgae grown on a biofilm photobioreactor. *Algal Res.*, 25, 421-430.

MARTINS, A. A., MARQUES, F., CAMERIA, M., SANTOS, E., BADENES, S., COSTA, L., VIEIRA, V. V., CAETANO, S. N. & MATA, M. T. 2018. Water footprint of microalgae cultivation in photobioreactor. *Energy Procedia*, 153, 426-431.

MARTINS, S. C. S., MARTINS, C. M., FIUZA, L. M. C. G. & SANTAELLA, S. T. 2013. Immobilization of microbial cells: A promising tool for treatment of toxic pollutants in industrial wastewater. *Afr. J. Biotechnol.*, 12, 4412-4418.

MASMOUDI, F., BESSADOK, A., DAMMAK, M., JAZIRI, M. & AMMAR, E. 2016. Biodegradable packaging materials conception based on starch and polylactic acid (PLA) reinforced with cellulose. *Environ. Sci. Pollut. Res.*, 23, 20904-20914.

MAZARI, S. A., GHALIB, L., SATTAR, A., BOZDAR, M. M., QAYOOM, A., AHMED, I., MUHAMMAD, A., ABRO, R., ABDULKAREEM, A., NIZAMUDDIN, S., BALOCH, H. & MUBARAK, N. M. 2020. Review of modelling and simulation strategies for evaluating corrosive behavior of aqueous amine systems for CO_2 capture. *Int. J. Greenh. Gas Control.*, 96, 103010-103021.

MCGOWAN, T., SHEAHAN, D., CUNHA, I., OLIVERIA, H. & SANTOS, M. 2013. ARCOPOLplus. European Union.

MEDRANO, H., ESCALONA, J. M., BOTA, J., GULIAS, J. & FLEXAS, J. 2002. Regulation of photosynthesis of C3 plants in response to progressive drought: stomatal conductance as a reference parameter. *Ann. Bot.*, 89, 895-905.

MEEHL, A. G. & STOCKER, F. T. 2007. Chapter 10 Global climate projections. IPCC.

MELIS, A. 2009. Solar energy conversion efficiencies in photosynthesis: Minimizing the chlorophyll antennae to maximize efficiency. *Plant Sci. J.*, 177, 272-280.

MENDIARA, T., GARCÍA-LABIANO, F., ABAD, A., GAYÁN, P., DE DIEGO, L. F., IZQUIERDO, M. T. & ADÁNEZ, J. 2018. Negative CO_2 emissions through the use of biofuels in chemical looping technology: A review. *Appl. Energy*, 232, 657-684.

MICHELET, L., ZAFFAGNINI, M., MORISSE, S., SPARLA, F., PEREZ-PEREZ, M. E., FRANCIA, F., DANON, A., MARCHAND, C. H., FERMANI, S., TROST, P. & LEMAIRE, S. D. 2013. Redox regulation of the Calvin-Benson cycle: something old, something new. *Front. Plant Sci.*, 4, 470-491.

MÍGUEZ, J. L., PORTEIRO, J., PÉREZ-OROZCO, R., PATIÑO, D. & GÓMEZ, M. Á. 2020. Biological systems for CCS: Patent review as a criterion for technological development. *Appl. Energy*, 257, 114032-114040.

MIN, M., HU, B., MOHR, M. J., SHI, A., DING, J., SUN, Y., JIANG, Y., FU, Z., GRIFFITH, R., HUSSAIN, F., MU, D., NIE, Y., CHEN, P., ZHOU, W. & RUAN, R. 2014. Swine manure-based pilot-scale algal biomass production system for fuel production and wastewater treatment--a case study. *Appl. Biochem. Biotechnol.,* 172, 1390-406.

MINX, J. C., LAMB, W. F., CALLAGHAN, M. W., FUSS, S., HILAIRE, J., CREUTZIG, F., AMANN, T., BERINGER, T., DE OLIVEIRA GARCIA, W., HARTMANN, J., KHANNA, T., LENZI, D., LUDERER, G., NEMET, G. F., ROGELJ, J., SMITH, P., VICENTE VICENTE, J. L., WILCOX, J. & DEL MAR ZAMORA DOMINGUEZ, M. 2018. Negative emissions—Part 1: Research landscape and synthesis. *Environ. Res. Lett.,* 13, 1-29.

MIYAIRI, S. 1995. CO_2 assimilation in a thermophilic cyanobacterium. *Energy Convers. Manag.,* 36, 763-766.

MOHEIMANI, N. R., BOROWITZKA, M. A., ISDEPSKY, A. & SING, S. F. 2013. Standard methods for measuring growth of algae and their composition. *In:* BOROWITZKA, M. & MOHEIMANI, N. (eds.) *Algae for biofuels and energy.* Dordrecht: Springer. 265-284.

MÖLLERS, K. B., CANNELLA, D., JORGENSEN, H. & FRIGAARD, N. U. 2014. Cyanobacterial biomass as carbohydrate and nutrient feedstock for bioethanol production by yeast fermentation. *Biotechnol. Biofuels,* 7, 64-75.

MONDAL, M., KHANRA, S., TIWARI, O. N., GAYEN, K. & HALDER, G. N. 2016. Role of carbonic anhydrase on the way to biological carbon capture through microalgae—A mini review. *Environ. Prog. Sustain.,* 35, 1605-1615.

MOORE, K. A., ALTUS, S., TAY, J. W., MEEHL, J. B., JOHNSON, E. B., BORTZ, D. M. & CAMERON, J. C. 2020. Mechanical regulation of photosynthesis in cyanobacteria. *Nat. Microbiol.,* 5, 757-767.

MORALES-GARCIA, A. L., BAILEY, R. G., JANA, S. & BURGESS, J. G. 2019. The role of polymers in cross-kingdom bioadhesion. *Philos. Trans. R Soc. Lond. B Biol. Sci.,* 374, 20190192-20190201.

MORAN, S. 2016. Pump sizing: briding the gap between theory and practice. *American Institute of Chemical Engineers (AlChE).*

MOREIRA, D. & PIRES, J. C. M. 2016. Atmospheric CO_2 capture by algae: Negative carbon dioxide emission path. *Bioresour. Technol.,* 215, 371-379.

MORENO-GARRIDO, I. 2008. Microalgae immobilization: Current techniques and uses. *Bioresour. Technol.,* 99, 3949-3964.

MØRETRØ, T. & LANGSRUD, S. 2004. Listeria monocytogenes: Biofilm formation and persistence in food-processing environments. *Biofilms,* 1, 107-121.

MORONTA-BARRIOS, F., ESPINOSA, J. & CONTRERAS, A. 2013. Negative control of cell size in the cyanobacterium *Synechococcus elongatus* PCC 7942 by the essential response regulator RpaB. *FEBS Lett.,* 587, 504-509.

MORSE, J. W. & MACKENZIE, F. T. 1990. The CO_2-carbonic acid system and solution chemistry. *Geochemistry of sedimentary cearbonates.* 1-38.

MURPHY, C. F. & ALLEN, D. T. 2011. Energy-water nexus for mass cultivation of algae. *Environ. Sci. Technol.,* 45, 5861-5868.

MURTHY, G. S. 2011. Overview and assessment of algal biofuels production technologies. *Biofuels.* 415-437.

NADERI, G., TADE, M. O. & ZNAD, H. 2015. Modified photobioreactor for biofixation of carbon dioxide by *Chlorella vulgaris* at different light intensities. *Chem. Eng. Technol.,* 38, 1371-1379.

NAGAR, E., ZILBERMAN, S., SENDERSKY, E., SIMKOVSKY, R., SHIMONI, E., GERSHTEIN, D., HERZBERG, M., GOLDEN, S. S. & SCHWARZ, R. 2017. Type 4 pili are dispensable for biofilm development in the cyanobacterium *Synechococcus elongatus. Environ. Microbiol.,* 19, 2862-2872.

NANDY, A., LOHA, C., GU, S., SARKAR, P., KARMAKAR, M. K. & CHATTERJEE, P. K. 2016. Present status and overview of chemical looping combustion technology. *Renew. Sustain. Energy Rev.,* 59, 597-619.

NOBLE, R. R. P., STALKER, L., WAKELIN, S. A., PEJCIC, B., LEYBOURNE, M. I., HORTLE, A. L. & MICHAEL, K. 2012. Biological monitoring for carbon capture and storage - A review and potential future developments. *Int. J. Greenh. Gas Con.,* 10, 520-535.

NOGUEIRA JUNIOR, E., KUMAR, M., PANKRATZ, S., OYEDUN, A. O. & KUMAR, A. 2018. Development of life cycle water footprints for the production of fuels and chemicals from algae biomass. *Water Res.,* 140, 311-322.

NOMANBHAY, S. M. & HUSSAIN, R. 2015. Immobilization of *Escherichia coli* mutant strain for efficient production of bioethanol from crude glycerol. *J. Appl. Sci.,* 15, 415-430.

NOTLEY, S. M., PETTERSSON, B. & WÅGBERG, L. 2004. Direct measurement of attractive van der Waals' forces between regenerated cellulose surfaces in an aqueous environment. *J. Am. Chem. Soc.,* 126, 13930-13931.

NOVOVESKÁ, L., ROSS, M. E., STANLEY, M. S., PRADELLES, R., WASIOLEK, V. & SASSI, J. F. 2019. Microalgal carotenoids: A review of production, current markets, regulations, and future direction. *Mar. Drugs,* 17, 640-661.

OGBONNA, J. C., LIU, Y. C., LIU, Y. K. & TANAKA, H. 1994. Loofa (*Luffa cylindrica*) sponge as a carrier for microbial cell immobilization. *J. Ferment. Bioeng.,* 78, 437-442.

OLAIZOLA, M. 2003a. Commercial development of microalgal biotechnology: From the test tube to the marketplace. *Biomol. Eng.,* 20, 459-466.

OLAIZOLA, M. 2003b. Microalgal removal of CO_2 from flue gases: Changes in medium pH and flue gas composition do not appear to affect the photochemical yield of microalgal cultures. *Biotechnol. Bioproc. E.,* 8, 360-367.

ONO, E. & CUELLO, J. L. 2007. Carbon dioxide mitigation using thermophilic cyanobacteria. *Biosyst. Eng.,* 96, 129-134.

ORGANICSEEDSTHAILAND.COM. 2020. *Organic Spirulina powder – Organic Seeds Thailand* [Online]. Available: https://www.organicseedsthailand.com/en/product/organic-spirulina-powder/ [Accessed 8/26/2020].

OZKAN, A., KINNEY, K., KATZ, L. & BERBEROGLU, H. 2012. Reduction of water and energy requirement of algae cultivation using an algae biofilm photobioreactor. *Bioresour. Technol.,* 114, 542-548.

PANDIT, S. & DAS, D. 2015. Role of microalgae in microbial fuel cell. *In:* DAS, D. (ed.) *Algal biorefinery: An integrated approach.* Springer.

PAPADOPOULOS, K. P., ECONOMOU, C. N., TEKERLEKOPOULOU, A. G. & VAYENAS, D. V. 2020. Two-step treatment of brewery wastewater using electrocoagulation and cyanobacteria-based cultivation. *J. Environ. Manage.,* 265, 110543-110550.

PARK, J. P., CHOI, M. J., KIM, S. H., LEE, S. H. & LEE, H. 2014. Preparation of sticky *Escherichia coli* through surface display of an adhesive catecholamine moiety. *Appl. Environ. Microbiol.,* 80, 43-53.

PARMAR, A., SINGH, N. K., PANDEY, A., GNANSOUNOU, E. & MADAMWAR, D. 2011. Cyanobacteria and microalgae: A positive prospect for biofuels. *Bioresour. Technol.,* 102, 10163-10172.

PARNASA, R., NAGAR, E., SENDERSKY, E., REICH, Z., SIMKOVSKY, R., GOLDEN, S. & SCHWARZ, R. 2016. Small secreted proteins enable biofilm development in the cyanobacterium *Synechococcus elongatus. Sci. Rep.,* 6, 32209-32219.

PASCU, A., STOICA, L., DINCA, C. & BEDEA, A. 2015. The package type influence on the performance of CO_2 capture process by chemical absorption. *U.P.B. Sci. Bull.*, 78, 201-213.

PERCIVAL, S., CHALMERS, R., EMBREY, M., HUNTER, P., SELLWOOD, J. & WYN-JONES, P. 2004. Cyanobacteria. *Microbiology of waterborne diseases*. Academic Press. 61-70.

PHILIPPIS, D. R., SILI, C. & VINCENZINI, M. 1992. Glycogen and poly-β-hydroxybutyrate synthesis in *Spirulina maxima*. *J. Gen. Microbiol.*, 138, 1623-1628.

PIRES, J. C. M., MARTINS, F. G., ALVIM-FERRAZ, M. C. M. & SIMÕES, M. 2011. Recent developments on carbon capture and storage: An overview. *Chem. Eng. Res. Des.*, 89, 1446-1460.

PISKORSKA, M., SOULE, T., GOSSE, J. L., MILLIKEN, C., FLICKINGER, M. C., SMITH, G. W. & YEAGER, C. M. 2013. Preservation of H_2 production activity in nanoporous latex coatings of *Rhodopseudomonas palustris* CGA009 during dry storage at ambient temperatures. *Microb. Biotechnol.*, 6, 515-525.

PLUZ, O., GERBSCH, N. & BUCHHOLZ, R. 1995. Light energy supply in plate-type and light diffusing optical fiber bioreactors. *J. Appl. Phycol.*, 7, 145-149.

POURJAMSHIDIAN, R., ABOLGHASEMI, H., ESMAILI, M., AMREI, H. D., PARSA, M. & REZAEI, S. 2019. Carbon dioxide biofixation by *Chlorella* sp. in a bubble column reactor at different flow rates and CO_2 concentrations. *Braz. J. Chem. Eng.*, 36, 639-645.

PRASAD, R., SHABNAM, N. & PARDHA-SARADHI, P. 2016a. Immobilization on cotton cloth pieces is ideal for storage and conservation of microalgae. *Algal Res.*, 20, 172-179.

PRASAD, R., SHABNAM, N. & PARDHA-SARADHI, P. 2016b. Immobilization on cotton cloth pieces is ideal for storage and conservation of microalgae. *Algal Research,* 20, 172-179.

PRICE, G. D. & BADGER, M. R. 1989. Isolation and characterization of high CO_2-requiring-mutants of the cyanobacterium *Synechococcus* PCC7942 : Two phenotypes that accumulate inorganic carbon but are apparently unable to generate CO_2 within the Carboxysome. *Plant Physiol.*, 91, 514-525.

PRICE, G. D., BADGER, M. R., WOODGER, F. J. & LONG, B. M. 2008. Advances in understanding the cyanobacterial CO_2-concentrating-mechanism (CCM): functional components, Ci transporters, diversity, genetic regulation and prospects for engineering into plants. *J. Exp. Bot.*, 59, 1441-1461.

PRICE, G. D., SULTEMEYER, D., KLUGHAMMER, B., LUDWIG, M. & BADGER, M. R. 1998. The functioning of the CO_2 concentrating mechanism in several cyanobacterial strains: a review of general physiological characteristics, genes, proteins, and recent advances. *Can. J. Bot.*, 76, 973-1002.

PRITCHARD, C., YANG, A., HOLMES, P. & WILKINSON, M. 2015. Thermodynamics, economics and systems thinking: What role for air capture of CO_2? *Process Saf. Environ. Prot.*, 94, 188-195.

PURWASASMITA, M., NABU, E. B. P., KHOIRUDDIN, K. & WENTEN, I. G. 2015. Non dispersive chemical deacidification of crude palm oil in hollow fiber membrane contactor. *J. Eng. Technol. Sci.*, 47, 426-446.

RAJENDRAN, A. & HU, B. 2016. Mycoalgae biofilm: Development of a novel platform technology using algae and fungal cultures. *Biotechnol. Biofuels*, 9, 112-125.

RAMANAN, R., KANNAN, K., DESHKAR, A., YADAV, R. & CHAKRABARTI, T. 2010. Enhanced algal CO_2 sequestration through calcite deposition by *Chlorella* sp. and *Spirulina platensis* in a mini-raceway pond. *Bioresour. Technol.*, 101, 2616-2622.

RAMKRISHNAN, U., BRUNO, B. & SWAMINATHAN, S. 2014. Sequestration of CO_2 by halotolerant algae. *J. Environ. Health Sci. Eng.*, 12, 81-88.

RAO, N. N., LÜTZ, S., WÜRGES, K. & MINÖR, D. 2009. Continuous biocatalytic processes. *Org. Process Res. Dev.,* 13, 607-616.

RAZA, A., GHOLAMI, R., REZAEE, R., RASOULI, V. & RABIEI, M. 2019. Significant aspects of carbon capture and storage – A review. *Petroleum,* 5, 335-340.

RAZZAK, S. A., ALI, S. A. M., HOSSAIN, M. M. & DELASA, H. 2017. Biological CO_2 fixation with production of microalgae in wastewater – A review. *Renew. Sustain. Energy Rev.,* 76, 379-390.

RAZZAK, S. A., HOSSAIN, M. M., LUCKY, R. A., BASSI, A. S. & DE LASA, H. 2013. Integrated CO_2 capture, wastewater treatment and biofuel production by microalgae culturing—A review. *Renew. Sustain. Energy Rev.,* 27, 622-653.

REALMONTE, G., DROUET, L., GAMBHIR, A., GLYNN, J., HAWKES, A., KOBERLE, A. C. & TAVONI, M. 2019. An inter-model assessment of the role of direct air capture in deep mitigation pathways. *Nat. Commun.,* 10, 3277-3289.

REIS, M. G. D. & RIBEIRO, A. 2020. Conversion factors and general equations applied in agricultural and forest meteorology. *Agrometeoros,* 27, 227-258.

REYES-MERCADO, Y., VÁZQUEZ, F., RODRÍGUEZ-GÓMEZ, F. J. & DUDA, Y. 2008. Effect of the acrylic acid content on the permeability and water uptake of poly(styrene-co-butyl acrylate) latex films. *Colloid Polym. Sci.,* 286, 603-609.

REYNHOUT, X. E. E., BECKERS, M., MEULDIJK, J. & DRINKENBURG, B. A. H. 2005. Electrosteric stability of styrene/acrylic acid copolymer latices under emulsion polymerization reaction conditions. *J. Polym. Sci., Part A-1: Polym. Chem.,* 43, 726-732.

REZAYIAN, M., NIKNAM, V. & EBRAHIMZADEH, H. 2019. Oxidative damage and antioxidative system in algae. *Toxicol. Rep.,* 6, 1309-1313.

REZVANI, S., MOHEIMANI, N. R. & BAHRI, P. A. 2016. Techno-economic assessment of CO_2 bio-fixation using microalgae in connection with three different state-of-the-art power plants. *Comput. Chem. Eng.,* 84, 290-301.

RITTIMA, A., SALEEKIJ, K., SAMARNWONGRAK, K., SRITAMMA, P. & CHEERANORAVANICH, I. 2013. The study on evaporation losses from large reservoirs in Thailand. *J. Res. Dev.,* 24, 17-26.

ROBESON, L. M. 2008. The upper bound revisited. *J. Membr. Sci.,* 320, 390-400.

ROBOPLANT. 2013. *Elsewhere in science: We need to talk about biofuels* [Online]. The Unviersity of Sheffield. Available: https://roboplant.wordpress.com/2013/07/23/elsewhere-in-science-we-need-to-talk-about-biofuels/ [Accessed].

ROCHA, A. C., REIS-HENRIQUES, M. A., GALHANO, V., FERREIRA, M. & GUIMARAES, L. 2016. Toxicity of seven priority hazardous and noxious substances (HNSs) to marine organisms: Current status, knowledge gaps and recommendations for future research. *Sci. Total Environ.,* 542, 728-749.

ROCHELLE, T. G. 2009. Amine scrubbing for CO_2 capture. *Science,* 325, 1652-1654.

ROGELJ, J., LUDERER, G., PIETZCKER, R. C., KRIEGLER, E., SCHAEFFER, M., KREY, V. & RIAHI, K. 2015. Energy system transformations for limiting end-of-century warming to below 1.5 °C. *Nat. Clim. Change,* 5, 519-527.

ROGELJ, J., SHINDELL, D., JIANG, K., FIFITA, S., FORSTER, P., GINZBURG, V., HANDA, C., KEHESHGI, H., KOBAYASHI, S., KRIEGLER, E., MUNDACA, L., SÉFÉRIAN, R. & VILARIÑO, M. V. 2018. An IPCC special report on the impacts of global warming of 1.5°C above pre-industrial levels and related global greenhouse gas emission pathways, in the context of strengthening the global response to the threat of climate change, sustainable development, and efforts to eradicate poverty.

ROJAS-GRAU, M. A., SOLIVA-FORTUNY, R. & MARTIN-BELLOSO, O. 2009. Edible coatings as tools to improve quality and shelf-life of fresh-cut fruits. *Fresh Produce,* 65-72.

ROSGAARD, L., DE PORCELLINIS, A. J., JACOBSEN, J. H., FRIGAARD, N. U. & SAKURAGI, Y. 2012. Bioengineering of carbon fixation, biofuels, and biochemicals in cyanobacteria and plants. *J. Biotechnol.*, 162, 134-147.

ROUSSANALY, S. 2019. Calculating CO_2 avoidance costs of carbon capture and storage from industry. *Carbon Manag.*, 10, 105-112.

RUBIN, E. S., CHEN, C. & RAO, A. B. 2007. Cost and performance of fossil fuel power plants with CO_2 capture and storage. *Energy Policy*, 35, 4444-4454.

RYU, H. J., OH, K. K. & KIM, Y. S. 2009. Optimization of the influential factors for the improvement of CO_2 utilization efficiency and CO_2 mass transfer rate. *J. Ind. Eng. Chem.*, 15, 471-475.

SAEED, A. & IQBAL, M. 2006. Immobilization of blue green microalgae on loofa sponge to biosorb cadmium in repeated shake flask batch and continuous flow fixed bed column reactor system. *World J. Microbiol. Biotechnol.*, 22, 775–782.

SAEED, A. & IQBAL, M. 2013. Loofa (*Luffa cylindrica*) sponge: Review of development of the biomatrix as a tool for biotechnological applications. *Biotechnol. Prog.*, 29, 573-600.

SAEED, I. M., ALABA, P., MAZARI, S. A., BASIRUN, W. J., LEE, V. S. & SABZOI, N. 2018. Opportunities and challenges in the development of monoethanolamine and its blends for post-combustion CO_2 capture. *Int. J. Greenh. Gas Control.*, 79, 212-233.

SAJJADI, B., CHEN, W.-Y., RAMAN, A. A. A. & IBRAHIM, S. 2018. Microalgae lipid and biomass for biofuel production: A comprehensive review on lipid enhancement strategies and their effects on fatty acid composition. *Renew. Sustain. Energy Rev.*, 97, 200-232.

SALIH, F. M. 2011. Microalgae tolerance to high concentrations of carbon dioxide: A review. *J. Environ. Prot.*, 02, 648-654.

SALVI, B. L. & JINDAL, S. 2019. Recent developments and challenges ahead in carbon capture and sequestration technologies. *SN Appl. Sci.*, 1, 885-905.

SANDERS, D. F., SMITH, Z. P., GUO, R., ROBESON, L. M., MCGRATH, J. E., PAUL, D. R. & FREEMAN, B. D. 2013. Energy-efficient polymeric gas separation membranes for a sustainable future: A review. *Polymer*, 54, 4729-4761.

SANZ-PEREZ, E. S., MURDOCK, C. R., DIDAS, S. A. & JONES, C. W. 2016. Direct capture of CO_2 from ambient air. *Chem. Rev.*, 116, 11840-11876.

SARTORY, D. P. & GROBBELAAR, J. U. 1984. Extraction of chlorophyll a from freshwater phytoplankton for spectrophotometric analysis. *Hydrobiologia*, 114, 117-187.

SASSANO, C. E. N., GIOIELLI, L. A., FERREIRA, L. S., RODRIGUES, M. S., SATO, S., CONVERTI, A. & CARVALHO, J. C. M. 2010. Evaluation of the composition of continuously-cultivated *Arthrospira* (Spirulina) *platensis* using ammonium chloride as nitrogen source. *Biomass Bioenerg.*, 34, 1732-1738.

SAUER, J., SCHREIBER, U., SCHMID, R., VOLKER, U. & FORCHHAMMER, K. 2001. Nitrogen starvation-induced chlorosis in *Synechococcus* PCC 7942. Low-level photosynthesis as a mechanism of long-term survival. *Plant Physiol.*, 126, 233-243.

SAYARI, A., BELMABKHOUT, Y. & SERNA-GUERRERO, R. 2011. Flue gas treatment via CO_2 adsorption. *Chem. Eng. J.*, 171, 760-774.

SAYRE, R. 2010. Microalgae: The potential for carbon capture. *BioScience*, 60, 722-727.

SCHATZ, D., NAGAR, E., SENDERSKY, E., PARNASA, R., ZILBERMAN, S., CARMELI, S., MASTAI, Y., SHIMONI, E., KLEIN, E., YEGER, O., REICH, Z. & SCHWARZ, R. 2013. Self-suppression of biofilm formation in the cyanobacterium *Synechococcus elongatus*. *Environ. Microbiol.*, 15, 1786-1794.

SCHMIDT, H., THOM, M., KING, L., WIEPRECHT, S. & GERBERSDORF, S. U. 2016. The effect of seasonality upon the development of lotic biofilms and microbial biostabilisation. *Freshw. Biol.*, 61, 963-978.

SCHWARZ, R. & FORCHHAMMER, K. 2005. Acclimation of unicellular cyanobacteria to macronutrient deficiency: emergence of a complex network of cellular responses. *Microbiology (Reading)*, 151**,** 2503-2514.

SERP, D., CANTANA, E., HEINZEN, C., STOCKAR, U. V. & MARISON, I. W. 2000. Characterization of an encapsulation device for the production of monodisperse alginate beads for cell immobilization. *Biotechnol. Bioeng.*, 70**,** 41-53.

SEYED HOSSEINI, N., SHANG, H. & SCOTT, J. A. 2018. Biosequestration of industrial off-gas CO_2 for enhanced lipid productivity in open microalgae cultivation systems. *Renew. Sustain. Energy Rev.*, 92**,** 458-469.

SHEPARD, D. 2016. Closing Paris agreement signing press release. UNFCCC.

SHILTON, A. 2006. *Pond treatment technology*, IWA Publishing.

SHIN, R. & SEARCY, C. 2018. Evaluating the greenhouse gas emissions in the craft beer industry: An assessment of challenges and benefits of greenhouse gas accounting. *Sustainability*, 10**,** 4191-4221.

SIAGIAN, U. W. R., RAKSAJATI, A., HIMMA, N. F., KHOIRUDDIN, K. & WENTEN, I. G. 2019. Membrane-based carbon capture technologies: Membrane gas separation vs. membrane contactor. *J. Nat. Gas. Sci. Eng.*, 67**,** 172-195.

SIEGELMAN, R. L., MILNER, P. J., KIM, E. J., WESTON, S. C. & LONG, J. R. 2019. Challenges and opportunities for adsorption-based CO_2 capture from natural gas combined cycle emissions. *Energy Environ. Sci.*, 12**,** 2161-2173.

SIERRA, E., ACIÉN, F. G., FERNÁNDEZ, J. M., GARCÍA, J. L., GONZÁLEZ, C. & MOLINA, E. 2008. Characterization of a flat plate photobioreactor for the production of microalgae. *Chem. Eng. J.*, 138**,** 136-147.

SILVERSTEIN, A., SILVERSTEIN, V. B. & NUNN, L. S. 2007. *Photosynthesis*, Twenty-First Century Books.

SIMBECK, D. & BEECY, D. 2011. The CCS paradox: The much higher CO_2 avoidance costs of existing versus new fossil fuel power plants. *Energy Procedia*, 4**,** 1917-1924.

SINGH, J. & DHAR, D. W. 2019. Overview of carbon capture technology: Microalgal biorefinery concept and state-of-the-art. *Front. Mar. Sci.*, 6**,** 29-38.

SINGH, J. S., KUMAR, A., RAI, A. N. & SINGH, D. P. 2016. Cyanobacteria: A precious bio-resource in agriculture, ecosystem, and environmental sustainability. *Front. Microbiol.*, 7**,** 529-548.

SINGH, R. N. & SHARMA, S. 2012. Development of suitable photobioreactor for algae production – A review. *Renew. Sustain. Energy Rev.*, 16**,** 2347-2353.

SINGLETON, J. 2019. Online monitoring of beer fermentation by measurement of evolved carbon dioxide using an infrared sensor. Newcastle University.

SLADE, R. & BAUEN, A. 2013. Micro-algae cultivation for biofuels: Cost, energy balance, environmental impacts and future prospects. *Biomass Bioenerg.*, 53**,** 29-38.

SMITH, M. J. 2018. *Statistical Analysis Handbook*, Edinburgh, The Winchelsea Press.

SMITH, P., BUSTAMANTE, M., AHAMMAD, H., CLARK, H., DONG, H., ELSIDDIG, E. A., HABERL, H., HARPER, R., HOUSE, J., JAFARI, M., MASERA, O., MBOW, C., RAVINDRANATH, N. H., RICE, C. W., ROBLEDO ABAD, C., ROMANOVSKAYA, A., SPERLING, F. & TUBIELLO, F. 2014. Agriculture, forestry and other land use (AFOLU). *Climate Change 2014: Mitigation of Climate Change. Contribution of Working Group III to the Fifth Assessment Report of the Intergovernmental Panel on Climate Change.* Cambridge, United Kingdom and New York, NY, USA: IPCC.

SONG, C., HU, X., LIU, Z., LI, S. & KITAMURA, Y. 2020. Combination of brewery wastewater purification and CO_2 fixation with potential value-added ingredients production via different microalgae strains cultivation. *J. Clean. Prod.*, 122332-122342.

SONG, C., LIU, Q., DENG, S., LI, H. & KITAMURA, Y. 2019a. Cryogenic-based CO_2 capture technologies: State-of-the-art developments and current challenges. *Renew. Sustain. Energy Rev.*, 101, 265-278.

SONG, C., LIU, Q., QI, Y., CHEN, G., SONG, Y., KANSHA, Y. & KITAMURA, Y. 2019b. Absorption-microalgae hybrid CO_2 capture and biotransformation strategy—A review. *Int. J. Greenh. Gas Control.*, 88, 109-117.

SONG, C., PAN, W., SRIMAT, S. T., ZHENG, J., LI, Y., WANG, Y.-H., XU, B.-Q. & ZHU, Q.-M. 2004. Tri-reforming of methane over Ni catalysts for CO_2 conversion to syngas with desired H_2/CO ratios using flue gas of power plants without CO_2 separation. *Carbon Dioxide Utilization for Global Sustainability, Proceedings of 7ththe International Conference on Carbon Dioxide Utilization.* 315-322.

SONG, C.-F., KITAMURA, Y., LI, S.-H. & OGASAWARA, K. 2012. Design of a cryogenic CO_2 capture system based on stirling coolers. *Int. J. Greenh. Gas Control.*, 7, 107-114.

SRIHARSHA, D. V., KUMAR R, L. & SAVITHA, J. 2017. Immobilized fungi on *Luffa cylindrica*: An effective biosorbent for the removal of lead. *J. Taiwan Inst. Chem. Eng.*, 80, 589-595.

STELLA, S. M. & VIJAYALAKSHMI, U. 2019. Influence of chemically modified *Luffa* on the preparation of nanofiber and its biological evaluation for biomedical applications. *J. Biomed. Mater. Res. A.*, 107, 610-620.

STEWARD, P. A., HEARN, J. & WILKINSON, M. C. 2000. An overview of polymer latex film formation and properties. *Adv. Colloid Interface Sci.*, 86, 195-267.

STIRLING, A. & PAPAI, I. 2010. H_2CO_3 forms via HCO_3^- in water. *J. Phys. Chem. B.*, 114, 16854–16859.

STRIETH, D., ULBER, R. & MUFFLER, K. 2018. Application of phototrophic biofilms: from fundamentals to processes. *Bioprocess Biosyst. Eng.*, 41, 295-312.

SUAREZ GARCIA, E., VAN LEEUWEN, J., SAFI, C., SIJTSMA, L., EPPINK, M. H. M., WIJFFELS, R. H. & VAN DEN BERG, C. 2018. Selective and energy efficient extraction of functional proteins from microalgae for food applications. *Bioresour. Technol.*, 268, 197-203.

SUBRAMANIAN, G. & SUNDARAM, S. S. 1986. Uninduced ammonia release by the nitrogen-fixing cyanobacterium *Anabaena*. *FEMS Microbiol. Lett.*, 37, 151–154.

SUBRAMANIYAM, V., SUBASHCHANDRABOSE, S. R., GANESHKUMAR, V., THAVAMANI, P., CHEN, Z., NAIDU, R. & MEGHARAJ, M. 2016. Cultivation of *Chlorella* on brewery wastewater and nano-particle biosynthesis by its biomass. *Bioresour. Technol.*, 211, 698-703.

SUH, S. I., PARK, B. C., HAN, K. J. & LEE, B. S. 1998. Cultivation of cyanobacterium in various types of photobioreactors for biological CO_2 fixation. *Advances in chemical conversions for mitigating carbon dioxide.* Elsevier. 471-474.

SUSTAINABLES, C. 2020. *Auro 321 White natural economic emulsion* [Online]. Available: https://www.celticsustainables.co.uk/auro-natural-emulsion-321/ [Accessed 30/09/2020].

SWOPE, K. L. & FLICKINGER, M. C. 1996. The use of confocal scanning laser microscopy and other tools to characterize *Escherichia coli* in a high-cell-density synthetic biofilm. *Biotechnol. Bioeng.*, 52, 340-356.

SYDNEY, E. B., STURM, W., DE CARVALHO, J. C., THOMAZ-SOCCOL, V., LARROCHE, C., PANDEY, A. & SOCCOL, C. R. 2010. Potential carbon dioxide fixation by industrially important microalgae. *Bioresour. Technol.*, 101, 5892-5896.

TAMPONNET, C., COSLANTINO, F., BARBOTIN, J.-N. & CALVAYRAC, R. 1985. Cytological and physiological behaviour of *Euglena gracillis* cells entrapped in a calcium alginate gel. *Physiol. Plant.*, 63, 277-283.

TAN, Y., NOOKUEA, W., LI, H., THORIN, E. & YAN, J. 2017. Evaluation of viscosity and thermal conductivity models for CO_2 mixtures applied in CO_2 cryogenic process in carbon capture and storage (CCS). *Appl. Therm. Eng.,* 123, 721-733.

TAVASSOLI-KAFRANI, E., SHEKARCHIZADEH, H. & MASOUDPOUR-BEHABADI, M. 2016. Development of edible films and coatings from alginates and carrageenans. *Carbohydr. Polym.,* 137, 360-74.

THEPENIER, C. & GUDIN, C. 1985. Immobilization of *Porphyridium cruentum* in polyurethane foams for the production of polysaccharide. *Biomass,* 225-240.

THIAGARAJAN, V. S., HUANG, Z., SCRIVEN, L. E., SCHOTTEL, J. L. & FLICKINGER, M. C. 1999. Microstructure of a biocatalytic latex coating containing viable *Escherichia coli* cells. *J. Colloid Interface Sci.,* 215, 244-257.

THIMIJAN, R. W. & HEINS, R. D. 1982. Photometric, radiometric, and quantum light units of measurement: a review of procedures for interconversion. *HortScience,* 18, 818-822.

TOLA, V. & PETTINAU, A. 2014. Power generation plants with carbon capture and storage: A techno-economic comparison between coal combustion and gasification technologies. *Appl. Energy,* 113, 1461-1474.

TOSA, T., SATO, T., MORI, T., YAMAMOTO, K., TAKATA, I., NISHIDA, Y. & CHIBATA, I. 1979. Immobilization of enzymes and microbial cells using carrageenan as matrix. *Biotechnol. Bioeng.,* 21, 1697-1709.

TOWLER, G. & SINNOTT, R. K. 2013a. 7.6.3 Materials factors. *In:* TOWLER, G. & SINNOTT, R. K. (eds.) *Chemical Engineering Design - Principles, Practice and Economics of Plant and Process Design (2nd Edition).* Elsevier.

TOWLER, G. & SINNOTT, R. K. 2013b. Chapter 8 Estimating revenues and production costs. *Chemical Engineering Design - Principles, Practice and Economics of Plant and Process Design (2nd Edition).* Elsevier.

TRAVIESO, L., BENITEZ, F., WEILAND, P., SANCHEZ, E., DUPEYRON, R. & DOMINGUEZ, A. R. 1996. Experiments on immobilization of microalgae for nutrient removal in wastewater treatments. *Bioresour. Technol.,* 55, 181-186.

TSAI, D. D.-W., CHEN, P. H., CHOU, C. M.-J., HSU, C.-F. & RAMARAJ, R. 2015. Carbon sequestration by alga ecosystems. *Ecol. Eng.,* 84, 386-389.

TUINIER, M. J., HAMERS, H. P. & VAN SINT ANNALAND, M. 2011a. Techno-economic evaluation of cryogenic CO_2 capture—A comparison with absorption and membrane technology. *Int. J. Greenh. Gas Control.,* 5, 1559-1565.

TUINIER, M. J., VAN SINT ANNALAND, M. & KUIPERS, J. A. M. 2011b. A novel process for cryogenic CO_2 capture using dynamically operated packed beds—An experimental and numerical study. *Int. J. Greenh. Gas Control.,* 5, 694-701.

ULLAH, K., AHMAD, M., SOFIA, SHARMA, V. K., LU, P., HARVEY, A., ZAFAR, M. & SULTANA, S. 2015. Assessing the potential of algal biomass opportunities for bioenergy industry: A review. *Fuel,* 143, 414-423.

UMAR, A. 2018. *The screening, fabrication and production of microalgae biocomposites for carbon capture and utilisation.* Doctor of Philosophy PhD, Newcastle University.

VAN DER SPEK, M., FOUT, T., GARCIA, M., KUNCHEEKANNA, V. N., MATUSZEWSKI, M., MCCOY, S., MORGAN, J., NAZIR, S. M., RAMIREZ, A., ROUSSANALY, S. & RUBIN, E. S. 2020. Uncertainty analysis in the techno-economic assessment of CO_2 capture and storage technologies. Critical review and guidelines for use. *Int. J. Greenh. Gas Control.,* 100, 103113-103133.

VAZ, B. D. S., COSTA, J. A. V. & MORAIS, M. G. 2019. Innovative nanofiber technology to improve carbon dioxide biofixation in microalgae cultivation. *Bioresour. Technol.,* 273, 592-598.

VESER, G. & MÜLLER, C. R. 2016. Chemical looping for energy technology: A special issue. *Energy Technol.,* 4, 1127-1129.

VILLENA, G. K. & GUTIERREZ-CORREA, M. 2006. Production of cellulase by *Aspergillus niger* biofilms developed on polyester cloth. *Lett. Appl. Microbiol.,* 43, 262-8.

WAKEFIELD, C. 2019. Marketbeat Thailand industrial Q4 2019.

WALLACE, A. D. 2018. *Constructing an algae-based biomimetic artificial leaf device for CO_2 recycling and solar energy harvesting.* Master of Science, North Carolina State University.

WANG, H. Y. & HETTWER, D. J. 1982. Cell immobilization in k-carrageenan with tricalcium phosphate. *Biotechnol. Bioeng.,* XXIV, 1827-1838.

WANG, J., LIU, W. & LIU, T. 2017. Biofilm based attached cultivation technology for microalgal biorefineries-A review. *Bioresour. Technol.,* 244, 1245-1253.

WANG, M., JANOUT, V. & REGEN, L. S. 2013. Gas transport across hyperthin membrances. *Acc. Chem. Res.,* 46, 2743-2754.

WANG, M., LAWAL, A., STEPHENSON, P., SIDDERS, J. & RAMSHAW, C. 2011. Post-combustion CO_2 capture with chemical absorption: A state-of-the-art review. *Chem. Eng. Res. Des.,* 89, 1609-1624.

WANG, S., ZHANG, Y., JU, W., CHEN, J. M., CIAIS, P., CESCATTI, A., SARDANS, J., JANSSENS, I. A., WU, M., BERRY, J. A., CAMPBELL, E., FERNÁNDEZ-MARTÍNEZ, M., ALKAMA, R., SITCH, S., FRIEDLINGSTEIN, P., SMITH, W. K., YUAN, W., HE, W., LOMBARDOZZI, D., KAUTZ, M., ZHU, D., LIENERT, S., KATO, E., POULTER, B., SANDERS, T. G. M., KRÜGER, I., WANG, R., ZENG, N., TIAN, H., VUICHARD, N., JAIN, A. K., WILTSHIRE, A., HAVERD, V., S. GOLL, D. & PEÑUELAS, J. 2020. Recent global decline of CO_2 fertilization effects on vegetation photosynthesis. *Science,* 370, 1295–1300.

WANG, Y. & CHEN, Z. 2019. The properties of solvent-based and water-borne butyl acrylate/styrene copolymer films. *Adv. Polym. Technol.,* 2019, 1-10.

WATKINSON, S. C. 2015. *The fungi,* Elsevier Science & Technology.

WEBB, C. & DERVAKOS, G. A. 1996. *Studies in viable cell immobilization,* R.G. Landes.

WILBERFORCE, T., BAROUTAJI, A., SOUDAN, B., AL-ALAMI, A. H. & OLABI, A. G. 2019. Outlook of carbon capture technology and challenges. *Sci. Total Environ.,* 657, 56-72.

WINNIK, A. M. 1997. Latex film formation. *J. Colloid Interface Sci.,* 2, 192-199.

WOLSKY, A. M., DANIELS, E. J. & JODY, B. J. 1994. CO_2 capture from the flue gas of conventional fossil-fuel-fired power plants. *Environ. Prog.,* 13, 214-219.

WONDRACZEK, L., GRUNDLER, A., REUPERT, A., WONDRACZEK, K., SCHMIDT, M. A., POHNERT, G. & NOLTE, S. 2019. Biomimetic light dilution using side-emitting optical fiber for enhancing the productivity of microalgae reactors. *Sci. Rep.,* 9, 9600.

WONG, Y. S. & TAM, N. F. Y. 2013. *Wastewater treatment with algae,* Springer Berlin Heidelberg.

WU, X., CEN, Q., ADDY, M., ZHENG, H., LUO, S., LIU, Y., CHENG, Y., ZHOU, W., CHEN, P. & RUAN, R. 2019. A novel algal biofilm photobioreactor for efficient hog manure wastewater utilization and treatment. *Bioresour. Technol.,* 292.

WURZBACHER, J. A., GEBALD, C., PIATKOWSKI, N. & STEINFELD, A. 2012. Concurrent separation of CO_2 and H_2O from air by a temperature-vacuum swing adsorption/desorption cycle. *Environ. Sci. Technol.,* 46, 9191-9198.

XIAO, R. & ZHENG, Y. 2016. Overview of microalgal extracellular polymeric substances (EPS) and their applications. *Biotechnol. Adv.,* 34, 1225-1244.

XU, L., WEATHERS, P. J., XIONG, X.-R. & LIU, C.-Z. 2009. Microalgal bioreactors: Challenges and opportunities. *Eng. Life Sci.,* 9, 178-189.

XU, X.-Q., WANG, J.-H., ZHANG, T.-Y., DAO, G.-H., WU, G.-X. & HU, H.-Y. 2017. Attached microalgae cultivation and nutrients removal in a novel capillary-driven photo-biofilm reactor. *Algal Res.,* 27, 198-205.

XUE, S., ZHANG, Q., WU, X., YAN, C. & CONG, W. 2013. A novel photobioreactor structure using optical fibers as inner light source to fulfill flashing light effects of microalgae. *Bioresour. Technol.*, 138, 141-147.

YAMAK, B. H. 2013. Emulsion polymerization: Effects of polymerization variables on the properties of vinyl acetate based emulsion polymers. *Polymer Science*. 35-71.

YASHVEER, S. 2003. Photosynthetic activity, and lipid and hydracarbon production by alginate-immobilized cells of *Botryococcus* in relation to growth phase. *J. Microbiol. Biotechnol.*, 687-691.

YEH, K. L. & CHANG, J. S. 2011. Nitrogen starvation strategies and photobioreactor design for enhancing lipid content and lipid production of a newly isolated microalga *Chlorella vulgaris* ESP-31: implications for biofuels. *Biotechnol. J.*, 6, 1358-1366.

YU, H., LI, X., DUCHOUD, F., CHUANG, D. S. & LIAO, J. C. 2018. Augmenting the Calvin-Benson-Bassham cycle by a synthetic malyl-CoA-glycerate carbon fixation pathway. *Nat Commun*, 9, 2008.

ZAINAB, A., MERAJ, S. & LIAQUAT, R. 2019. Study on natural organic materials as biofilm carriers for the optimization of anaerobic digestion. *Waste Biomass Valori*.

ZEEBE, R. E. 2011. On the molecular diffusion coefficients of dissolved, and and their dependence on isotopic mass. *Geochim. Cosmochim. Acta*, 75, 2483-2498.

ZEMAN, F. 2014. Reducing the cost of Ca-based direct air capture of CO_2. *Environ. Sci. Technol.*, 48, 11730-11735.

ZHANG, X. 2015. Microalgae removal of CO_2 from flue gas. IEA Clean Coal Centre.

ZHAO, B. & SU, Y. 2014. Process effect of microalgal-carbon dioxide fixation and biomass production: A review. *Renew. Sustain. Energy Rev.*, 31, 121-132.

ZHAO, X., KUMAR, K., GROSS, M. A., KUNETZ, T. E. & WEN, Z. 2018. Evaluation of revolving algae biofilm reactors for nutrients and metals removal from sludge thickening supernatant in a municipal wastewater treatment facility. *Water Res.*, 143, 467-478.

ZHENG, H., LIU, M., LU, Q., WU, X., MA, Y., CHENG, Y., ADDY, M., LIU, Y. & RUAN, R. 2018. Balancing carbon/nitrogen ratio to improve nutrients removal and algal biomass production in piggery and brewery wastewaters. *Bioresour. Technol.*, 249, 479-486.

ZHOU, H., SHENG, Y., ZHAO, X., GROSS, M. & WEN, Z. 2018. Treatment of acidic sulfate-containing wastewater using revolving algae biofilm reactors: Sulfur removal performance and microbial community characterization. *Bioresour. Technol.*, 264, 24-34.

ZHOU, W., CHEN, P., MIN, M., MA, X., WANG, J., GRIFFITH, R., HUSSAIN, F., PENG, P., XIE, Q., LI, Y., SHI, J., MENG, J. & RUAN, R. 2014. Environment-enhancing algal biofuel production using wastewaters. *Renew. Sustain. Energy Rev.*, 36, 256-269.

ZHU, H., ZHU, C., CHENG, L. & CHI, Z. 2017. Plastic bag as horizontal photobioreactor on rocking platform driven by water power for culture of alkalihalophilic cyanobacterium. *Bioresour. Bioprocess.*, 4.

ZNAD, H., AL KETIFE, A. M. D. & JUDD, S. 2019. Enhancement of CO_2 biofixation and lipid production by *Chlorella vulgaris* using coloured polypropylene film. *Environ. Technol.*, 40, 2093-2099.

ZOHREHVAND, S. & NIJENHUIS, K. T. 2005. Film formation from monodisperse acrylic latices, part 4: The role of coalescing agents in the film formation process. *Colloid Polym. Sci.*, 283, 1305-1312.